

Remote Detection of Concealed Guns and Explosives

Matthew James Southgate

A thesis submitted in partial fulfilment of the requirements of the Manchester
Metropolitan University for the degree of Doctor of Philosophy

Department of Engineering and Technology
Faculty of Science and Engineering
Manchester Metropolitan University

2013

Blank page

*To my beautiful wife and wonderful family; without you,
this would not have been possible.*

Ability is nothing without opportunity.

NAPOLEON BONAPARTE

Blank page

Abstract

A reliable method of remotely detecting concealed guns and explosives attached to the human body is of great interest to governments and security forces throughout the world. This thesis describes the development and trials of a new remote non-imaging concealed threat detection method using active millimetre wave radar using the microwave and mm-wave frequencies bands 14 – 40 and 75 – 110 GHz (Ku, K, Ka and W). The method is capable of not only screening for concealed objects, like the current generation of concealed object detectors, but also of differentiating between mundane and threat objects. The areas focused upon during this investigation were: identifying the impact of different commonly worn fabrics as barriers to detection; consulting with end users about their requirements and operational needs; a comparison of different frequency bands for the detection of guns and explosives; exploring the effects of polarisation on object detection; a performance comparison of different detection schemes using Artificial Neural Networks; improving existing data acquisition systems and prototyping of a real-time capture system.

Blank page

Acknowledgements

I would like to thank my supervisor Nick for his encouragement and support, not just for this Ph.D. part over the past several years. Without Nick, the remote sensing research team would never have been formed and much of this work would never have been undertaken. My thanks also go to Nacer Ddine Rezgui for always offering his expert advice and regularly alternate point of view and David Andrews for his considered insight and patience.

My gratitude to my parents, for without them, none of this would have been possible. I hope you now appreciate in hindsight how amusing your initial confusion about my intent to become a doctor was and that hopefully you now understand that what I'm doing is 'a real job'.

Finally I would like to thank my wife Penny. For almost a decade you have supported me in my ideas and efforts. You're my best friend, my confidant, and my support pillar.

Without you I would not be where I am today (and still eating junk food). In addition, you have produced the most beautiful child on the planet. Our son Oscar is the motivation to keep doing with this. If I can do anything to make this world a little safer for him, then I feel it is all worthwhile.

Domestic life can now return to 'normal'.

Blank page

Declaration of Originality

This is to certify that the work is entirely my own and not of any other person, unless explicitly acknowledged (including citation of published and unpublished sources). The work has not previously been submitted in any form to the Manchester Metropolitan University or to any other institution for assessment for any other purpose.

Signed _____

Date _____

Blank page

Table of Contents

1	Introduction.....	1
1.1	Concealed Threat Detection.....	3
1.2	Contribution to Knowledge.....	5
1.3	Document Structure.....	6
2	Literature Review.....	9
2.1	Detection Energies and Detector Types.....	15
2.2	Acoustic-based Systems.....	16
2.2.1	Hard Object Detector.....	16
2.2.2	Non-linear Acoustic Object Detector.....	17
2.3	Electromagnetic Detection Systems.....	18
2.3.1	Passive Non Imaging Electromagnetic Detection Systems.....	18
2.3.1.1	Millimetre Wave Imagers.....	18
2.3.2	Passive Imaging Electromagnetic Detection Systems.....	21
2.3.3	Active Non-Imaging Electromagnetic Detection Systems.....	28
2.3.3.1	Pulsed Radar With Swept Frequency Detector.....	28
2.3.3.2	Millimetre Wave Radar Detectors.....	28
2.3.3.3	Electromagnetic Pulse Detector.....	33
2.3.4	Active Imaging Electromagnetic Detection Systems.....	34
2.3.4.1	Microwave Holographic Imagers.....	34
2.3.4.2	Microwave Dielectric Imagers.....	35
2.3.4.3	Microwave Radar Imagers.....	35
2.3.4.4	Terahertz Imagers.....	36
2.3.4.5	X-Ray Imagers.....	36
2.4	Magnetic Detection Systems.....	37
2.4.1	Walk-Through Metal Detection Portal.....	38
2.4.2	Hand-Held Metal Detectors.....	39

2.4.3	Magnetic Imaging Portals.....	39
2.4.4	MRI Body Cavity Imager.....	40
2.4.5	Gradiometer metal detectors.....	40
2.5	Summary.....	41
3	Background Theory.....	43
3.1	Electromagnetic Propagation.....	43
3.2	Background Theory of Detection.....	44
3.2.1	Active Illumination.....	49
3.2.2	Continuous or Pulsed Radiation.....	50
3.2.3	Controlled and Uncontrolled Environments.....	50
3.2.4	Refractive Index.....	51
3.2.5	Refraction and Reflection.....	53
3.2.6	Skin Depth.....	54
3.2.7	Radar Cross Section.....	54
3.2.8	Polarisation.....	55
3.2.9	Beam Generation and Focussing.....	57
3.2.10	Radiation Safety.....	57
3.3	Radar.....	58
3.3.1	Active Radar Types.....	58
4	Proof of Concept.....	61
4.1	Analysing the Problem.....	61
4.2	Threat Objects and Detection Scenarios.....	63
4.2.1	On Body Threat Concealment.....	64
4.2.2	Detection Scenarios.....	65
4.3	Basic Device Specification.....	65
4.3.1	Radar Types.....	66
4.3.2	Measurement of Ultra-Wideband Frequency Responses.....	67
4.3.2.1	Narrow Pulsed Radar.....	68
4.3.2.2	Swept FMCW Radar.....	69
4.3.2.3	Stepped Frequency FMCW.....	71
4.3.2.4	Direct Detection Radar	71
4.3.2.5	Resolution Limitations of FMCW Radar.....	72

4.3.2.6	Comparison of Pulsed and Frequency Modulated Systems.....	72
4.3.2.7	Pulsed and FMCW Radar Equivalence.....	73
4.3.2.8	Distance Resolution and Bandwidth.....	74
4.4	Atmospheric Signal Attenuation.....	75
4.5	Material Attenuation and Transmittance.....	77
4.6	Detection of Dielectrics.....	86
4.6.1	Measurements of a PTFE Disk Embedded with Mica	88
4.6.2	Application to Non-Fragmentation Based Explosives.....	91
4.6.3	Simulated Plastic Explosive in Isolation.....	92
4.6.4	Dielectric with Reflective Background (Simulated Body).....	95
4.6.5	Observation of a Water Backed Dielectric Layer Between 75 – 110 GHz.....	98
4.7	Detection of Metals.....	104
4.7.1	Edge Glint.....	104
4.7.2	Gun Barrel Detection.....	106
4.8	'Direct Detection' Radar Resolution and Maximum Range.....	108
4.9	Prototype One: Direct Detector Bench Top Feasibility System.....	109
4.10	Detection Using Multiple Polarisation.....	114
5	Portable Prototypes.....	125
5.1	Methods of Determining Target Range	126
5.1.1	IR Distance Sensor.....	127
5.1.2	Acoustic Range Finder.....	128
5.1.3	Ranging Device Interfacing.....	129
5.1.4	Signal Gain.....	132
5.2	Custom High Speed Compact Data Acquisition Boards.....	132
5.2.1	Rapid Scanner Board.....	134
5.2.2	Rapid Scanning Performance Benefits.....	141
5.3	Frequency Source.....	144
5.3.1	Rapid Sweeper.....	146
5.4	Target Screening and Localisation of Concealed Objects.....	148
5.4.1	Illumination Spot Size.....	148
5.5	Prototype Two: Direct Detector Tripod Prototype.....	151
5.6	Prototype Three: Portable Direct Detector Prototype.....	161
5.6.1	Proposed Improvements.....	164

5.7	Prototype Four: Mirlin.....	165
5.7.1	Future Work.....	169
5.8	Interpolation of FFT Binned Data for Improved Dielectric Detection.....	170
6	Data Classification and Results.....	173
6.1	Artificial Neural Networks.....	173
6.1.1	Prototype Artificial Neural Network Structure.....	176
6.2	Alternative Classifiers.....	177
6.2.1	Principal Component Analysis.....	177
6.2.2	Thresholding.....	177
6.2.3	Self Organising Maps.....	177
6.3	Performance Metrics.....	178
6.4	Detection of Non-Fragmentation Based Explosives.....	179
6.4.1	ANN Classification of Direct Detector Generated Data.....	181
6.4.2	ANN Classification of Super-heterodyne Generated Data.....	185
6.5	Detection of Fragmentation Based Explosives.....	187
6.6	Detection of Concealed Handguns.....	187
6.7	Identifying The Effect Of Thresholding On Accuracy and Data Utility.....	194
6.7.1	Receiver Operating Characteristic (ROC) Space.....	199
6.8	Identification of Features Used In Classification: Signal Intensity or Structure....	201
6.9	Evaluation.....	204
7	Conclusion and Future Work.....	207
7.1	Conclusion.....	207
7.2	Future Work.....	210
	Bibliography.....	211
	A Radiation Safety.....	233
	B PCB Polariser.....	235
	C Comparison of PIC Compiler USB Throughput.....	237

Table of Figures

Figure 2.1: High resolution image from a Rapiscan Systems scanner.....	11
Figure 2.2: Smiths Detection TADAR system.....	13
Figure 2.3: ThruVision T4000 installation in Wayne County Courthouse, Michigan, USA.	14
Figure 2.4: CWD-2002 hand-held acoustic imager (Wild, 2003).....	16
Figure 2.5: SPO-7 system (Transportation, 2007).....	19
Figure 2.6: SPO-20 system (Transportation, 2007).....	20
Figure 2.7: SPO-30 system (Appleby, 2008).....	20
Figure 2.8: ThruVision indoor passive imager T4000	22
Figure 2.9: T4000 image of a person carrying a wallet in his trouser pocket at 3 m.....	22
Figure 2.10: ThruVision active imaging system T5000.....	23
Figure 2.11: ThruVision T5000 staged image of a person at 25 m with concealed object around their torso	24
Figure 2.12: ThruVision T5000 staged image of a person at 20m with concealed object around their torso	24
Figure 2.13: ThruVision T5000 staged image of a person at 10m with concealed object around their torso	25
Figure 2.14: ThruVision THz top level system diagram	25
Figure 2.15: Maximum detection distance against time for a 1 kg explosive device strapped to the torso	26
Figure 2.16: ThruVision TS4	27
Figure 2.17: ThruVision TS4 imagery.....	27
Figure 2.18: Kapilevich hand-held object detector.....	29
Figure 2.19: Kapilevich refined hand-held object detector.....	30
Figure 2.20: Spinning disk to produce a pulsed illumination	30

Figure 2.21: Kapilevich detector sweep of man with explosives.....	31
Figure 2.22: Kapilevich detector sweep of man without explosive.....	31
Figure 2.23: Kapilevich FMCW non-imaging sensor system diagram.....	32
Figure 2.24: Kapilevich FMCW radar detecting a remote metal object.....	33
Figure 2.25: Basic pulse induction metal detection scheme (Nelson, 2004).....	37
Figure 2.26: Photograph of hands free metal detectors that can be worn under gloves.....	39
Figure 3.1: The electromagnetic spectrum.....	43
Figure 3.2: Spectral radiation of a 300 K Blackbody for wavelengths between 0.001 and 10.000 mm.....	45
Figure 3.3: Black body radiation of a 300 K body for wavelengths between 2.50 and 5.00 mm.....	46
Figure 3.4: Solid angle against wavelength (2.50 and 5.00 mm) for a unit area aperture. . .	47
Figure 3.5: Spectral radiation power of a Blackbody at 300 K seen by an antenna for wavelengths between 2.50 and 5.00 mm.....	48
Figure 3.6: Image from TADAR passive imager system using naturally occurring Black-body radiation to form an image.....	49
Figure 3.7: Absorption and refractive index of C-4.....	52
Figure 3.8: Angles of refraction and reflection.....	53
Figure 3.9: B274B Multi-pitch PCB Polariser.....	56
Figure 4.1: Areas of the body commonly used to conceal handguns (Met, 2008).....	64
Figure 4.2: The Doppler effect on the perceived frequency of illumination of a stationary and moving target.....	66
Figure 4.3: System diagram of a pulsed radar	67
Figure 4.4: Swept FMCW radar system diagram.....	68
Figure 4.5: Swept frequency FMCW radar response	69
Figure 4.6: Relative interface distance stepped FMCW radar system diagram.....	71
Figure 4.7: Radar resolution against bandwidth.....	73
Figure 4.8: Geometric, Mie, and Rayleigh atmospheric scattering regimes.....	75
Figure 4.9: Atmospheric attenuation across the EM spectrum at sea level.....	76
Figure 4.10: Atmospheric absorption 1 GHz to 1 THz.....	77

Figure 4.11: Side view of material transmittance experiment.....	78
Figure 4.12: Material transmittance experiment – part way through denim measurements	79
Figure 4.13: Stepper motor controlled rotational table.....	80
Figure 4.14: B194 Rotational table driver board.....	80
Figure 4.15: Energy transmission through various materials, normally irradiated.....	83
Figure 4.16: Background measurement prior to red leather energy transmittance experiment.....	84
Figure 4.17: Energy transmittance for red leather between 75 and 110 GHz.....	85
Figure 4.18: Normalised response of red leather between 75 and 110 GHz.....	85
Figure 4.19: 50 - 65 GHz frequency response of a 40 mm thick PTFE disc with embedded mica.....	89
Figure 4.20: Fourier transformed frequency response of a 40 mm thick PTFE disc with embedded mica.....	90
Figure 4.21: Principal reflections of an EM signal caused by a paraffin wax block.....	91
Figure 4.22: 8 cm by 8 cm calibration wax block used for antenna alignment.....	93
Figure 4.23: Sinusoidal response of paraffin wax block.....	94
Figure 4.24: Result of adapted Fourier Transform on FMCW data showing the optical depth of a paraffin wax block of dimensions 8 cm by 8 cm	94
Figure 4.25: Wax block with full water barrel backing simulating a human torso.....	95
Figure 4.26: Paraffin wax block of dimensions 8 cm by 8 cm backed by a full water bottle backing.....	96
Figure 4.27: Paraffin wax block backed by a full water bottle optical depth plot.....	97
Figure 4.28: Frequency spectrum of a barrel only, wax block and barrel and wax block only (offset vertically)	98
Figure 4.29: Frequency spectrum of a body only, wax block and human body and wax block only (offset vertically)	99
Figure 4.30: Fourier transformed optical depth for barrel only, wax block and barrel and wax block only (offset vertically)	100
Figure 4.31: Fourier transformed optical depth for body, wax block and body and wax block only (vertically offset).....	100

Figure 4.32: Range gated response from barrel only, wax block and barrel and wax block only (offset vertically) taken using the VNA.....	101
Figure 4.33: Range gated response from body only, wax block and human body and wax block only (offset vertically) taken using the VNA.....	102
Figure 4.34: Irregular dielectric test piece one.....	103
Figure 4.35: Irregular dielectric test piece two.....	103
Figure 4.36: Experimental apparatus to measure the FMCW response of a rotating thin metal plate (unetched PCB).....	104
Figure 4.37: Rotating thin metal sheet optical depth transform results.....	105
Figure 4.38: Experimental apparatus to measure the response of a gun barrel.....	106
Figure 4.39: Frequency response of a 9mm internal diameter 10cm long simulated gun barrel aligned between 0 and 60 degrees and illuminated between 14 and 40 GHz (plots vertically offset).....	107
Figure 4.40: Direct Detector bench prototype antennas and a gun with simulated torso...	109
Figure 4.41: Direct Detector bench prototype RF and PC hardware.....	110
Figure 4.42: 14 – 40GHz Direct Detector Prototype Block Diagram.....	110
Figure 4.43: Rotational table in a direct detection reflective object experiment.....	112
Figure 4.44: Direct detection of wax slab on torso experiment.....	113
Figure 4.45: Top level diagram of a single channel of the 60 dB variable gain and offset voltage amplifier.....	114
Figure 4.46: Co-polarised antennas.....	115
Figure 4.47: Cross-polarised antennas.....	115
Figure 4.48: Cross-polarised response of a person rotating with no gun present.....	117
Figure 4.49: Cross-polarised response of a person rotating with a concealed handgun....	117
Figure 4.50: Experimental VNA setup for measuring the time domain co and cross-polarised responses of a range of objects scanning between 14 and 40 GHz.....	117
Figure 4.51: Co and cross-polarised response of a gun between 14 and 40 GHz.....	118
Figure 4.52: Co and cross-polarised response of a gun between 14 and 40 GHz.....	118
Figure 4.53: Co and cross-polarised response of a body between 14 and 40 GHz orientated face on.....	119
Figure 4.54: Co and cross-polarised response of a body between 14 and 40 GHz at an angle	

showing the signal from the arms and torso.....	119
Figure 4.55: Co and cross-polarised response of a body with gun between 14 and 40 GHz face on.....	120
Figure 4.56: Co and cross-polarised response of a gun on the side of the body between 14 and 40 GHz angled side on.....	120
Figure 4.57: Co and cross-polarised response of a body with camera between 14 and 40 GHz face on.....	121
Figure 4.58: Co and cross-polarised response of a bunch of keys between 14 and 40 GHz face on.....	121
Figure 5.1: Sharp 2Y0A700 infra-red distance sensor.....	125
Figure 5.2: Measured against actual distance results for a GP2Y0A700	126
Figure 5.3: SensComp #615088 50kHz ultrasonic instrument grade Smart Sensor	126
Figure 5.4: Measured against actual distance results for a SensComp 615088 50kHzUltrasonic Instrument Grade Smart Sensor	128
Figure 5.5: The compact B246A and ultrasonic sensor assembly.....	128
Figure 5.6: B246A Range Finder Multiple Target firmware flowchart.....	130
Figure 5.7: Typical apparatus for using a rapid scanning board.....	132
Figure 5.8: Time against frequency for a E8257D PSG Analogue Signal Generator (007 analogue ramp option) ramping from 12.5 to 18.33 GHz	133
Figure 5.9: Rapid scanning board v1 top level block diagram.....	134
Figure 5.10: Rapid Scanner v3.....	138
Figure 5.11: Rapid Scanner v3 top level block diagram.....	139
Figure 5.12: VCO output power output against frequency.....	142
Figure 5.13: VCO output frequency against driver voltage.....	142
Figure 5.14: Rapid scanner top level system diagram.....	144
Figure 5.15: Tuning sensitivity for Sivers IMA VCO at different temperatures.....	144
Figure 5.16: Spot size (half power) as a function of distance.....	147
Figure 5.17: First portable direct detector prototype.....	148
Figure 5.18: Top level systems of the first portable direct detector prototype, only one receive channel is shown.....	149

Figure 5.19: Video feed provided by a Trust HiRes USB 2.0 Webcam.....	151
Figure 5.20: AMC-10 frequency against output power (Millitech, 2011).....	153
Figure 5.21: Diagram of lens.....	154
Figure 5.22: Spot size measurements with lens, range against beam-width.....	155
Figure 5.23: MMIC output voltage against frequency at room temperature.....	157
Figure 5.24: Top level systems of the first portable direct detector prototype, only one receive channel is shown.....	158
Figure 5.25: Image of prototype four.....	162
Figure 5.26: Top level system diagram for Mirlin.....	163
Figure 5.27: Top level system diagram of Mirlin control electronics.....	165
Figure 5.28: Mirlin homodyne range finder top level system diagram.....	166
Figure 5.29: Interpolation of FFT example.....	167
Figure 6.1: ANN with six inputs, a hidden layer of three neurons and a single output....	170
Figure 6.2: Superimposed time domain scans for body only aligned on the body peak ...	176
Figure 6.3: Superimposed time domain scans for body and wax block aligned on the body peak.....	176
Figure 6.4: Performance metrics for ANN classification of direct detector generated optical depth spectrum in the 75 – 105 GHz band at ranges 2 – 4 m.....	179
Figure 6.5: Performance metrics for ANN classification of direct detector generated frequency spectrum in the 75 – 105 GHz band at ranges 2 – 4 m.....	180
Figure 6.6: Performance metrics for ANN classification of super-heterodyne generated data in the 14 – 40 GHz for concealed wax block with segmented range	182
Figure 6.7: Aligned time domain responses of a stationary body 14 – 40 GHz.....	184
Figure 6.8: Aligned time domain responses of body with gun in front 14 – 40 GHz.....	184
Figure 6.9: Performance for ANN classification of heterodyne range gated data between 14 – 40 GHz for concealed guns.....	185
Figure 6.10: Performance of an ANN with variable output thresholding using range gated data from a heterodyne system operating between 14 – 40 GHz.....	189
Figure 6.11: Plot of Efficiency metric for various confidence upper thresholds on gun and mundane item classification using a direct detection system operating between 75 – 110 GHz.....	194

Figure 6.12: ROC space.....	195
Figure 6.13: ROC curves for various upper thresholds of an unseen dataset consisting of body only; camera in the waistband; keys; gun held in the waistband and in the hand, at ranges of 2, 4 and 6 metres.....	196
Figure 6.14: Performance of an ANN classifying unscaled and scaled data for body only and body with gun at 2 m using a direct power detect based system with a single cross-polar receiver operating between 80 – 100 GHz.....	199
Figure 6.15: Performance of an ANN classifying unscaled and scaled data for body only and body with gun at 5 m using a direct power detect based system with a single cross-polar receiver operating between 80 – 100 GHz.....	200
Figure 1: GUI of test and verify data terminal application.....	234

Blank page

List of Tables

Table 2.1: List of detector types.....	15
Table 2.2: T5000 field trial detection results for concealed explosive vest tests.....	26
Table 5.1: Prototype two top level parts list.....	150
Table 5.2: MMIC LNA and detector properties.....	156
Table 5.3: Prototype three top level parts list.....	159
Table 5.4: Prototype four top level parts list.....	164
Table 6.1: Performance metric confusion matrix.....	174
Table 6.2: ANN classification of body only and body with wax for normalised datasets generated using a direct detector system.....	178
Table 6.3: Sum of test data results for correctly and incorrectly classified by ANN supplied with dataset from a direct detection system operating between 75 – 105 GHz	179
Table 6.4: Optical depth spectrum performance metrics for direct detector operating between 75 – 105 GHz using a concealed paraffin wax block.....	180
Table 6.5: Frequency spectrum performance metrics for direct detector operating between 75 – 105 GHz using a concealed paraffin wax block.....	180
Table 6.6: ANN classification of body only and body with wax for normalised, body aligned datasets generated using a super-heterodyne detector.....	181
Table 6.7: Performance metrics for super-heterodyne data, segmented by range for body only and body with wax.....	182
Table 6.8: ANN classification of body only and body with gun for normalised, distance gated, body aligned datasets generated using a co-polar heterodyne detector.....	185
Table 6.9: Performance metrics for the ANN classification of range gated co-polar heterodyne generated data between 14 – 40 GHz for concealed guns	186
Table 6.10: ANN classification of body only, body with two different guns for normalised, distance gated, body aligned datasets generated using a co-polar heterodyne detector.....	186

Table 6.11: Performance metrics for cross testing of two ANNs trained on a starter pistol and Glock using range gated data from a heterodyne system between 14 – 40 GHz.....	187
Table 6.12: ANN classification with 50% threshold of body only and body and gun using a heterodyne system operating between 14 – 40 GHz.....	188
Table 6.13: Performance metrics for an ANN network with variable output thresholding using range gated data from a heterodyne system operating between 14 – 40 GHz.....	189
Table 6.14: TPR for various confidence thresholds on gun and mundane item classification using a direct detection system operating between 75 – 110 GHz.....	190
Table 6.15: FPR for various confidence thresholds on gun and mundane item classification using a direct detection system operating between 75 – 110 GHz.....	191
Table 6.16: TNR for various confidence thresholds on gun and mundane item classification using a direct detection system operating between 75 – 110 GHz.....	191
Table 6.17: FNR for various confidence thresholds on gun and mundane item classification using a direct detection system operating between 75 – 110 GHz.....	192
Table 6.18: Accuracy for various confidence thresholds on gun and mundane item classification using a direct detection system operating between 75 – 110 GHz.....	192
Table 6.19: Data Utility (%) for various confidence thresholds on gun and mundane item classification using a direct detection system operating between 75 – 110 GHz.....	193
Table 6.20: Efficiency metric for various confidence thresholds on gun and mundane item classification using a direct detection system operating between 75 – 110 GHz.....	194
Table 6.21: Comparison of Efficiency selected threshold pair (85/05) with the standard classification threshold (50/50) for an unseen dataset of body only; camera in the waistband; keys; gun held in the waistband and in the hand, at ranges of 2, 4 and 6 metres	197
Table 6.22: ANN classification results for original and normalised data from a direct power detector based system with a single cross-polar receiver between 80 – 100 GHz.....	198
Table 6.23: Performance metrics for ANN classifying unscaled and scaled data for body only and body with gun at 2 m using a direct power detect based system with a single cross-polar receiver operating between 80 – 100 GHz.....	199
Table 6.24: Performance metrics for ANN classifying unscaled and scaled data for body only and body with gun at 5 m using a direct power detect based system with a single cross-polar receiver operating between 80 – 100 GHz.....	200

Table 6.25: Comparison of Kapilevich detection systems and Mirlin.....	202
Table 7.1: Sections relating to fulfilment of Academic Aims.....	205
Table 1: PIC18F2550 USB data throughput using usb_cdc_putc(“payload”).....	235
Table 2: PIC18F2550 USB data throughput using looped usb_cdc_putc('1').....	235
Table 3: PIC18F2550 USB data throughput using looped usb_cdc_putc('1').....	236
Table 4: PIC18F2550 USB data throughput using isochronous transfers and manual buffer flushing of the Endpoint and sending data using putsrsUSBUART (‘payload’).....	236

Blank page

Publications

This thesis contains material which has been previously included in the following publications:

- 1 N. J. Bowring, J. G. Baker, N. D. Rezgui, M. Southgate, and J. F. Alder. Active millimetre wave detection of concealed layers of dielectric material. *Optics and Photonics in Global Homeland Security III*, Vol. 6540, No. 1. (2007), 65401M.
- 2 D. A. Andrews, N. D. Rezgui, S. E. Smith, N. J. Bowring, M. Southgate, J. G. Baker. Detection of concealed explosives at stand-off distances using wide band swept millimetre waves. *Millimetre Wave and Terahertz Sensors and Technology*, Vol. 7117, No. 1. (2008), 71170J.
- 3 Nacer Rezgui, David Andrews, Nicholas Bowring, Stuart Harmer and Matthew Southgate. Standoff detection of concealed handguns. *Passive Millimetre-Wave Imaging Technology XI*, Vol. 6948, No. 1. (2008), 69480L.
- 4 David A. Andrews, Nicholas Bowring, Nacer D. Rezgui, Matthew Southgate, Elizabeth Guest, Stuart Harmer and Ali Atiah. A multifaceted active swept millimetre-wave approach to the detection of concealed weapons. *Millimetre Wave and Terahertz Sensors and Technology*, Vol. 7117, No. 1. (2008), 711707.
- 5 David A. Andrews, Sarah Smith, Nacer Rezgui, Nicholas Bowring, Matthew Southgate and Stuart Harmer. A swept millimetre-wave technique for the detection of concealed weapons and thin layers of dielectric material with or without fragmentation. *Passive Millimetre-Wave Imaging Technology XII*, Vol. 7309, No. 1. (2009), 73090H.
- 6 Matt Southgate, David Andrews, Nacer Rezgui, Stuart W. Harmer and Nicholas

Bowring. Millimetre Radar Threat Level Evaluation at Stand Off Ranges. SPIE European Security and Defence Conference 2011 Paper.

- 7 Stuart Harmer, Nicholas Bowring, David Andrews, Nacer Ddine Rezgui, Matthew Southgate and Sarah Smith. A Review of Non-imaging Stand-Off Concealed Threat Detection with Millimetre-Wave Radar. IEEE Microwave magazine, Vol. 13. (2012) pp. 160 – 167.

Abbreviations

ADC	analogue to digital converter
AM	amplitude modulation
DAC	digital to analogue converter
DC	direct current
DSP	digital signal processor
EM	electromagnetic
FAR	false alarm rate
FFT	Fast Fourier transform
FMCW	frequency modulated continuous wave
FN	false-negative
FP	false-positive
IED	improvised explosive device
IF	intermediate frequency
INSTINCT	innovative science and technology in counter terrorism
IR	infra-red
LNA	low noise amplifier
LO	local oscillator
LSb	least significant bit
MMIC	monolithic microwave integrated circuit
PBIED	person borne improvised explosive device
PC	personal computer
PD	probability of detection

PFA	probability of false alarm
PLL	phase locked loop
RCS	radar cross-section
RF	radio-frequency
TD	time domain
TEM	transverse electromagnetic
VCO	voltage controlled oscillator
VNA	vector network analyser

1 Introduction

This Chapter introduces the project, its aims, objectives and scope; the subject of concealed threat detection and terminology; the contribution to knowledge; and finally a structural outline of this document.

The aim of this project was to develop a novel method to remotely detect weapons and explosives carried upon the human body, concealed by everyday fabrics. Secondly, to design, realise and field trial prototypes of various configurations implementing the proposed method and quantify their real-world performance metrics. A real-time threat detection method would represent a significant improvement in capability, with widespread applicability because of the ability to distinguish between different objects in addition to establishing their presence. If successful, this research and associated technology will greatly benefit society.

The problem statement concisely defines the scope of a research project and the problem statement addressed by this thesis is:

Research and develop a method, potentially portable, capable of the remote detection of threat items concealed upon a human body with an acceptable level of accuracy. Detection could be covert, providing the operator with the nature of the object and location. Concealment will consist of everyday clothing. The project will lead to a demonstration of a prototype, working in real-time at multiple frames per second.

Academic aims for the project include investigation of the physical and engineering mechanisms associated with the remote detection of concealed objects and to identify suitable discoveries for publication and patenting.

In the process of developing a prototype, the following areas were investigated for the detection of both concealed weapons and explosives:

- a) Identification of the optimum frequency bands within the electromagnetic spectrum and power levels for object detection.
- b) Identification of the effects of different commonly worn materials on electromagnetic transmission.
- c) Investigation of the use of continuous wave and pulsed illumination for concealed object detection.
- d) The design of a signal processing and classification system and database for radar signatures.
- e) Construction and testing a radar that can inspect a remote individual for concealed objects.
- f) The development of analysis routines that discriminate between threat objects in the database and mundane clutter such as keys and mobile telephones.

Threats to the security of the public and the UK have perceptibly increased since the beginning of the millennium (Agurto et al., 2007). The chance of war on UK soil is negligible and the danger of concealed weaponry comes from criminal elements and terrorists. Given the opportunity and ability, the author hopes the proposed system will improve the world we live in.

The requirement for a technology capable of reliable and consistent detection of remote and concealed guns and weapons has grown in urgency during recent years. This need has always existed for governments and the security forces, but changes in the nature of the perceived threat and demands by the public reinforce this urgency. To date, details of a system or collection of systems capable of reliably detecting concealed threats at a stand off distance in situations where portability and rapid response are requirements, have not been published (Agurto et al., 2007) The objective of this project is to identify the physical fundamentals of concealed threat detection that can be measured and exploited.

1.1 Concealed Threat Detection

Concealed threat detection is a broad subject concerned with the non-invasive detection of items capable of causing substantial harm. Items considered in this application are typically guns, explosives and knives. Protection of community and property are a motivator for having a reliable detection system. Secondary objectives include exposing illegal activities and where attacks are likely, act as an effective deterrent. The UK counter-terrorism strategy, known as CONTEST (UKHO, 2010), focuses on the most significant security threat to the people of the UK today – the threat from international terrorism (BBC, 2010b). One strand of the CONTEST strategy is to encourage the development of systems to 'augment the situational awareness' of security personnel. National security is the primary duty of the government (UKHO, 2011).

The UK Home Office hold regular events as part of the INSTINCT (innovation in science and technology in counter terrorism) programme inviting proposals from companies and academic institutions for innovative research and development in the field of explosives and weapons detection (UKHO, 2009).

Detection techniques are as numerous as they are wide-ranging and ingenious. There are typically many ways to effect a detection, with differing levels of public visibility. Sniffer dogs are a good example of a method known to the public for the detection of explosives in our ports, but the use of trained moths to fulfil the same role (with much shorter training times) is less well known (King et al., 2004) Equally the use of x-ray machines to screen baggage for contraband and weapons is a well known method, but not the use of magnetic fields to do the same (Goya & Sibley, 2007).

Development of the proposed system will benefit the security forces in numerous ways, for example detection of objects on bodies will be possible not only through everyday clothing, but also through other obscurants such as smoke and fog. By providing a capability to remotely inspect a person without physical contact, operator safety is thereby improved by distancing them from potential threats. Since the technique is non-invasive the possibility exists for covert use and inspection of uncooperative persons. An additional benefit of all of the above, is that public throughput may be increased compared to conventional threat detection regimes.

Unfortunately there are problems associated with concealed threat detection, not all of which are technical in nature. Public acceptance of concealed threat detectors as thorough and reliable security tools has been slow – familiarity will come in time and with advances in technology. Currently and understandably there are privacy and legal issues for imaging systems producing revealing pictures of targets with piercings, prosthetic limbs and false breasts (BBC, 2010a). Concerns about the availability of detailed images post inspection, despite assurances to the contrary were proven valid with the leak of tens of thousands such images (McCullagh, 2010).

Most issues are technical or operational in nature and still the subject of debate; most relate to the type and level of radiation used by active systems and in particular backscatter systems that use 'soft x-rays' (Knox, 2010). The opposing requirements to reduce radiation levels and improve performance result in a compromise, with image resolution and contrast balanced against inspection speed and system noise. Passive millimetre wave imaging systems, particularly, can suffer from this problem, often necessitating long integration times, even for systems designed and optimised for a specific and carefully controlled environment, such as an airport security suite.

1.2 Contribution to Knowledge

The method and detector described herein has been developed by a team of researchers.

Contributions specifically made by the author include:

- (a) refinement and optimisation of algorithms used to measure the dielectric properties of low loss dielectrics; these routines were initially used with a Fabry-Perot interferometer and later implemented on the prototypes;
- (b) development of deterministic, high speed, non-PC based data acquisition systems with integrated signal post-processing, providing capabilities not currently available;
- (c) incorporation of these systems described in (b) into a direct power detection concealed threat detection system, significantly improving performance;
- (d) development of a reliable, high speed, Voltage Controlled Oscillator (VCO) programmable frequency source with supporting test, calibration and configuration algorithms, providing capabilities for real-time inspection of targets, not currently available;

- (e) incorporation of these systems into a direct power receiver concealed threat detection system significantly improving performance;
- (f) development of algorithms and electronic systems to enable a compact, sensitive heterodyne radar receiver to be developed for future enhanced variants of the detector described in this work;
- (g) devising and realising a covert method of relaying scan information to the operator without line of sight using a discrete wireless headset.

1.3 Document Structure

This thesis is organised into seven chapters, each describing a different aspect of the project.

The Literature Review contains an introduction to the field of concealed threat detection and a critique of the prior state of the art. Phenomenology is explained and details of the workers in the different fields is given. Different system types are described with associated issues and limitations highlighted. State of the art non-imaging active radar based systems are covered in more detail for comparison with the proposed method.

Background Theory describes the engineering concepts underpinning the operation of the devices and the types of radar used by active illumination concealed threat detectors. The metrics used to compare system performance in this document are defined.

Proof of Concept describes in detail the experiments and development work undertaken to realise a bench-top prototype FMCW single pixel mm-wave pattern matching radar capable of the remote detection of concealed threat objects.

Portable Prototypes describes the steps involved realising portable versions of the bench-top version. The description includes details on methodology, hardware, data acquisition and analysis in real time.

Data Classification and Results describes the instrument and presents the results generated by trials and laboratory experiments to measure its performance. An analysis of the results and suggestions for improvement are given.

Conclusion and Future Work presents a final summary of achievements and a description of techniques and ideas identified during the project as potentially useful and worthy of further investigation.

Blank page

2 Literature Review

I start where the last man left off.

THOMAS A. EDISON

This Chapter presents a critical review of the previous state-of-the-art; introducing and describing all major techniques. Methods and technologies using electromagnetic waves are emphasised since they have the greatest relevance to the project. Related research will be referred to, providing a rounded critique.

Concealed threat detection techniques and systems developed in the past two decades are reviewed in this Chapter. The emphasis of existing systems is object screening. The purpose of object screening is to detect and locate objects concealed upon a person, prompting a manual search, rather than to identify the nature of an object.

Such an approach is unsuitable for discrete checking of individuals suspected of carrying concealed threat items, a scenario requiring a very low false positive rate.

Stimulated by grant offerings (UKHO, 2009) and the large homeland security market worth approximately \$200 B (Raza, 2012), research and development companies and institutions have generated solutions to satisfy the demand of governments and security forces to remotely detect concealed guns and explosives (UK Government, 2000; Hill et al., 2002; Sutton & Bromley, 2005).

This research project takes inspiration from this prior art and investigates and develops techniques to detect concealed guns and explosives in particular to address this requirement.

The field of concealed threat detection is broad and the subject of many publications. A comprehensive review within a single chapter would be impossible; therefore, this Chapter focuses on the area to which this thesis contributes: the use of electromagnetic waves for the detection of concealed threats on humans. Related technologies and systems are covered briefly for completeness.

Comprehensive literature reviews covering the field of concealed threat detection can be found in a number of review papers, (Agurto et al., 2007; Costianes, 2005; Paulter, 2001). Agurto reviewed the advantages and constraints of existing sensors, focusing on passive imaging systems, which has the second largest user base after metal detectors, and concluded that the most critical weaknesses of this approach were the short range, insufficient scanning speed per person scanned and the vulnerability of some sensors to weather in outdoor environments.

Two approaches to detecting concealed weapons and explosives at a distance are imaging and non-imaging. Imaging systems use a detector or arrays of detectors, mechanically or electronically rastered to measure the intensity of EM waves at specific points, called pixels. A set of pixels make up an image that can be automatically analysed (Connolly, 2006) or more typically operator interpreted (Detection, 2006). Non-imaging systems instead measure specific properties of a target to determine whether a weapon is present.

These two categories of detector are sub-divided into active and passive systems. An active system generates radiation to illuminate the target, whereas a passive system relies on naturally occurring radiation and emanations to detect concealed weapons. Active systems have the advantage of control over the type, power level, polarisation and frequency of the illumination.

A prevalent imaging approach to detection generates grey-scale images for an operator to check and identify items. Figure 2.1 shows the high resolution image generated by a Rapiscan 1000 (BBC, 2009b). The Rapiscan Secure 1000 system is an active x-ray back scatter imager (Rapiscan, 2009).



Figure 2.1: High resolution image from a Rapiscan Systems scanner

Non-imaging EM systems take the form of a directional radar (the focus of this project) to detect and sometimes identify concealed objects by exploiting the physical properties of threat items. Recent and relevant work in this field has been conducted at Ariel University Centre of Samaria, Israel, to develop a hidden object detection system that locates objects by the specular reflections that occur on the edges of objects and the lower than expected

power levels of signals returning from lossy materials (Kapilevich & Einat, 2010). This work builds on a previous device and the focus of an international patent (Kapilevich & Einat, 2007).

The picture quality of imaging systems has improved to the extent that there are concerns about privacy (Telegraph, 2009; BBC, 2010a) with potential breaches of the Human Rights Act (BBC, 2010a) and such systems being understandably referred to as 'naked scanners' (BBC, 2009b). An effective detection system will most likely need to overcome these concerns to gain public acceptance.

Concealed threat detection systems are used in many high-profile areas such as: airports, sea ports, border security, mass surface transportation, infrastructure and public events. Typically a zoned approach is adopted with a first line of metal detectors followed by a second line of body scanners to identify and locate detected anomalies or failing that resort to the traditional pat down (Elias, 2011; Foster, 2011).

Physical examination of an individual by security personnel places them implicitly in close proximity with the person(s) being searched and therefore in potential danger, while also broadcasting that a search is being conducted to anyone nearby.

Detection technology has yet to advance to the point where there exists a single system capable of reliable detection of threats. It is conventional to use zone detection, with systems developed to detect specific objects in very limited circumstances. The practicalities of where and when to scan are based on the available equipment. An appreciation of the range and size of existing systems would be helpful to understand the extent with which they vary. The illustration in Figure 2.2 is of a passive millimetre-wave imaging portal system called the TADAR and manufactured by Smiths Detection (Detection, 2006).



Figure 2.2: Smiths Detection TADAR system

This system performs by scanning an array of detectors across the target, generating an image similar to that is shown in Figure 2.1. The TADAR system requires an operator to interpret the image and spot suspicious items. Operation is only effective within a carefully controlled environment (the booth) requiring the full co-operation of the individual being screened. System performance would suffer without the carefully controlled environment provided by the booth enclosure. Moreover, a successful inspection requires a cooperative individual to follow the instructions of the operator and remain perfectly still during image acquisition. The intended application of this machine is passenger screening within an airport; such a system would be less suitable for operation outside these conditions. In comparison a later and more advanced system, using similar technology but operating at a higher frequency of 250 GHz instead of 94 GHz, the T4000 manufactured by ThruVision is much smaller. Note that although the T4000 does not require a booth to operate, a backdrop is used behind the target to increase contrast. SDN (2008) reported commencement trials of the T4000 within a Wayne County courthouse during late 2008. Figure 2.3 shows the T4000 trial installation and the size of the device alongside the existing security systems.



Figure 2.3: ThruVision T4000 installation in Wayne County Courthouse, Michigan, USA.

The predominant approach of modern detection systems and the focus of this project is the use of electromagnetic (EM) radiation to remotely detect the presence of concealed threat items.

The quantity and complexity of information presented to the user of a system can take many forms. At the most basic level, 'yes/no' or binary detectors indicate when a specific object or collection of objects enter its detection volume, without providing any additional information. An example of a binary system is an unzoned metal detector. An audible alert is produced when a substantial metal object enters the detection field. No information about the location, size, composition, orientation or threat value of the object is provided, except its presence. Comparing an unzoned walk through metal detector with a hand-held detector, they have significantly different applications. Both can indicate the presence of metal objects, but the hand-held metal detector is able to pinpoint the location of metal objects because of its smaller detection volume. However the hand-held device must be swept over the entire body to give the same body coverage as its walk-through equivalent, resulting in a longer inspection time.

2.1 Detection Energies and Detector Types

A variety of technologies are being used or developed for concealed threat detection; these include acoustic and ultrasonic inspection, and electromagnetic-based techniques such as x-ray and microwave imaging. Systems formats are just as varied and include hand-held close proximity scanning; walk by scanning and stand-off scanning. Current technology limits the feasibility of different combinations of system type, performance and form. Those forms that are not always possible using current technology, but may with future advances, become available. Table 2.1 lists detectors grouped by energy type and the remainder of the Chapter, describes each in turn.

Acoustic	Hard object detector Non-linear acoustic object detector
Electromagnetic	Microwave dielectric imager Microwave radar imager Microwave holographic imager, mm-wave radar detector mm-wave imager EM pulse detector Pulsed radar with swept frequency Terahertz imager IR imager X-Ray imager
Magnetic	Walk through and hand held metal detectors Magnetic imaging portal MRI cavity scanner Gradiometer metal detectors

Table 2.1: List of detector types

2.2 Acoustic-based Systems

2.2.1 Hard Object Detector

Hard materials reflect acoustic energy more efficiently than soft materials. Since guns are generally made of hard materials, such as metal and ceramic and the human body is comparatively soft, acoustic systems work by detecting the glint produced by a hard object against the 'soft' background of the body. Consequently this technology is capable of detecting plastic weapons as well as metal weapons, however hard innocuous objects will also trigger the system.

Early designs were binary detection systems, unable of producing an image (Wild, 2001; Felber, 1998). Subsequent developments produced a system capable of creating an image using a single focused transducer using 40 kHz ultrasonic waves operating at ranges up to eight metres (Wild et al., 2001). Unfortunately the prototype suffered from low signal to noise ratio caused by reflections from the clothing and was very sensitive to weapon aspect. The false alarm rate depended entirely upon the type of clothing, varying from a rate below 10% for relatively transparent materials such as cotton, wool, polyester to 80% for reflective materials like leather (Wild, 2003). Figure 2.4 shows a photograph of the CWD-2002 hand held acoustic imager.



Figure 2.4: CWD-2002 hand-held acoustic imager (Wild, 2003)

An alternate system developed by Jaycor operating at higher frequencies up to a 100kHz at a range of up to four and a half metres (Jaycor, 2002; Currie & Stiefvater, 2003). The increase in frequency provided the ability to resolve smaller items to a size of 10cm. This is small enough to detect most, but not all guns and other small threat items.

Ultrasonic energy can be easily blocked by thick clothing. Air-coupled transducers generate a high-frequency signal that is needed to reach the target and create a small inspection area, however to effectively penetrate clothing a low-frequency signal is needed (Nacci & Mockensturm, 2001). These two contradictory requirements led to the development of non-linear acoustic object detectors.

2.2.2 Non-linear Acoustic Object Detector

This advanced approach uses a non-linear technique developed by (Achanta et al., 2005) that combines ultrasonic and acoustic energy. The technique employs multiple ultrasonic sources to generate a localised acoustic wave (a sum and difference interaction) that is better suited to penetrating clothing than direct ultrasonics (Achanta et al., 2005) The resulting wave significantly modifies the velocity of sound at the point of inspection on the target (due to dynamic pressure changes) and the resulting reflections are measured by an audio frequency sensor and processed for information.

Scan speed is significantly affected by the distance between the source and the target. Detection of weapons is possible at distances up to 4.5m. An image can be generated by scanning the ultrasonic beam across the target (Achanta et al., 2005). The image does not contain any anatomical details of the inspected individual. This work has been patented (Heyman, 2008). Threat detection is based on pattern matching and classification.

2.3 Electromagnetic Detection Systems

This type of detector is in widespread use and constitutes the majority stand off detection systems deployed today. All four permutations of system type are represented and are covered in the following order: passive non-imaging, passive imaging, active non-imaging and active imaging.

2.3.1 Passive Non Imaging Electromagnetic Detection Systems

2.3.1.1 Millimetre Wave Imagers

The millimetre wave imager is a family of passive detection systems that rely on naturally emitted radiation. All bodies, at temperatures above absolute zero emit black-body radiation and the temperature determines the peak radiated wavelength. Total power emitted is dependent on the size and emissivity of the target. The human body has a emissivity approximately five times greater than most concealed weapons at millimetre wavelengths (McMillan et al., 1998). Systems using this principle work by detecting the difference in the product of temperature and emissivity between areas of the body with and without concealed threats. This appears as an area of different contrast on the captured image. Operation is similar to that of a thermal imager (Huguenin, 1997). This type of system does not have the temperature sensitivity of thermal imagers and it is difficult to detect concealed weapons that have been in contact with the body and are at body temperature. The person being scanned must remain relatively stationary to avoid a blurred image.

An practical example passive non-imaging mm-wave devices are the SPO family of systems produced by QinetiQ. The SPO-7R is a small mobile system, claiming to be capable of revealing the presence of large objects concealed by clothing a stand-off distance of 4 to 15m, it is a real-time sensor and requires minimal training due to its red light/green light indication. The system works by comparing two separate areas on the

target and if the difference in response is greater than a predetermined threshold the user is alerted. The technique relies upon the proposition that two areas of a target will give similar emissivity readings and whereas interposing an object in one area will result in a suitably different response and trigger the system. Figure 2.5 shows an image of the SPO-7R.



Figure 2.5: SPO-7 system (Transportation, 2007)

A larger system with a working range of 20 m operating in exactly the same way as the SPO-7, is available as the SPO-20, see Figure 2.6 or the SPO-30 shown in Figure 2.7.



Figure 2.6: SPO-20 system (Transportation, 2007)

The SPO-20 houses 64 MMIC receivers with a refresh rate of 15 Hz and are conically scanned with an off axis rotating mirror. The 80 cm aperture gives a spatial resolution of 0.3 degrees (Kemp, 2006).



Figure 2.7: SPO-30 system (Appleby, 2008)

All three systems work by comparing the temperature or emissivity contrast of two points on the target around 94 GHz. If the difference of contrast between the two points of inspection is greater than a predefined threshold the system alarms. The device is aimed using a carefully aligned CCTV camera. Throughput varies, but a claimed 380 people can be inspected in an hour (QinitiQ, 2012).

2.3.2 Passive Imaging Electromagnetic Detection Systems

All matter radiates and reflects EM waves, including humans. Since the human body is approximately 90% water it has relatively high emissivity and reflectivity properties 0.35 and 0.65 at 100 GHz respectively (Appleby & Wallace, 2007). In comparison metals, plastics and composites have higher levels of reflectivity. When an object such as explosives, weapons, liquids, gels, electronics are concealed upon a person, it appears as an area of different contrast. The sensitivity and dynamic range of a passive system is proportional to the contrast it can render with its image. Techniques to image people (Coward & Appleby, 2003; Sheen et al., 2001) have been refined by Pacific Northwest National Laboratories; mm-wave and terahertz imagers by www.brijot.com and www.thruvision.com and backscatter x-ray systems by www.as-e.com.

ThruVision passive detection systems are generally considered to be state of the art (Sheen et al., 2010). The first passive imaging system to be covered is the ThruVision T4000, an indoor only model, designed 'primarily to detect objects with a fairly large thermal signature' with an operating range of 3 to 15 metres (Seymour et al., 2010) and is shown in Figure 2.8.



Figure 2.8: ThruVision indoor passive imager T4000

The T4000 is an indoor passive imager with a low rate of 1 – 3 frames per second and 12 cm aperture giving a spatial resolution of 3 cm (Kemp, 2006). Figure 2.9 shows an image from the operator interface of the T4000.



Figure 2.9: T4000 image of a person carrying a wallet in his trouser pocket at 3 m

The T5000 is the outdoor version shown in Figure 2.10, with a smaller scanning angle and longer operating range of 7 m to 25 m. The T5000 is only suitable for detecting large concealed items and it is claimed that a wide selection of materials can be detected including metals, plastics, liquids, gels, ceramics and narcotics. It is clear from the example images, that the material nature of an object is not identified.



Figure 2.10: ThruVision active imaging system T5000

The T5000 works by detecting the reflections from concealed items of the cold sky. The sky is 100-200 K cooler than ambient (Kemp, 2006) . Metal objects show up particularly well, but equally if the reflection is from an ambient temperature source, the temperature contrast drops below the sensitivity of the detector and the the concealed object is effectively masked.

Figures 2.11 through 2.13 show images from a T5000 system taken at distances of 25, 20 and 10 m of an individual approaching the system with a large concealed object wrapped around their torso. The panes labelled A – F are an image of the scene measured by the detector with increasing levels of exposure.



Figure 2.11: ThruVision T5000 staged image of a person at 25 m with concealed object around their torso

The small patch of light grey on the lower torso is the concealed object reflecting the cold sky.

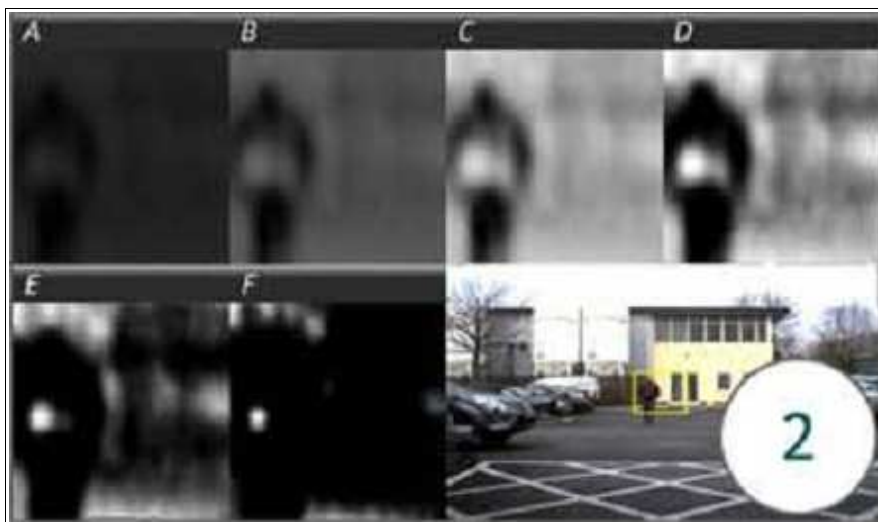


Figure 2.12: ThruVision T5000 staged image of a person at 20m with concealed object around their torso

Reflections of the cold sky on the concealed object are clear at 20 m, by inspection of panes C and D.

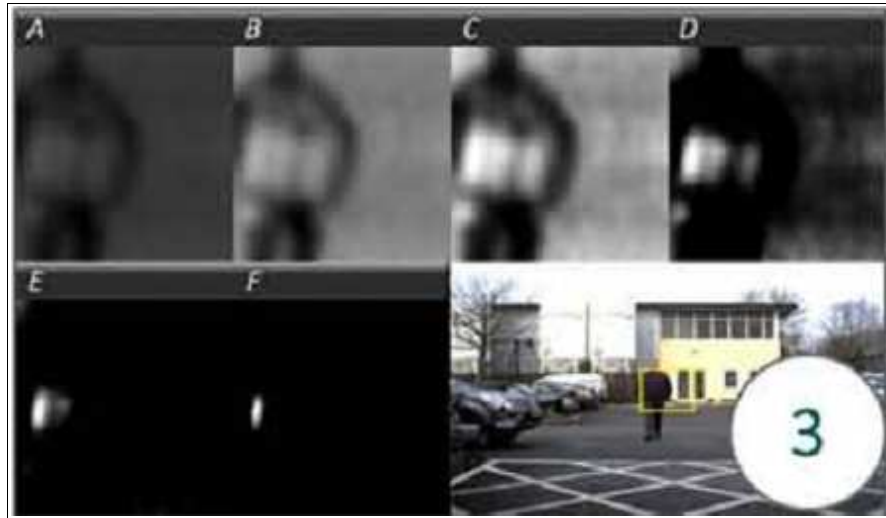


Figure 2.13: ThruVision T5000 staged image of a person at 10m with concealed object around their torso

At 10 m it is possible to see the concealed object consists of several discrete forearm sized blocks, rather than a single block.

The T4000 and T5000 images are formed by scanning a mirror and 8 receivers. Figure 2.14 is a top level diagram of the ThruVision THz system (Seymour et al., 2010).

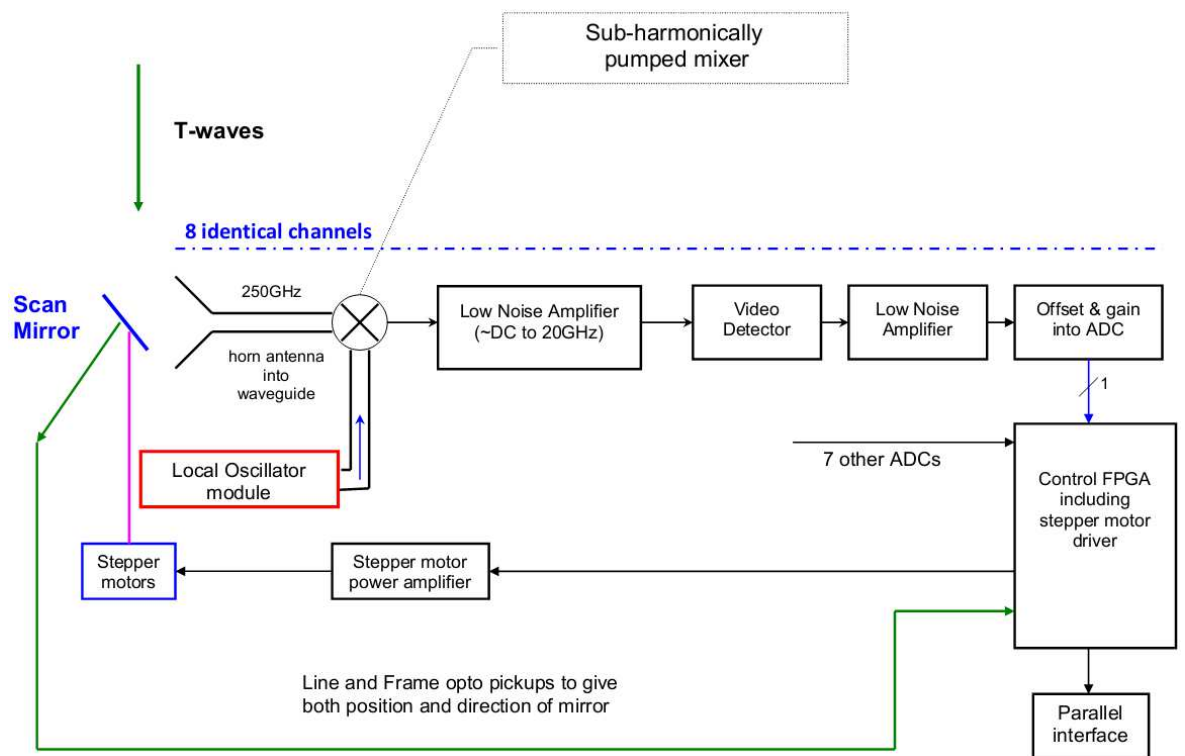


Figure 2.14: ThruVision THz top level system diagram

Since passive detection systems rely upon the contrast between the body and the concealed object for detection, an experiment was conducted to determine the visibility of a 1 kg explosive device strapped to the torso over time. It was observed that the maximum range of detection with time, up to a point where the contrast did not reduce further (Kennedy, 2009).

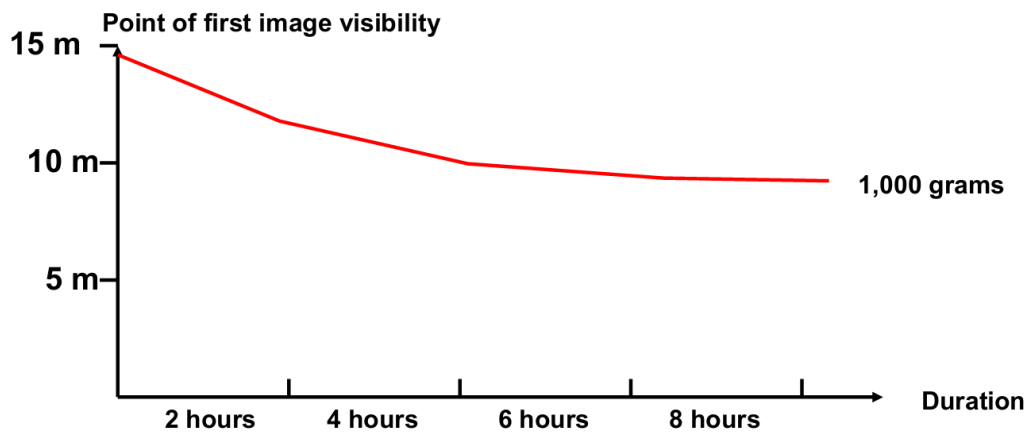


Figure 2.15: Maximum detection distance against time for a 1 kg explosive device strapped to the torso

Field trials results for the T5000 generated for a test population of 100 subjects, with 70 wearing a concealed explosive vest and the remainder with no such vest, are shown in Table 2.2. No other test details are provided (Kennedy, 2010).

Accuracy	95.00%
False Negatives	2.80%
False Positives	10.00%

Table 2.2: T5000 field trial detection results for concealed explosive vest tests

The latest product TS4 uses a similar imaging system to the T4000 and T5000 systems and shown in Figure 2.16.



Figure 2.16: ThruVision TS4

The TS4 features several improvements over the T5000 design with a smaller lighter chassis and higher scan rate (Kennedy, 2010). The improved frame rate of 5 – 10 Hz is due to a reduction in the field of view (Met, 2008). TS4 operator interface imagery is shown in Figure 2.17.



Figure 2.17: ThruVision TS4 imagery

The mm-wave imagery is accurately superimposed over the video feed of a bore sighted camera. Operator interpretation of images is necessary, because the system alone does not discriminate between threat and non-threat items and technical challenges still exist for automatic image exposure and increasing the frame rate (Kennedy, 2010).

2.3.3 Active Non-Imaging Electromagnetic Detection Systems

2.3.3.1 Pulsed Radar With Swept Frequency Detector

This type of system uses radar to determine the range to the object and a frequency scan to obtain information about the object. Range is measured by the return time for a pulse or swept frequency measurements are taken. The swept frequency return from the object is analysed to determine whether it contains the resonant signature of a threat item. This type of system does not generate an image and the ability of the system to detect threat items requires a signature database. A disadvantage of this approach is that new threats will not be detected unless, a representative database of radar signatures is maintained.

2.3.3.2 Millimetre Wave Radar Detectors

Microwave radar detectors typically have a short effective range of less than 10 m (Kemp, 2006) and consist of a detector and source (McMillan et al., 1998). The radiation source is often a frequency modulated continuous wave and centred around 94 GHz. The requirement to have a large aperture to produce a small spot is avoided, so generally this type of system is small and lighter than its imaging equivalent (Novak et al., 2005). System operation consists of measuring the energy reflected from an individual in the detection volume. The distance from the system can be determined by mixing the reflected signal with a coherent reference. The resulting frequency is proportional to target range (Komarov & Smolskiy, 2003).

From a safety perspective MMW radar-based systems use low levels of non-ionising radiation, unlike x-ray based systems that use potentially damaging ionising radiation (Appleby, 2004a; Andrews et al., 2009).

An example of this type of device developed by Kapilevich & Einat (2010). The system is a hand-held millimetre-wave sensor for the detection of metallic and dielectric objects with a claimed detection rate of up to 90% and the subject of a patent (Kapilevich & Einat, 2007) An image of the original device is shown in Figure 2.18 and an image of the refined version taken from a later publication (Kapilevich & Einat, 2010) is shown in Figure 2.19. Operating range is up to 3 m, and detection is achieved by analysing the signal returns at a rate of 1 kHz. The presence of a concealed object is determined by the return signal level, looking specifically for specular reflections and signal returns of low power potentially indicating the presence of a lossy material. The spot size for the system is elliptical with dimensions of approximately 3 cm wide by 30 cm tall. Scanning of a target is achieved by manually moving the beam of the system across the target to identify the presence if any, location, size and shape of hidden objects. The nature of the object is presented to the operator if the structure in time and magnitude of the reflected signal match values stored in a calibration table of pre-measured objects.



Figure 2.18: Kapilevich hand-held object detector



Figure 2.19: Kapilevich refined hand-held object detector

The hardware consists of a single transmitter and receiver with high gain horns and lens(s).

The transmitter source is a Gunn diode modulated at 1 kHz operating at 94 GHz and producing 10 mW. A spinning disc was used to alternately block and allow the transmission of illumination (Kapilevich & Einat, 2007), see Figure 2.20.

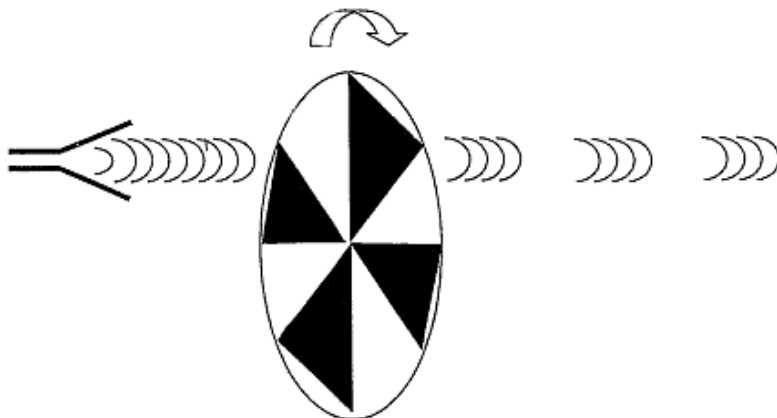


Figure 2.20: Spinning disk to produce a pulsed illumination

The detector operates in a synchronised demodulation regime using a zero biased Schottky diode to measure signal power. The relative signal technique compares the signal from the target with and without illumination.

A 20 L water bottle full of tap water was used to simulate a human torso while gathering measurements for calibration. Detection of a C4 stimulant is achieved by looking for a drop in return signal, due to the absorption of the incident RF power, compared to the same signal reflected by the human body without C4, see Figures 2.21 and 2.22. Figure 2.22 has a much higher peak as comparatively more power is reflected from the human torso.

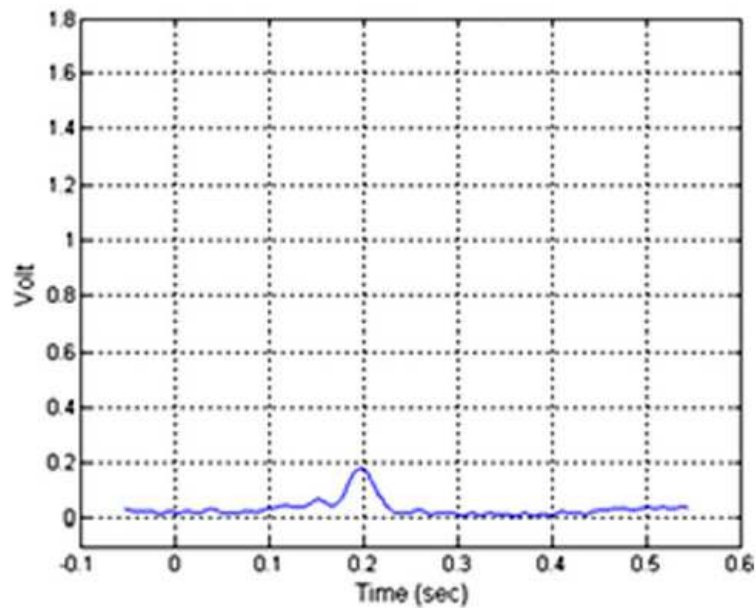


Figure 2.21: Kapilevich detector sweep of man with explosives

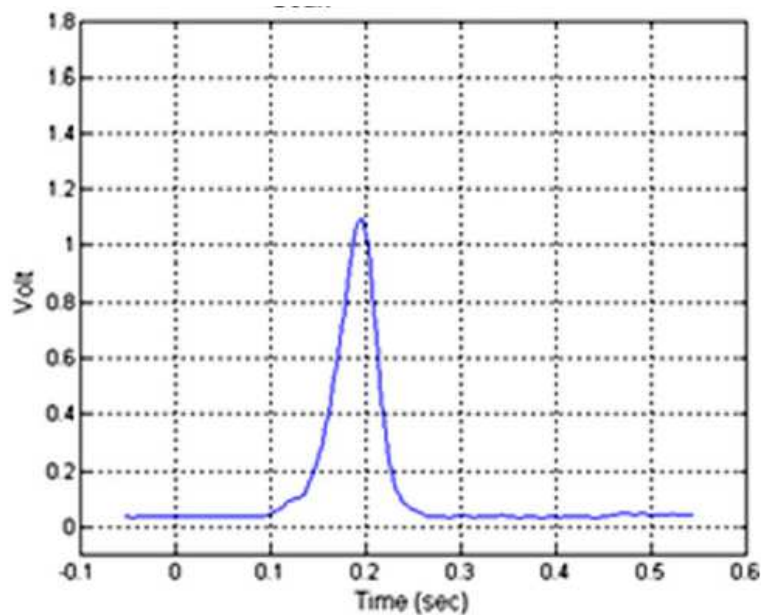


Figure 2.22: Kapilevich detector sweep of man without explosive

Building on his earlier work Kapilevich developed a homodyne system with an operating range greater than 3 m and incorporated a range detecting capability using a FMCW radar (Kapilevich et al., 2011). The laboratory prototype uses even higher gain horn antennas and some RF power amplifiers. The system diagram (Kapilevich et al., 2011) is shown in Figure 2.23.

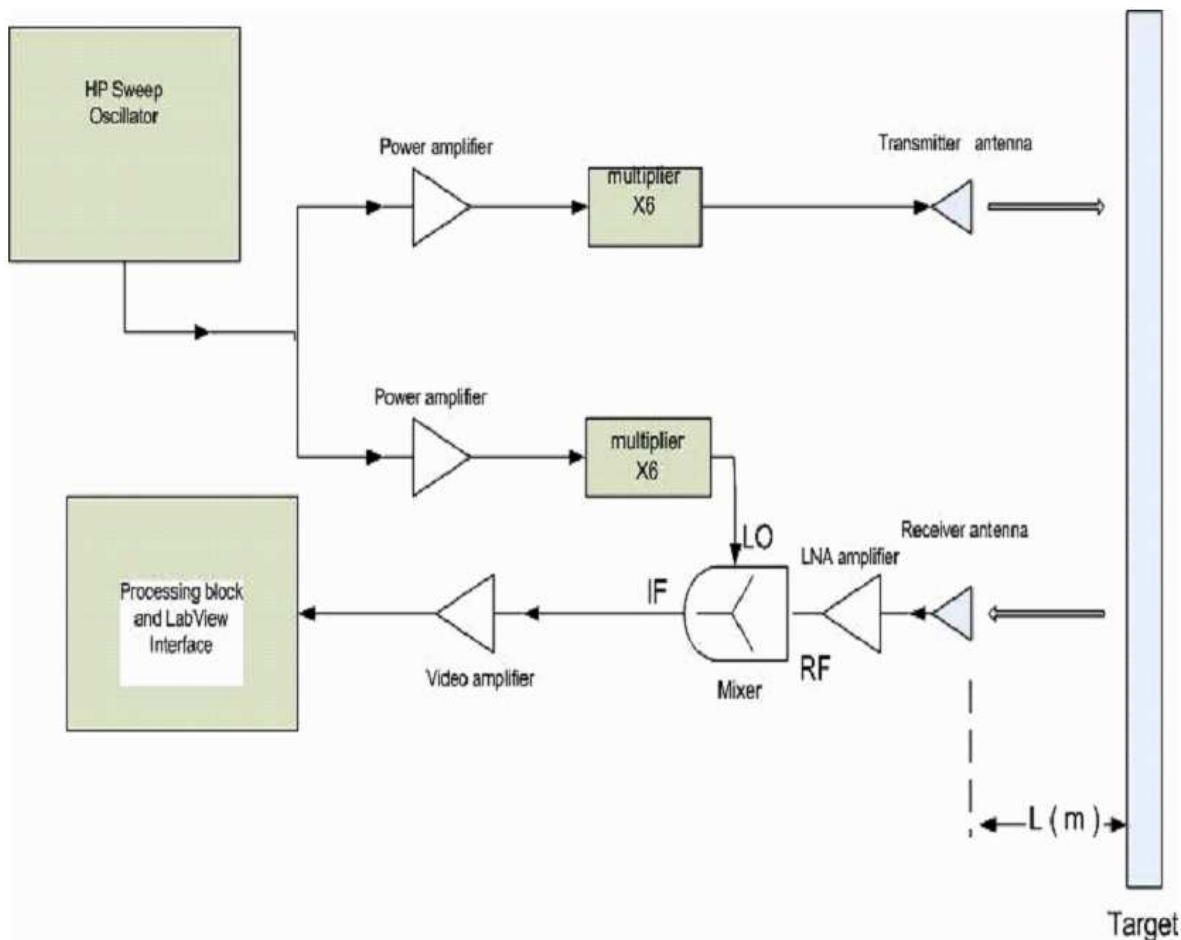


Figure 2.23: Kapilevich FMCW non-imaging sensor system diagram

The system embodies a homodyne based detector with 35dB horns, power amplifiers sweeping in the 90 – 96 GHz frequency band with a claimed accuracy of several centimetres (based on a 6 GHz sweep a range resolution of 25 mm should be possible). The remote detection capabilities of the device are similar to its predecessor, for metal and dielectric objects. Detection of small metal items was demonstrated at 9.5 m; large metal

objects at 14 m and dielectric rods at 3 m. Figure 2.24 shows the demonstration of the detection of a small handgun in a plastic bag at 9.5 m with the corresponding measurement.

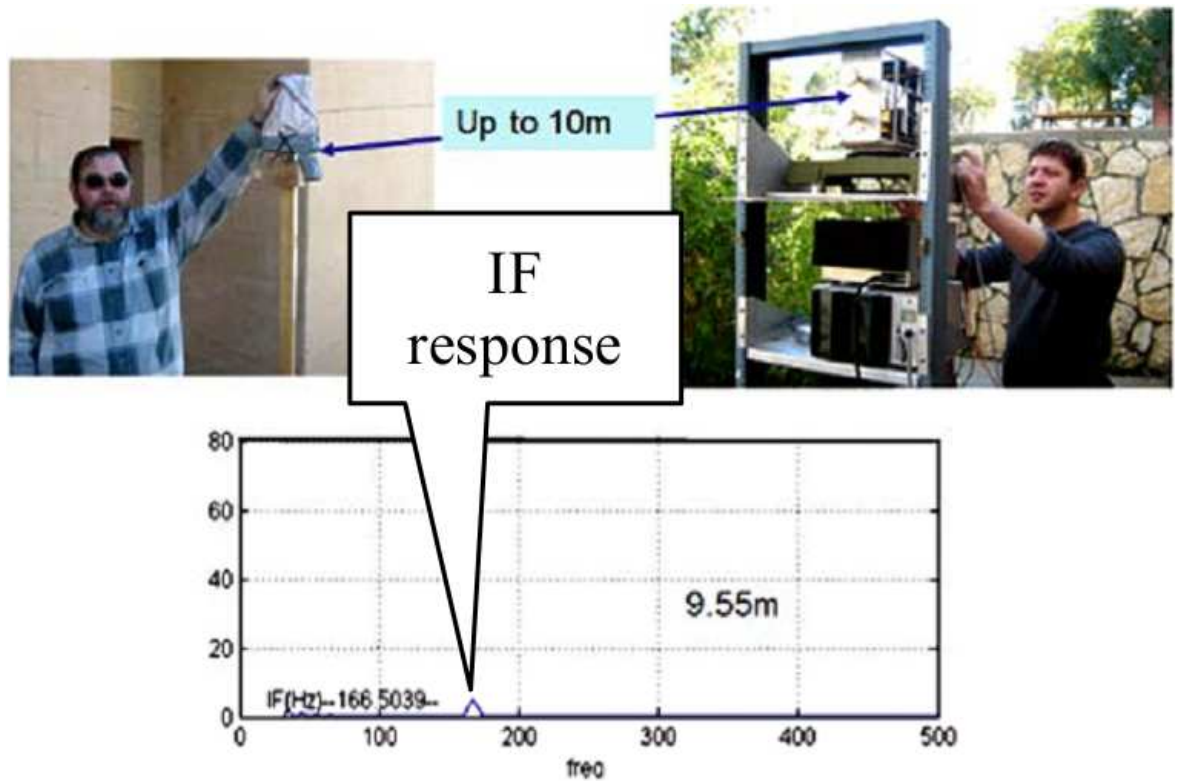


Figure 2.24: Kapilevich FMCW radar detecting a remote metal object

Although a handgun is used in the demonstration, it is suspected that any metal object would produce similar results.

Operating speeds have not been specified, but based on the described hardware and the quantity of back end processing undertaken it is thought that either analysis is performed offline or is likely to be significantly slow by may be two orders of magnitude compared to its predecessor, with an inspection rate of 1 kHz.

2.3.3.3 Electromagnetic Pulse Detector

This type of system is similar in many ways to millimetre wave radar; they both rely upon the electromagnetic properties of target objects for identification. They function by illuminating objects with a pulsed radiation source, rather than continuous radiation and

then very rapidly measure the reflected signal, measuring the time domain response. Every object has an associated electromagnetic signature. The person carrying the concealed object also has an associated electromagnetic signature. The combined signature is then checked against a comprehensive library of known signatures to determine if a threat object is present, assuming an average human signature. The disadvantage of this approach is that it is not possible to obtain an average human signature because of the diversity of human shapes and sizes.

2.3.4 Active Imaging Electromagnetic Detection Systems

2.3.4.1 Microwave Holographic Imagers

Work is being conducted by (Fernandez-Cull et al., 2010) at 350 GHz using a single receiver to generate a Gabor hologram and using compressive sensing to approximate depth information from the composite 2D hologram. This system is effectively a 3D surface mapping portal.

This is a portal type detector, where a person being scanned is illuminated with microwave energy by a column containing a set of vertically arranged emitters, which rotate around the person. These emitters radiate coherent continuous wave energy and the detected signal is used to map the surface of the person. Mapping is achieved by measuring the distance to the target from the source and spatial resolution is a function of frequency bandwidth, the greater the frequency bandwidth the higher the spatial resolution. Capture time is a signal to noise issue and depends upon illumination intensity. The target must be stationary during image capture to avoid image distortion. This device works on the principle that microwave radiation readily penetrates most clothing but not the human body (Gandhi & Riazi, 1986), therefore objects concealed within the body cannot be detected. This type of scanner is referred to as “naked scanners” and involve privacy issues

(Telegraph, 2009; BBC, 2009b, 2010a; McCullagh, 2010). Images must be taken with a stationary object and current acquisition time is a few seconds. There are also concerns about scanning or difficulty of scanning children or claustrophobic people.

2.3.4.2 Microwave Dielectric Imagers

This type of imager is based on measuring the dielectric constant of materials (Bertl & Detlefsen, 2010). This is similar to a microwave holographic imager in that it scans different surfaces of the person with microwave radiation. The person must remain stationary during scanning to avoid image distortion. Each detection element consists of an emitter detector pair. The emitter generates a pulse and the detector measures the amplitude and propagation delay of the return signal. The dielectric permittivity and electrical conductivity of the material are different from that of air. The amplitude of the signal is a measure of the material property values and the delay gives distance information. The principal differentiation between systems is the size of the detection volume. No anatomical detail is recorded and the operator is presented with a wire frame representation of the body.

2.3.4.3 Microwave Radar Imagers

This type of detector uses a frequency modulated continuous wave source. This system forms an image from reflections of the microwave energy within the detection area. Range information is obtained by mixing a fraction of the incident energy with the return energy, in such a way to be able to calculate the distance between the source and target. Spatial resolution of the microwave radar imager is dependent upon the microwave wavelength used. A smaller wavelength produces a finer spatial resolution. However, absorption of microwaves by clothing increases with frequency (Bjarnason et al., 2004). Image acquisition time is dependent on the area to be scanned.

2.3.4.4 Terahertz Imagers

The 300 to 1000 GHz section of the electromagnetic spectrum represents sub-millimetre wave or Terahertz frequencies. These frequencies possess an advantage of higher spatial resolution, but reduced penetration of clothing occurs with increasing frequency much above 100 GHz (Dunayevskiy et al., 2007; Gatesman et al., 2006; Dickinson et al., 2006; Bjarnason et al., 2004)

The Pacific North West National Laboratory has developed a prototype wideband active imaging system. Operating at 350 GHz for the feasibility testing of sub-millimetre imaging for stand-off detection applications. The operating range is greater than 10 m and image acquisition takes between ten and twenty seconds. Wideband operation gives good spatial resolution of 7.8 mm axially and a 1 cm diffraction limited lateral resolution at 5 m (Sheen et al., 2010).

2.3.4.5 X-Ray Imagers

X-ray imagers use the same technology as conventional medical x-ray imagers (Morris, 2005), except very low energies are used (Smith, 1991; Chalmers, 2005). This type of system using soft x-rays is a backscatter detector, as this type of radiation penetrates only a few millimetres into the body. Consequently, these x-ray systems cannot find items hidden within body cavities or concealed under flesh, for example under a breast (Schauer, 2011). Every part of the body that may conceal an object must be scanned and the images produced by this type of system contain detailed anatomical information raising issues of privacy (McCullagh, 2010; BBC, 2010a; Telegraph, 2009; BBC, 2009b). There are also safety concerns, because x-ray radiation is ionising, despite using known dosage levels well below published safety limits (Zanotti-Fregonara et al., 2011) The European Commission have a moratorium on their use within the European Union (European Commission, 2011)

2.4 Magnetic Detection Systems

Magnetic field intensity drops off rapidly with distance (WHO, 2012) from the source requiring close proximity operation for all of the systems described in this section.

Metal detectors detect more than just metal, they detect electrically conductive objects. However and importantly from a concealed threat perspective they are unable to distinguish between threat or mundane items. Basic operation is similar for all systems with a detection element which consists of two coils, a source coil that generates a time varying magnetic field and a second coil that measures the resulting magnetic field(s). If an electrically conductive object is present it will generate its own additional magnetic field in response the varying magnetic field of the source coil, see Figure 2.25. Detection of this additional signal indicates the presence of a conducting object. Unfortunately large numbers of mundane objects also contain metal and would trigger the system.

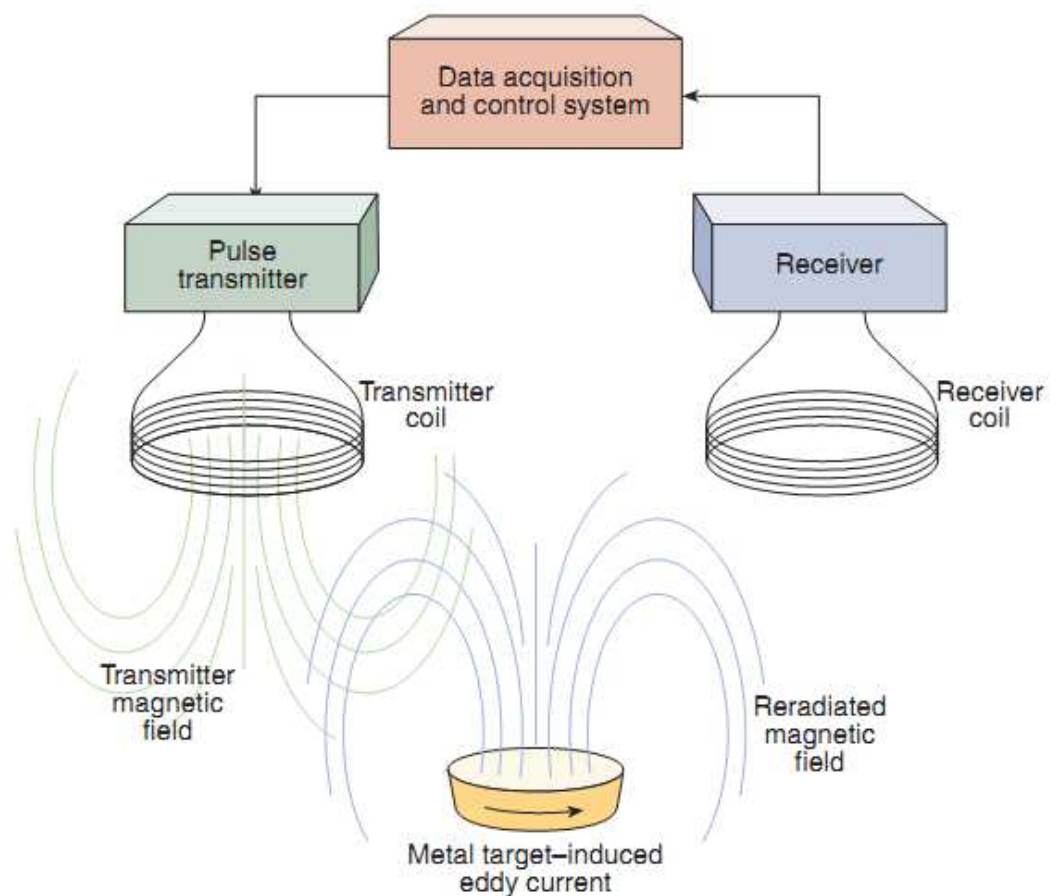


Figure 2.25: Basic pulse induction metal detection scheme (Nelson, 2004)

There are sensitivity issues limiting the minimum size of a detectable object due to the induced magnetic field of the human body. Although the human body is a poor conductor it is physically large and can swamp the faint signals produced by small objects.

As magnetic field strength rapidly decreases portal sizes are limited and non-metallic and small metal objects often go undetected.

2.4.1 Walk-Through Metal Detection Portal

Walk-through metal detectors are common sights at nightclubs and airports. Operation requires individuals to be screened to walk through them one at a time. Since most weapons contain a significant amount of metal they are a good means of detecting weapons. As already noted it is unfortunate that many mundane objects with no threat value whatsoever also contain metal. The human body has conductive properties and due to its large size and this limits the potential sensitivity of the system to minimise the false alarm rate and this may result in small metal objects not being detected. Unless a walk-through detector is zoned with multiple detection elements, no information is obtained about the location of a detected object.

To overcome the limitations of limited operating range and individual scanning of targets through a portal, a system was proposed to screen large crowds consisting of a spatially distributed metal detectors (Nelson, 2003b); such a system uses steerable magnetic field sensors (Nelson, 2003a) and has a with patent granted (Nelson, 2006b).

This technology can also be applied to detect land mines (Nelson, 2006a) and IEDs (Nelson, 2007). A steerable magnetic sensor has also been incorporated into a 3D metal detector (Humphreys & Keene, 2009) extending earlier zoned work by (Keller, 1999, 1996; Keene, 2003).

2.4.2 Hand-Held Metal Detectors

These lightweight devices are used in very close proximity to the target, typically a few centimetres. They are used to search over the target to identify the presence of and location of metallic items. Because they are used in close proximity to the target the operator can be placed in potential danger.

Figure 2.26 shows a pair of hands-free metal detectors that can be covertly worn under gloves. They are commercially available (Interconnective, 2010) costing less than £300. They have been trialled and are in use by UK police to enhance pat down searches (Herald, 2010).



Figure 2.26: Photograph of hands free metal detectors that can be worn under gloves

2.4.3 Magnetic Imaging Portals

This is a walk-through type detector which uses multiple receivers and a single transmitter arranged around a door. Similar to conventional metal detectors, the time varying magnetic field generated by the transmitter antenna interacts with items within the detection volume, but multiple detectors are used. Analysis of these signals enables an image to be constructed of the portal contents. Spatial resolution is approximately 5 cm

(Zollars, 1997) In a hand gun example it could not be identified, but may show up as a patch area of different contrast. It would not be possible to identify conclusively the presence of a handgun from the image, but it may be discernible.

The time varying magnetic field generated by the transmitter antenna interacts with items within the detection volume, similarly to current conventional metal detectors.

2.4.4 MRI Body Cavity Imager

Body cavity imagers use the same magnetic resonance imaging techniques used by medical MRI systems. MRI works by exposing the target to large pulsed-magnetic fields and using high-frequency microwaves to probe the interaction of the magnetic field with the body. By investigating the internal cavities of the body which would normally contain food and liquid in the digestive tract, foreign objects can be located. The large pulsed magnetic fields used by MRI systems are dangerous to people with pacemakers and other medical electronic devices.

MRI imagers are very large devices and require very close proximity for inspection. As such, they are unsuitable for mass screening, due to the necessary safety precautions and lengthy inspection times.

2.4.5 Gradiometer metal detectors

These passive devices detect ferromagnetic metals by measuring the localised distortion they create in the Earth's magnetic field (Roybal, 1997; Allen, 1999). Ferrous metals distort the Earth's magnetic field because they are magnetically permeable and may even possess a permanent magnetic moment, that creates its own magnetic field. A solitary gradiometer is susceptible to background fluctuations of the Earth's magnetic field, so in practice a pair of detectors are connected in differential mode. This configuration has the dual benefits of overcoming these natural fluctuations and reducing the false alarm rate. Zoned detectors consist of multiple gradiometer pairs. (Paulter, 2001; Allen, 1999).

Gradiometers are more sensitive than current metal detectors, however they can still only detect ferromagnetic materials (Paulter, 2001) Early systems were portal based, but as greater dynamic range detectors have been developed, mobile platform mounted systems have been developed (Keene et al., 2005).

2.5 Summary

The field of concealed threat detection is broad and complex with the inevitable conflicting requirements. The most common systems use EM radiation for detection and work by either generating an image for interpretation by an operator or by analysing the radar returns of the target for signatures characteristic of threats. Currently the most effective systems work in carefully controlled environments with co-operative targets – a prime example is airport passenger screening.

Systems currently exist, but their effectiveness is limited by the extent to which the environment can be tightly controlled. An example system manufactured by Smiths Detection called the TADAR (Detection, 2006) was previously considered cutting edge and operated well within an airport, but ignoring its size, performance outside would be variable, due to the changing environmental conditions. Systems like the TADAR use passive detection of mm-waves from background sources to form an image. Subsequent systems like the Rapiscan Secure 1000 (Rapiscan, 2009) are considered current state of the art and by actively illuminating the target using x-ray backscatter they overcome the need for a carefully controlled environment while also producing superior imagery, but unfortunately they retain the weight and size. Backscatter x-ray are currently the subject of a safety investigation by the European Commission (European Commission, 2011) and their use has been withdrawn until the use of soft x-rays is deemed safe. A system capable of working safely with equal efficacy inside and outside where the environment is not as easily controlled is needed.

Blank page

3 Background Theory

This Chapter presents some of the concepts employed by the novel prototype for the remote detection of concealed guns and explosives. The relevance with regards to the detection of guns or fragmentation based explosives (PBIED's) is explored.

3.1 Electromagnetic Propagation

EM radiation has amplitude, frequency and polarisation. These properties dictate how the radiation propagates through different mediums, determining for example transmission speed and opacity. Figure 3.1, shows the different bands of the electromagnetic spectrum with accompanying physical examples (NASA, 2011).

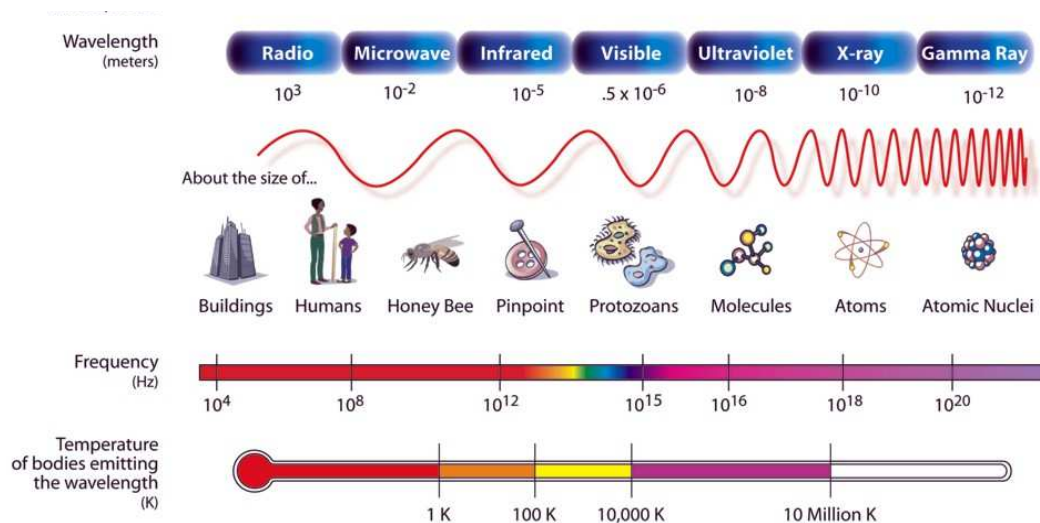


Figure 3.1: The electromagnetic spectrum

3.2 Background Theory of Detection

This section describes the portion of the electromagnetic spectrum used by the concealed threat detection systems developed during this work, to remotely detect objects and the conventions used to classify and distinguish between these systems.

For detection to occur, energy must be measured. That energy must travel from the target to the detection system. Either the target itself must radiate or the target must be illuminated by an external energy source and the reflected/re-radiated energy measured.

In the microwave/millimetre wave arena, viable detection systems rely on either naturally occurring energy emitted by the target, or active illumination of the target. A system that relies upon the naturally occurring radiation for detection is classified as a passive system and a system that generates radiation to illuminate a target is classified as an active system.

Passive detection systems use naturally occurring radiation. The principal radiation sources for passive systems are:

- a) The Sun - the Sun is a broadband radiation source.
- b) Blackbody radiation - this radiation is generated by the target itself with a peak emission frequency based on the temperature of the body.

The science behind passive millimetre wave technology was discovered in the 1930s and has been part of radio astronomy ever since (Appleby, 2004b).

Anything above the temperature of absolute zero, emits black-body radiation and is called a black-body radiator. Practically all objects are non-ideal black bodies and referred to as Grey bodies (Annaratone, 2009; Seymour et al., 2010) as they exhibit an emissivity of less than unity that varies as a function of wavelength, but for calculation of maximum emitted power purposes only Blackbodies are considered herein.

The peak wavelength of emission of a Blackbody can be obtained using Wein's Displacement Law:

$$\lambda_{max} = \frac{b}{T} \quad (3.1)$$

where T is the absolute temperature of the object in Kelvin and b is Wein's displacement Constant of 2.898×10^{-3} K.m. For a body at 300 K the peak emission wavelength is 9.66×10^{-6} m or frequency 31.1 THz.

However passive detection systems operate in the millimetre wave regime at much lower frequencies. Using Planck's law the spectral radiation of an object can be calculated:

$$E(\lambda) = \frac{2hc^2}{\lambda^5} \frac{1}{e^{\frac{hc}{\lambda kT}} - 1} \quad (3.2)$$

where h is Planck's constant (6.63×10^{-34} J.s), c is the speed of light (3×10^8 m.s⁻¹), k is Boltzmann's constant (1.38×10^{-23} J.K⁻¹) and T is the absolute temperature of the object. For an object at 300 K the spectral plot looks like:

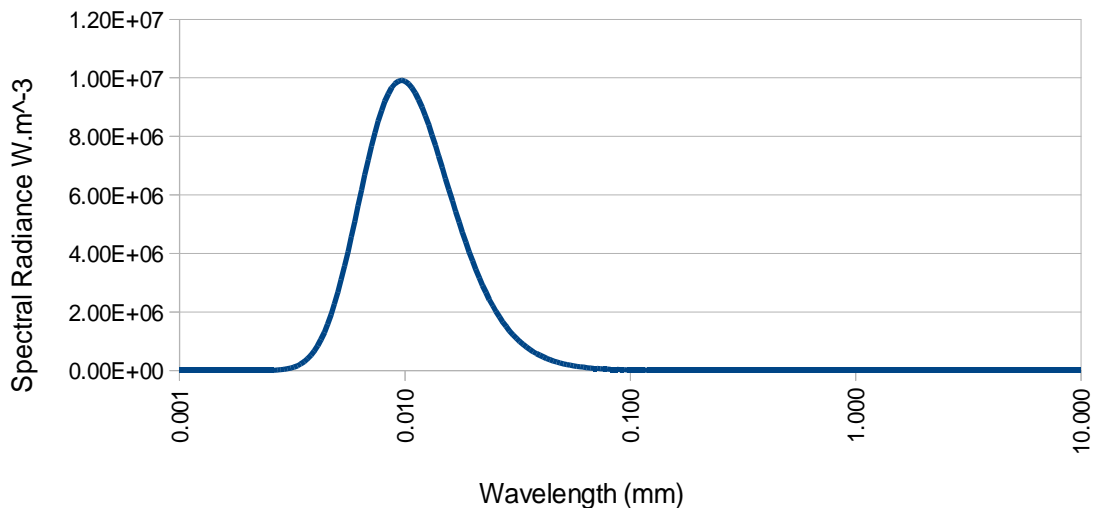


Figure 3.2: Spectral radiation of a 300 K Blackbody for wavelengths between 0.001 and 10.000 mm

Fig 3.2 shows the energy distribution of radiation against wavelength. Examination of the wavelengths of interest 2.7 to 4.0 mm (75 to 110 GHz) is difficult, because of the low gradient of the curve at this point, so Figure 3.3 shows this sub-section of the curve.

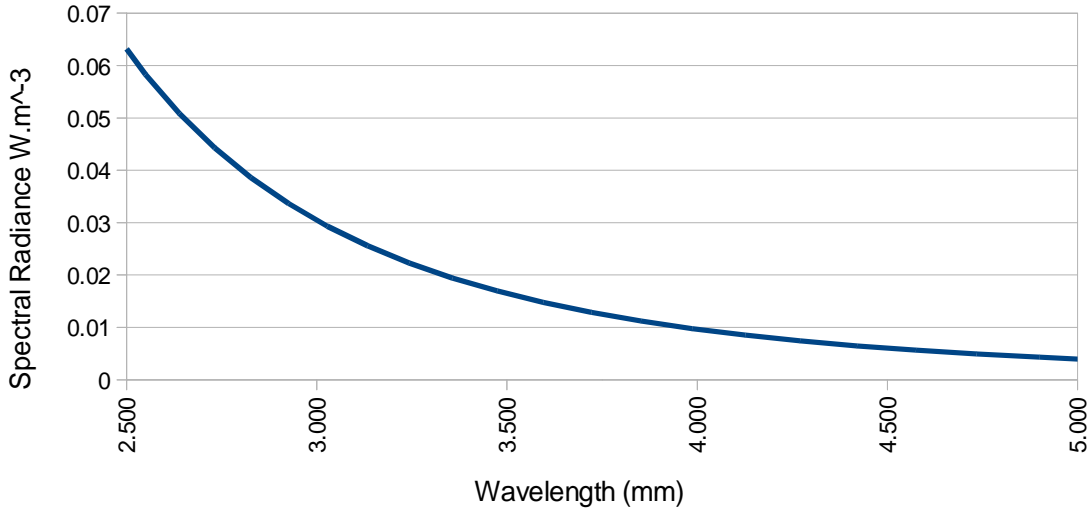


Figure 3.3: Black body radiation of a 300 K body for wavelengths between 2.50 and 5.00 mm

Summing the spectral radiance of wavelengths between 2.72mm and 4.50mm (75 – 110 GHz) gives the power radiated is $3.94 \times 10^{-5} \text{ W.m}^{-2}$.

The gain of a horn antenna is (Narayan, 2007):

$$G = \eta \frac{4\pi A}{\lambda^2} \quad (3.3)$$

where η is the antenna efficiency which for a optimum horn of pyramidal construction this is 0.511 (Teshirogi & Yoneyama, 2001); A is the area of the horn flare and λ is the wavelength of the radiation.

Conventionally the gain of an antenna is in dB:

$$G_{dB} = 10 \log \left(\eta \frac{4\pi A}{\lambda^2} \right) \quad (3.4)$$

The gain of an antenna is also equal to:

$$G = \frac{4\pi}{\Omega} \quad (3.5)$$

where Ω is the solid angle of the beam pattern in steradians. Removing G by combining equations (3.3) and (3.5) gives:

$$\eta \frac{4\pi A}{\lambda^2} = \frac{4\pi}{\Omega} \quad (3.6)$$

simplifying for Ω this is:

$$\Omega = \frac{\lambda^2}{\eta A} \quad (3.7)$$

substituting effective aperture (A_e) for ηA gives the solid angle of the antenna as a function of wavelength:

$$\Omega = \frac{\lambda^2}{A_e} \quad (3.8)$$

By inspection of equation (3.8) the area of an antenna and its directionality are inversely proportional. If the area of an antenna is constant, then:

$$\Omega \propto \lambda^2 \quad (3.9)$$

Therefore the acceptance solid angle of a horn antenna is a function of wavelength.

Consequently, the previously calculated radiation figure of $3.94 \times 10^{-5} \text{ W.m}^{-2}$ for an object at 300 K is only correct for a fixed Ω across the wavelengths of interest and so cannot be used. To calculate the energy received the product of the wavelength and the spectral radiance of a body are needed. Figure 3.4 is a plot of Ω against λ generated using Equation (3.9):

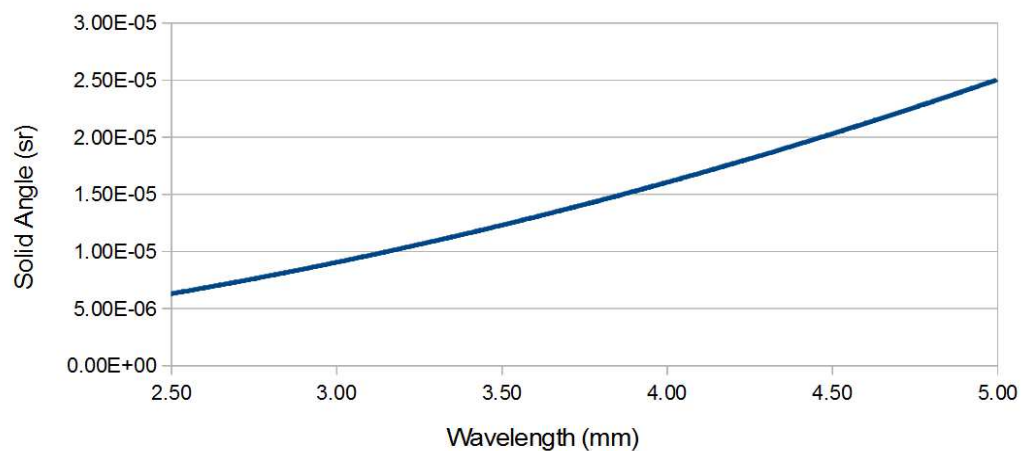


Figure 3.4: Solid angle against wavelength (2.50 and 5.00 mm) for a unit area aperture

Multiplying the graphs in Figures 3.3 and 3.4 together creates a spectral radiation power plot for an antenna with acceptance solid angle spot lies within the boundary of the measured object:

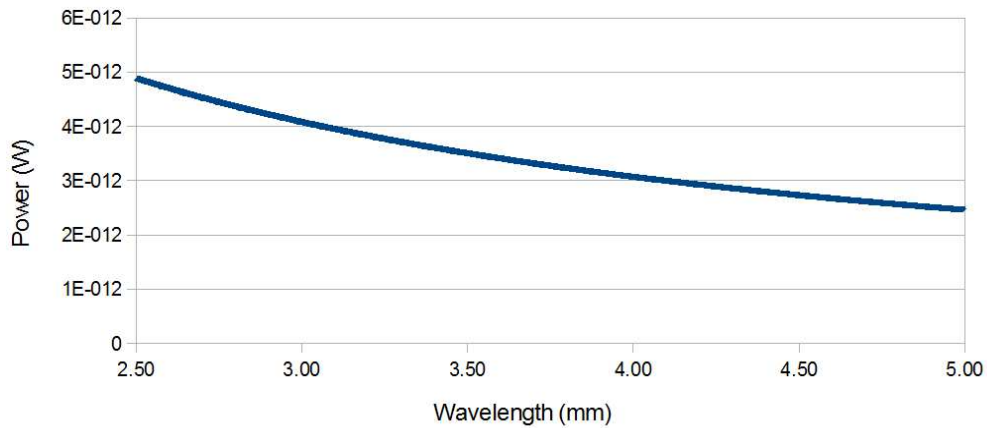


Figure 3.5: Spectral radiation power of a Blackbody at 300 K seen by an antenna for wavelengths between 2.50 and 5.00 mm

Summing the area under the curve for wavelengths between 2.73 and 4.00 mm (75 – 100 GHz) gives the best case power measured by a pyramidal horn antenna from an extensive Blackbody object at 300K of 2.88×10^{-10} W. For a practical system this figure will be smaller (Annaratone, 2009).

To mitigate the very low power levels received by passive systems, MMIC receivers are used. MMIC receivers are a type of monolithic integrated-circuit operating at microwave and mm-wave frequencies performing low-noise, wideband signal amplification with a typical gain of approximately 17dB (Infineon, 2010). but gain can be as high as 40dB (Lo et al., 1995)

Examples of passive imaging systems include the TADAR manufactured by Smith's Detection a manufacturer of security systems operating at 3mm wavelengths (Detection, 2006). At these wavelengths clothing is mostly transparent, but other objects such as dielectrics and metallic weapons are opaque (Anscombe, 2005).



Figure 3.6: Image from TADAR passive imager system using naturally occurring Black-body radiation to form an image

3.2.1 Active Illumination

An active illumination based detection system provides its own radiation to illuminate the target. The energy transmitted by the system is reflected or re-radiated by objects in a field of view. Active systems have control over the type, power level, polarisation and frequency of the illumination they generate, whereas passive systems have no such control. The amount of energy reflected from objects is a function of their structure and composition. Any reflected energy is affected by barriers between their detection system and the object, including concealing barriers such as clothing. Masking of objects is possible by blocking the incident energy. Mundane objects within the detection volume can also reflect a significant level of energy and affect the responsiveness of the detector. As an example, the glint (directly reflected energy) from the perfectly aligned flat surface of a mobile phone can swamp the return signal potentially overwhelming the smaller return signal from threat objects.

3.2.2 Continuous or Pulsed Radiation

The difference is based on how output power varies with time. Continuous wave sources as the name implies, continuously produce radiation. The amplitude and frequency of such energy can be modulated. Conversely pulsed sources produce a short burst of energy spread over many frequencies. Pulsed sources typically have a greater peak power than continuous wave sources for a given average power, providing them with a relative performance increase. This can result in superior image quality or faster scan rates. With the use of Fourier transforms and the ability to change domain, the two approaches are mathematically equivalent (Cooley & Tukey, 1965). The realisation of a FMCW radar is simpler by not having to implement the very high speed receiver sub-systems needed when using pulsed radiation (Stove, 1992).

3.2.3 Controlled and Uncontrolled Environments

A controlled environment is a location where the conditions can be accurately predetermined in terms of radiation sources, fixtures, temperature etc. A controlled environment is a prerequisite for optimum performance of passive detection systems. Examples of controlled environments include installations within buildings and the booth of a detector.

Conversely, the number, intensity, orientation and type of radiation sources cannot be predicted in an uncontrolled environment. Therefore the number of unknowns for a passive illumination based system is greater than for the equivalent active system and hence an active system producing known radiation (coherent or incoherent) to illuminate the target may provide better performance in a greater range of environments compared to passive systems.

To work in an uncontrolled environment a successful system must in addition to mitigating changes in naturally occurring radiation, be able to accommodate changes of temperature and variable weather conditions.

3.2.4 Refractive Index

The complex refractive index N of a material is a frequency dependent complex value determining the speed and attenuation of EM waves travelling through it:

$$N = n + i \kappa \quad (3.10)$$

where n is the real refractive index of the material affecting refraction and reflection and κ determines the extinction coefficient (Hecht, 2001). Energy not coupled into or absorbed by the material is reflected at the interface. The proportion of energy R reflected is a function of the properties of the materials forming the interface:

$$R = \left(\frac{n_1 - n_2}{n_1 + n_2} \right)^2 \quad (3.11)$$

where n_1 and n_2 are real parts of the refractive indexes for the materials. The coefficient of extinction is a measure of attenuation of a EM wave through the material. Absorbed energy can be re-radiated in a different form, for example thermal radiation.

Normally Refractive index is positive, but for a special type of the artificially created structures called meta-materials it can be negative (Eleftheriades & Balmain, 2005).

The dielectric constant of a material is important when trying to identify the presence of a non-fragmentation based explosive because n affects the apparent thickness of the explosive because phase speed is a function of n :

$$v_{phase} = \frac{c}{n} \quad (3.12)$$

where c is the speed of light. Measurement of objects with EM radiation generates an optical dimension not the physical dimension; with knowledge of the refractive index of a

material the physical dimension can be derived. For example, paraffin wax has a similar refractive index to plastic explosives (Baker, n.d.) Therefore the measurement of block with refractive index 1.5 and thickness 8cm will show an optical thickness of 12cm.

The absorption and refractive index of mass manufactured C-4 are shown in Figure 3.7, (Yamamoto et al., 2004) In the frequency band of interest the absorption coefficient is very small and the refractive index is approximately 1.8.

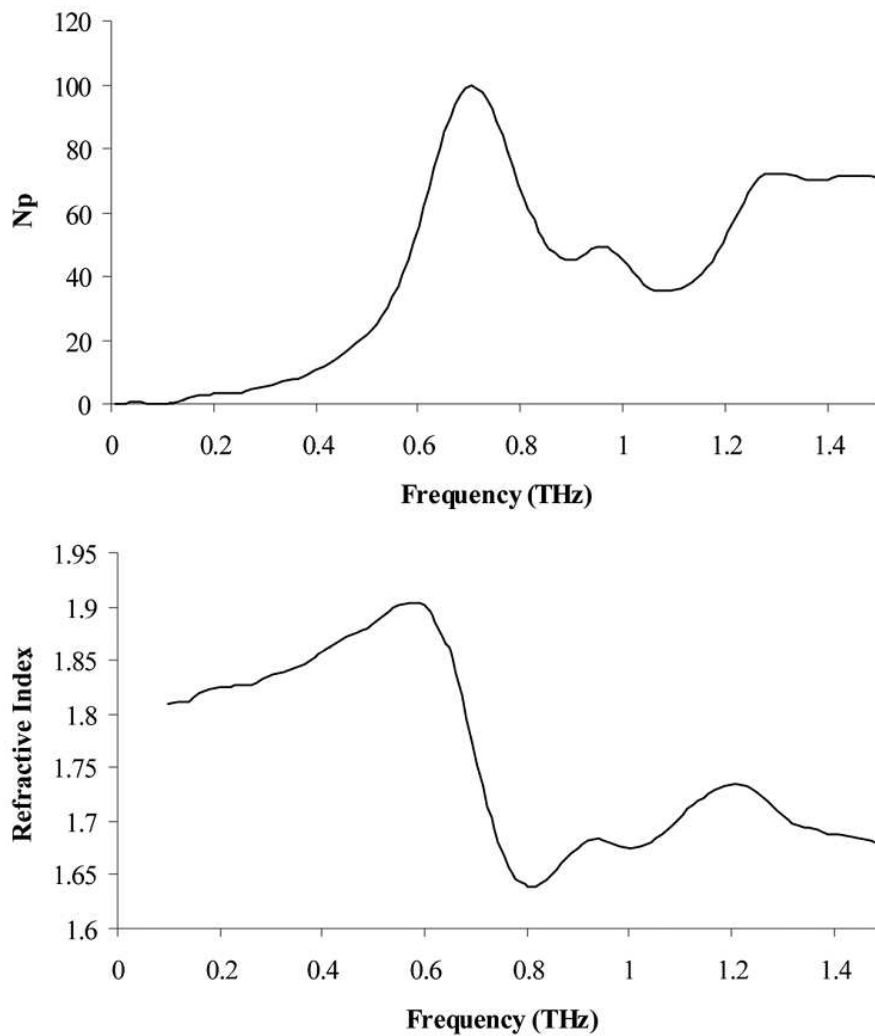


Figure 3.7: Absorption and refractive index of C-4

The above is only true for transparent materials and a material can be opaque if the imaginary component of ϵ is high at a particular frequency (Yamamoto et al., 2004). An opaque material can absorb, scatter or reflect the incident wave.

3.2.5 Refraction and Reflection

Refraction and reflection occur at the boundary between mediums of different refractive index. Since this occurs in each detection scenario, this is applicable to gun, dielectric and fragmentation based explosive detection. In free space an EM wave travels in a straight line, however when an EM wave crosses the boundary between two dissimilar materials, the direction of propagation of the wave changes. This change in direction is called Refraction and described by Snell's Law (otherwise known as the Law of Refraction):

$$n_1 \sin \theta_1 = n_2 \sin \theta_2 \quad (3.13)$$

where θ_1 is the angle between the direction of the initial wave and the normal to the boundary of the two media and θ_2 is the corresponding angle for the refracted wave. The change of direction is due to the change in velocity experienced by the wave as described by Equation (3.12). Any energy not refracted is reflected. The reflected wave is at the same angle as the incident wave because they are travelling in the same material and hence travel at the same speed. Figure 3.8 shows these two phenomenon.

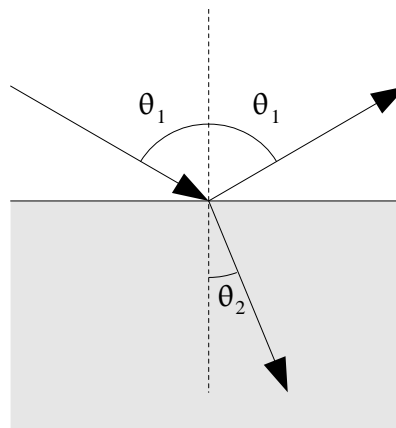


Figure 3.8: Angles of refraction and reflection

The fraction of the incident wave power that is reflected for radiation normal to the material is given by Equation (3.11). Using the same example for air ($n_1 = 1$) and paraffin wax ($n_2 = 1.5$), the reflected energy is approximately 4% of the incident energy. Thus 96% is refracted into the wax.

Non-conducting solids and liquids behave as dielectrics with a typical refractive index between 1 and 3 at millimetre wave frequencies. Therefore, most materials reflect at most 25% of the incident radiation (Kemp, 2006).

3.2.6 Skin Depth

Skin depth is a measure of the depth into a conducting material, where current density has fallen to 1/e and defined by Johnson (1950):

$$\delta_s = \sqrt{\frac{\rho}{\pi f \mu}} \quad (3.14)$$

where ρ is bulk resistivity ($\Omega \cdot m$), f is frequency (Hz) and μ is the absolute magnetic permeability of the conductor (H/m). The skin depth of metals is very shallow preventing the measurement of its interior. For example, copper at 100 GHz has a skin depth of 0.2062×10^{-6} m (Lide, 1996). Therefore only the surface of a metal can be irradiated for measurement purposes and the proportion of energy reflected at the interface approaches 100%.

For comparison the skin depth of a lossy dielectric is:

$$\delta = \left(\frac{\sqrt{\epsilon'}}{2\pi \epsilon''} \right) \lambda \quad (3.15)$$

where ϵ' and ϵ'' are the real and imaginary parts of the absolute permittivity and λ is the wavelength.

Since the imaginary part of the refractive index is large relative to air in the frequencies of interest, metals are almost perfect reflectors (Polyanskiy, 2008).

$$\kappa \approx c \sqrt{\frac{\mu}{4\pi f \rho}} \gg 1 \quad (3.16)$$

3.2.7 Radar Cross Section

The power received by a mono-static radar from a remote metal object can be calculated (ignoring atmospheric attenuation) using:

$$P_r = \frac{G^2 P_t \sigma \lambda^2}{64 \pi^3 R^4} \quad (3.17)$$

where P_r is received power, G is antenna gain, P_t is transmitted power, σ is the Radar Cross Section (RCS) for the object, λ is the wavelength of the signal and R is the distance to the object (Renato, 2002). It should be noted the received signal strength is inversely proportional to the fourth power of the range.

The RCS of an object is the apparent area intercepting that amount of power which, when scattered equally in all directions, produces a power at the receiver equal to that from the target (Skolnik, 2002) and is equal to (IEEE, 1984):

$$\sigma = 4 \pi R^2 \frac{S_r}{S_t} \quad (3.18)$$

where S_r is power density at the range R and S_t is the power density intercepted by the object. This simplifies producing a gain figure:

$$\sigma = G A \quad (3.19)$$

where G is the effective RCS gain of the object and A the irradiated area of the object.

3.2.8 Polarisation

Polarisation is a property of an EM wave describing the orientation of electric field oscillations within the wave. A polarised EM wave can be produced by one or more correlated sources. When the sources of an EM wave are uncorrelated it is described as incoherent. Active EM based detection systems often use polarised energy and this can be either planar or circularly polarised. Planar polarisation can be at any angle, but normally refers to the electric field component of the wave and can be described as horizontal or vertical relative to the planet surface. The other type is circularly polarised, where the polarisation rotates as the wave travels; this is either right handed polarisation or left handed describing the direction of rotation. Where the amplitude or phase of the two fields are not equal for a circular polarisation, it is referred to as elliptically polarised.

The intensity of a linearly polarised electromagnetic wave is:

$$I = \frac{cn\epsilon_0}{2} |E|^2 \quad (3.20)$$

where E is the complex amplitude of the electric field, n is the refractive index, c is the speed of light and ϵ_0 is the permittivity of free space.

The polarisation of an EM may change due to scattering of an object. This depends upon the size, form, structure and composition of the object and the type of radiation. A polariser is such a device and is used to change the polarisation of a millimetre waves in a controlled manner. It achieves this by only transmitting the component of the wave that is perpendicular to the traces of the polariser (Alba, 2006). For linearly polarised waves a polariser typically takes the form of a grid of thin parallel conducting lines.

The PCB polariser shown in Figure 3.9 was designed with variable line pitches to assist in experiments. Appendix B contains a detailed description and results.

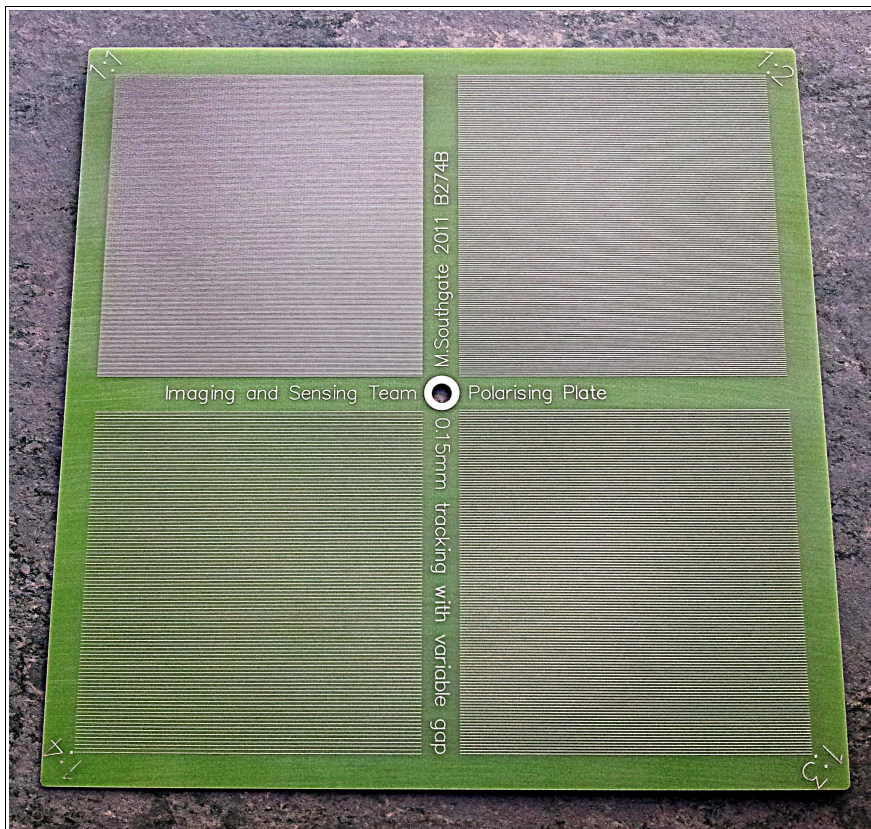


Figure 3.9: B274B Multi-pitch PCB Polariser

Structures such as isolated spheres (symmetric in all orientations) and flat metallic surfaces (symmetric about one axis) do not alter polarisation, whereas a complex shape such as a gun or shrapnel containing explosive device, changes the polarisation to some extent. In this project only linear polarisation was used, but the properties of complex metallic shapes do considerably affect the polarisation of the return signal. This is especially applicable to the detection of concealed guns and explosives. The polarisation modifying properties of complex shapes such as handguns and fragmentation may be used to indicate the presence of a concealed threat (Andrews et al., 2008a; Rezgui et al., 2008; Andrews et al., 2009)

3.2.9 Beam Generation and Focussing

The intensity of an EM wave is inversely proportional to the distance from a compact wave source. As the wave spreads out radially from an isotropic source covering the surface area of a sphere, the greater the radius the larger the surface area. For an isotropic antenna radiating power P the intensity I at distance r is given by:

$$I = \frac{P}{A} = \frac{P}{4\pi r^2} \quad (3.21)$$

The effective range of a system is limited by the SNR of the signal. Lenses or antennas can be used to focus radiation and reduce the loss of intensity due to dispersion of a wave as it propagates, compared to an undisturbed wave.

3.2.10 Radiation Safety

High energy radiation, such as X-rays and gamma rays are capable of ionising atoms whereas low energy non-ionising radiation is not. Ionising radiation is dangerous and low energy non-ionising radiation is not thought to be damaging for low levels of exposure. Only non-ionising radiation is used in this project at levels well below internationally accepted safety guidelines (ICNIRP, 1998). The levels of radiation used in this research

project are small compared to the the guide levels, however we were mindful to minimise levels where possible. An assessment and examination of the radiation used in this research project can be found in Appendix A. This fulfils aim (a) of the project.

Passive detection systems do not share this risk.

3.3 Radar

3.3.1 Active Radar Types

It is worthwhile at this point to cover the different types of active mm-wave radar. The main types are pulsed radar, continuous wave radar and frequency modulated continuous wave radar:

- (a) Pulse radar – emit wave usually less than a metre long at set frequencies. These are used to detect range, by measuring the time taken to receive a reflection. To be accepted the pulse has to be received within a period called the range gate.
- (b) Continuous Wave (CW) Radar – these operate at a fixed frequency similar to a pulse radar but on a continuous basis. This type of radar measures velocity by exploiting the Doppler Effect. Energy levels are much lower than for pulsed radar.
- (c) Frequency Modulated Continuous Wave (FMCW) Radar – use ramped frequency modulation and mix the outgoing wave with the reflected signal at the detector to allow continuous measurement of distance and velocity, by measuring the amplitude and phase of the return, or the average power of the returned transmission.

FMCW was chosen despite its complexity compared with pulsed radar because of the recent availability of wideband RF components, as an alternative to the high cost of the equivalent pulsed radar parts. In (Hunt, 2001) the performance of FMCW was comparable with pulsed radar. (Mikhnev, 2008) covers the reconstruction of a FMCW signal set. The

disadvantages of the FMCW approach to detection also include the longer detection time and the processing overhead. However there are advantages of greater flexibility in antenna design and system imperfections can be quantified and calibrated at different frequencies, permitting automatic compensation. Lastly the calculated time-domain performance of FMCW schemes have superior signal-to-noise ratios, giving superior resolution, this is crucial to discriminating between multiple co-located targets (Mikhnev, 2008).

Blank page

4 Proof of Concept

It doesn't matter how beautiful your theory is, it doesn't matter how smart you are.

If it doesn't agree with experiment it's wrong.

RICHARD P. FEYNMAN

This Chapter describes the steps taken to build a bench-top non-imaging radar based demonstrator capable of remotely detecting concealed threats object using microwave and mm-wave radiation. Starting with an analysis of the Problem Statement, a basic device specification is presented and important phenomenology is identified. Secondly the diversity and scope of threat objects and their concealment are quantified. Thirdly, experiments to establish the proof of concept are described.

4.1 Analysing the Problem

This section breaks down and analyses the requirement defined in the Problem Statement, see Chapter 1. The requirements of the solution will now be outlined.

Threat items to be detected by the prototype consist of guns and explosives, knives and needles are not included. The type, size and composition of each threat item are considered in section 4.2.

The final device needs to be reasonably small for covert use and light enough to be easily carried by a single adult, probably in a bag. The user interface and operation of the device must not alert the target that they are being covertly screened for threat items. This requires that the detection method to be entirely non-invasive.

Since the final device will be portable, it must also be possible to power it using batteries, precluding the use of high power consumption components.

Since the device is not intended to be deployed in a fixed installation, it is unlikely that it will be used within carefully controlled environment. To be effective in an uncontrolled environment requires a degree of control over target illumination. The mechanical scanning mechanism used in passive imaging systems adds size and weight, making it attributes inconsistent with a compact and lightweight device. Therefore, the device must use active illumination of the target.

Remote detection in this context, is defined as a stand-off distance greater than five metres (Bowring, 2006). Since covert use within a reasonably busy environment is expected and maintaining a line of sight to the target over a distance of more than ten metres is difficult, an effective upper range of eight metres is assumed.

The device could either automatically scan over the target and produce an image for the operator, or the device could be manually scanned over the target by the operator, indicating the presence of concealed objects during an inspection. Inclusion of a mechanical scanning mechanism is however precluded because of the design requirement for a compact and lightweight device.

The device must be capable operating in real time, handling data acquisition and processing measurements at multiple frames per second. It is anticipated that the operating speed should be comparable with the frame rate of a video, giving a minimum target rate of fifteen inspections per second.

4.2 Threat Objects and Detection Scenarios

Threats come in different forms and the most effective method of detection is not always the same. This section identifies the different threat types and it is anticipated that multiple variants of the device could be developed, each optimised for a particular threat.

PBIEDs may be divided into two types, with and without fragmentation. The efficacy of a bomb is related to the detonation environment and its composition. For example, explosive devices without fragmentation kill by over pressure and are effective in enclosed or underground environments where the pressure wave is confined. Explosive devices without fragmentation normally consist of a substantial volume of explosive material. The exception is an airtight environment, such as an aeroplane, where very little explosive material would be required which makes them the most difficult explosive device to detect.

Conversely, fragmentation based explosives contain a significant proportion of fragmentation and little explosive material. This type of explosive is normally intended to be detonated in the open.

In summary, to be effective, explosives generally consist of either a substantial volume of dielectric material or fragmentation. With these distinct differences, the detection method should be tailored to the characteristics of each type of explosive. This project focuses exclusively on person borne improvised explosive devices (PBIEDS) mostly with fragmentation present.

The form of a hand gun is fixed and is equally effective in open and confined environments.

4.2.1 On Body Threat Concealment

Large quantities of explosive material are most readily concealed when attached to the torso, as in the archetypical suicide bomber.

Assault rifles and other large guns are rarely recovered by the security forces in the UK, indicating their low availability. As they are also difficult to conceal, it is reasonable to exclude them from the scope of detection. This gun detection aspect of the project focuses on smaller handguns, that can be easily concealed. The body locations most commonly used to conceal handguns are the shown in Figure 4.1.

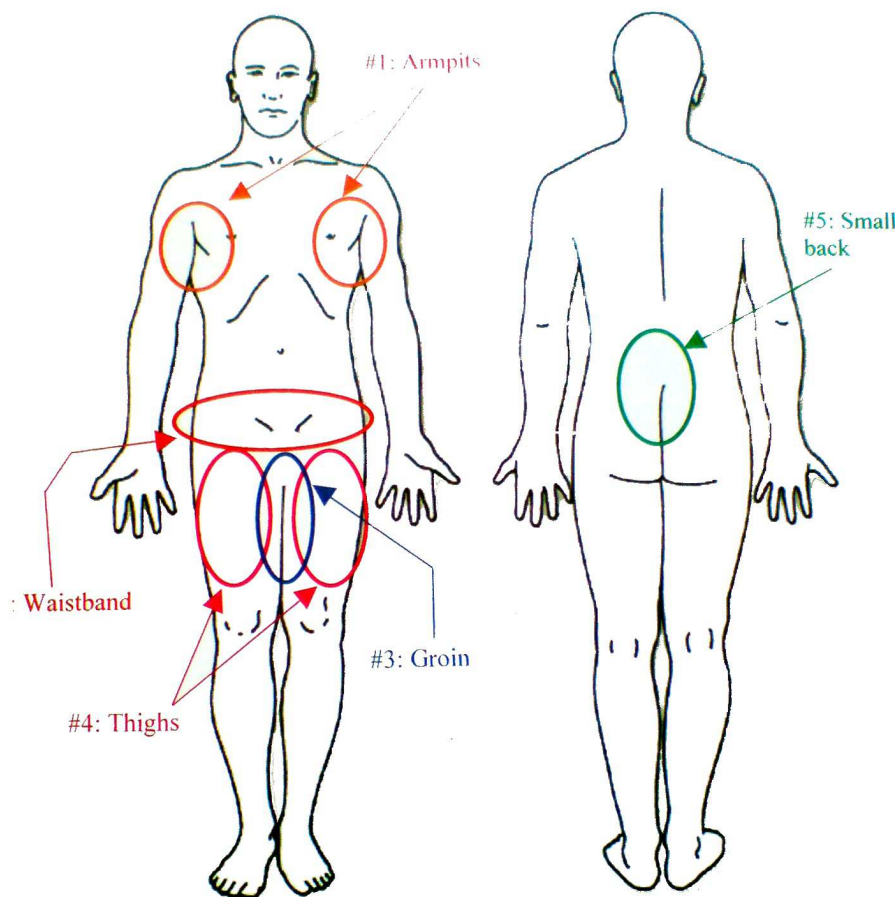


Figure 4.1: Areas of the body commonly used to conceal handguns (Met, 2008)

A mundane item is an object that is not a threat object, but may be confused for a threat object. Examples of mundane items are keys, mobile phones, glasses cases, wallets, cameras etc. Unfortunately, from a threat detection perspective, almost everyone carries concealed mundane items upon their person.

4.2.2 Detection Scenarios

Different environments include indoor and outdoor, controlled and uncontrolled areas, day and night, etc. and these have been outlined previously. The different scenarios that the proposed method is required to be capable of distinguishing between are: body only; body and gun; body and explosive; body and mundane object; body, gun and mundane object; and body, explosive and mundane object.

4.3 Basic Device Specification

The device consists of an ultra wideband active single pixel highly focused radar producing a beam pattern of dimensions comparable to that of a threat object. The beam pattern should be comparable in size to the object being illuminated to minimise measurement of the area surrounding the object.

The device must be able to discriminate between threat and mundane items on the human body that are concealed by commonly worn items of clothing at a distance greater than five metres. Screening rates will be approximately fifteen scans per second.

It is a requirements to have low power consumption and offer flexible power options either running off a small battery pack or an external mains powered DC switched mode power supply (SMPS).

The following section gives a review of the design decisions for the initial prototype.

4.3.1 Radar Types

There are four distinct active radar types. The first is continuous wave radar. This type of radar transmits a continuous, unmodulated wave and is unable to determine the range to a target, but instead, is designed to detect the Doppler shift of radiation reflected by a moving target. Doppler is the perceived variation upon the true frequency of a signal when a target is moving relative to the receiver. If the target is moving then effect of Doppler must be considered. If the target is moving toward the receiver the signal is perceived to be of a higher frequency (LHS of moving target) and of lower frequency (RHS of moving target) for a target moving away from the receiver.

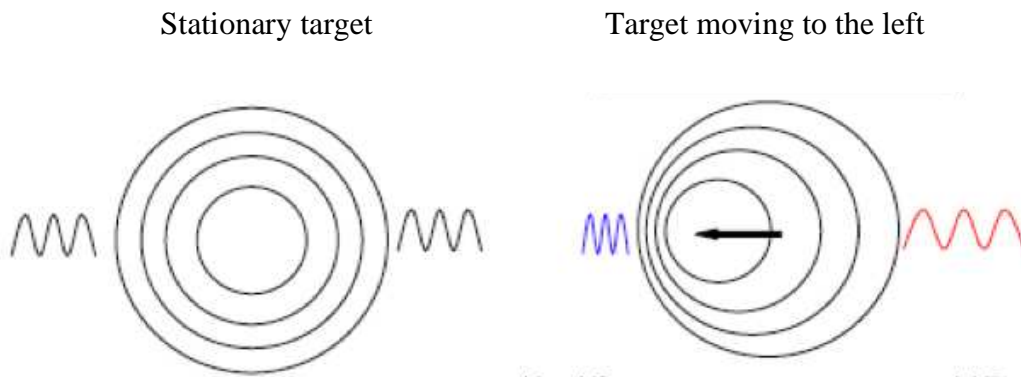


Figure 4.2: The Doppler effect on the perceived frequency of illumination of a stationary and moving target.

The Doppler shift f_d is given by:

$$f_d = 2v_r \left(\frac{f_0}{c} \right) \quad (4.1)$$

where v_r is the relative velocity of the target and source, f_0 is the transmitter frequency and c is the velocity of light. The signal frequency seen at the receiver f_r is given by:

$$f_r = f_0 \pm f_d \quad (4.2)$$

where the frequency is greater if the radar and source are moving closer and lower if they are moving away from each other. By mixing the received signal with the transmitted signal it is possible to extract the Doppler frequency directly. A system with a single mixer directly generating a baseband signal is called a Homodyne (Langman et al., 1996)

A similar approach is heterodyne detection where the incoming signal is down converted using a local oscillator to an intermediate frequency (IF) as is done in a super-heterodyne system (Iizuka et al., 1984). Following amplification of the IF the Doppler signal is extracted by further down mixing to produce a baseband signal.

One way to overcome the inability of CW radar to detect the range is to modulate the amplitude or frequency of the transmitter. These systems are considered in the following sections.

4.3.2 Measurement of Ultra-Wideband Frequency Responses

Techniques for producing UWB are discussed in (Taylor, 2001, 1995). Ultra wide band frequency measurements are either obtained by amplitude modulation using a narrow pulse generator and a very fast receiver to measure the target response in real time, see Figure 4.31 or frequency modulation using a stepped or swept frequency source (Currie & Brown, 1987).

4.3.2.1 Narrow Pulsed Radar

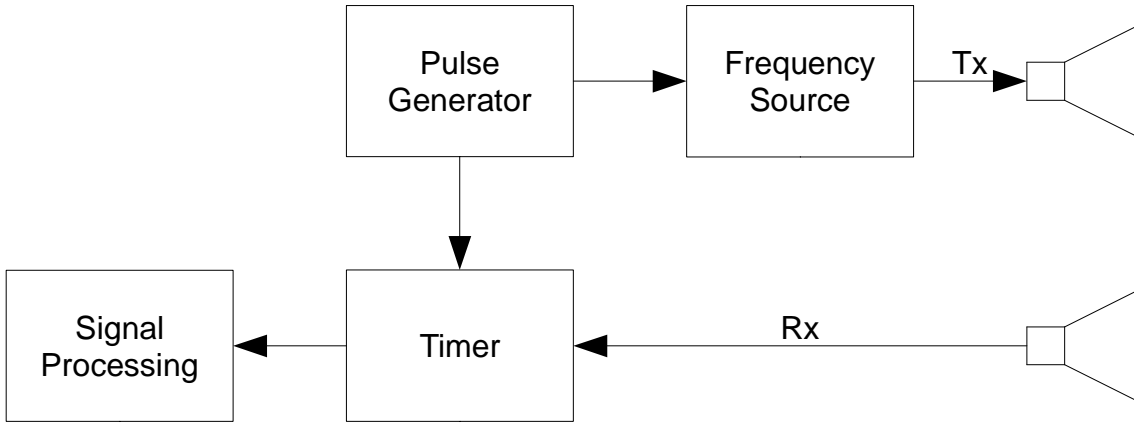


Figure 4.3: System diagram of a pulsed radar

Pulsed radar is used in many industrial applications (Weib & Knochel, 1997; Motzer, 2000). The simplest form of radar uses AM modulation producing a pulse that is scattered at a distance d_{target} . The time return journey time for the pulse is:

$$T_p = \frac{2d_{target}}{c} \quad (4.3)$$

where c is the speed of light. To resolve more than one spatially separated target, the pulse length τ must be smaller than twice the separation of the targets Δd :

$$\tau \leq \frac{2\Delta d}{c} \quad (4.4)$$

To improve resolution the pulse length needs to be shortened:

$$\Delta d \geq \frac{c\tau}{2} \quad (4.5)$$

The problems of high-speed acquisition associated with narrow pulse radar, can be overcome by using a continuous wave modulated frequency technique.

There are two main types of FMCW radar: swept and stepped.

4.3.2.2 Swept FMCW Radar

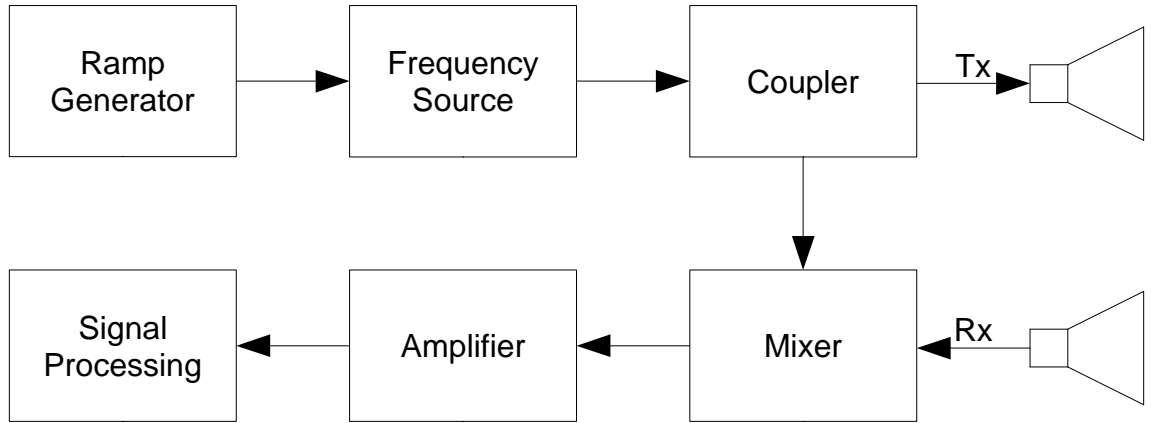


Figure 4.4: Swept FMCW radar system diagram

A swept frequency radar typically has a linearly modulated frequency source that transmits and measures the scattered target response. Due to the journey time, the scattered response is at a different frequency to the currently transmitted frequency. Using the source oscillator as the reference oscillator and mixing the received signal into a baseband signal can be achieved in a single step, without an IF. In contrast a super-heterodyne system has an intermediate step producing an IF. The journey time of a signal reflected from a remote object can be determined by examination of the phase difference of the outgoing and incoming signal. The products of this multiplication are the sum and difference frequencies, based on the trigonometric identity (Abramowitz & Stegun, 1965):

$$\sin \theta \sin \varphi = \frac{1}{2} \cos(\theta - \varphi) - \frac{1}{2} \cos(\theta + \varphi) \quad (4.6)$$

where the product of the two sine waves on the left hand side result in the difference and sum of the original frequencies on the right hand side. Using this to multiply two signals gives:

$$\sin(2\pi f_1 t) \sin(2\pi f_2 t) = \frac{1}{2} \cos[2\pi(f_1 - f_2)t] - \frac{1}{2} \cos[2\pi(f_1 + f_2)t] \quad (4.7)$$

The journey time is proportional to the difference of the transmitted and received frequencies (Stove, 1992, 1992; Brandwood, 2003).

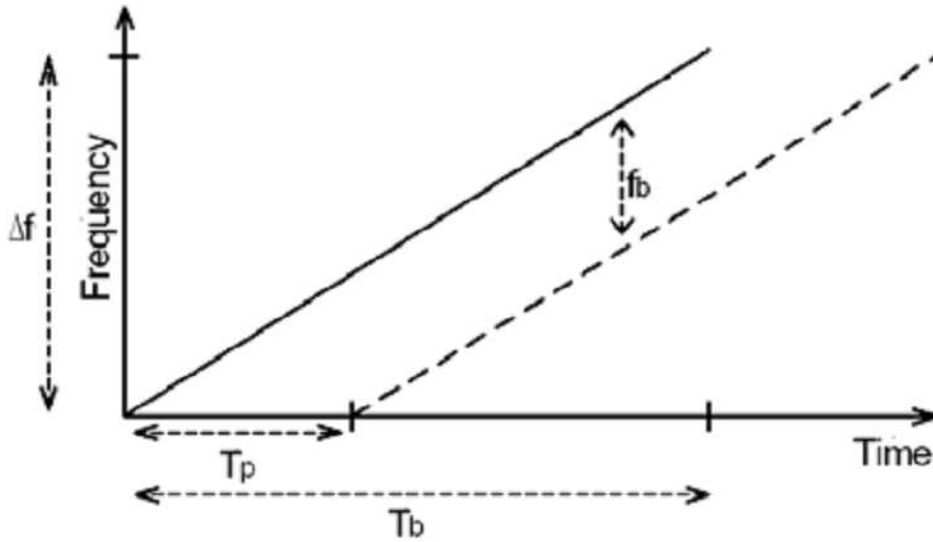


Figure 4.5: Swept frequency FMCW radar response

By rapid sweeping the transmitter frequency and monitoring the instantaneous difference between the transmitted frequency and received frequency, a difference or beat frequency f_b can be obtained. The range to the target can be calculated from the difference frequency:

$$f_b = T_p \left(\frac{\Delta f}{T_b} \right) \quad (4.8)$$

Where the round trip time T_p has been previously defined by Equation 4.3, Δf is the bandwidth of the frequency sweep, T_b is the time period of the sweep, as shown in Figure 4.5. If the target is moving the Doppler shift imposed on f_b must be considered for a continuous frequency ramp. Fortunately for a swept or stepped frequency system the Doppler shift is small (1312Hz for a target walking at 4mph at a transmitter frequency of 110GHz) comparing the typical values of f_b to our frequency step size it can be ignored.

If the error due to Doppler can be ignored, the range to the target is proportional to the difference frequency of the transmitter and receiver frequencies, see Figure 4.5, (Brooker et al., 2008).

4.3.2.3 Stepped Frequency FMCW

Very similar to swept frequency radar and using the same hardware, see Figure 4.4, a stepped frequency radar uses multiple discrete frequency steps equally spaced on the frequency ramp. Transmission and reception of the signal occurs simultaneously. To determine the relative phase the two signals can be mixed to produce a baseband signal. This allows absolute ranging to an interface (surface). The resulting oscillating response in the frequency domain can be transformed and analysed using the Fourier transform (Currie et al., 1992) or MUSIC to obtain an improved resolution in the presence of noise (Yuehua et al., 1998) in the time domain.

4.3.2.4 Direct Detection Radar

The 'Direct Detection' radar is another and less common type of FMCW radar without a mixer. The system diagram is shown in Figure 4.6. Removal of the mixer eliminates the capability to determine the absolute distance to a surface or interface, but for a dielectric target, the distance between surfaces can still be measured.

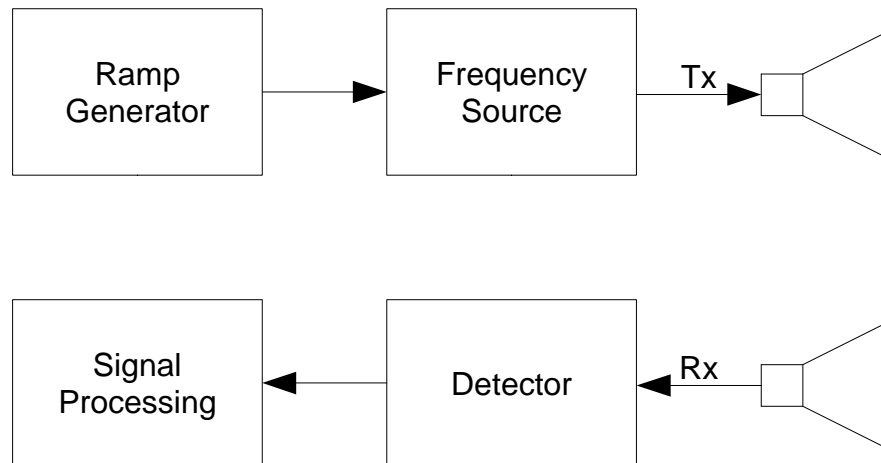


Figure 4.6: Relative interface distance stepped FMCW radar system diagram

When a dielectric object is illuminated, there will exist multiple reflections between its surfaces, producing a series of interference patterns as described in section 4.6. The mixing of signals that would normally occur in the radar, occurs instead at the target.

Fourier analysis of the received power in the frequency spectrum will produce a series of relative optical measurements related to the relative distances between the surfaces of the target.

4.3.2.5 Resolution Limitations of FMCW Radar

Two limitations exist for FMCW radar: the bandwidth Δf and the linearity of the frequency sweep. The resolution d_{res} achievable is the larger value from equations (4.9) and (4.11):

$$d_{res} = \frac{c}{2\Delta f} \quad (4.9)$$

Brooker et al., (2005) state the achievable range resolution with a non-linear sweep is:

$$d_{lin} = d_{target} Lin \quad (4.10)$$

where d_{target} is the distance to the target and Lin is the non-linearity of the sweep:

$$Lin = \frac{S_{max} - S_{min}}{S_{min}} \quad (4.11)$$

where S_{min} and S_{max} are the extreme rates of change of frequency sweep with time.

The combined effect of non-linearity with the system frequency bandwidth is (Brooker et al., 2008):

$$d_{res} = \sqrt{\left(\frac{c}{2\Delta f}\right)^2 + (d_{target} Lin)^2} \quad (4.12)$$

4.3.2.6 Comparison of Pulsed and Frequency Modulated Systems

The advantage of using a pulsed system is faster acquisition time and greater peak power (SiversIMA, 2011) but the equipment is expensive requiring high speed switches and ultra-fast detectors and digitisation processes. Conversely, the swept frequency technique is slower and dependant on the number of points and the dwell time for signal capture. The equipment is however more affordable and although FMCW radar has a higher average power compared to pulsed radar (Wolff, 2009), it can suffer from sensitivity issues with reflected power (Brooker et al., 2008).

4.3.2.7 Pulsed and FMCW Radar Equivalence

These two approaches are equivalent if the phase is measured (Komarov & Smolskiy, 2003). Transformation of data between the time domain and frequency domain can be achieved using the Fourier transform (Cooley & Tukey, 1965). Where u and U are two functions related by:

$$u(t) = \int_{-\infty}^{\infty} U(f) e^{2\pi i t f} df \quad (4.13)$$

and

$$U(f) = \int_{-\infty}^{\infty} u(t) e^{-2\pi i t f} dt \quad (4.14)$$

U is the Fourier transform of u , and u is the inverse Fourier transform of U :

$$u \Leftrightarrow U \quad (4.15)$$

The transforms have 2π in the exponent (so in the spectral analysis, we can use f instead of $\omega=2\pi f$) to maintain the symmetry between the variables (Brandwood, 2003). These equations relate to the general case with an infinitely long series of samples, however for a finite series the equations are:

$$u_n = \frac{1}{N} \sum_{k=0}^{N-1} U_k e^{2\pi i n \left(\frac{k}{N}\right)} \quad (4.16)$$

and

$$U_n = \sum_{k=0}^{N-1} u_k e^{-2\pi i n \left(\frac{k}{N}\right)} \quad (4.17)$$

4.3.2.8 Distance Resolution and Bandwidth

The absolute bandwidth available within a frequency band increases with frequency. A greater bandwidth is therefore available in the mm-wave band than the microwave band.

More information is available in the scattered signals of an object with shorter pulses because a greater range of frequencies existing in a short pulse (Immoriev, 2003). This can be shown numerically with the formula devised by Shannon that relates the information content of a channel H to the channel frequency bandwidth Δf :

$$H = \Delta f \log(1 + P_s/P_n) \quad (4.18)$$

Where P_s is the signal power and P_n the noise power. For a given signal-to-noise ratio the information content of a channel is limited by the frequency bandwidth. System bandwidth is important because it determines radar range resolution, see Equation (4.9).

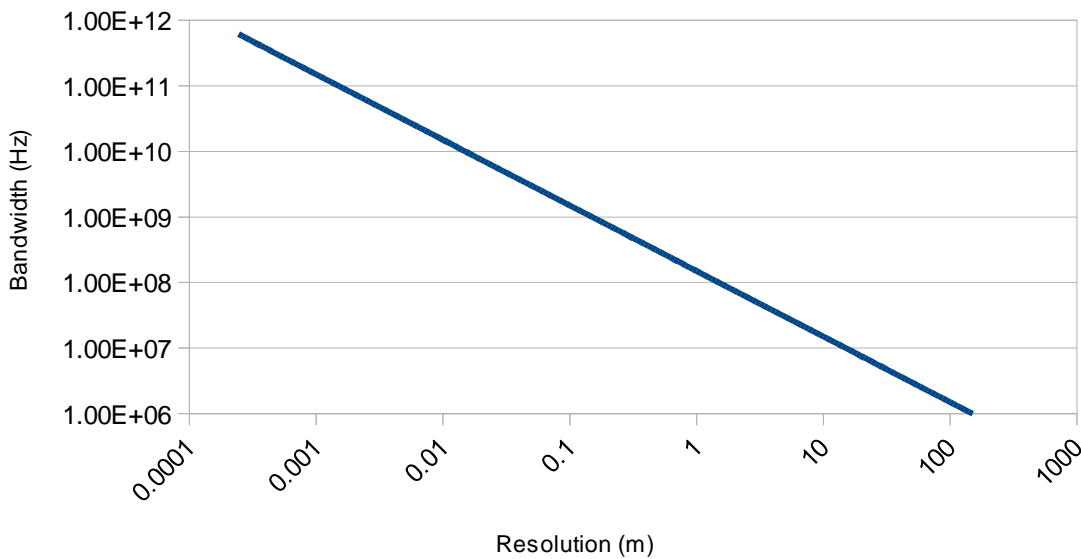


Figure 4.7: Radar resolution against bandwidth

To summarise, the greater the bandwidth the better the resolution and in this case the absolute frequency of the sweep is only relevant for the hardware required (Andrews et al., 2009). Due to ease of implementation, availability of parts and the equivalence of the measurements, stepped FMCW radar was chosen for active target illumination.

4.4 Atmospheric Signal Attenuation

Atmospheric attenuation of electromagnetic waves is frequency dependent. In the lower frequency microwave or millimetre ranges, this is limited to specific absorption lines, where attenuation is due to scattering and absorption by atmospheric particles (Crane, 1980; Liebe, 1989). Three discrete regimes of scattering based on frequency wavelength and atmospheric particle size are shown in Figure 4.8.

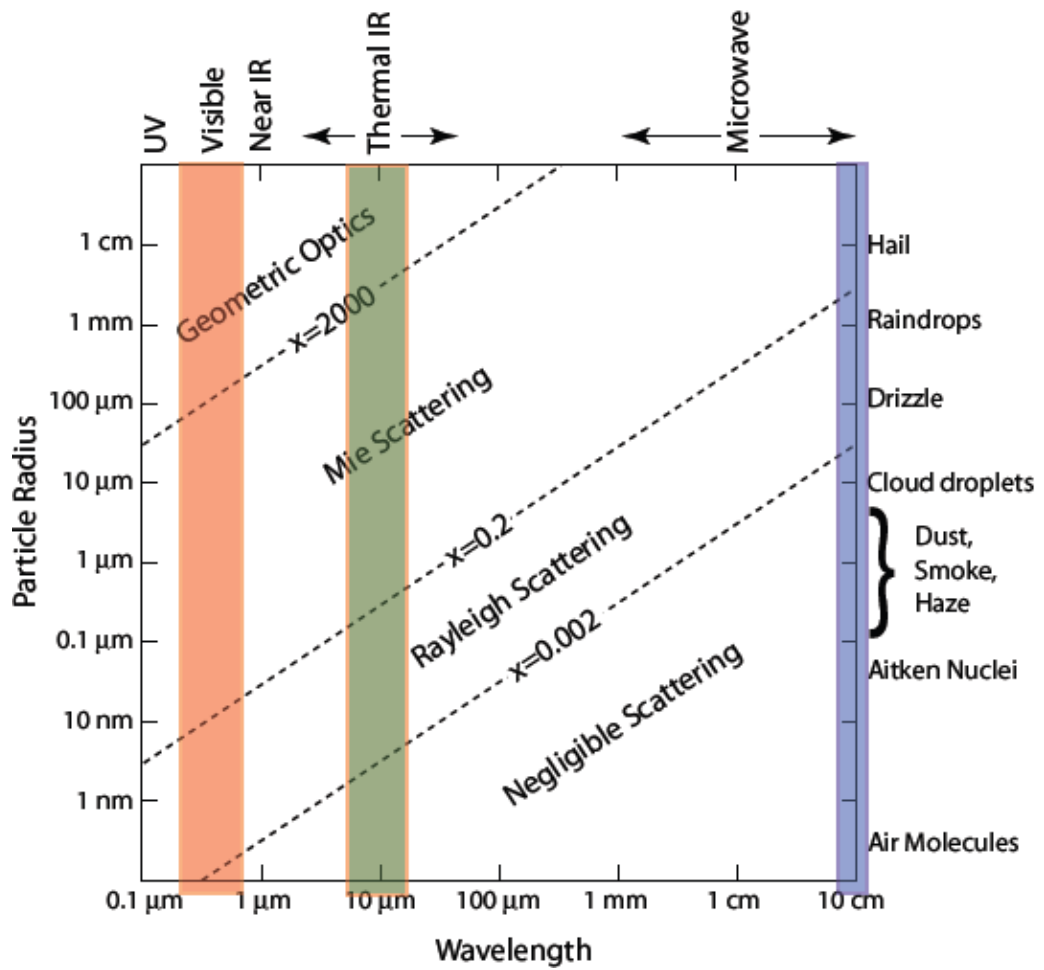


Figure 4.8: Geometric, Mie, and Rayleigh atmospheric scattering regimes

The normalised size x is defined as:

$$x = \frac{2\pi r}{\lambda} \quad (4.19)$$

where r is the characteristic dimension of the object and λ is wavelength.

Figure 4.9, taken from (Appleby & Wallace, 2007) shows atmospheric attenuation across the EM spectrum, at sea level based on current models with rain = 4 mm/h, fog = 100m visibility, STD (standard atmospheric) = 7.5 gm/m³ water vapour and 2 × STD (humid conditions) = 15gm/m³ water vapour.

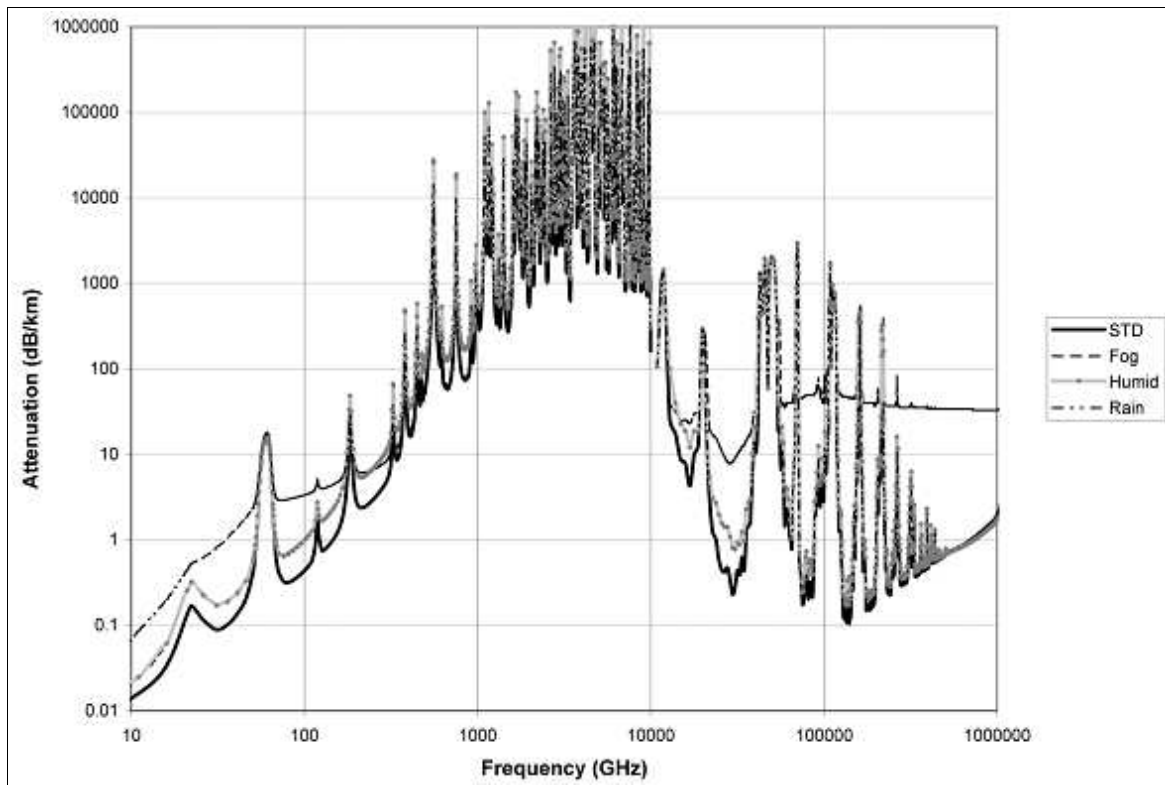


Figure 4.9: Atmospheric attenuation across the EM spectrum at sea level

Except for the spikes in attenuation at 22 GHz and 63 GHz due to water and oxygen respectively, the general trend is of increasing attenuation until 10 THz, beyond which several atmospheric windows exist. Therefore it is advantageous to operate at lower frequencies. Figure 4.10 taken from (Cafe, 2008) focuses on these lower frequencies and breaks down the contributions of oxygen and water so their effects can be seen more easily.

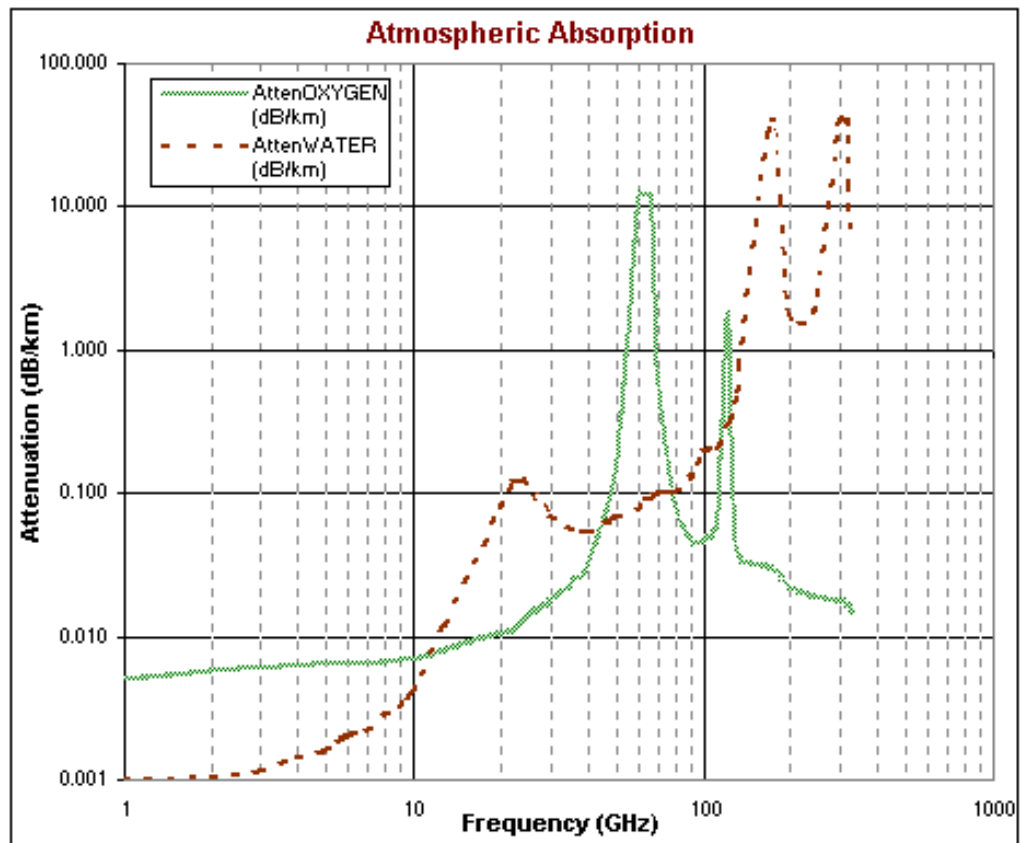


Figure 4.10: Atmospheric absorption 1 GHz to 1 THz

Under standard conditions, worst case atmospheric attenuation in the 14 – 110 GHz frequency band, is approximately 0.2 dB due to oxygen for a target at ten metres.

Atmospheric attenuation would start to be a problem if the device operated above 500 GHz. Comparatively, the attenuation due to clothing is expected to be greater.

4.5 Material Attenuation and Transmittance

Data on the attenuation effects of clothing and different fabrics at mm-wave frequencies is available beyond 100GHz in (Dunayevskiy et al., 2007; Gatesman et al., 2006; Dickinson et al., 2006; Bjarnason et al., 2004), but in 2008 information below this frequency was lacking. Therefore it was necessary to obtain appropriate data for a variety of fabrics below 100GHz, so the optimum operating band and power levels for item detection can be

identified. The process involved measuring the transmittance of a selection of fabrics at different angles of incidence for frequencies between 14 and 110GHz, using the methods outlined in Chapter 3 and (Harmer et al., 2008).

Figure 4.11 shows the apparatus seen from the side and consists of a frequency modulated source, a frame to hold the sample, a rotational table to turn the sample in the beam and finally a receiver to measure the signal passing through the sample. The purpose for this configuration is to test the relative attenuation of different materials at different frequencies and angles.

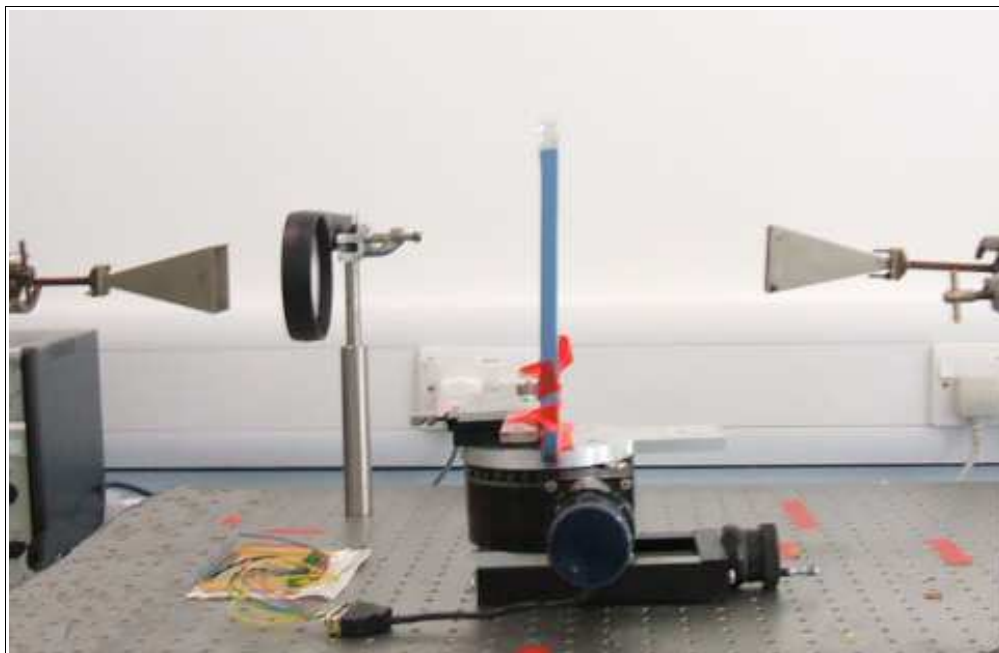


Figure 4.11: Side view of material transmittance experiment

The rotational table is used to easily measure the response of the material under test at different angles, between 0° and 75° in 5° increments. The software was created in LabVIEW. The apparatus produced the data for Harmer et al., (2008) and a proposed paper by Southgate et al., (2008) investigating the EM properties of commonly worn fabrics.

Without an automated means of rotating the sample, collection of data on numerous materials at many repeatable angles would be tedious and error prone. Figure 4.12 shows the experiment part way through measurement of a denim sample.



Figure 4.12: Material transmittance experiment – part way through denim measurements

A stepper motor controlled rotating stage would address this issue and is described next.

During an experiment to measure the permittivity of fabrics (Harmer et al., 2008) it is necessary to examine an object from an array of angles, because of structure and surface texture. This could be achieved by manually rotating the object or automatically using a rotational table such as the one shown in Figure 4.13.

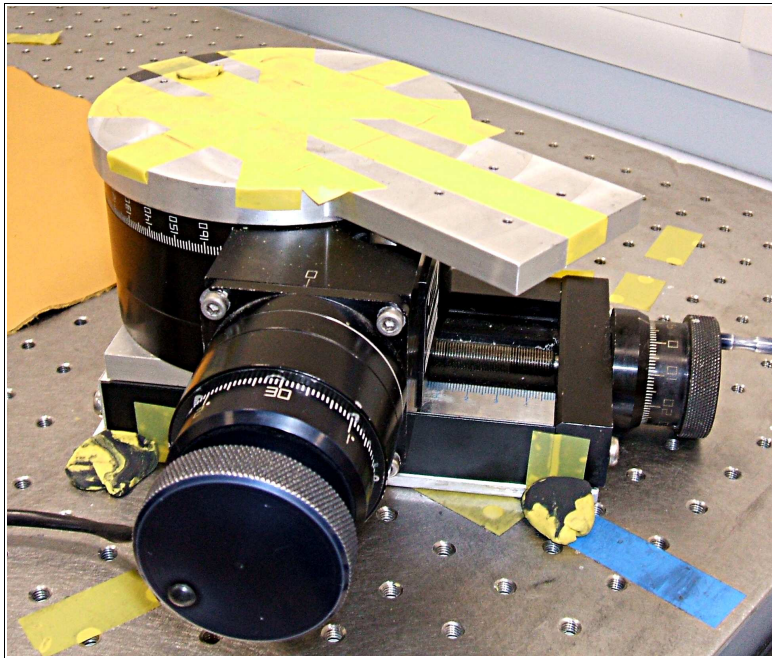


Figure 4.13: Stepper motor controlled rotational table

A driver board controlled by a Microchip PIC microcontroller was designed and built to specifically power and control this rotational table. The driver board is shown in Figure 4.14.

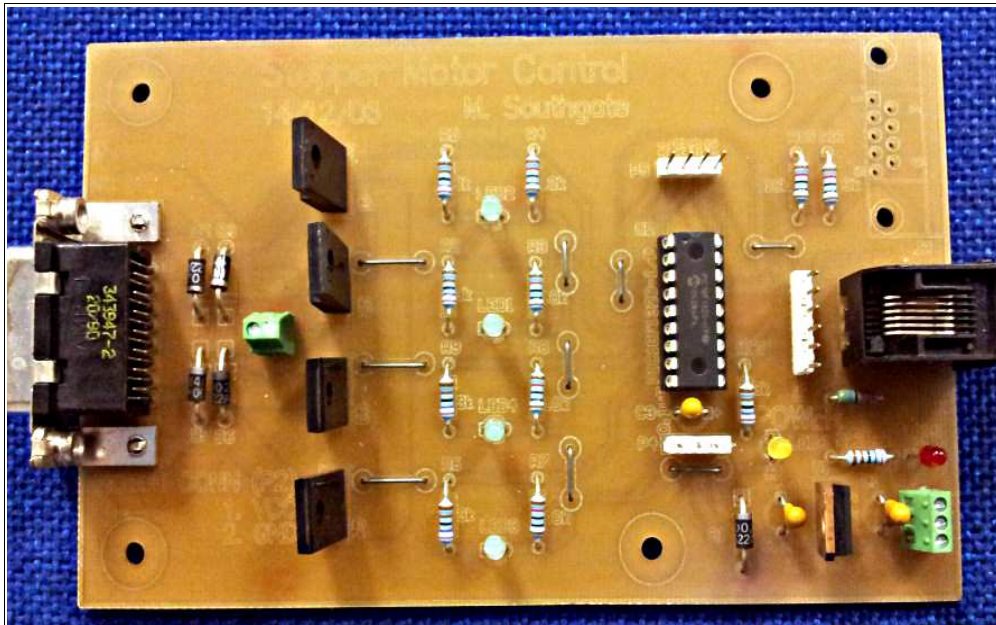


Figure 4.14: B194 Rotational table driver board

The circuit uses an 8-bit PIC18F1320 micro-controller and discrete power transistors to switch power to the coils of the stepper motor and worked very well. Implementing the design and having the ability to change the firmware allowed full and deterministic control of a stepper motor over a ubiquitous RS232 connection.

The list of materials tested included commonly worn fabrics and other materials of interest:

- a. Cotton shirt
- b. Cotton polyester shirt mix – stripped blue, black and white
- c. Denim – two lots pale blue and dark blue
- d. Kevlar
- e. Leather – colours: natural, red, white and yellow
- f. Paper white 85g/m²
- g. Polar fleece blue
- h. Polyester film
- i. Paraffin wax block 8cm square

An analysis of measurements for from the 14 – 40 GHz experiment can be found in (Harmer et al., 2008). The summed measurements of transmittance for each material are shown in Figure 4.15 for frequencies between 75 and 110 GHz. The radiation was normally incident for this data. The measurements show that Kevlar is the most attenuating material, but apart from personal body armour, this is not a commonly worn material. Of the most commonly worn materials red leather was the most attenuating of all the fabrics tested and represents the baseline to aim for when detecting concealed objects. The case for red leather is discussed next.

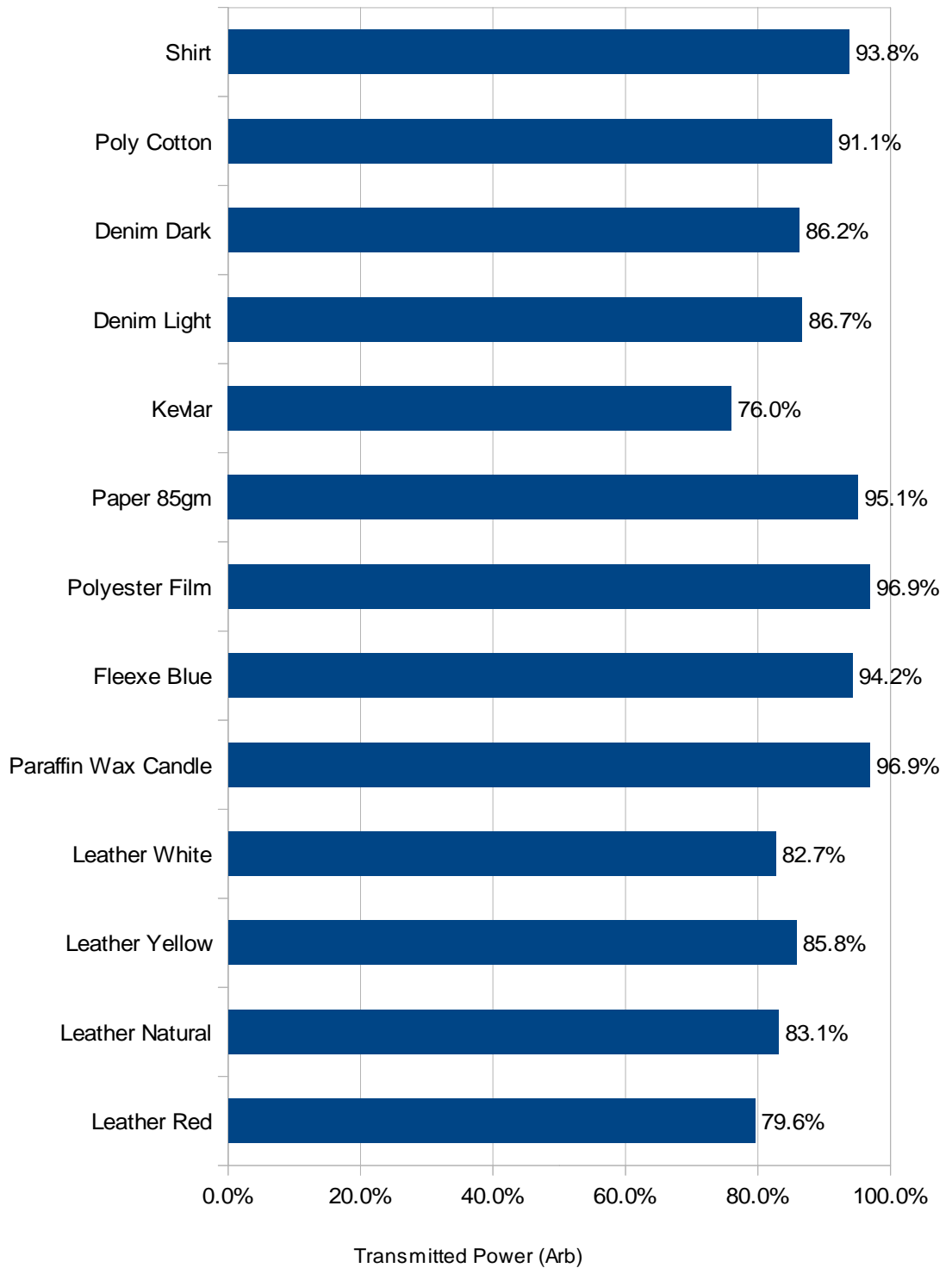


Figure 4.15: Energy transmission through various materials, normally irradiated

Since red leather gave the smallest normalised signal levels at different frequencies for a commonly worn dry fabric, it represents the most difficult material through which to detect a threat and helps establish the level of sensitivity needed in the first prototype.

The effect of applying water to a fabric sample to simulate wet conditions gave results with higher levels of attenuation. The different leather samples were similar, except for their colour. It was therefore concluded that the pigment was probably responsible for the different levels of attenuation. Natural iron oxide (Fe_2O_3) pigments are used for in material colouring processes to produce a red colour. A by-product of this process is an increase in the metal content of the leather that could explain the increased levels of attenuation. Hence the unanticipated impact of material colouring on transmission performance was identified and must be considered. Figures 4.16 and 4.17 show the measurements the background and red leather between 75 and 110 GHz (Southgate, 2009).

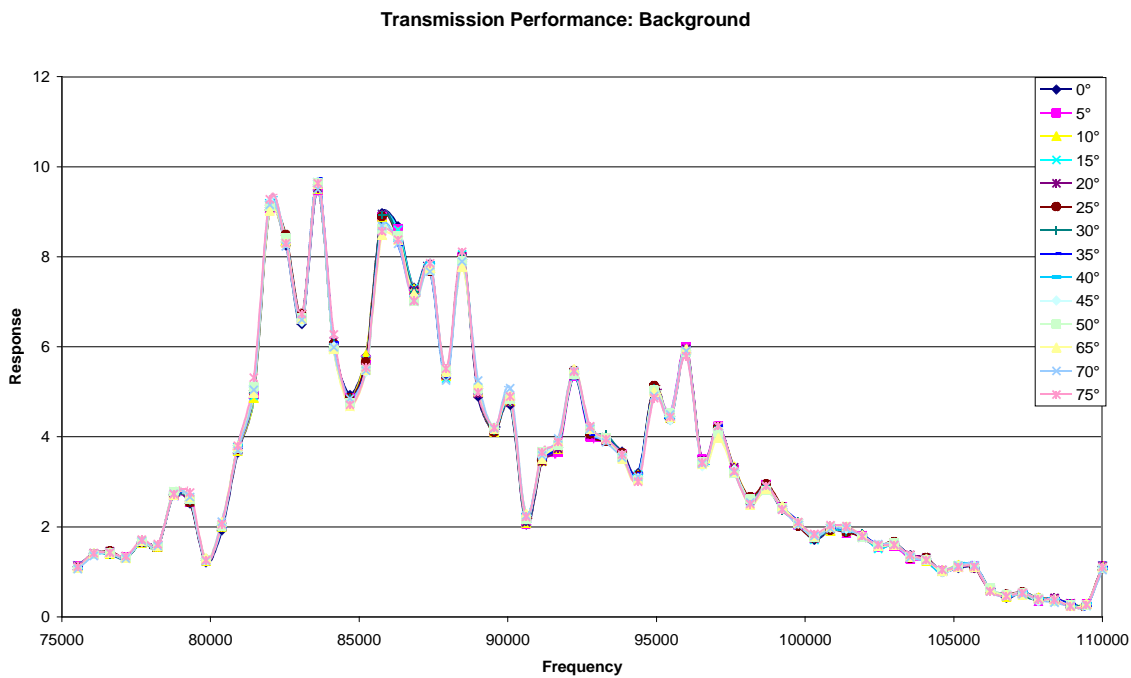


Figure 4.16: Background measurement prior to red leather energy transmittance experiment

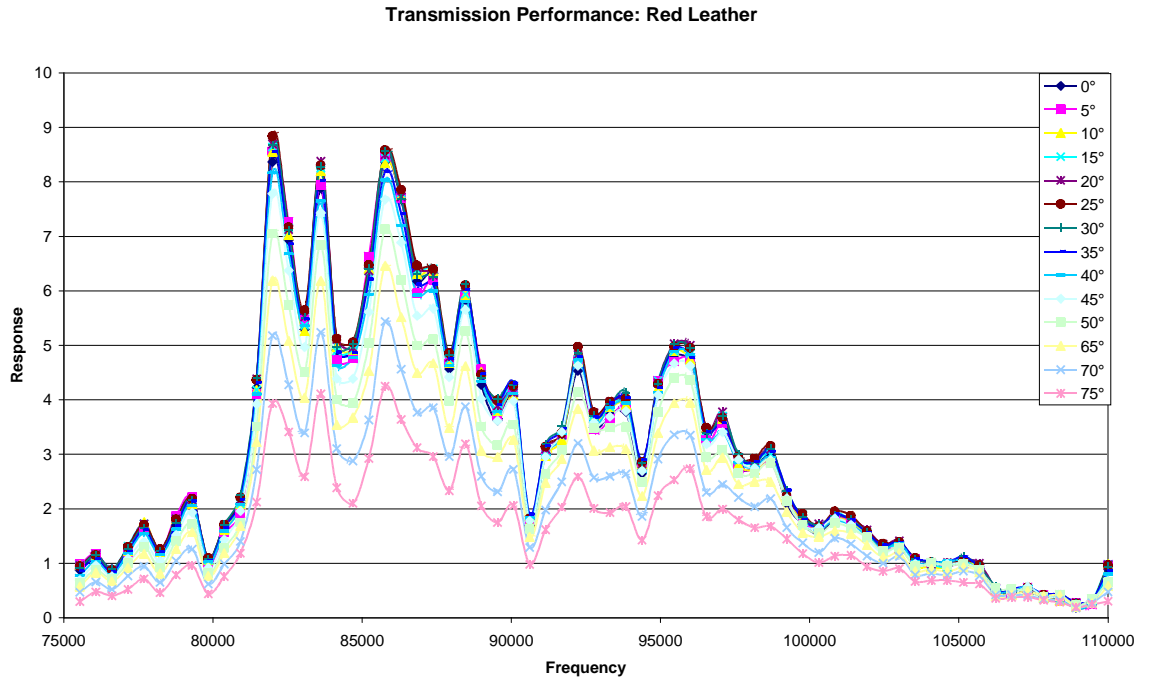


Figure 4.17: Energy transmittance for red leather between 75 and 110 GHz

Figure 4.18 shows the normalised response for the red leather.

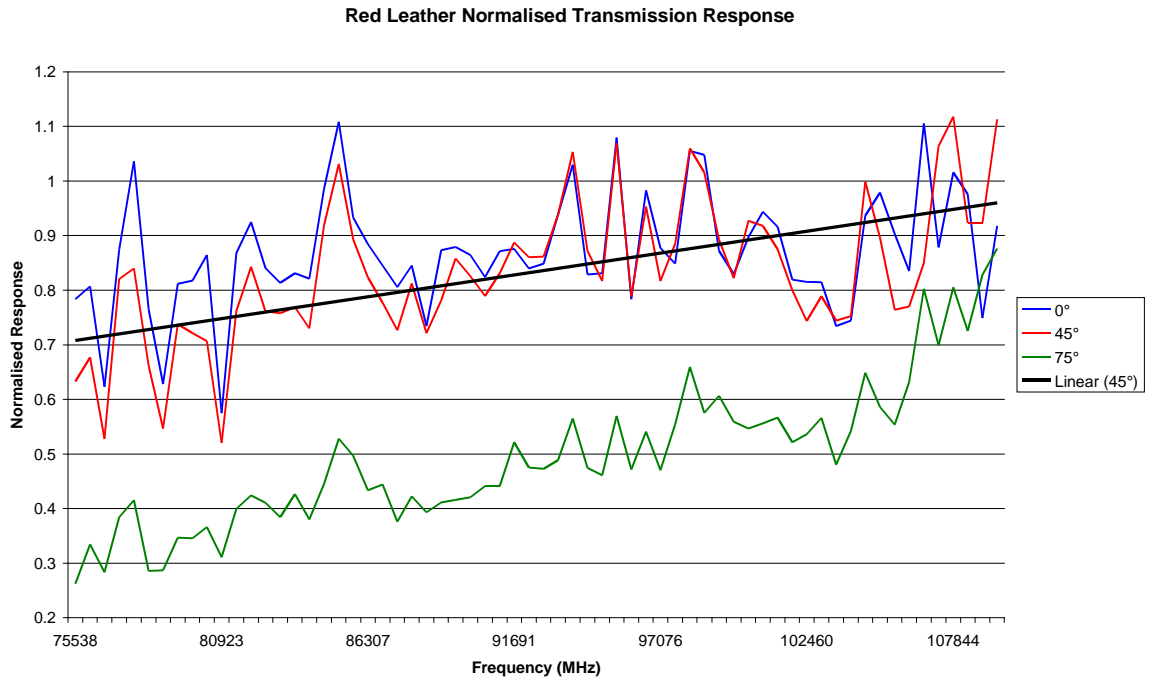


Figure 4.18: Normalised response of red leather between 75 and 110 GHz

After examination of the results for the different fabrics, it was concluded that an optimal window does not exist in range of frequencies that would give significantly better results, than the average across the range.

The benefit of this conclusion is the absence of any restriction on operating frequency for the detection system, although this early work was restricted to lower frequencies (Andrews et al., 2009). This is a definite advantage for systems using active swept frequency radar since the wider the swept frequency range, the finer the spatial resolution (Immoreev & Taylor, 2005).

4.6 Detection of Dielectrics

Most non-conducting materials reflect up to 25% of a 75 to 110 GHz signal in air. Water reflects 40% (Rønne & Keiding, 2002) and human skin has similar properties, but with a lower reflectance (Pickwell et al., 2004). Therefore a large plastic bottle full of water can be used to approximate a human torso (Bowring et al., 2007b). Metals are almost perfect reflectors.

The Fabry-Perot Interferometer (FPI) was used extensively during the early stages of this research project to measure the properties of dielectrics. The contribution to knowledge gained through using this enhanced the control and analysis software available for faster data collection.

Interference between the front and back surfaces of a dielectric slab forms the basis of detecting explosive layers, by generating an oscillatory signal in the frequency domain. The interference pattern is a result of the combination of reflections from the parallel sides of the dielectric, acting in a similar way to the plates of a FPI. Reflections occur due to a step change in refractive index between two dielectric materials creating a partial mirror reflecting a fraction of the incident radiation, see equation 4.20.

$$R = \left(\frac{n_1 - n_2}{n_1 + n_2} \right)^2 \quad (4.20)$$

Where R is the fraction of the incident wave power reflected and n_1 and n_2 are the refractive indices for the interface materials. The two partially reflecting surfaces act in a similar fashion to the two fixed plates of an etalon resulting in the oscillatory frequency response. The frequency difference of successive cycles δf of oscillation is inversely proportional to the thickness of the dielectric (Bowring et al., 2008)

$$\delta f = \frac{c}{2} l_n = \frac{c}{2l_s n} \quad (4.21)$$

Therefore the lowest maxima is at:

$$f = \frac{c}{2l_s n} \quad (4.22)$$

where c is the speed of light, n is the refractive index of the material, l_s is the physical thickness of the sample. This technique is applied to measuring a PTFE disc in the next section.

For a transmitted signal $E_0 e^{-j\omega t}$, return signal E_R , primary target distance L and amplitude reflection r :

$$|E_R|^2 = \left| r E_0 e^{-j\omega t} e^{\left(\frac{2j\omega L}{c} \right)} \right|^2 \quad (4.23)$$

where $\omega = 2\pi f$, f is frequency and c is the speed of light. A detector measuring only power will measure $|E_R|^2$, which for a single interface does not vary based on frequency.

However for two interfaces located at L_1 and L_2 , the reflected power is:

$$\begin{aligned} |E_R|^2 &= \left| r_1 e^{\left(\frac{2j\omega L_1}{c} \right)} + r_2 e^{\left(\frac{2j\omega L_2}{c} \right)} \right|^2 \\ &= |r_1|^2 + |r_2|^2 + 2|r_1||r_2| \cos\left(\frac{2\omega}{c} (L_1 - L_2) \right) \end{aligned} \quad (4.24)$$

This contains a cosine term that produces an oscillating response, proportional to the difference in L_1 and L_2 , with respect to frequency. By Fourier Transforming this response it is possible to extract the apparent distance between the two interfaces.

This analysis can be adapted to provide the absolute range to a target at a distance L_2 and the first interface is at the transmitter, forming a cavity. Since the first interface is at the radar $L_1 = 0$:

$$|E_R|^2 = |r_1|^2 + |r_2|^2 + 2|r_1||r_2|\cos\left(\frac{2\omega}{c}(L_2)\right) \quad (4.25)$$

and if the frequency is being swept linearly with time t :

$$\omega = 2\pi \left[f_0 + \left(\frac{\delta f}{\delta t} \right) t \right] \quad (4.26)$$

then the frequency of the interference pattern is:

$$f_{if} = \frac{2L_2}{c} \left(\frac{\delta f}{\delta t} \right) \quad (4.27)$$

4.6.1 Measurements of a PTFE Disk Embedded with Mica

Figure 4.19 shows the interference pattern for a PTFE disk containing embedded mica of thickness 40 mm illuminated between 50 and 65 GHz.

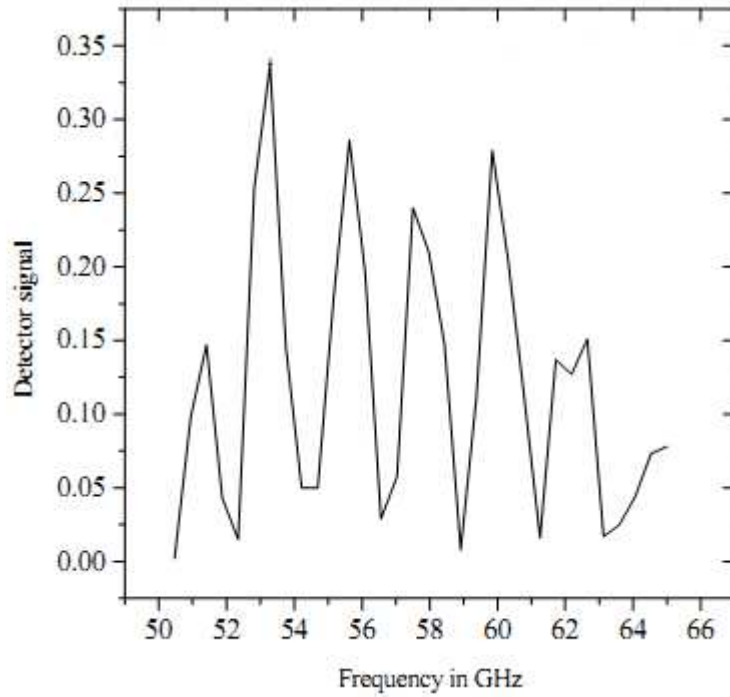


Figure 4.19: 50 - 65 GHz frequency response of a 40 mm thick PTFE disc with embedded mica

Applying Equation (4.22) to the 5 oscillations between 51 and 62 GHz the refractive index of mica embedded PTFE may be determined:

$$\delta f = \frac{c}{2nl_s} \quad (4.28)$$

$$\therefore n = \frac{3 \times 10^8 \times 5}{2 \times 0.04 \times (62 - 51) \times 10^9} = 1.70$$

The oscillations in the frequency domain relate to the optical depth of the dielectric and the existence of such a pattern is a clear indicator that a dielectric object is present. It is important that the range resolution of the system is better than the minimum optical depth of a explosive device for detection to occur:

$$\frac{c}{2\Delta f} \leq nl_s \quad (4.29)$$

A Fourier Transformation of the frequency data shown in Figure 4.19 generates a time domain/optical depth plot (Bowring et al., 2007a), giving an observed peak shown in Figure 4.20.

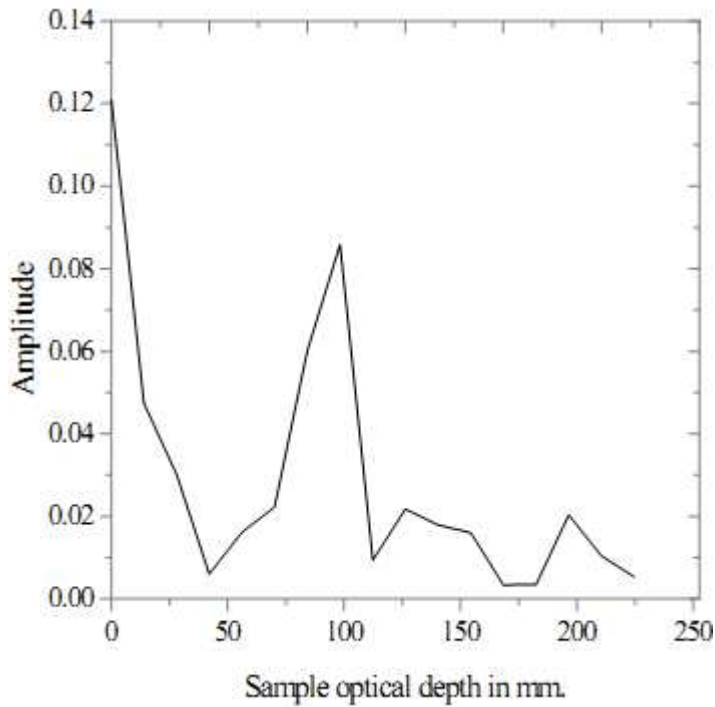


Figure 4.20: Fourier transformed frequency response of a 40 mm thick PTFE disc with embedded mica

The difference of the observed thickness from the measured thickness of 40 mm is a product of the mica in the sample with a refractive index of approximately 2, which may be compared to 1.44 for the PTFE matrix alone (Lamb, 1996).

The large non-zero frequency component generated by the variations in illumination power and receiver sensitivity is difficult to mitigate and obscures low optical depth measurements. Also it is significant that dielectric objects with irregular surfaces but parallel surfaces produce a sinusoidal oscillatory response in the frequency domain despite the additional scattering caused by the irregular surfaces (Bowring et al., 2007b).

An improvement in optical depth resolution could be achieved by increasing the frequency sweep and the maximum extent of separate dimensions measurable extent is a function of the number of frequency samples points taken:

$$d_{\text{extent}} = \frac{c(N-1)}{2\Delta f} \quad (4.30)$$

where c is the speed of light, N is the number of samples and Δf is the system bandwidth.

The disadvantage of this method is that the Fourier transform expects the datasets to be periodic (Smith, 1997). A distinct advantage of this method is that it is independent of absolute frequency, requiring only a frequency bandwidth to achieve a specific resolution. By changing the operational frequency band of the prototypes up to 75 – 110 GHz an optical depth resolution of better than 5 mm could be achieved.

4.6.2 Application to Non-Fragmentation Based Explosives

A practical illustration of this phenomenon uses air and paraffin wax. Paraffin wax has similar dielectric properties to plastic explosives (Lamb, 1996; Kemp et al., 2006; Hu et al., 2006). The refractive index of paraffin wax at 120 GHz is 1.48 with a imaginary component of 27×10^{-4} (Lamb, 1996). For a normally illuminated flat surface the coefficient of reflected power is 4% and since only 4% of the incident signal is reflected the signal strength rapidly diminishes, anything after the first reflection has little effect on the results. Figure 4.21 shows in three stages, the principal reflections and the quantities of interest are in bold:

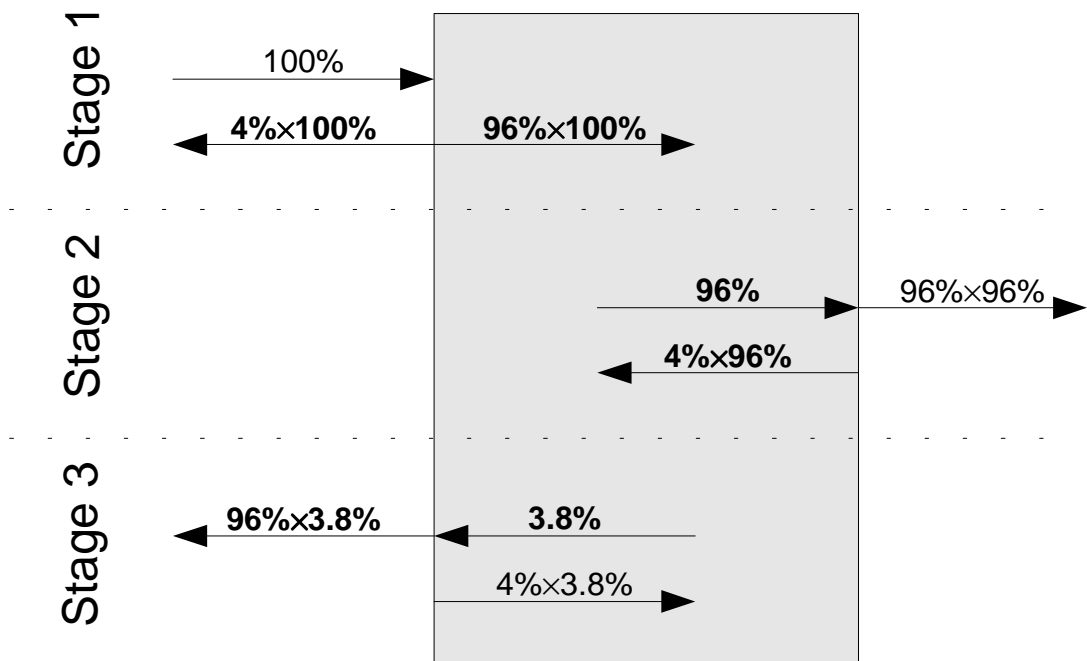


Figure 4.21: Principal reflections of an EM signal caused by a paraffin wax block

The first stage shows the original incident wave, the reflected component and the transmitted component (96%). Stage two occurring at the back surface of the dielectric, shows most of the signal passing out of the dielectric and a small internal reflection (4% of 96%). Step three sees most of signal reflected in stage two, passing back out of the dielectric towards the receiver (96% of 3.8%). The EM waves add and interfere when measured on the detector diode. Depending upon three variables, the thickness of the dielectric, the dielectric's refractive index and the wavelength of the radiation interference will occur causing a sinusoidal response. If the distance between the partial reflectors is equal to:

$$\Delta d = \frac{k \lambda}{2} \quad (4.31)$$

where k is an integer and λ is the wavelength of the radiation then all the waves passing through are in phase and a maximum signal will be measured. If the distance between the surfaces is not a multiple of $\lambda/2$, then some degree of destructive interference will occur and the signal will not be a maximum. Figure 4.23, shows detector voltage representing measured power against frequency (sample number) for a linearly stepped frequency source.

This simple example considers a uniform sample of loss-free material, since signal attenuation has no effect upon the the optical depth of the object.

4.6.3 Simulated Plastic Explosive in Isolation

This technique can be applied to a dielectric block, simulating a plastic explosive device. Paraffin wax shares similar dielectric characteristics with conventional explosives and has been used as a replacement in experiments (Farinelli & Roth, 2003; Bowring et al., 2007b).

This technique can be applied to objects that are outside the Fabry-Perot interferometer (FPI), since at any discrete change in refractive index (and depending on the angle of incidence) portions of the EM wave are coupled into and reflected at the boundary.

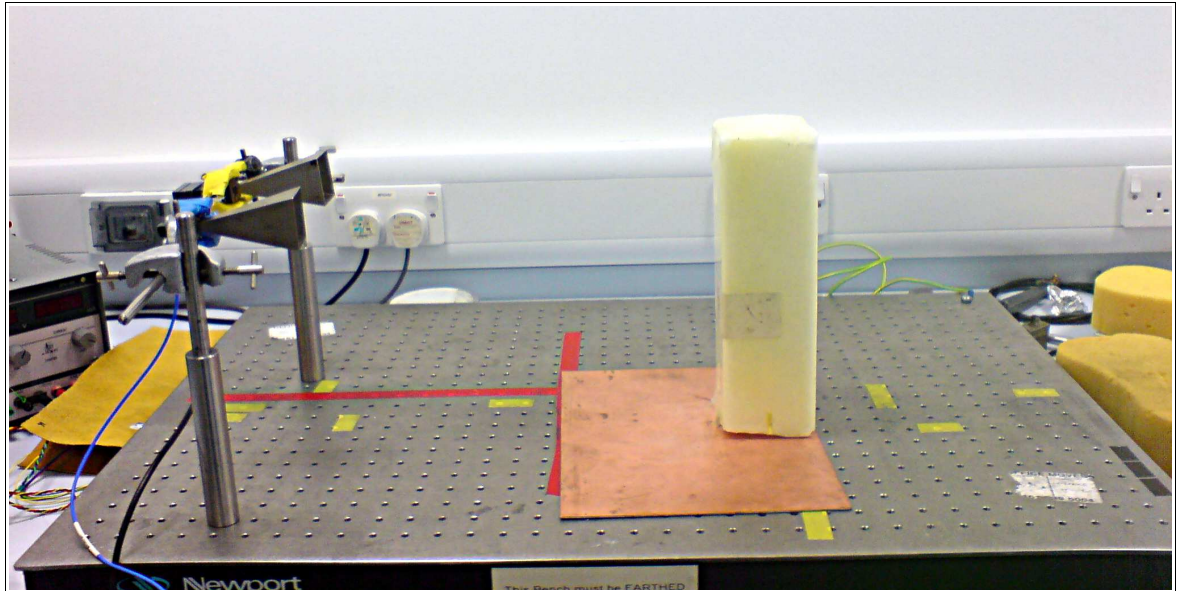


Figure 4.22: 8 cm by 8 cm calibration wax block used for antenna alignment

By analysing the frequency response of an object across a wide band, it is possible to determine its dimensions if the object's dielectric properties are known. Figure 4.22 shows a wax block used to align the apparatus. It has a simple shape with flat parallel sides, ideal for testing the adapted FPI technique. The response is shown in Figure 4.23 from Southgate (2009).

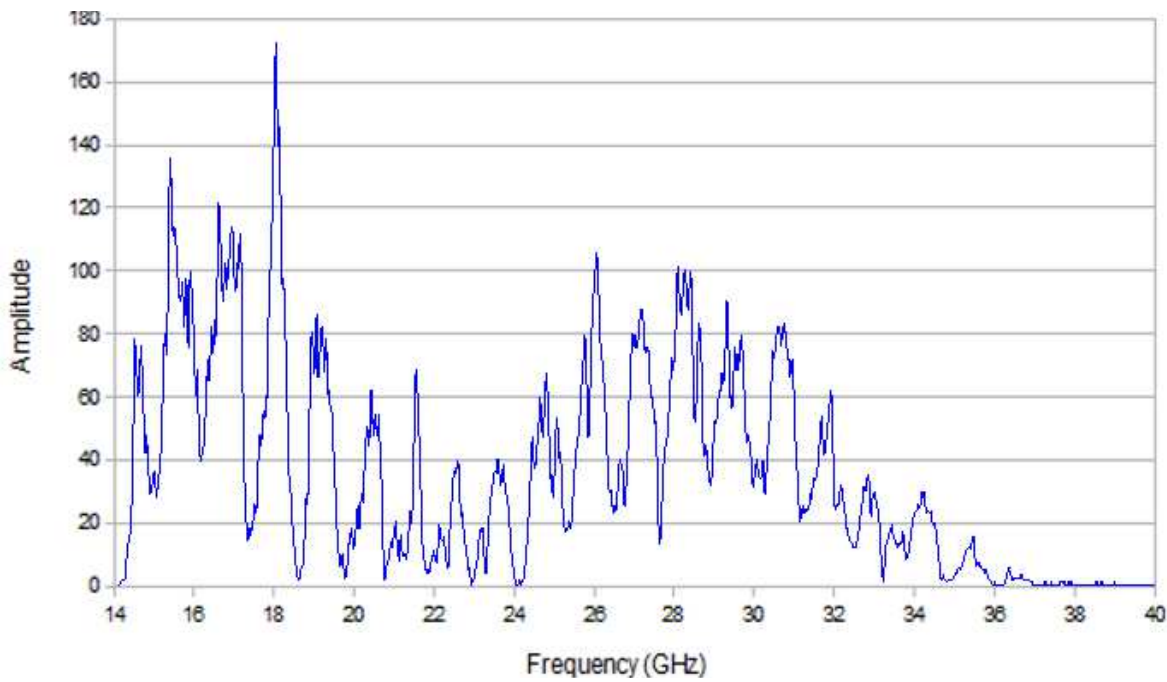


Figure 4.23: Sinusoidal response of paraffin wax block

Performing an adapted Fourier Series transform on this dataset and after removing the DC component (0Hz) a peak can be seen at 12cm in Figure 4.24. The FFT was adapted to directly output the optical depth for paraffin wax. The peak corresponds not to the thickness of the wax block, but instead to its optical thickness (actual thickness 8cm multiplied by its refractive index of approximately 1.5, giving 12cm).

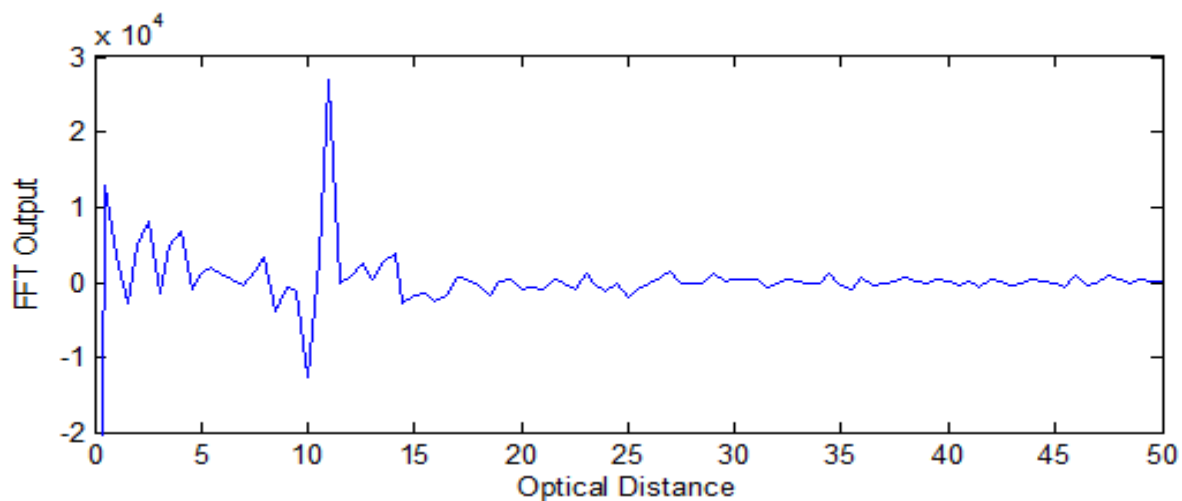


Figure 4.24: Result of adapted Fourier Transform on FMCW data showing the optical depth of a paraffin wax block of dimensions 8 cm by 8 cm

This happens because the front and back faces of the wax block act as boundaries or step change in refractive index. Peaks in the response occur when the EM radiation is at a frequency of wavelength similar to an integer multiple of the optical thickness of the wax block and troughs when the reflected wave is out of phase with the incoming wave. The distance to the wax block is not determined using this technique.

4.6.4 Dielectric with Reflective Background (Simulated Body)

To more fully simulate the effects of an explosive device strapped to the torso, the wax block from the previous experiment was positioned in front and against a large water bottle full of water used to simulate a human torso. The use of a large water bottle as a simulated human torso has been adopted by other researchers (Kapilevich & Einat, 2010), due to the similarity between the dielectric properties of the human torso and water.

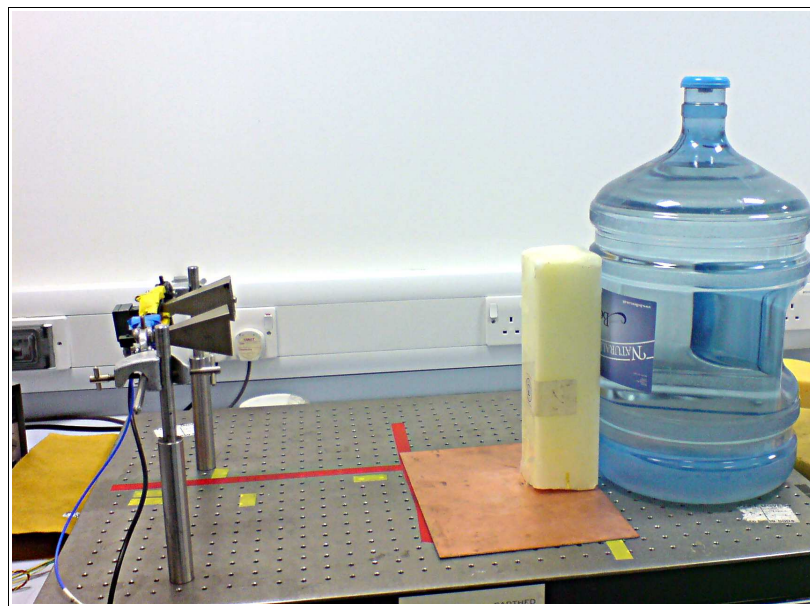


Figure 4.25: Wax block with full water barrel backing simulating a human torso

The raw data collected during this experiment is shown in Figure 4.26 and applying the adapted Fourier Transform, produces Figure 4.27.

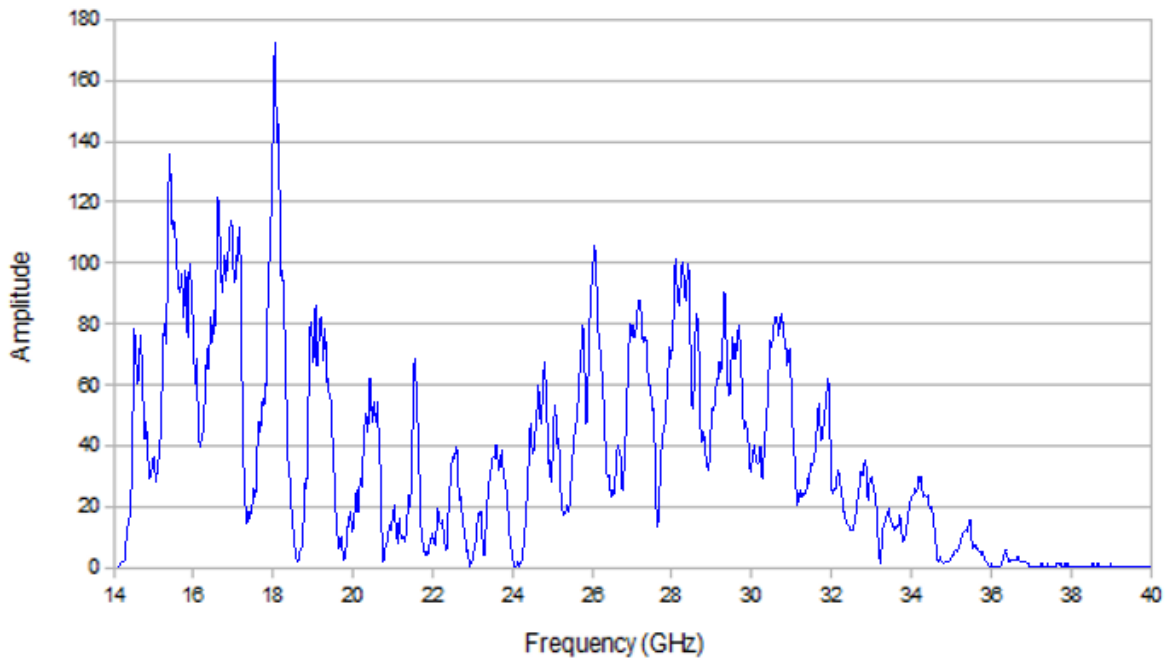


Figure 4.26: Paraffin wax block of dimensions 8 cm by 8 cm backed by a full water bottle backing

The resulting plot shown in Figure 4.27 is similar to that for the wax block alone, with the system seeing an optical depth of 120 mm, except for the large low frequency variation seen in the raw data plot which produces a peak in the optical depth plot at 14mm. Again the refractive index of paraffin wax was 1.5, which explains why the peak for the 80 mm square wax block appears at 120 mm; the peak at 14 mm is attributed to the shape of the ribbed wall of the water bottle, which causes a gap of this dimension between the wax block and the water.

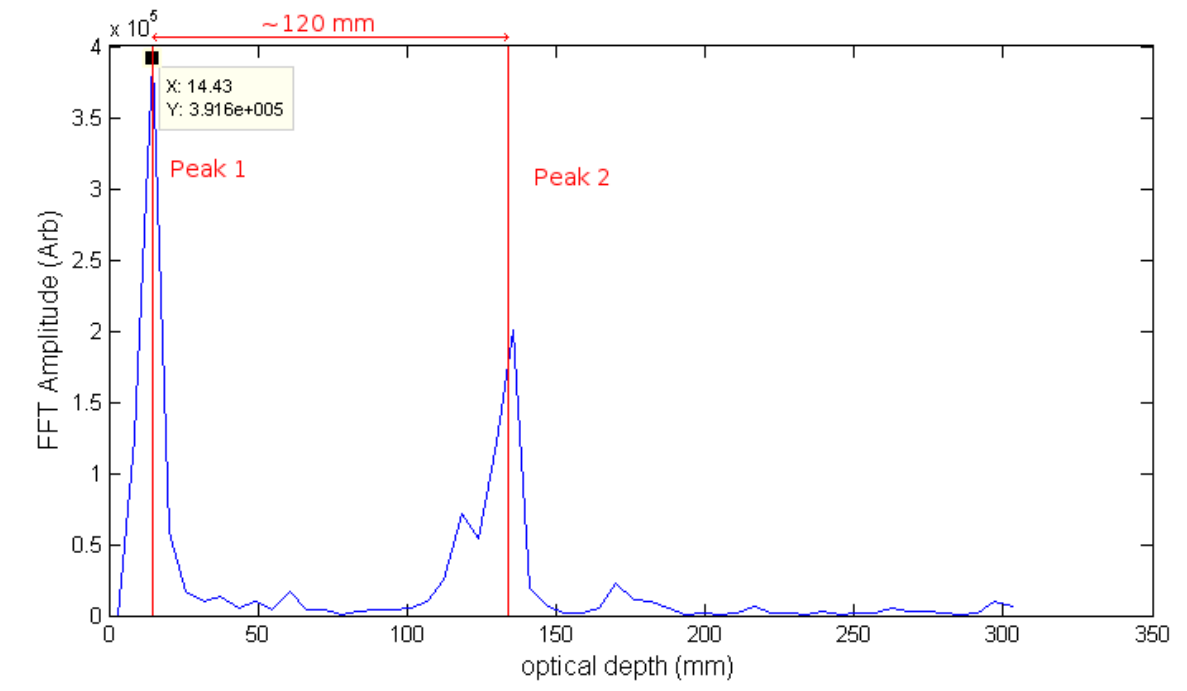


Figure 4.27: Paraffin wax block backed by a full water bottle optical depth plot

Although the data shown in Figure 4.26 has a distinct oscillatory nature, there are problems converting this data into distinct optical depths. The experimental data in addition to a zero offset, contains the source and receiver characteristics. The zero offset can be removed numerically while the variations in source and receiver characteristics can be modelled.

Direct power detection can be used to measure the distance between interfaces, but since the phase of the reflected signal is not compared with the phase of the source only relative time and hence distance measurements are possible. Everything in the beam is measured simultaneously and it is not possible to gate out objects in the beam, whereas a heterodyne based radar with access to phase information can determine the range, permitting time gating of the signal to remove clutter.

4.6.5 Observation of a Water Backed Dielectric Layer Between 75 – 110 GHz

Figures 4.28 and 4.29 using a 75 – 105 GHz system show the results for a rectangular block of paraffin wax between 25 – 30 mm thick, simulating a plastic explosive layer. The graph shows the wax target alone, mounted on a full water barrel (in the case of Figure 4.25) and strapped to a human torso.

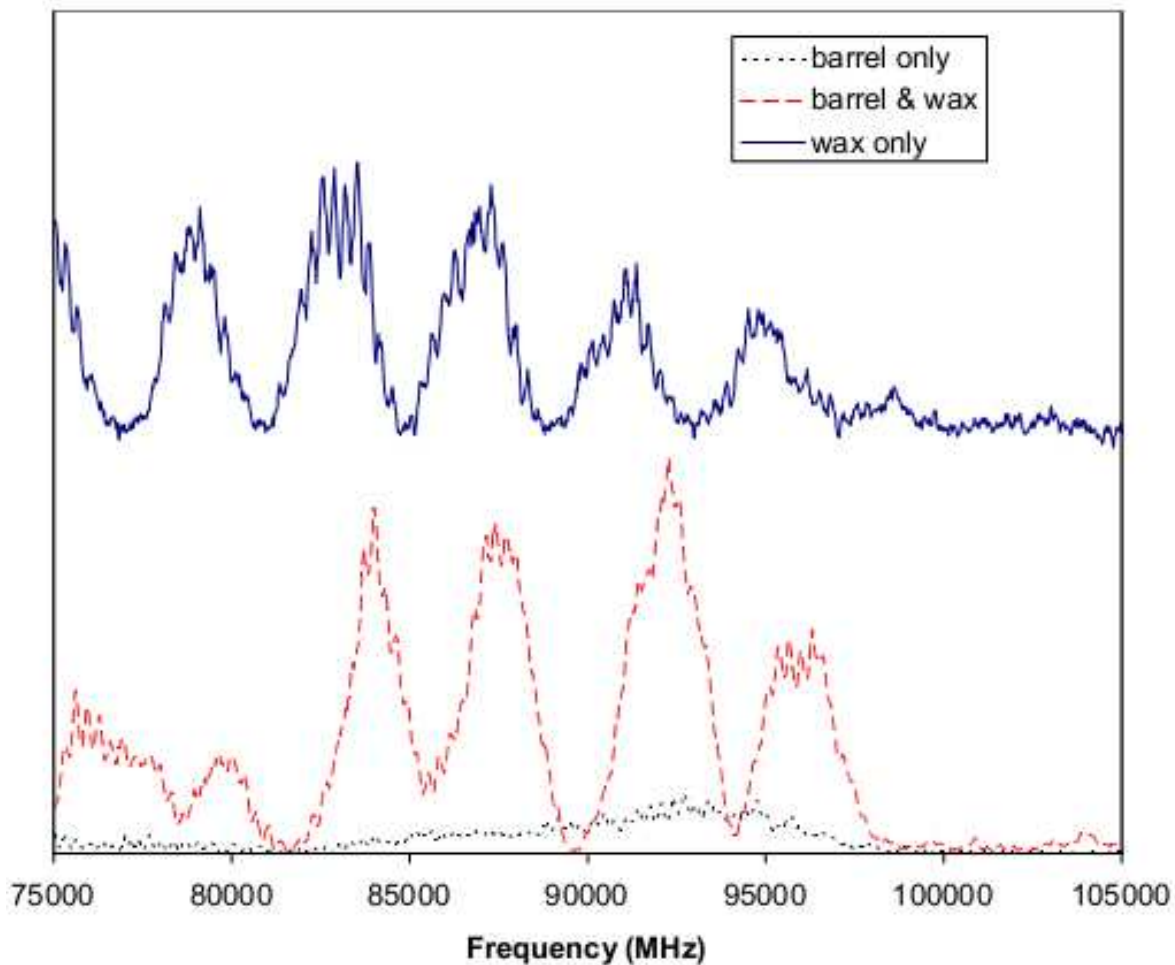


Figure 4.28: Frequency spectrum of a barrel only, wax block and barrel and wax block only (offset vertically)

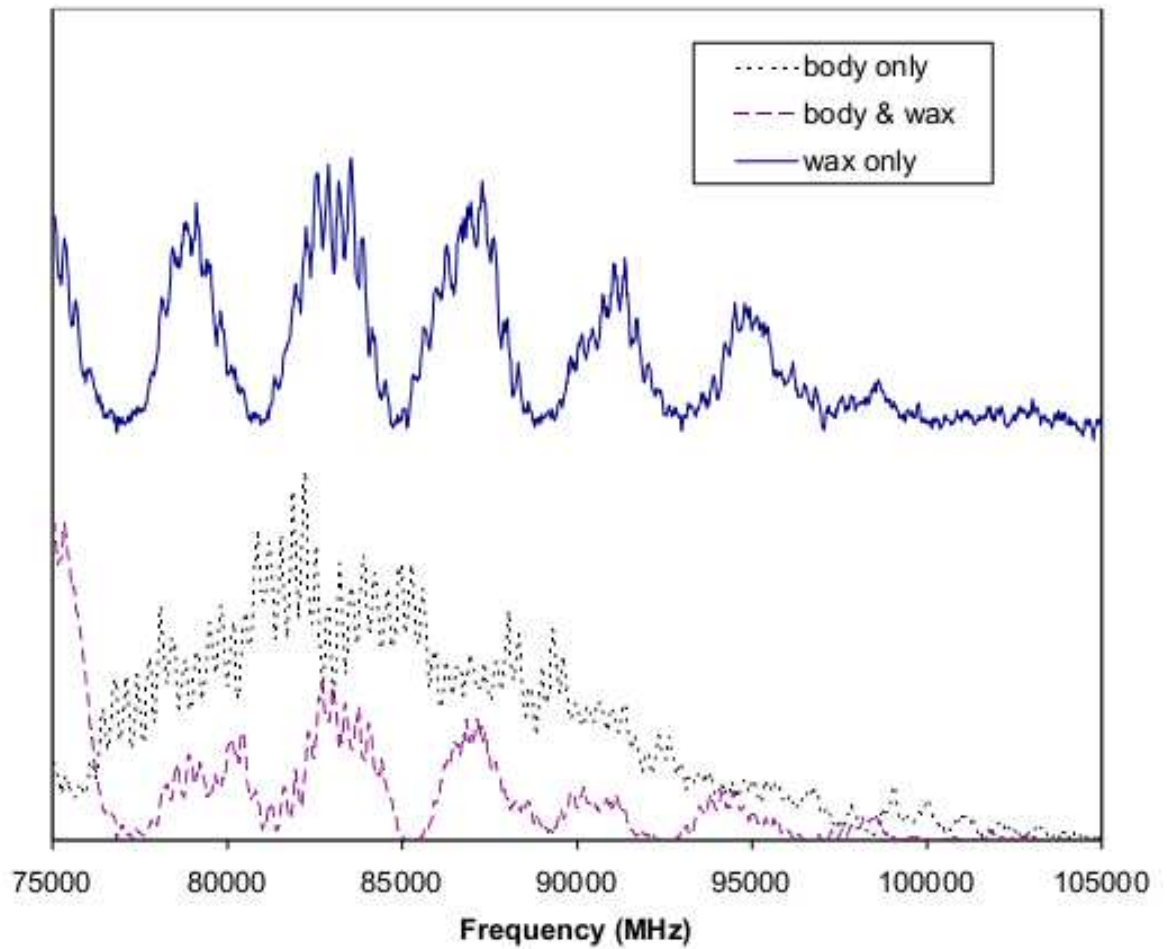


Figure 4.29: Frequency spectrum of a body only, wax block and human body and wax block only (offset vertically)

The oscillation in the data due to the wax block is clearly seen even when backed by an aqueous body. Transforming the data into an optical depth produces a clear peak at 40 mm corresponding to the wax block, shown in Figures 4.30 and 4.31.

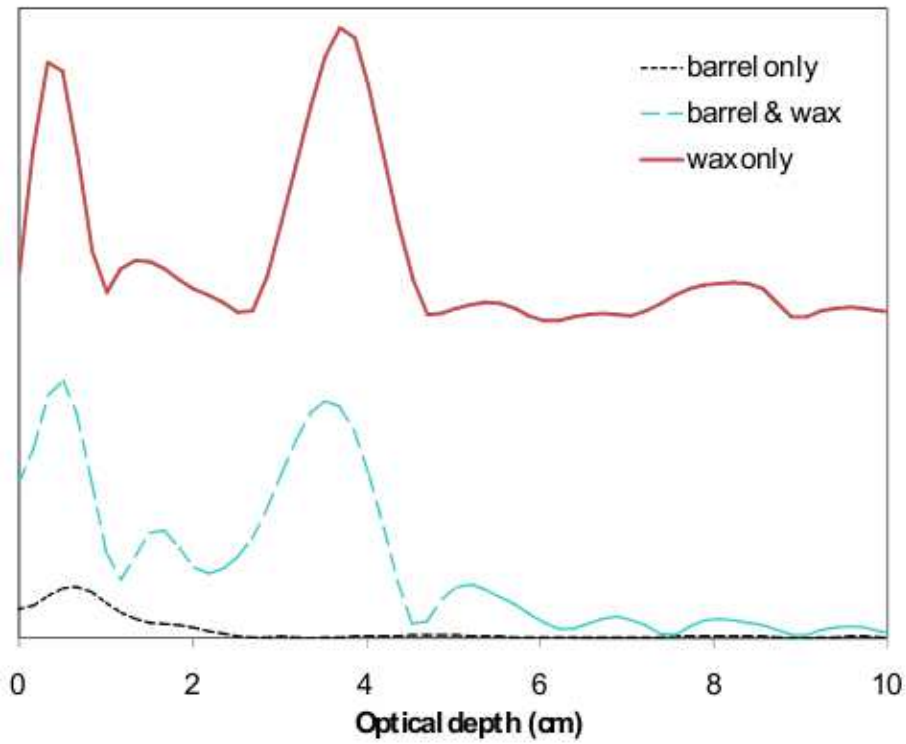


Figure 4.30: Fourier transformed optical depth for barrel only, wax block and barrel and wax block only (offset vertically)

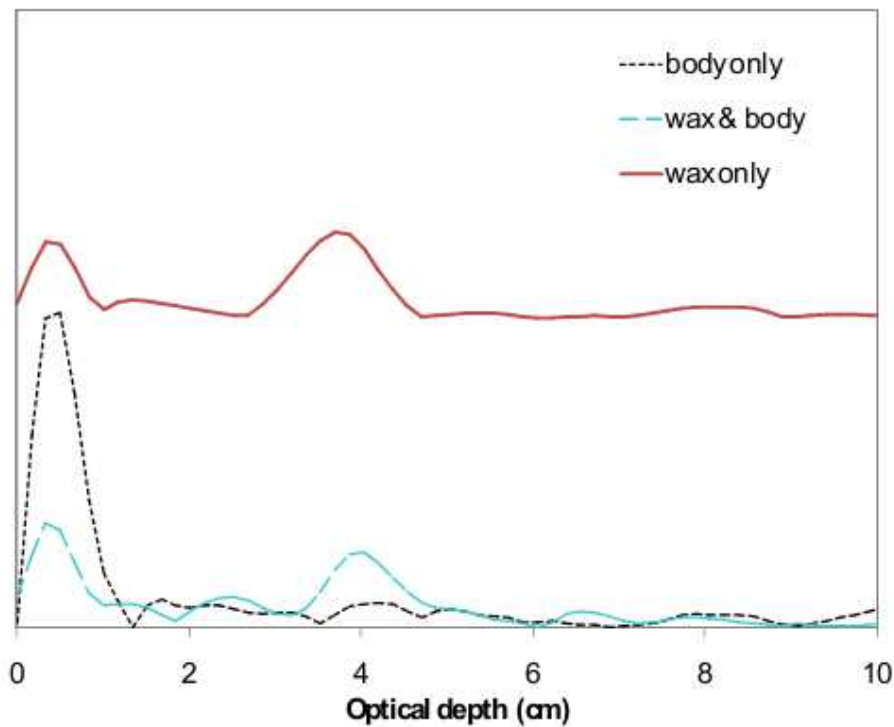


Figure 4.31: Fourier transformed optical depth for body, wax block and body and wax block only (vertically offset)

This may be compared with results taken using a VNA (Agilent E8363B/N4420B). This heterodyne measures the range dependent response from the same targets and by sweeping from 14 to 40 GHz. Figure 4.32 and 4.33 shows the range gated responses for body, barrel and wax.

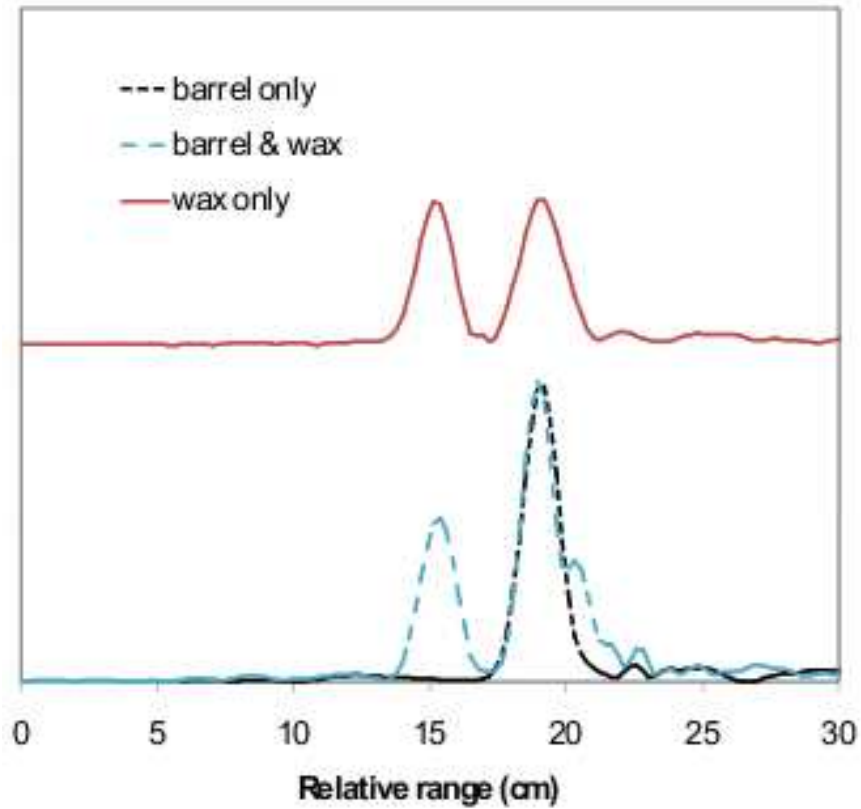


Figure 4.32: Range gated response from barrel only, wax block and barrel and wax block only (offset vertically) taken using the VNA

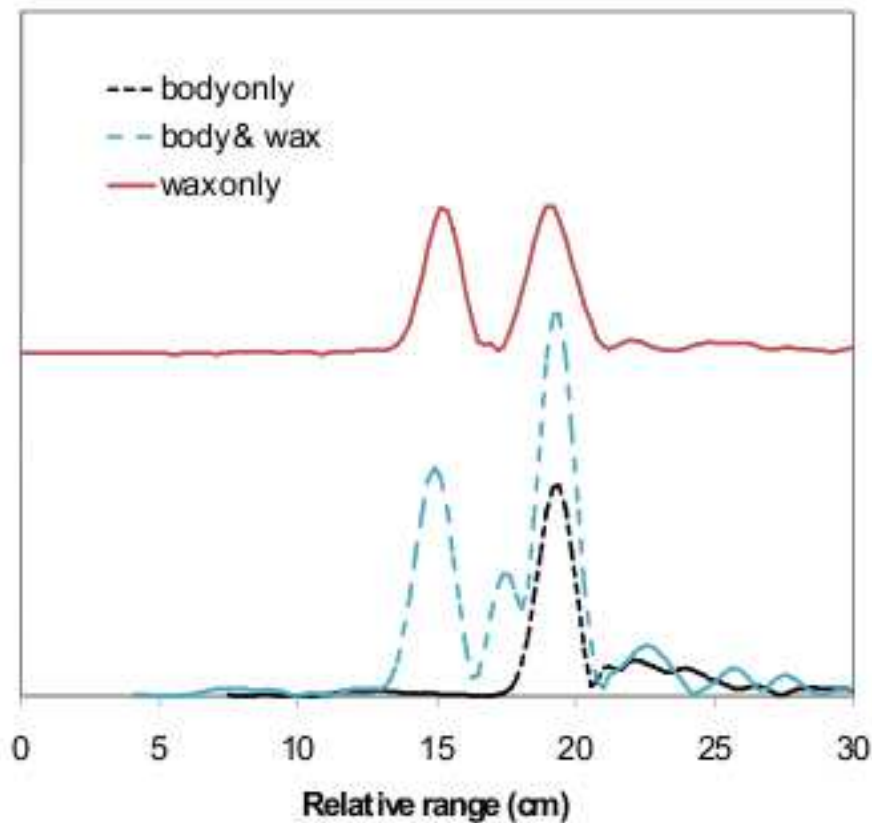


Figure 4.33: Range gated response from body only, wax block and human body and wax block only (offset vertically) taken using the VNA

The presence of the wax block is clearly indicated by the peak in front of the body and barrel corresponding to its optical depth. These results suggest that time domain analysis using a super-heterodyne based system can be used to detect the presence of a concealed dielectric. However in practice, with a moving target with body rotation of approximately $\pm 10^\circ$ combined with Doppler blur, the response from the body changes and additional peaks occur where the peak for the explosive is expected. Therefore it is necessary to scan faster than the VNA in a practical system. The VNA used takes approximately 200 ms to complete the aforementioned scan (Agilent, 2012).

It could be argued that the technique for detecting the thickness of a dielectric block would give results of little or no significance if the block is of irregular shape or thickness.

Results show that dielectric blocks of irregular shape and surface texture still display strong directional reflectance at millimetre wavelengths. The location and approximate thickness can still be determined (Bowring et al., 2007b).

Two test samples are shown below:

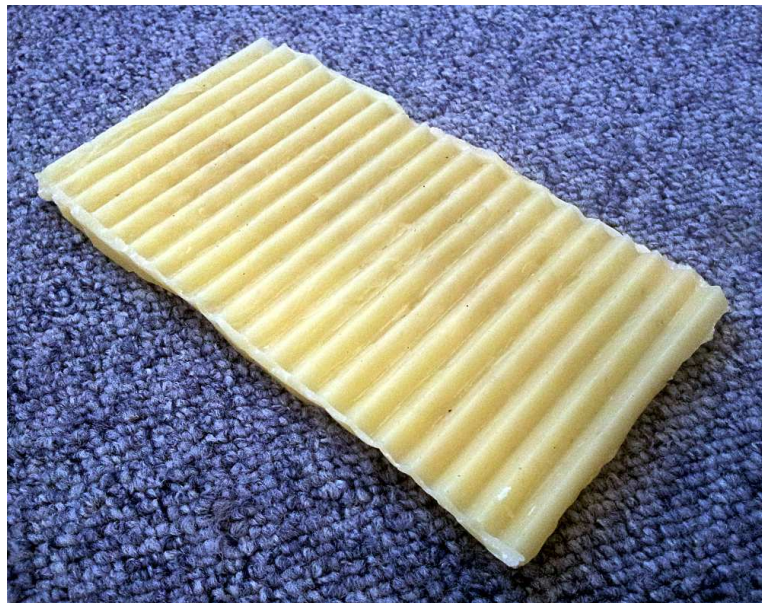


Figure 4.34: Irregular dielectric test piece one



Figure 4.35: Irregular dielectric test piece two

4.7 Detection of Metals

4.7.1 Edge Glint

The edges of a metal object can be easily detected from their to scattered signal. This can be seen by rotating a simple thin metal sheet (an unetched PCB), see Figure 4.36, in the beam and the lateral distance between the edges can be calculated from the frequency of the peaks in the raw data.



Figure 4.36: Experimental apparatus to measure the FMCW response of a rotating thin metal plate (unetched PCB)

Since the metal sheet is conductive and is within an alternating EM field, an electric current is generated within it. The radiation of the induced surface currents can be measured and analysed (Novak et al., 2005; Gashinova et al., 2006). The measurements taken for Figure 4.37 were taken using a VNA and using the method described in (Rezgui et al., 2008).

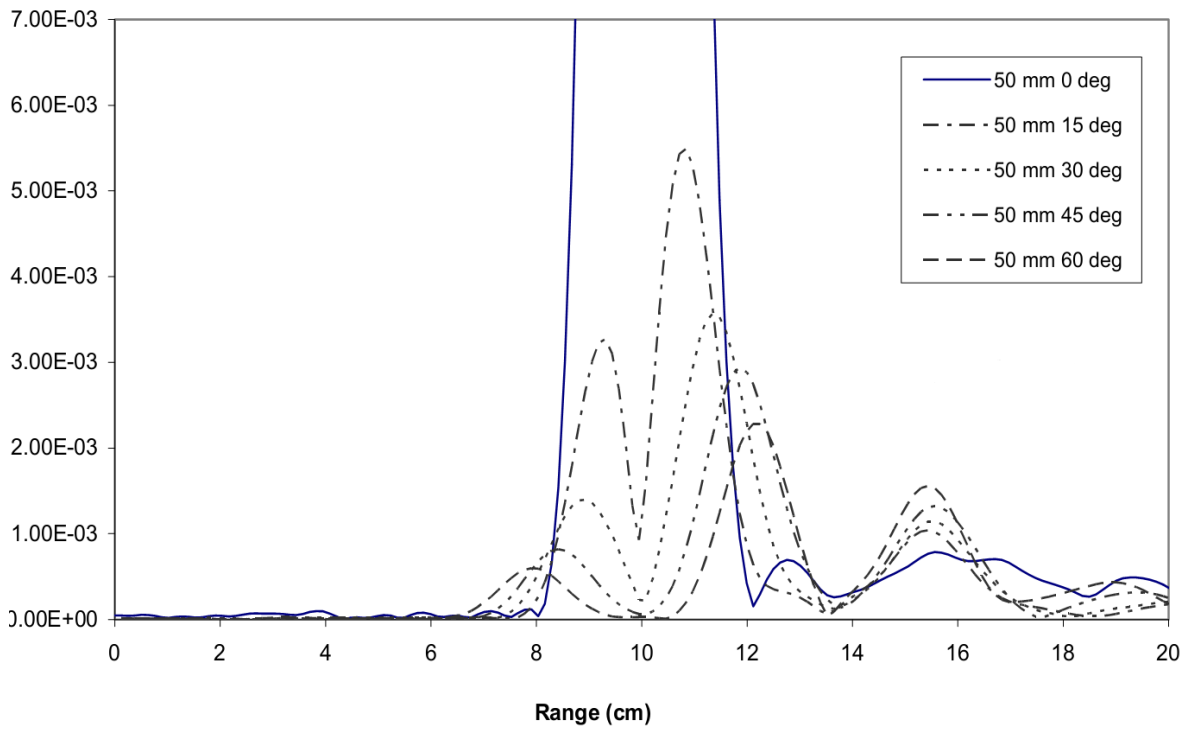


Figure 4.37: Rotating thin metal sheet optical depth transform results

The metal plate is geometrically simple, conserving the polarisation of the incoming EM radiation. The distance l between the peaks is a function of the angle θ through which the plate is rotated and width L of the metal plate in the relationship:

$$l = L \cos \theta \quad (4.32)$$

It can be seen from this that the response from a simple metal object is not aspect independent and a poor choice for the detection of simple metal objects. However a gun is a complex shape with many dimensions, edges and corners. The multiple and curved surfaces scatter and alter the polarisation of the incident radiation which when measured can indicate the presence of a complex object such as a gun.

4.7.2 Gun Barrel Detection

One feature of every gun is the barrel. The signal response due to glint varies for a simple metal object as described in section 4.7.1, but the barrel has a distinctive response that has some aspect independence.

The experimental apparatus to measure the response of a metal barrel at different angles is shown in Figure 4.38.

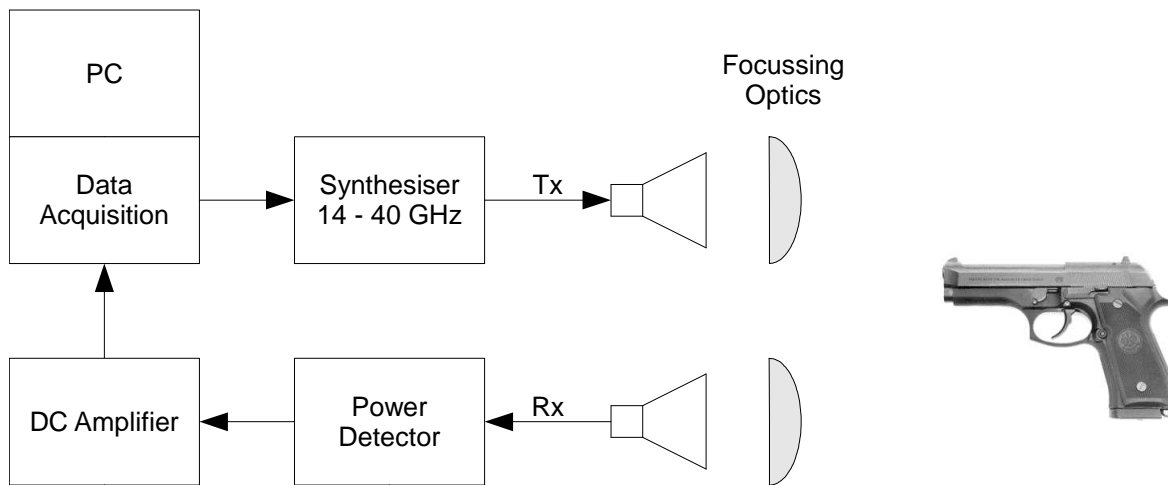


Figure 4.38: Experimental apparatus to measure the response of a gun barrel

Synthesiser	Agilent E8257D 40 GHz
Antennas	20dB gain horns
Detector	HP 11585A zero-bias detector
DC Amplifier	80dB with variable gain and offset
Data Acquisition	National Instruments NI-6132 PCI card
Object	10cm long barrel closed at one end with 9 mm ID and 19 mm OD

The difference between the response from the exterior of the gun to the response of the barrel is that it has a cut off frequency and being a cavity has greater aspect independence.

Rotating the barrel the measurements in Figure 4.39 were taken.

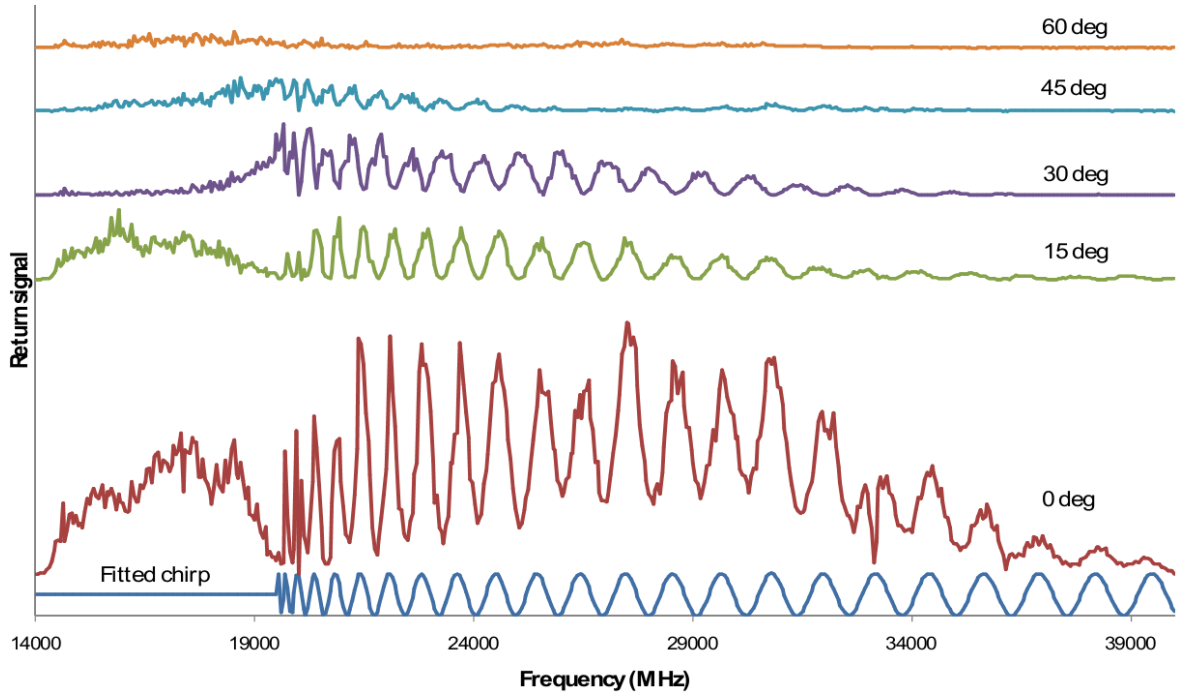


Figure 4.39: Frequency response of a 9mm internal diameter 10cm long simulated gun barrel aligned between 0 and 60 degrees and illuminated between 14 and 40 GHz (plots vertically offset)

An oscillating response can be clearly seen when the wavelength of the signal is small enough to propagate into the barrel. The minimum frequency f_0 to propagate into the barrel is given by:

$$f_c = \frac{1.8412 c}{2 \pi r} \quad (4.33)$$

where c is the speed of light, and r is the radius of the circular cross section (Bevelacqua, 2008). For a 4.5 mm radius the calculated cut off frequency of 19.5 GHz agrees with the empirical results.

For a cavity length L , the response for when f is greater than f_c is given by (Rezgui et al., 2008):

$$|E_r|^2 \propto \cos\left(2\pi\sqrt{(f^2 - f_c^2)}\left(\frac{2L}{c}\right) + \varphi\right) \quad (4.34)$$

where c is the speed of light. The results show the oscillatory response occurs at a range of angles up to and over 45° and oscillation period relating to the cavity length L . The period seen is independent of rotation angle unlike the response produced by a simple metal plate given in section 4.7.1, where the period is proportional to the angle of orientation. This signal behaviour provides a potential method of determining the presence of a metal barrel which in most cases would constitute a suspicious object when concealed.

4.8 'Direct Detection' Radar Resolution and Maximum Range

For a practical 'direct detection' based system, the system antenna forms one interface and the approximately parallel surfaces of remote objects form other interfaces. Spatial resolution is a function of the bandwidth with a theoretical distance d_{res} between adjacent channels of:

$$d_{res} = \frac{c}{2\Delta f} \quad (4.35)$$

Where Δf is the bandwidth of the system and c is the speed of light. With a frequency sweep between 14 and 40GHz, $d = 5.77\text{mm}$. This is the best possible resolution for this bandwidth and can be applied in exactly the same way in stepped and swept FMCW radar that measure the phase, by a non-linear frequency ramp, see equations (4.9) to (4.12).

The maximum unambiguous distance between two interfaces measurable by the the system is a function of the resolution d_{res} and the number of frequency points taken n_s :

$$d_{unambiguous} = d_{res} n_s \quad (4.36)$$

For a distance of 10 m, 1734 points are required or practically 2048 for FFT purposes. The unambiguous range of a system is only the maximum distance an object can be from the antenna for unambiguous extraction of range, not the maximum range at which an object

can be detected. The maximum range that an object can be detected is a function of the transmitted power, the receiver sensitivity, the RCS of the object and the minimum detected noise limited power:

$$S_{min} = (S/N)_{min} k T_0 B (NF) \quad (4.37)$$

where S/N_{min} is the minimum signal to noise ratio needed to detect a signal, k is Boltzmann's Constant [1.38×10^{-23} J/°K], T_0 is the Absolute Temperature of the receiver input [°K], B is the receiver bandwidth [Hz] and NF is the Noise figure.

4.9 Prototype One: Direct Detector Bench Top Feasibility System

This system was the first prototype and was built to demonstrate feasibility. The system consists almost entirely of off the shelf parts and bench equipment. The hardware and experimental apparatus is shown in Figures 4.40 and 4.41.



Figure 4.40: Direct Detector bench prototype antennas and a gun with simulated torso

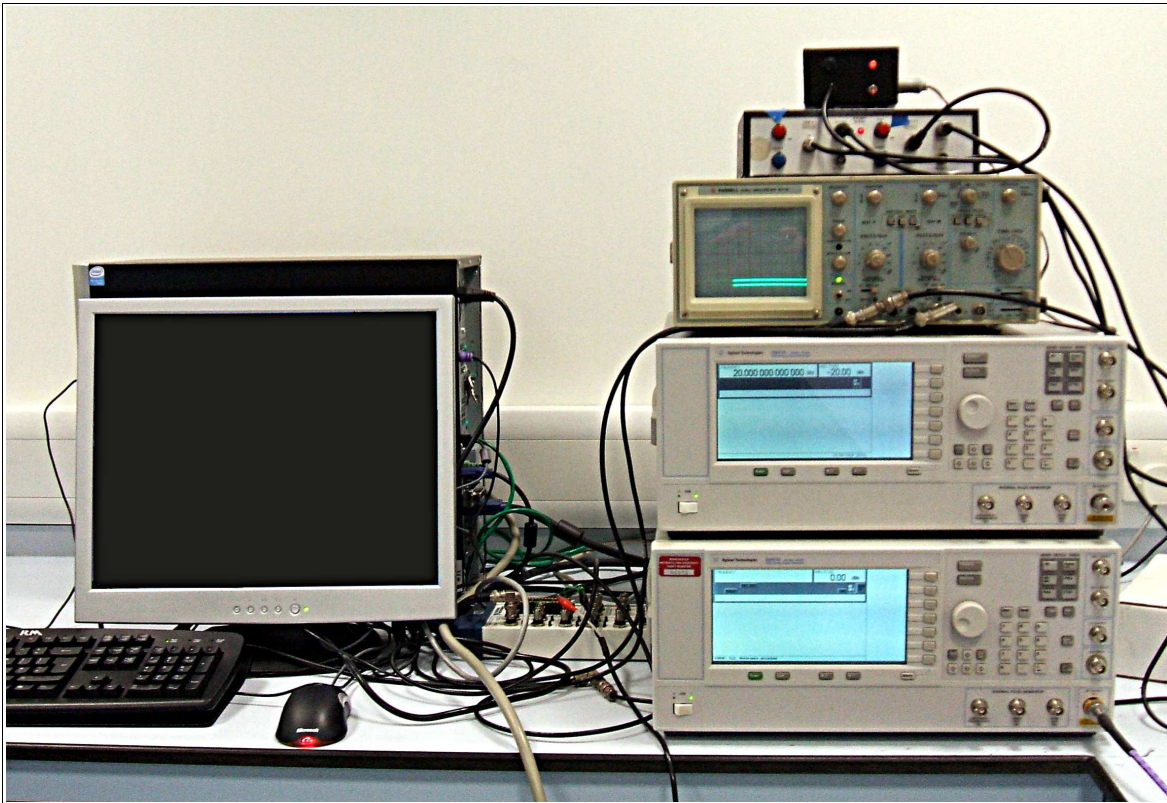


Figure 4.41: Direct Detector bench prototype RF and PC hardware

A LabVIEW program handled control of the equipment and signal processing. The top level diagram for the system is shown in Figure 4.42.

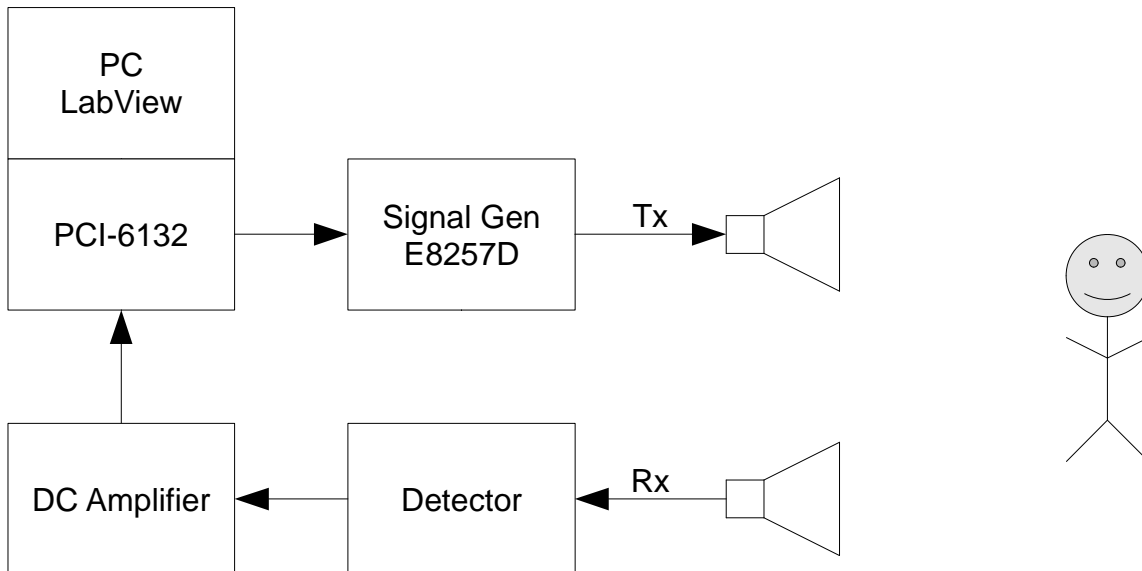


Figure 4.42: 14 – 40GHz Direct Detector Prototype Block Diagram

The bench equipment used to test the detection technique is listed below:

- An Agilent E8257D PSG Analogue Signal Generator – 40GHz, for generation of the FMCW signal to illuminate the target.
- Two 20dB high gain horns to focus radiation onto the target and minimise the collection of radiation from surround objects.
- A microwave zero-biased detector to convert the intensity of the received radiation into a proportional analogue voltage.
- A DC coupled amplifier to amplify the voltage produced by the detector and provide a low source impedance for the subsequent ADC.
- A National Instruments PCI-6132 – 14-bit 2.5MS/s/ch, Simultaneous Sampling Multifunction DAQ card to digitise the receiver signal and trigger the E8257D PSG.
- A PC running Windows and LabVIEW to control and process the signal data acquired by the PCI-6132 card.

The only component that was not bought off the shelf was the DC coupled amplifier.

The control and analysis was implemented using LabVIEW. The source and receiver antennas were located and the object under measurement positioned as in Figure 4.40, with a reflective background and in this case a water barrel full of water to simulate a human torso. Aiming was achieved by manually aligning the horns and target to obtain the maximum signal at the detector. The signal source is stepped in frequency and the response is measured using a single receiver. The receiver produces a unipolar DC voltage response. The frequency response of the target is then processed using an FFT and the

resulting data plotted with an arbitrary amplitude against optical depth. The plot is against optical depth because without knowledge of the target material, geometric thickness is a function of optical depth and refractive index.

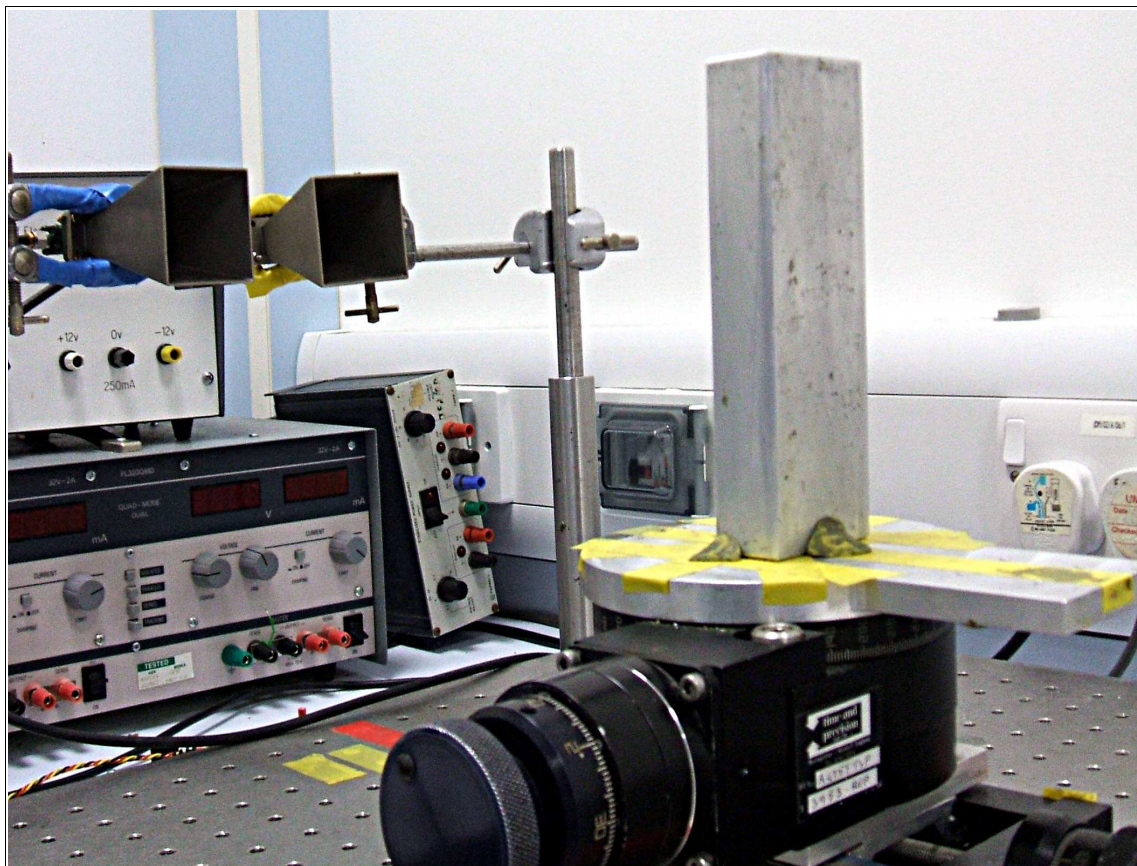


Figure 4.43: Rotational table in a direct detection reflective object experiment

This information could then be fed into a pattern matching artificial neural network for classification. Classification consisted of attributing a threat level to each set of measurements. Physical shape, construction, material composition and distance all affect the results. In the context of this research direct detection has come to describe an experimental apparatus used to detect the reflected response of a remote target as shown in Figure 4.43. Time for a single inspection was approximately three seconds.

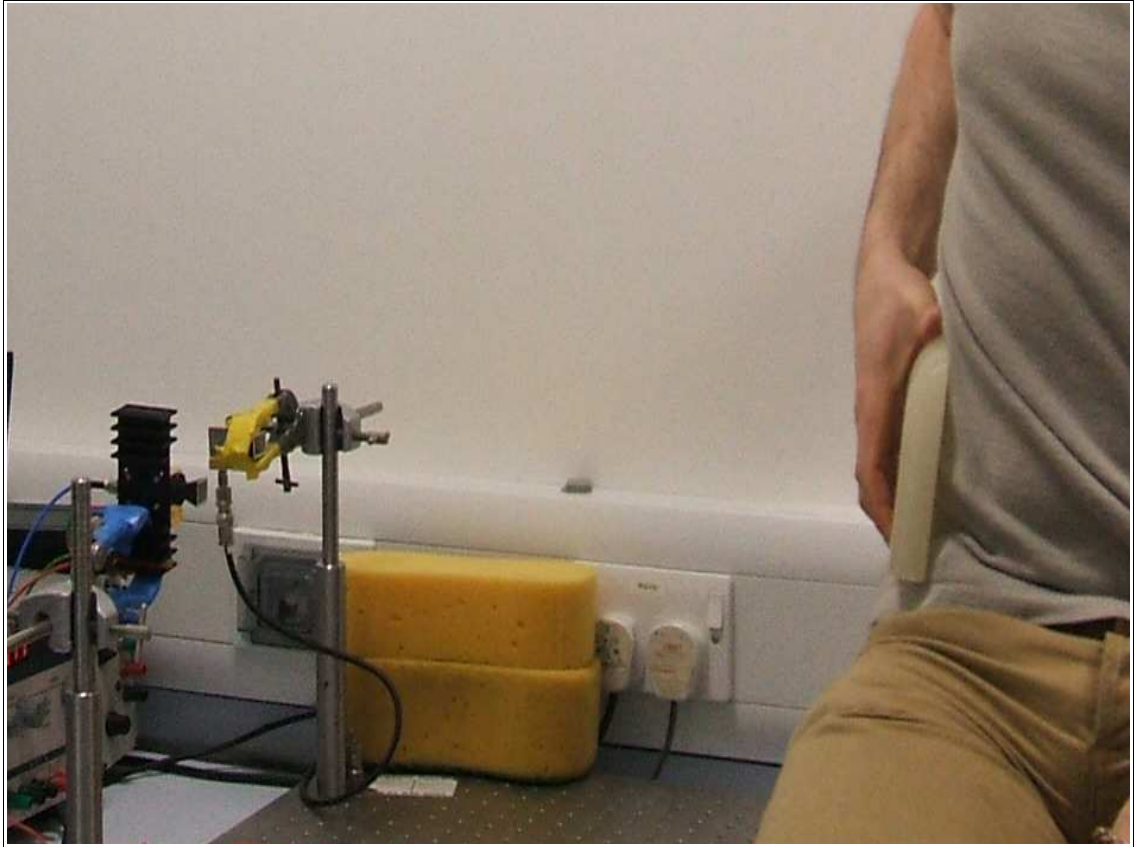


Figure 4.44: Direct detection of wax slab on torso experiment

Initially samples were held against the body as shown in Figure 4.44, however more regularly and conveniently a water barrel was used to simulate a human torso backing for the object under test, as previously shown in Figure 4.40. This approach was later adopted by another research group (Kapilevich & Einat, 2010). The use of a water bottle gave increased repeatability, because the position of the object and 'torso' were constant.

Even using high gain horns on the transmit and receive paths the measured signal at the receiver is tiny, due to distribution of the EM signal and scattering. A two stage amplifier with optional inverting stage was constructed to provide up to 60 dB of gain. A top level diagram of a single channel of the amplifier is shown in Figure 4.45.

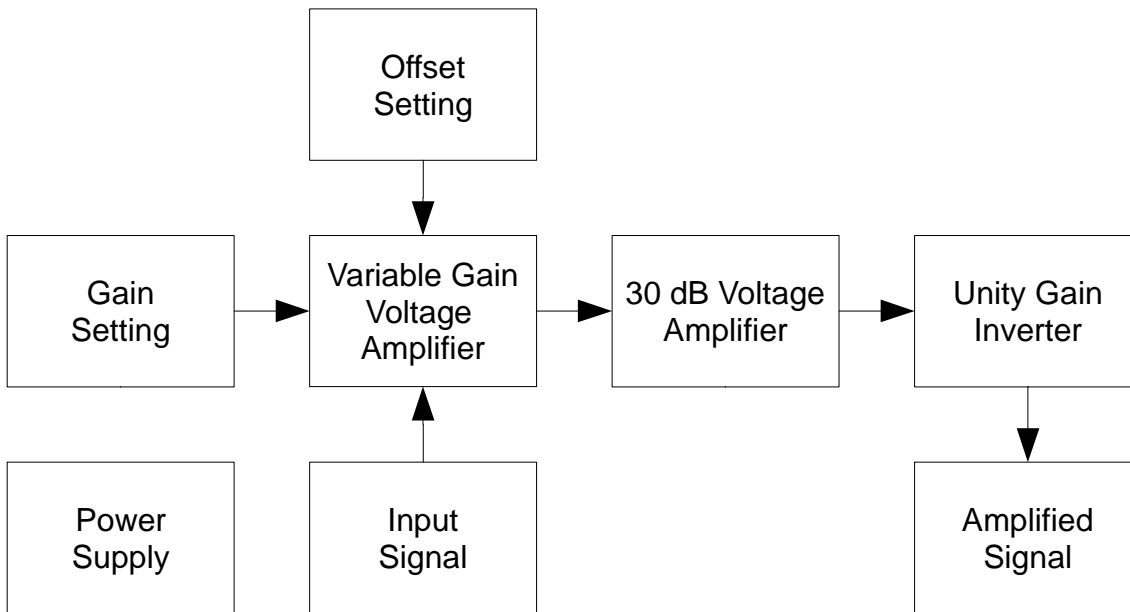


Figure 4.45: Top level diagram of a single channel of the 60 dB variable gain and offset voltage amplifier

The gain and offset were manually set to fill the input of the ADC, later systems would need a means of automatically adjusting gain in a controlled manner to respond to the range to target. A ranging system was incorporated into the subsequent prototypes.

4.10 Detection Using Multiple Polarisations

It was found that complex targets could be more readily identified by rotating the polarisation of the receiver horn. Since complex objects are capable of changing the polarisation of an EM wave, the effects of changing the polarisation of the receiver were investigated. The signal response was measured at 0° and 90° with respect to the transmitter horn. These are known respectively as co-polarisation and cross-polarisation. For co-polarised measurements, antennas are orientated so they are sensitive to EM waves in the same polarisation. Practically, this is achieved by orienting the horn feeds in the same direction as shown in Figure 4.46. For cross-polarised measurements the horn feeds are perpendicular as shown in Figure 4.47.

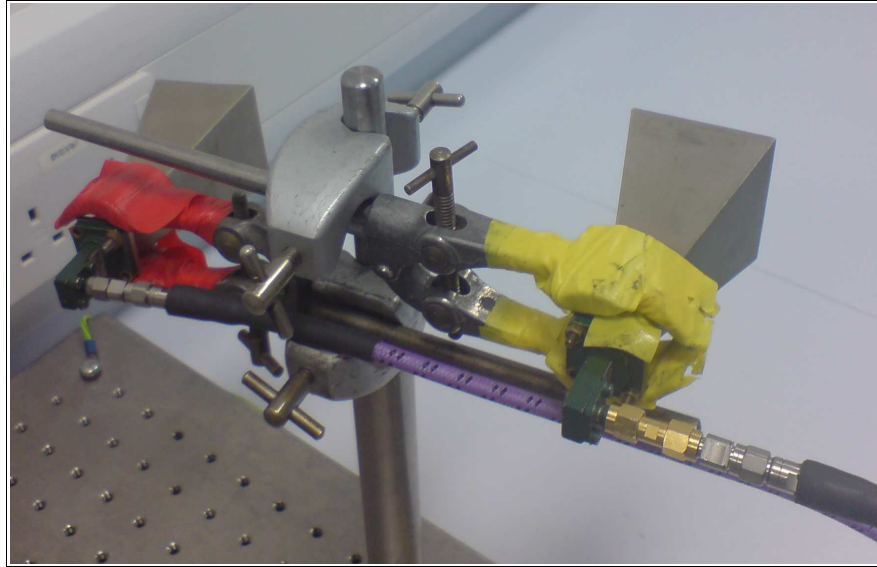


Figure 4.46: Co-polarised antennas

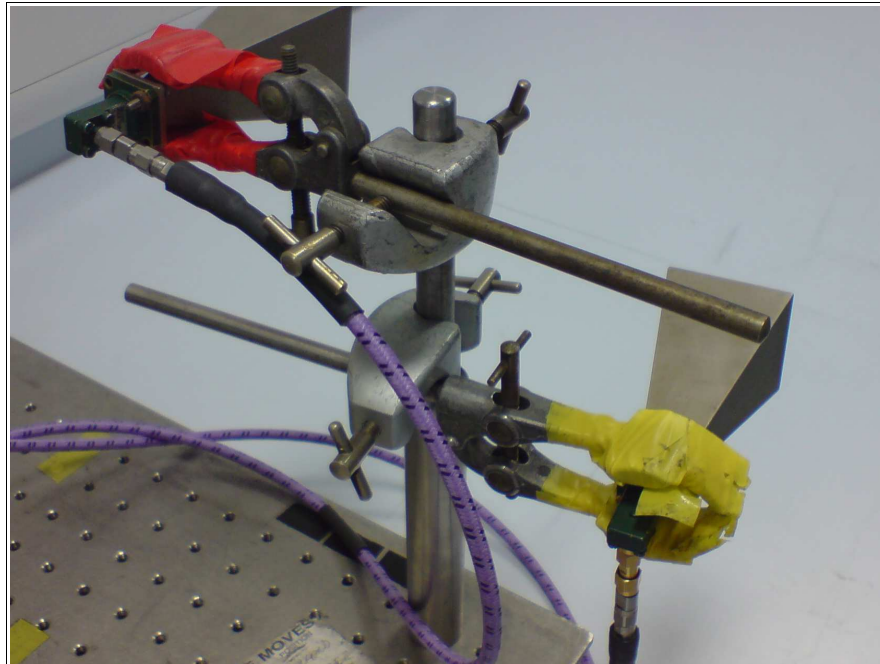


Figure 4.47: Cross-polarised antennas

Since wave-guide horns act as excellent polarisers, the polarisation of a signal may be measured by careful orientation of the antenna. For example, if the transmitter and receiver horns are orientated in the same plane (co-polarised configuration) only the signal where the polarisation has been conserved is measured. Conversely if the receiver antenna

is rotated about its axis only the amplitude component a of a signal of amplitude A in the plane of the antenna will be measured, where θ is the difference in angle between the polarisation of the antenna and the radiation:

$$a = A \cos \theta \quad (4.38)$$

The radiation from a horn antenna is linearly polarised (Markov, 1965), therefore by using horn antennas the polarisation of outgoing signals and the parallel component of received signals can be measured. If a signal is exactly 90° out of alignment with a receiver then theoretically no signal is measured. This phenomenon can be exploited, by manipulating the polarisation of the antennas. Normally shifting the polarisation of EM waves is achieved using a polariser, but instead we use the physical characteristics of a small handgun to shift the polarisation. The two graphs below show the results of cross polarising the antennas for a person with and without a small handgun present on their person, see Figures 4.48 and 4.49. The data was gathered using apparatus shown in Figure 4.50.

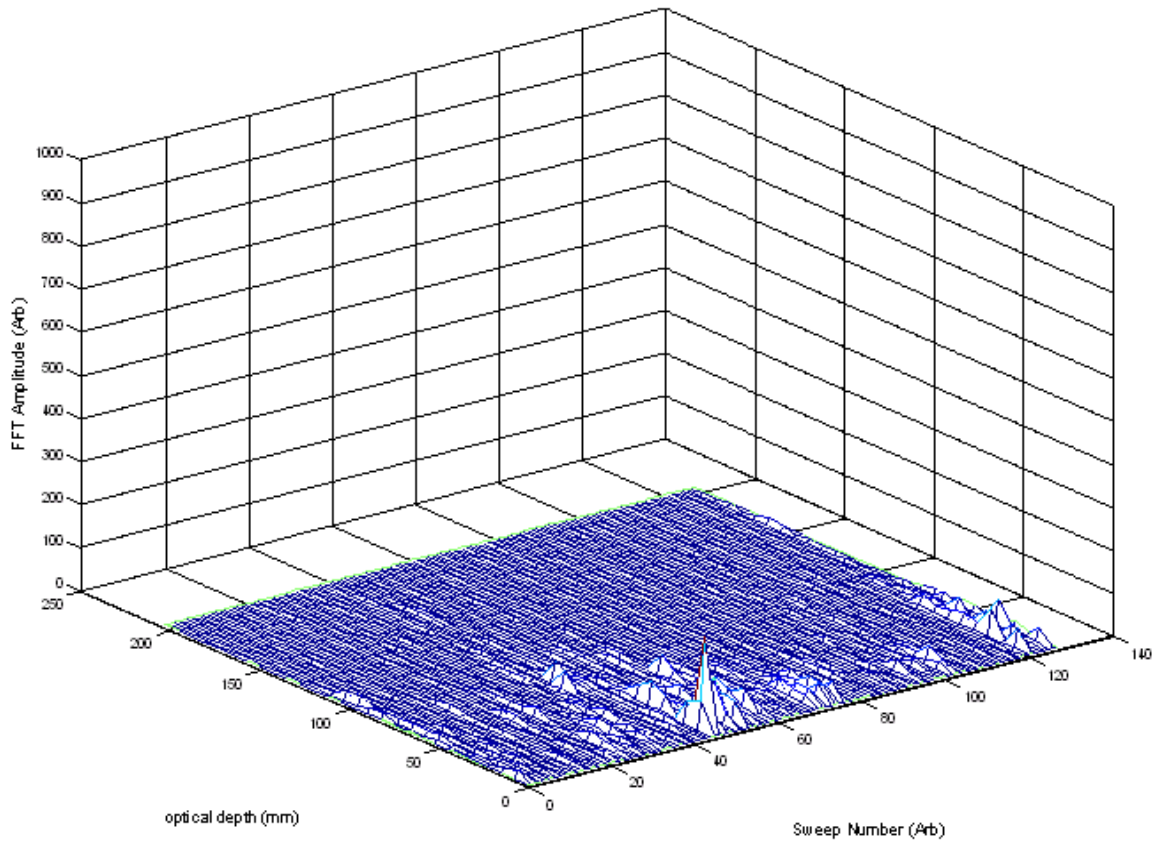


Figure 4.48: Cross-polarised response of a person rotating with no gun present

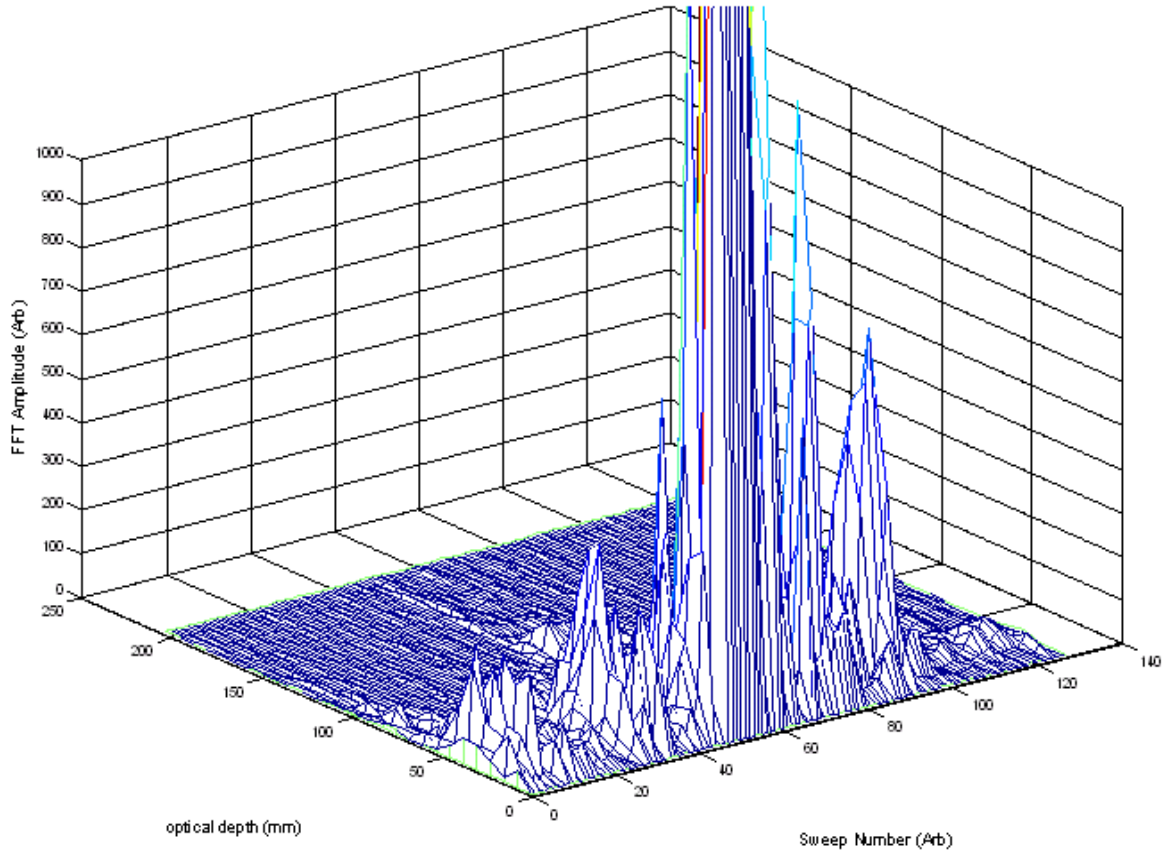


Figure 4.49: Cross-polarised response of a person rotating with a concealed handgun

The co and cross polarised time domain responses for a selection of targets can be seen in Figures 4.51 to 4.58. The co and cross polarised measurements were taken using a Agilent VNA operating between 14 and 40 GHz. The experimental apparatus is shown by Figure 4.50. and a more detailed description of the method can be found in (Rezgui et al., 2008).

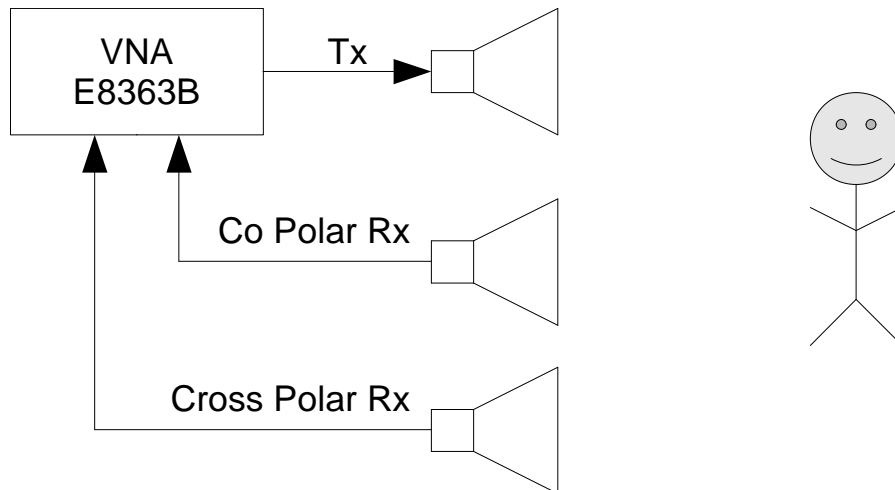


Figure 4.50: Experimental VNA setup for measuring the time domain co and cross-polarised responses of a range of objects scanning between 14 and 40 GHz

The targets were positioned approximately 2 m from the antennas and the resulting data range gated, so the ranges given in the plots are all relative. The co and cross polarised responses are shown by the smooth pink and crossed blue traces respectively. Figures 4.51 and 4.52 show a gun in different orientations and Figures 4.53 and 4.54 show the body face on and at an angle. The features from different parts of the body can be seen clearly in Figure 4.54.

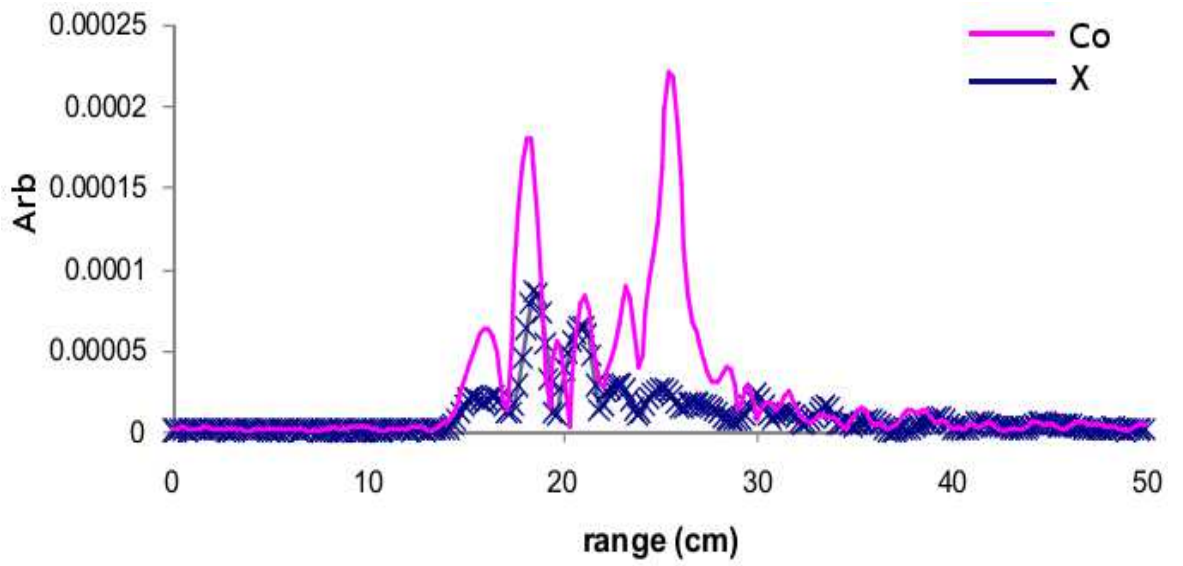


Figure 4.51: Co and cross-polarised response of a gun between 14 and 40 GHz

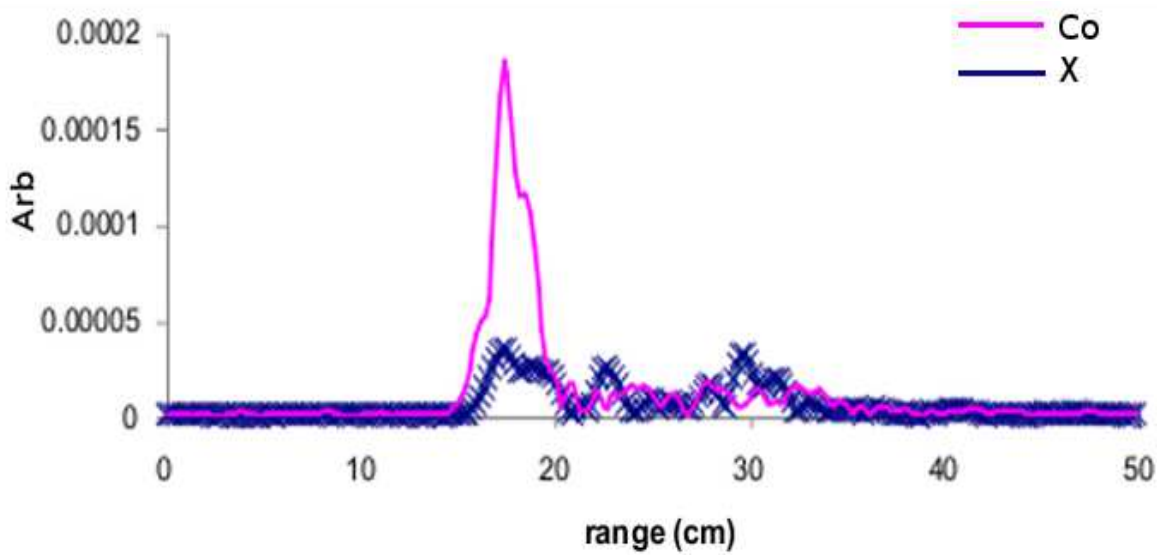


Figure 4.52: Co and cross-polarised response of a gun between 14 and 40 GHz

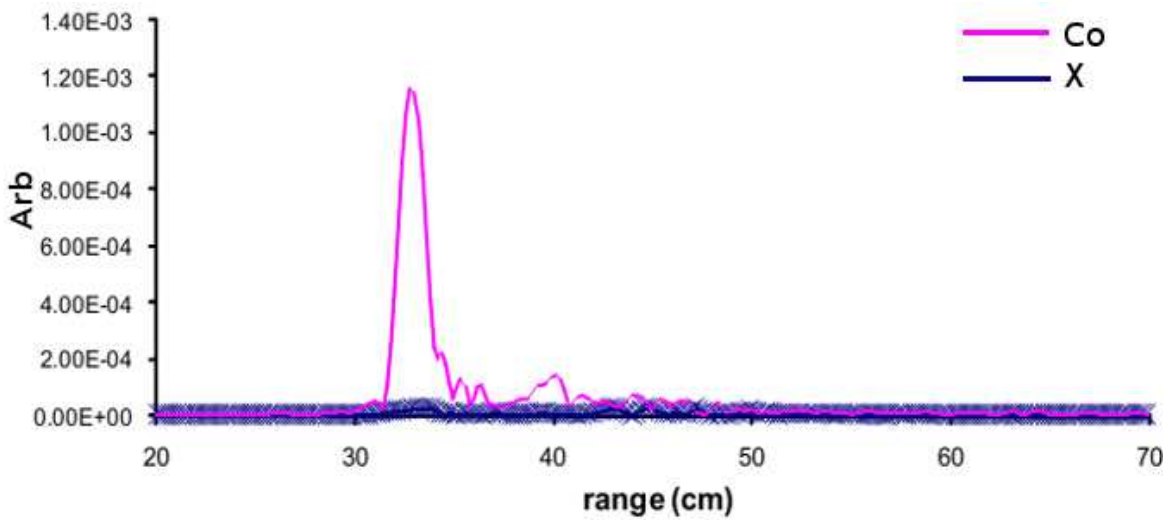


Figure 4.53: Co and cross-polarised response of a body between 14 and 40 GHz orientated face on

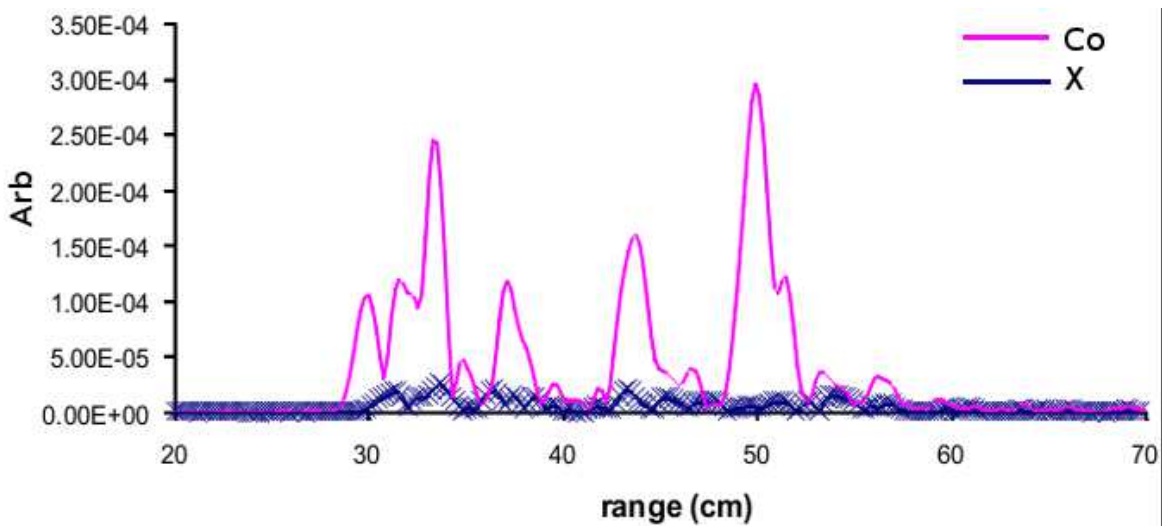


Figure 4.54: Co and cross-polarised response of a body between 14 and 40 GHz at an angle showing the signal from the arms and torso

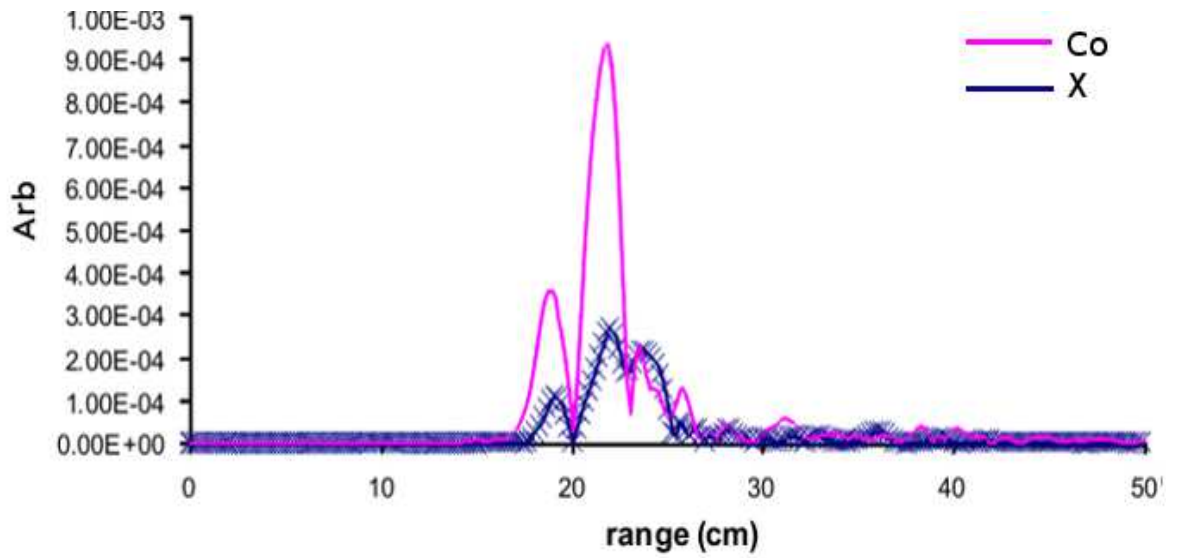


Figure 4.55: Co and cross-polarised response of a body with gun between 14 and 40 GHz
face on

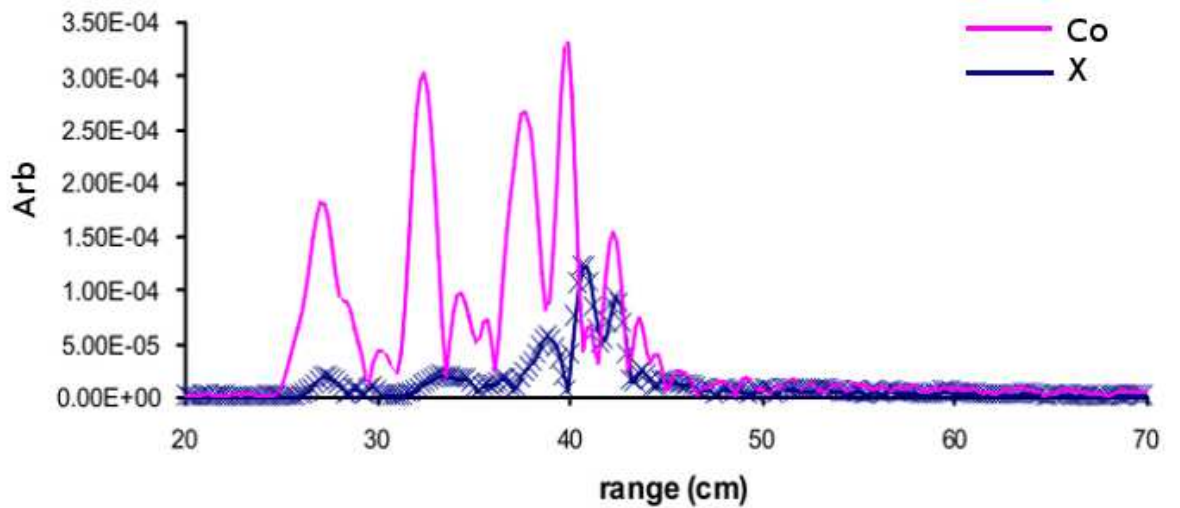


Figure 4.56: Co and cross-polarised response of a gun on the side of the body between 14
and 40 GHz angled side on

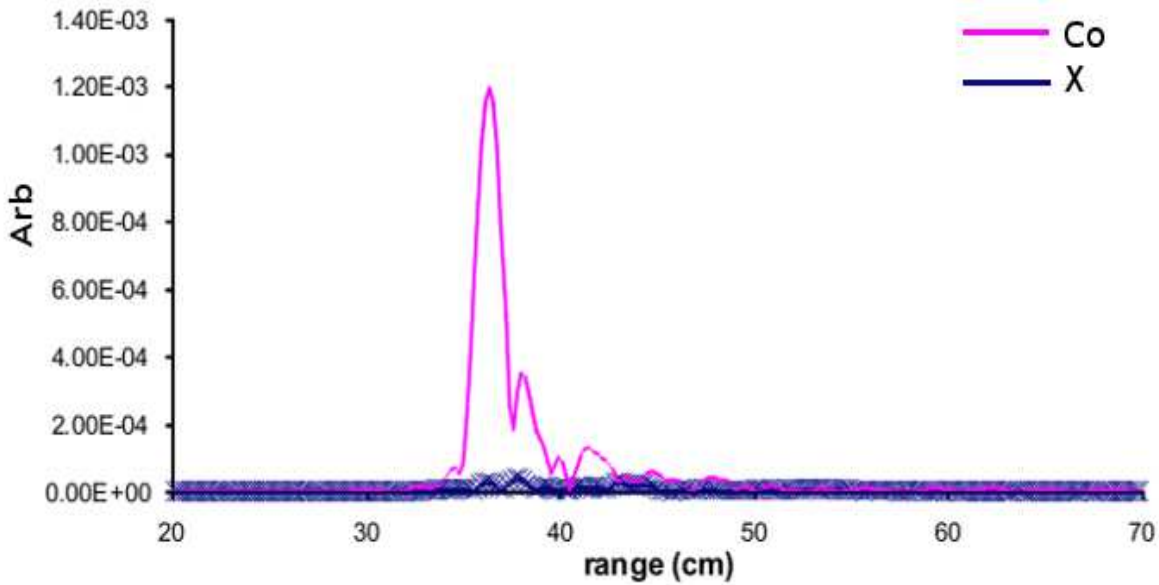


Figure 4.57: Co and cross-polarised response of a body with camera between 14 and 40 GHz face on

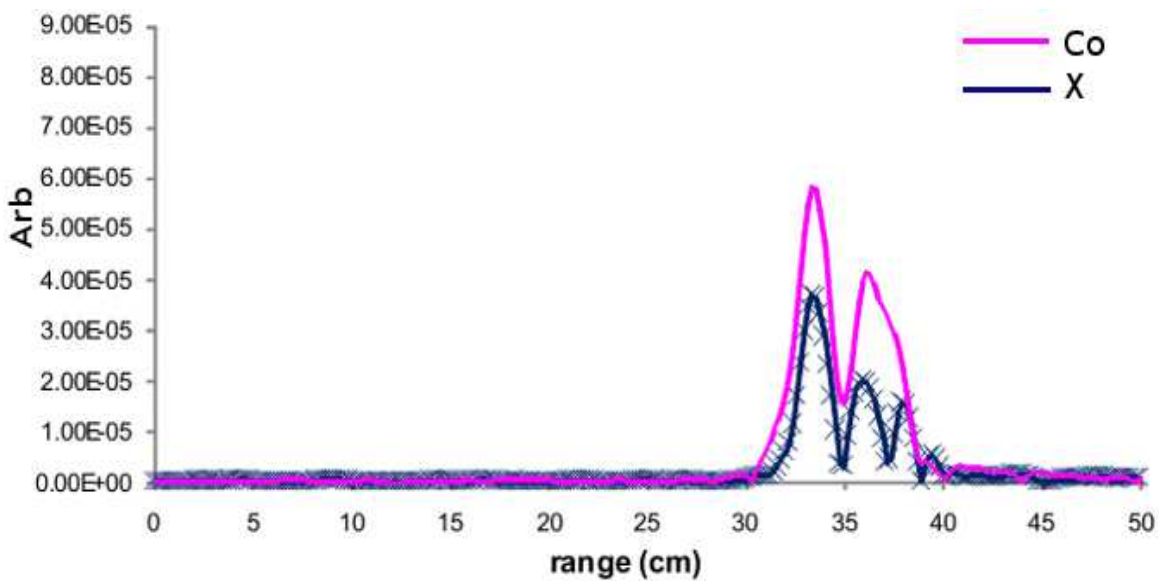


Figure 4.58: Co and cross-polarised response of a bunch of keys between 14 and 40 GHz face on

The cross polarised response produced by complex structures such as the gun are absent from the plots for the body alone. The measurements for the bunch of keys has a significant a cross-polarised component, so using the presence of a cross polar response alone is insufficient to reliable indicate the presence of a gun. However, significantly the

co and cross polar response for the keys are similar in amplitude, unlike those for the gun and due to the smaller RCS of the keys they are also an order of magnitude smaller than the measurement for the gun.

Blank page

5 Portable Prototypes

This chapter describes the development of portable prototypes based on the techniques discussed in Chapter 4.

The feasibility prototype techniques see 4.6.1 to 4.6.5 and 4.7.2, use a lot of equipment unsuited to the realisation of a portable version. To implement a portable device the functionality of the test equipment in compact low power form factors is required. The systems requiring a portable version to be developed were the controllable mm-wave source; DC amplification of the detector signals; ADC circuitry for sampling of detected signals; synchronisation and control circuitry, firmware and software and power supplies. Although designed to be portable the system chassis was designed with a tripod mount to ease setup, configuration and calibration.

The bench top prototype required the target object to be placed and moved into the detection volume of the system. By making the prototype portable or tripod mounted its detection volume can be moved by just pointing it in a new direction. Inspection of a individual would be achieved by manually rastering the detection volume over the target to identify the presence, nature, size and position of any concealed objects.

A method of detecting the range to the target is needed to mitigate variations in the return signal level due to distance and permit deterministic normalisation of measurements prior to analysis. Methods of determining target distance are described in section 5.1.

Both stepped and swept approaches have been used to obtain target data. Initially the stepped approach was used where it was possible to easily synchronise receiver sampling with steps in the transmission frequency, but this is slow and prohibitive for large numbers of data points. Their frequency stepping speed is relatively slow taking tens of milliseconds per frequency point, resulting in anything more than a basic scan taking tens of seconds, even minutes. This is impractical for taking reliable data from a human with object target due to sway and breathing movement. A secondary and beneficial side effect of rapid scanning is that spontaneity of research and experimentation are easily stifled when data collection and processing times are excessive or off-line. The same data can be collected in a fraction of the time.

The analog sweep approach required a deterministic sampling system that could monitor the state of the signal generator and suspend sampling during a band switch. However, even the relatively fast analog sweep option (option 007) for the Agilent PSG was slower than our requirements. The circuitry for the next prototype will need to include the facility to sweep the mm-wave source more rapidly with a matched increase in receiver digitisation rates. This is accomplished by the rapid scanning prototypes described in section 5.2.

5.1 Methods of Determining Target Range

In order to determine the range to a target such that radar returns can be effectively normalised a method of measuring target range is needed. Ideally the system itself would be capable of determining target range by phase sensitive detection (homodyne based ranging), removing the need for a separate ranging peripheral; such a system was implemented by the later Mirlin prototype, described later in Section 5.7. Meanwhile a compact, lightweight, low power device was needed to measure the proximity of a individual with a suitable interface. A number of devices were investigated for purposes of

range normalisation of the signal including laser, acoustic, video and capacitive, but ultimately two devices were selected for trial and comparison. These were the Sharp 2Y0A700 IR distance sensor and the SensComp 615088 50kHz ultrasonic ranger.

5.1.1 IR Distance Sensor

Sharp 2Y0A700 IR Distance Sensor



Figure 5.1: Sharp 2Y0A700 infra-red distance sensor

The selected part was a Sharp IR Distance Sensor part number 2Y0A700, with a quoted maximum range of 550cm. The small package of this sensor with an equally small power consumption, silent operation and easy to interface analogue voltage output made this an ideal part, however the range was less than that for the acoustic sensor. In practice this maximum range was nearer 450cm and dependant upon the reflector properties. It was found that clothing is a poor reflector and the quoted range is for a white sheet of paper. This approach did have a much smaller beam pattern than the acoustic methods, but ultimately the range was insufficient for our purposes. Figure 5.2 shows the measured accuracy of the device.

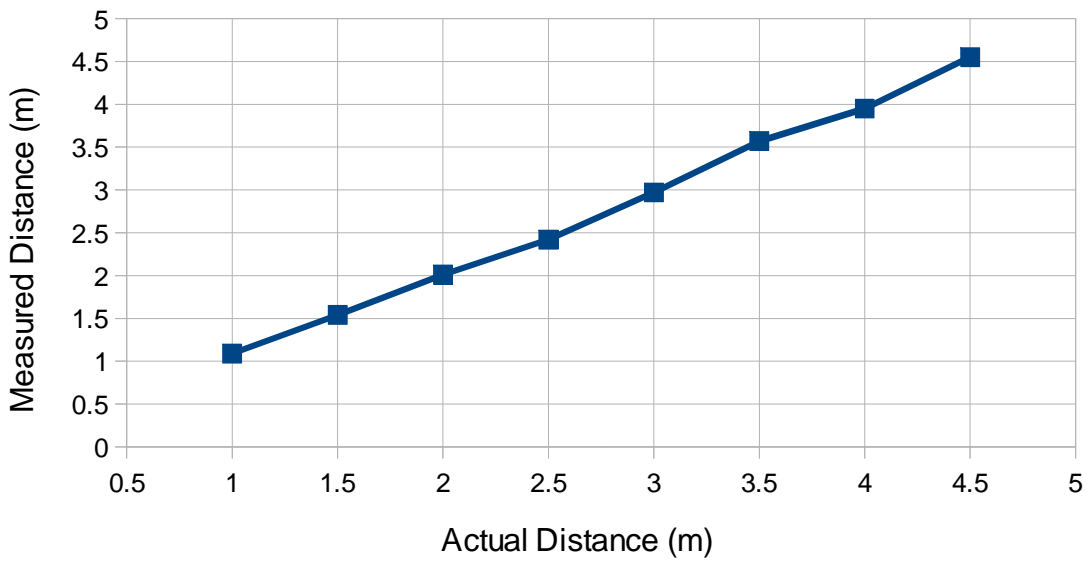


Figure 5.2: Measured against actual distance results for a GP2Y0A700

5.1.2 Acoustic Range Finder

SensComp 615088 50kHz Ultrasonic Instrument Grade Smart Sensor

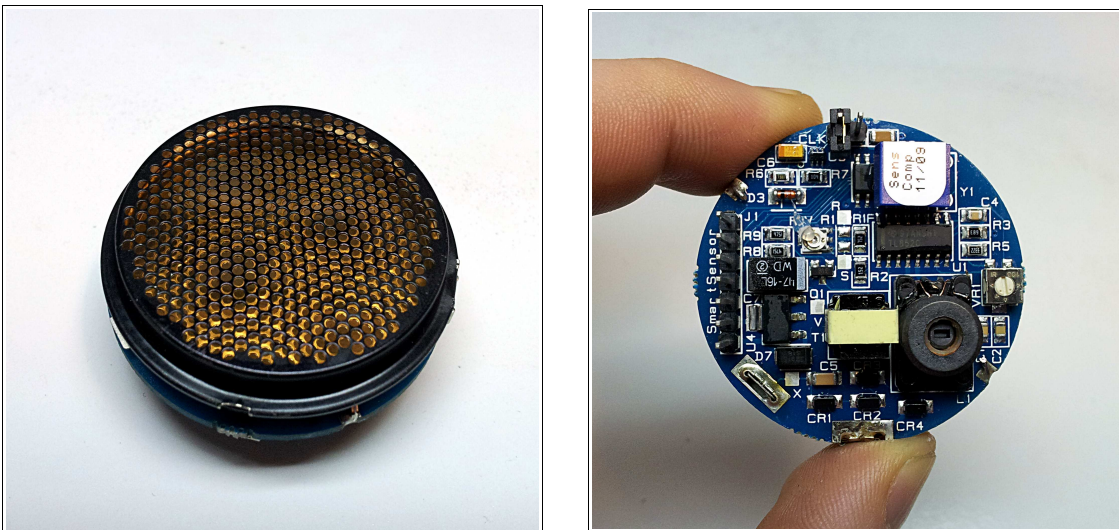


Figure 5.3: SensComp #615088 50kHz ultrasonic instrument grade Smart Sensor

The quoted range of the sensor is 10.7 m with a nominal beam pattern of 15°. In practice for clothing the maximum obtainable range was 8.0m. The width of the beam pattern was significant, because objects off axis and closer than the intended target were detected in

error. Fortunately, the sensor can be configured to allow multiple targets to be detected with a separation of greater than 8 cm between them. This device was selected to be used on the next prototype.

5.1.3 Ranging Device Interfacing

The Smart Sensor is controlled and target distance measured by toggling and measurement a series of IO pins. Reception of acoustic echoes is indicated on the ECHO pin and must be reset if multiple echoes are to be received. To distinguish between clustered targets the relative arrival time of an echo must be recorded and the ECHO output reset with a low latency. The maximum latency is a function of the length of the acoustic pulse train, consisting of sixteen 50 kHz oscillations and the desired range. The minimum delay before the ECHO output can be reset allowing reception of the acoustic pulse train and the internal delay times of the device is 0.44 ms (SensComp, 2009). This corresponds to a maximum achievable resolution of:

$$d_r = \frac{V_s T_{bd}}{2} \quad (5.1)$$

where V_s is the speed of sound (343.2 ms^{-1} and in dry air at $20 \text{ }^\circ\text{C}$) and T_{bd} is the minimum delay time before reset (0.44 ms). The maximum obtainable d_r given this constraint is 75.5 mm.

The process of extracting accurate range information about multiple targets from the sensor is a timing and latency critical task, unsuited to a MATLAB script running on a PC. Hence an intelligent peripheral interface (IPI) was designed and built by the author to manage the SensComp device with a minimum of latency and supervision. The heart of the intelligent peripheral is a PIC18F2420, a fully deterministic RISC architecture microcontroller (Microchip, 2008). The IPI was designed to fit the footprint of the sensor and send regular messages containing measured range over a serial interface to MATLAB, while automatically triggering and measuring the outputs of the ultrasonic sensor in a fully

deterministic manner. Practical measurements using the device are shown in Figure 5.4.

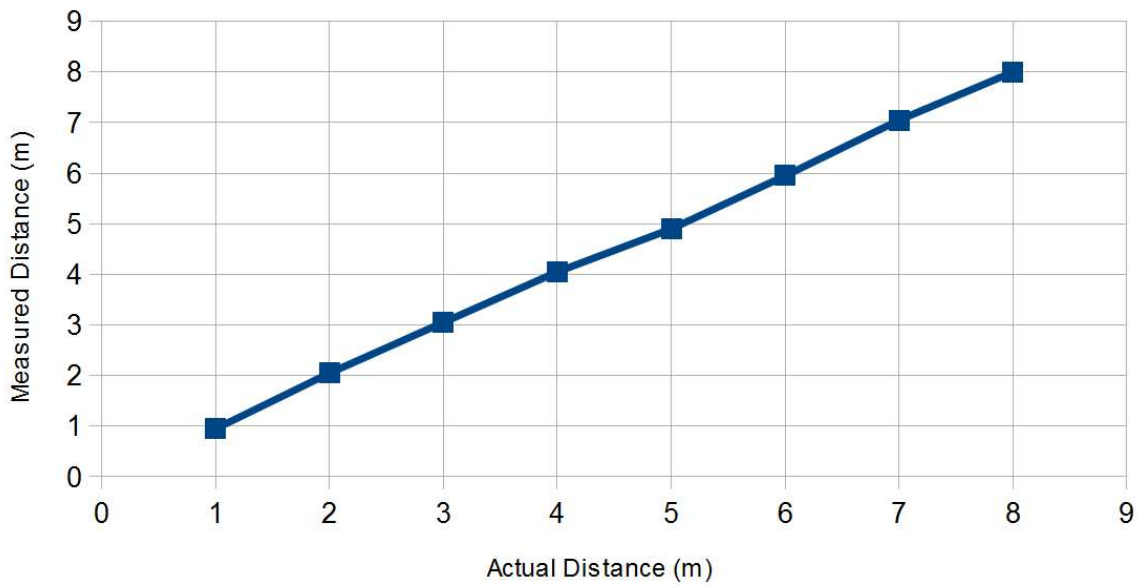


Figure 5.4: Measured against actual distance results for a SensComp 615088

50kHz Ultrasonic Instrument Grade Smart Sensor

The IPI features power LEDs and on board indicators showing the number of targets visible to aid debugging and assist commissioning. Figure 5.5 illustrates the compact footprint of the board making it very easy to integrate into the existing design.

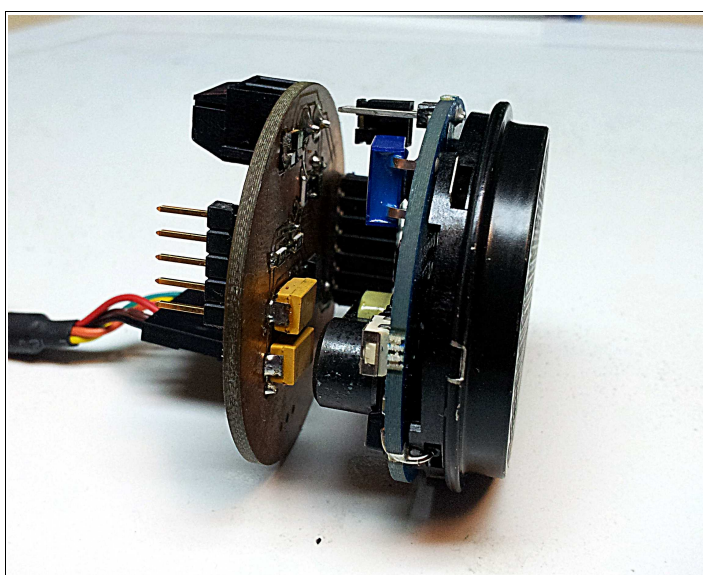


Figure 5.5: The compact B246A and ultrasonic sensor assembly

The firmware flowchart is shown in Figure 5.6.

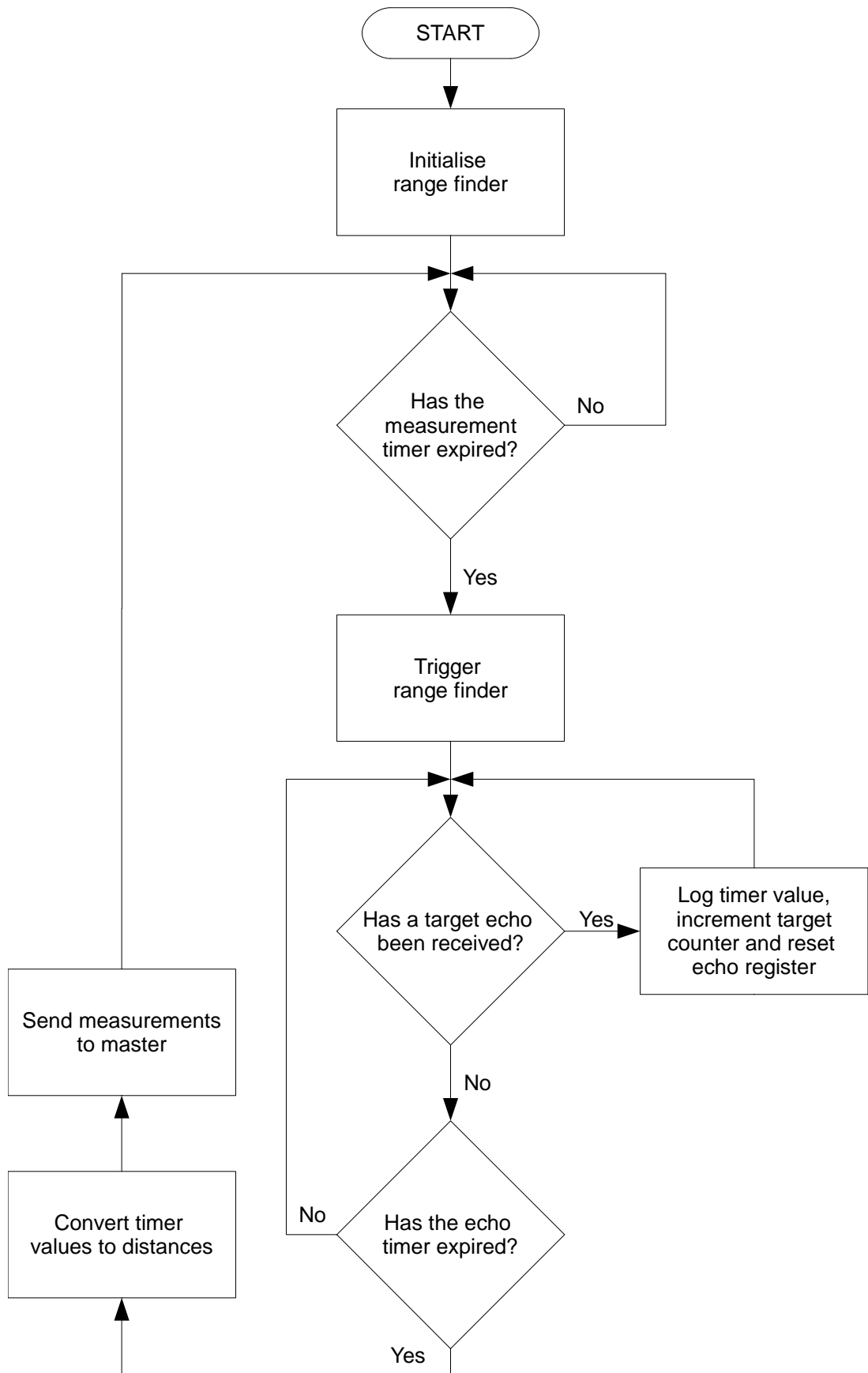


Figure 5.6: B246A Range Finder Multiple Target firmware flowchart

5.1.4 Signal Gain

Two methods of normalising the signal response of a target were considered: numeric and physical. The numeric method of multiplying the signal level in software is possible provided the input signal level fills a sufficient fraction of the ADC dynamic range. When it is decided that an insufficient fraction of the ADC input is used or the dynamic range of the ADC is small or the detector is prone to saturation then variable physical amplification of the signal prior to digitisation is required.

Prototype One uses zero biased millimetre wave power detector and amplifier, the output of which provides a suitable signal for the ± 10 V 14-bit ADC of the NI-6132 to digitise over the possible variations of target distance. Numeric gain of the detected signal was implemented in software by the host PC.

5.2 Custom High Speed Compact Data Acquisition Boards

Real time operation requires rapid scanning of targets. Lab based experiments measuring the response of static objects and bodies are indispensable tools for understanding mechanisms of operation, but inadequate for even slow moving real world targets. A means of dramatically reducing the scan time of the system was needed to ‘freeze’ in time a moving target. This was the design aim for the rapid scanning prototypes, by providing a synchronised deterministic method of recording the receiver response, thereby enabling faster and faster sweep speeds to be achieved. In essence, the shorter the scan time the smaller the degree of movement of the target and the subsequent minimisation of the spatial blurring of the raw data.

For the target to be effectively frozen in time as far as range is concerned the limit acquisition time was set as a distance the target can move as a fraction of the range resolution. Using range resolution equation 4.35, the optimal resolution (range interval) for a 35 GHz frequency sweep is 4.29 mm:

$$\begin{aligned}
 d &= \frac{c}{2 \Delta F} \\
 d &= \frac{3 \times 10^8}{2 \times 35 \times 10^9} \\
 d &= 4.29 \text{ mm}
 \end{aligned}
 \tag{5.2}$$

Assuming the worst case scenario of the device operator and target walking (3 mph) towards each other the time taken to travel a single range interval is:

$$\begin{aligned}
 1 \text{ mile per hour} &= 0.447 \text{ ms}^{-1} \\
 \text{Relative Speed} &= 6 \times 0.447 \text{ ms}^{-1} = 2.682 \text{ ms}^{-1} \\
 \text{Time taken to travel range interval} &= \frac{4.29 \times 10^{-3}}{2.682 \text{ ms}^{-1}} = 1.6 \text{ ms}
 \end{aligned}
 \tag{5.3}$$

For the Fourier Transformations to operate correctly, the time for a complete scan must be at least less than half this value, or 0.8 ms.

For maximum effectiveness these circuits required a matching Rapid Scanning DAC circuit B226 (described later in section 5.3.1) to produce the drive signal for the microwave Voltage Controlled Oscillator (VCO) generating the mm-waves and ADC boards to measure the detector signals.

A diagram of the initial apparatus using the custom rapid scanning data acquisition board is shown in Figure 5.7.

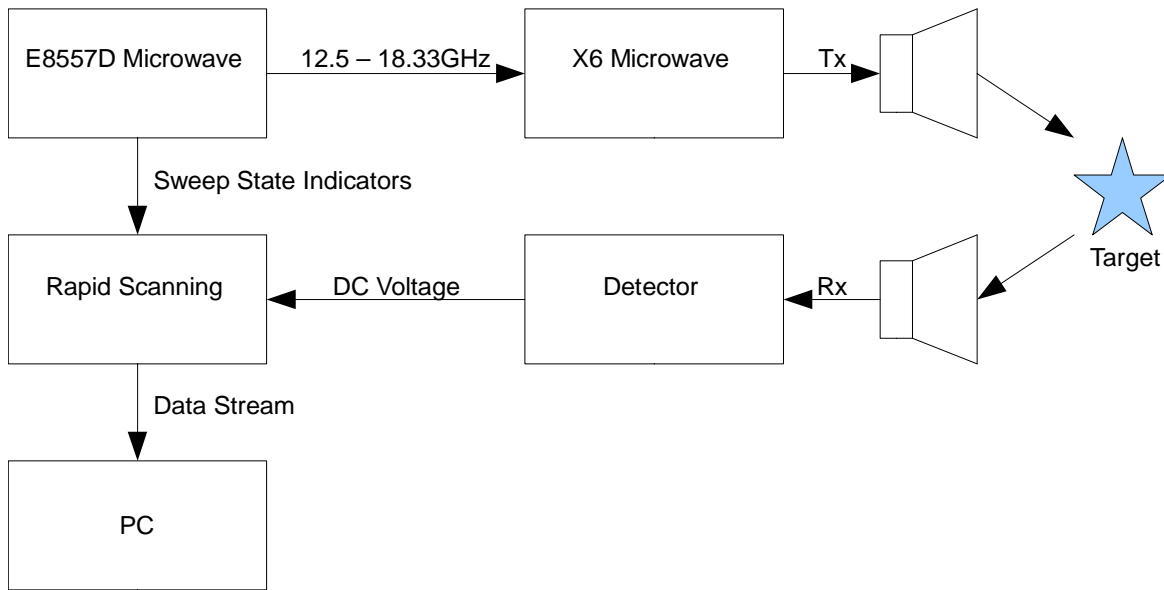


Figure 5.7: Typical apparatus for using a rapid scanning board

A collection of progressively refined circuits were realised to fulfil this requirement of an non-PC based high-speed sampling device that could be used with or without a computer. The experience in developing these was applied in the actual portable prototypes.

5.2.1 Rapid Scanner Board

This system underwent a three iterations until a satisfactory version was produced. The board was originally designed to provide a non-pc based alternative to National Instruments analogue interface cards capable of synchronising with the synthesiser and only digitise when a valid signal is being generated. In analogue sweep mode the synthesiser is capable of sweeping from 12.50 to 18.33 GHz in 58 ms. By controlling the synthesiser using the Sweep Stop In/Out interface, a practically unlimited number of samples could be taken during a frequency sweep by stopping the sweep during data acquisition. However for the fastest possible sweep, a synthesiser with the 007 analog sweep option is required. The shortest sweep time configurable for a 12.50 to 18.33 GHz sweep is shown as 16 ms on the GUI, but unexpectedly only 17 sweeps per second were observed to occur in practice, in free running mode. Free running mode produces a continuous sequence of frequency sweeps.

The output of the synthesiser was measured and instead of the expected single frequency ramp the ramp was split into three parts, as shown in Figure 5.8.

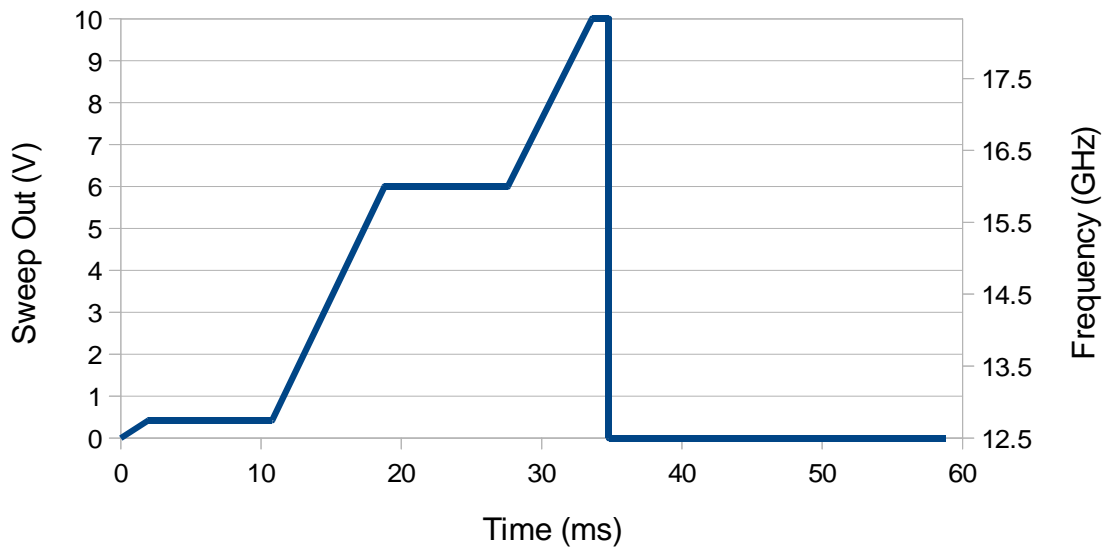


Figure 5.8: Time against frequency for a E8257D PSG Analogue Signal Generator (007 analogue ramp option) ramping from 12.5 to 18.33 GHz

The plot was created by measuring the output of the Sweep Out connector on the back of the signal generator which outputs a voltage proportional to the frequency sweep ranging from 0 V and the start of the programmed sweep and 10 V at the end of the programmed sweep. The periods of the graph when the frequency is not increasing are due to the switched oscillator architecture of the signal generator and the delay at the end of the sweep is the fly-back preparation time for a new sweep. A means of monitoring the Sweep Out output was initially implemented, but dropped when triggered monitoring and receiver sampling performance were proven to be repeatable. This was fortunate as it transpired design and realisation of the sampling circuitry was relatively simple compared to the task of transporting the generated data in a timely manner.

The initial decision was to sample and buffer an entire sweep was made as it gave the lowest latency between samples, transmitting the data to the host between sweeps, thereby maintaining peak samples per second. The PIC18F2620 with its large quantity of RAM –

3968 bytes the largest of any 8-bit PIC was selected for the sampling task and the PIC18F2550 was selected for its 'Full-Speed' USB connectivity.

The block diagram shown in Figure 5.9 shows the top level subsystems of the prototype.

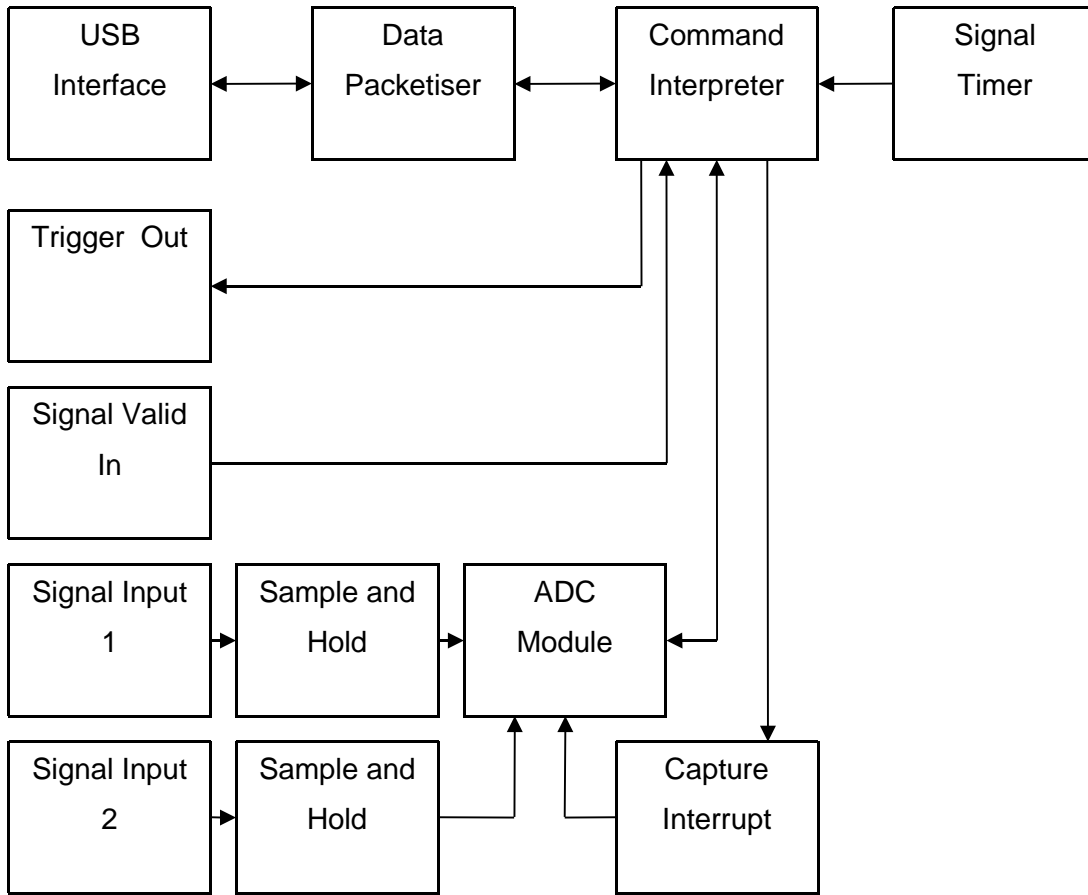


Figure 5.9: Rapid scanning board v1 top level block diagram

The data throughput calculations started with the sample time T_s were:

$$T_s = \frac{1}{\text{Sample Rate}} = \frac{1}{110 \times 10^3} = 9.09 \times 10^{-6} \text{ s} \quad (5.4)$$

and the maximum number of samples D_{mss} that could be taken during the shortest configurable sweep available on the synthesiser:

$$D_{mss} = \frac{T_{\text{sweep}}}{T_s} = \frac{15 \times 10^{-3}}{9.09 \times 10^{-6}} = 1650 \text{ samples/inspection} \quad (5.5)$$

The maximum number of sweeps per second (inspection rate) with a synthesiser total sweep time including band switches and fly-back of 58 ms is:

$$f_{inspection} = \frac{1}{T_{inspection}} = \frac{1}{58 \times 10^{-3}} = 17.24 \text{ Hz} \quad (5.6)$$

the the total expected average data generated per second with a message size per sample of 40 bits is:

$$Data \text{ Payload} = f_{inspection} \times D_{msss} \times Message \text{ Size} = 1.14 \text{ Mb} \quad (5.7)$$

Fitting this into the band switch and fly-back period of each inspection gives a data rate of:

$$\frac{Data \text{ Payload}}{f_{inspection} \times (T_{flyback} + T_{bandswitching})} = \frac{1.14 \times 10^6}{17.24 \times 31.6 \times 10^{-3}} = 2.09 \text{ Mbaud} \quad (5.8)$$

These figures assume no handshaking, line returns or checksums.

A USB connection was chosen over a standard serial connection because of the additional speed needed for the quantity of data to be transferred. A standard serial connection would have been insufficient for transferring captured data for real time processing. USB is ubiquitous on modern computers and satisfies the bandwidth requirements for real time transfers with a theoretical bandwidth of Low Speed (1.5Mbps) and Full Speed (12Mbps) for USB 1.0 and 480Mbps for USB 2.0. USB 1.0 is sufficient for our requirements and the Microchip PIC18F2550 high performance USB 2.0 compliant micro-controller supporting Full-Speed USB 1.0 connections (Microchip, 2009). Although capable of simultaneous dual channel signal capture the USB capable micro-controller a Microchip PIC18F2550 was unable to fully utilise the available USB bandwidth. A significant time was spent trying to improve the throughput of the micro-controller. Both CCS and Microchip compilers were evaluated, see Appendix C, but ultimately even rewriting firmware to interface directly with the USB Engine instead of using the standard library only an improvement of 34% was achieved, this performance was inadequate. An alternative was needed and a commercial USB to UART bridge was identified TTL-232R-3V3. Manufactured by FTDI the bridge is capable of 3Mbaud.

The next board revision dropped the second digitisation channel in exchange for a higher maximum speed and reduced circuit and firmware complexity.

Even so, when using only a single ADC the system is capable of saturating the 3Mbps data channel offered by the bridge. The throughput the hardware serial port of a PIC18F is:

$$Baud\ Rate = \frac{F_{osc}}{4(n+1)} \quad (5.9)$$

where F_{osc} is the system oscillator speed and n is the value in the SPBRG register.

Therefore, by inspection of Equation (5.9), the maximum achievable baud rate and hence throughput for the serial port, is a quarter of the system oscillator speed. The maximum oscillator frequency for this chip is 40 MHz giving a maximum throughput of 13.33 Mbaud, however the baud rates supported by the USB converter are different (FTDI, 2010):

$$Baud\ Rate = \frac{3000000}{y+0.125x} \quad (5.10)$$

where y can be any integer between 2 and 16384 and x can be an integer between 0 and 7, except when $y = 1$, x must equal 0. Thereby achieving baud rates between 183.1 baud and 3 Mbaud. The inter-relationship of all these variables influences the processing capability of the MCU via F_{osc} and the throughput of the data link in the following relationship:

$$\frac{F_{osc}}{4(n+1)} = \frac{3000000}{y+0.125x} \quad (5.11)$$

A 36 MHz system clock was selected, a reduction of 1 MIPS, but allowing full use of the serial link - 3 Mbaud.

Changing the oscillator also alters the ADC module clock. The original PIC18F2620 was swapped for a PIC18F2431 with an internal high resolution automatically clocked and buffered ADC module with automatic acquisition triggering.

The new T_{adc} can be calculated using the T_{AD} (typically 416 ns) for the PIC18F2431 (Microchip, 2010):

$$T_{AD} \leq \frac{F_{osc}}{ADC_{divisor}} = T_{adc} \quad (5.12)$$

where $ADC_{divisor}$ is a preselected conversion value and in this case 16, producing a T_{adc} of 444 ns for a 36 MHz system clock. Allowing sample time. The minimum acquisition time is:

$$T_{acq} = T_{amp} + T_{coff} + T_c \quad (5.13)$$

where T_{amp} is the amplifier (negligible) settling time, T_c is the holding capacitor charging time and T_{coff} is the temperature coefficient. T_{coff} is (Microchip, 2010):

$$T_{coff} = (Temp - 25^\circ C)(5 \times 10^{-9} s^\circ C^{-1}) \quad (5.14)$$

where $Temp$ is the operating temperature of the converter. Assuming the maximum operating temperature is $50^\circ C$, T_{coff} is:

$$T_{coff} = (50^\circ C - 25^\circ C)(5 \times 10^{-9} s^\circ C^{-1}) = 130 \times 10^{-9} s \quad (5.15)$$

T_c allowing for a conversion error of $\leq 1/2$ LSB is:

$$T_c = -(C_{hold})(R_{ic} + R_{ss} + R_s) \ln\left(\frac{1}{2047}\right) \times 10^{-6} s \quad (5.16)$$

where C_{hold} is the hold capacitor (9 pF), R_{ic} is the internal multiplexer switch impedance, R_{ss} is the internal sampling switch impedance and R_s is the source impedance. R_{ss} varies with V_{dd} and for a 5 V supply R_{ss} is 6 k Ω , therefore T_c is:

$$T_c = -(9 pF)(1 k \Omega + 6 k \Omega + 100 \Omega) \ln\left(\frac{1}{2047}\right) \times 10^{-6} s = 620 \times 10^{-9} s \quad (5.17)$$

Hence T_{acq} is:

$$T_{acq} = (0 + 130 + 620) \times 10^{-9} = 750 \times 10^{-9} s \quad (5.18)$$

The resulting maximum throughput was:

$$F_{\text{sample}} = \left(\frac{1}{\frac{12 \times 16}{36 \times 10^6} + 750 \times 10^{-9}} \right) = 164 \text{ ksps} \quad (5.19)$$

This completes the ADC calculations in preparation for coding.

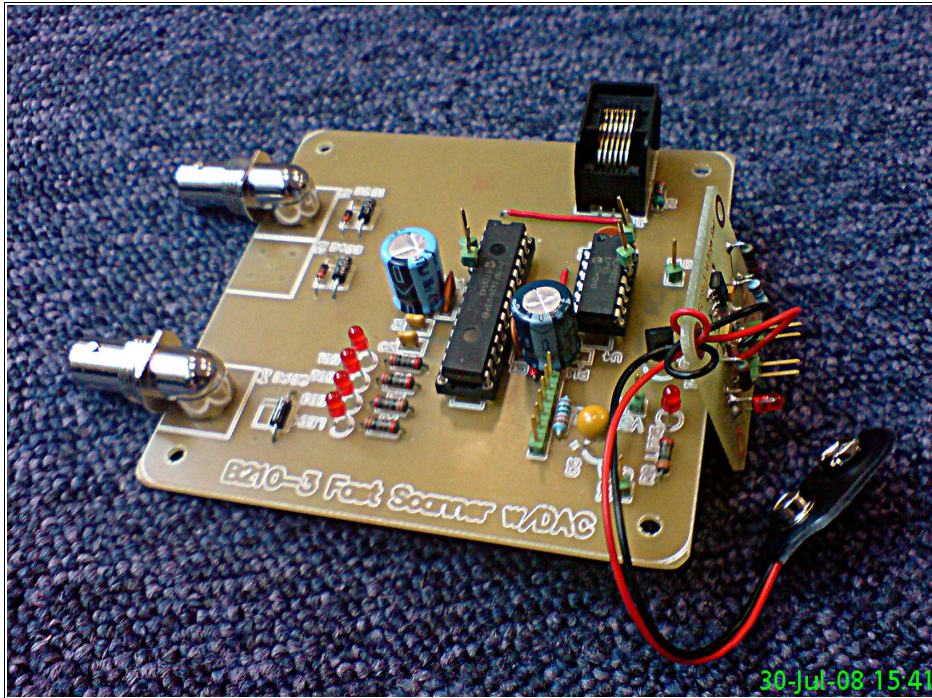


Figure 5.10: Rapid Scanner v3

The final version of the board and top level diagram are shown in Figures 5.10 and 5.11.

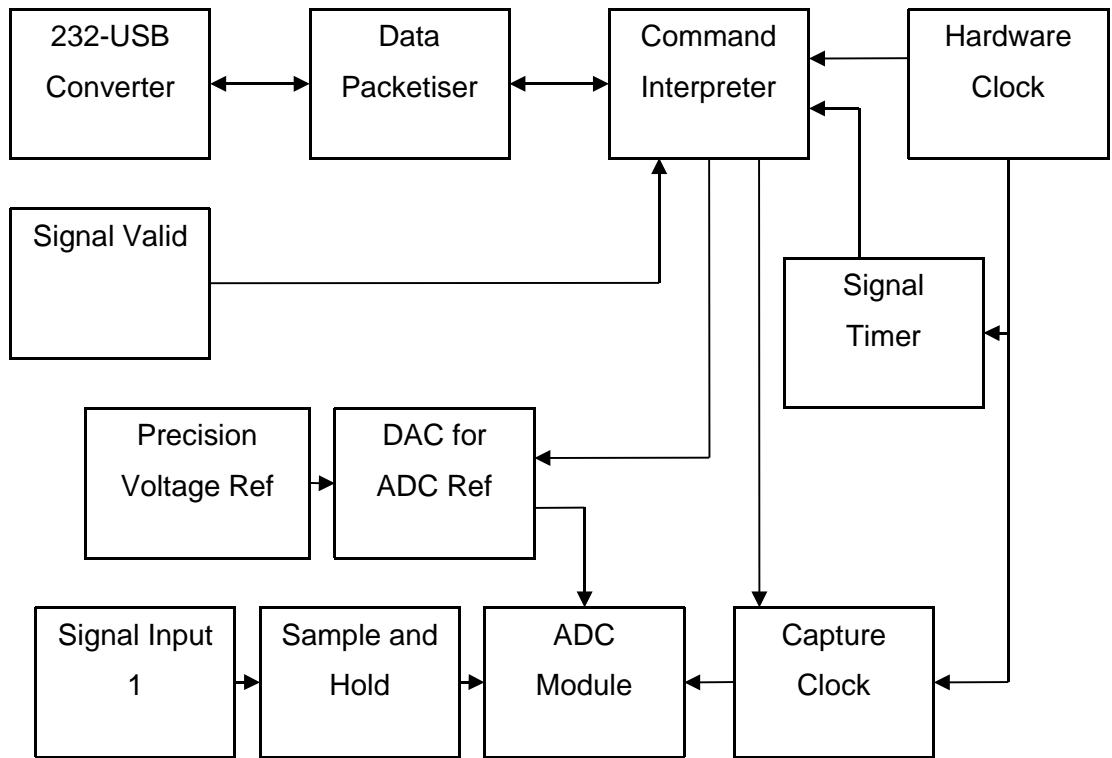


Figure 5.11: Rapid Scanner v3 top level block diagram

The resolution obtainable by the commercial NI-6132 card was exceeded and by controlling the ADC reference a variable inter-inspection dynamic input was created.

5.2.2 Rapid Scanning Performance Benefits

Speed increases in excess of 10,000% were achieved, by sweeping instead of stepping the frequency source, reducing the time taken to obtain a long scan of 32768 points (chosen from 2^n for numerical analysis) used for a long scan with the FPI where a large number of points gave good resolution over narrow bands reducing the time taken from three and a half minutes to well under a second. To enable ever faster sweep speeds faster prototypes are needed to maintain the number of scan points created within a sweep. For example, if 2048 points are required and the sweep time is 20ms then the minimum sample rate F_{min} would be:

$$F_{min} = \frac{I_s}{T_i} \quad (5.20)$$

where I_s is inspection size or number of samples and T_i is inspection time. To acquire 2048 samples in 20 ms, a minimum sample rate of 102 ksps is required.

A significant and inherent benefit of increasing signal acquisition rates was to produce a system capable of capturing inspection data almost instantly. This made examination and measurement of targets more intuitive, enabling interactive manipulation of targets in real-time, in a ways previously impossible.

The original software was written using MATLAB and it was later and unexpectedly discovered that MATLAB has limited high speed serial communications support. All debugging and throughput measurement had been fulfilled by a custom C# application. The maximum rate supported using MATLAB was 230 kbaud, much less than the 3 Mbaud that was planned. Typically 2400 samples would be generated for a 16 ms sweep with a 150 KSPS sample rate. The maximum number of samples that could be transmitted per second over the MATLAB limited serial link would be 11500. This would adversely impact the inspection rate and limit the maximum number of samples possible within an inspection. Using the existing process of sequentially sampling and transmitting data would result in a significant inter-inspection delays of approximately:

$$T_{inspection} = \frac{10 R_s n_s}{8 n_b} \quad (5.21)$$

where n_b is the baud rate of the serial link, R_s is the sample size in bits and n_s is the inspection size in data samples. Giving a MATLAB imposed inspection time of 209 ms, instead of the expected 16 ms for a 3 Mbaud connection.

Re-writing the rapid scanner firmware to buffer and asynchronously transmit the sample data was not an option due to lack of RAM. To overcome this issue, the number of samples taken was reduced to allow local buffering and asynchronous transmission to the host PC. However this approach proved insufficient and without data compression the

rate of inspections per second would suffer, dropping from the expected 18 fps to less than 6 fps. Lossy compression of the sample data would be an acceptable interim measure until the C# version of the software capable of Full Speed USB communication was ready.

The effect of lossy compression upon reconstruction and transformation of the data into the time domain would be to reduce the amplitude of high frequency signal components, representing large optical distances which would not be present anyway. The degree of compression would be proportional to the attenuation of high frequency components.

The time taken to bin and compress the data was similar to the time it would take to send it in its entirety. Therefore, apart from implementing a routine to reconstruct the data on the host PC prior to processing and analysis, the MATLAB imposed restriction on serial port baud rate was circumvented.

Bench tests have shown that 12 Mbaud is possible with enhanced hardware and an FTDI F232H IC, using PCB B251A FT2232H breakout board. It is expected this additional speed and more could be needed by future systems.

5.3 Frequency Source

The VCO used in all of the portable prototypes is a manufactured part made by Siverts IMA, model number VO3260P/04. This microwave primitive is the radiation source, producing a frequency roughly linear with control voltage. The power output varies by frequency and temperature as shown in Figure 5.12 and fulfils the input requirements of the AMC-10 Harmonic Generator, used to multiply the frequency to 75 – 110 GHz.

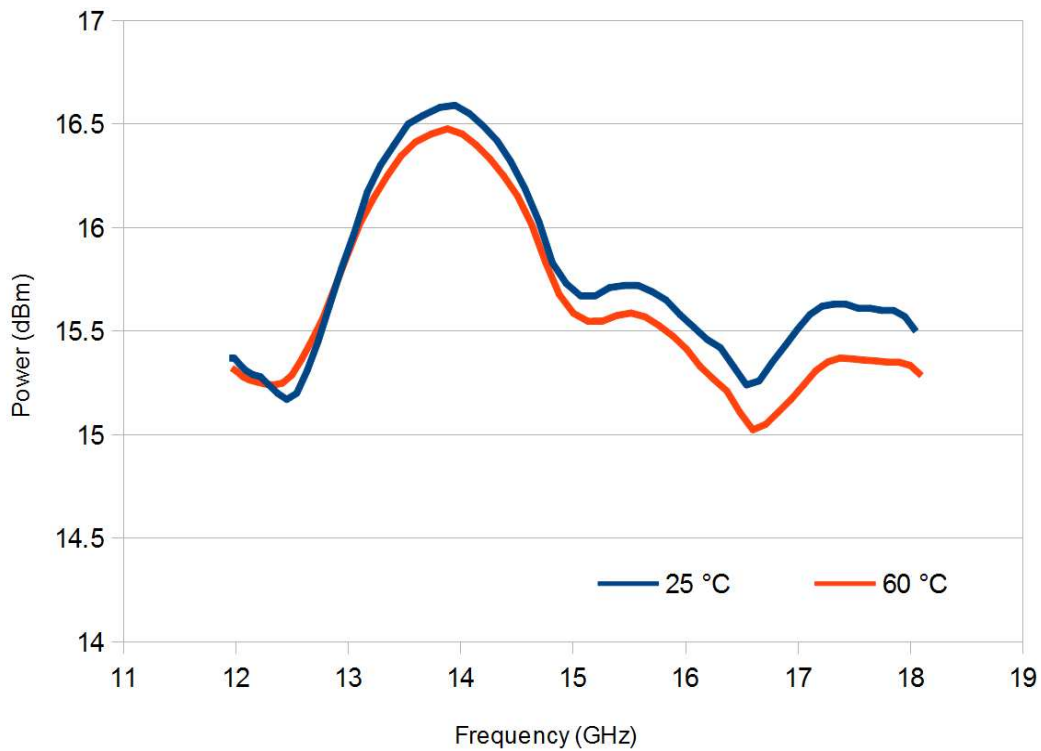


Figure 5.12: VCO output power output against frequency

The non-linear drive voltage frequency response is shown in Figure 5.13.

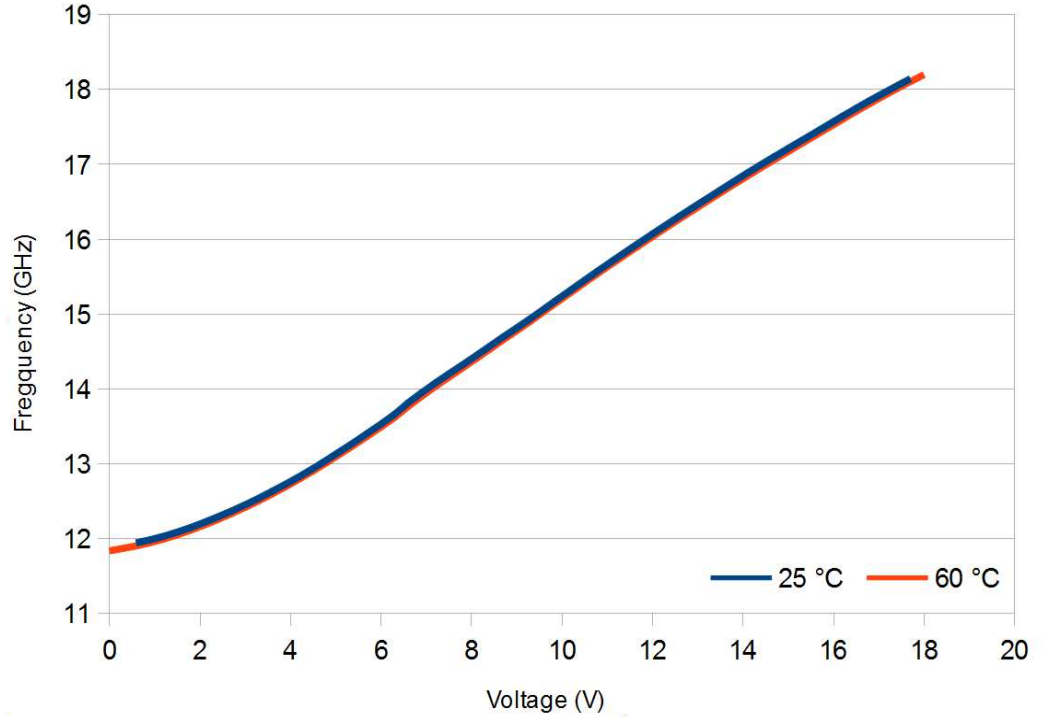


Figure 5.13: VCO output frequency against driver voltage

Driving the VCO with a linear voltage ramp will not produce equally spaced frequency steps resulting in a loss of resolution. Brooker et al., (2005) states the achievable resolution with a non-linear sweep is:

$$\Delta d_{lin} = d_{target} Lin \quad (5.22)$$

where d is the distance to the target and Lin is the linearity of the ramp defined as:

$$Lin = \frac{S_{max} - S_{min}}{S_{min}} \quad (5.23)$$

where S_{min} and S_{max} are the rate of change of frequency sweep with voltage ($\Delta F/\Delta V$).

This can be combined quadratically with the system frequency bandwidth:

$$\Delta d_{resolution} = \sqrt{\left(\frac{c}{2\Delta f}\right)^2 + (d_{target} Lin)^2} \quad (5.24)$$

For direct detection the non-linearity associated with using a linear voltage ramp to drive the non-linear response shown in Figure 5.13, did not significantly affect the depth spectra obtained as the effective value of d_{target} is small. However, for homodyne systems, for

example Prototype 4 (see Section 5.7), the range finder requires a closer to ideal linear frequency sweep and in this case the voltage sweep generated by the Rapid Sweeper circuitry (see Section 5.3.1) was designed to compensate for the VCO non-linearity. The non-linear voltage curve was generated by extracting the desired frequency and voltage pairs from a cubic spline interpolation of the measured response, shown in Figure 5.13.

5.3.1 Rapid Sweeper

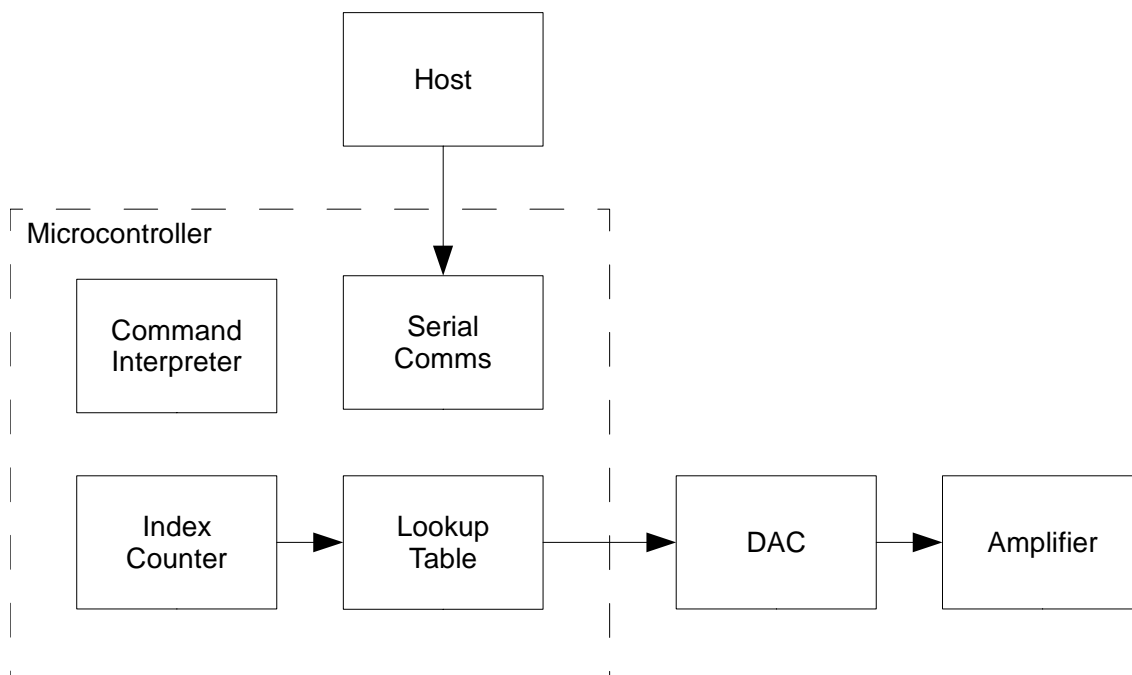


Figure 5.14: Rapid scanner top level system diagram

The Rapid Sweeper is a device developed to provide a non-linear drive voltage for non-linear VCOs, for generation of a linear frequency ramp. The frequency against voltage characteristics for the VCO are shown in Figure 5.13 and the non-linearities are easier to observe in Figure 5.15 plotting the voltage tuning sensitivity against frequency change.

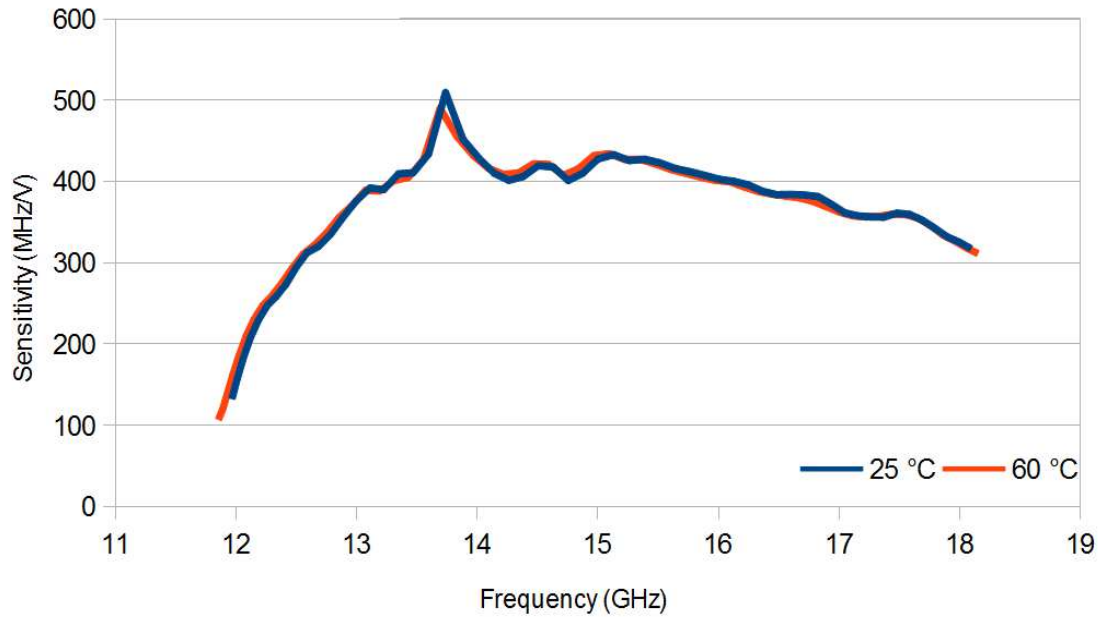


Figure 5.15: Tuning sensitivity for Siverts IMA VCO at different temperatures

Host communications were handled by a FTDI USB TTL converter part number TTL-232R-3V3. The command interpreter accepts instructions and configuration information from the host and initiates frequency sweeps as required. The DAC selected for this prototype was a 5V TTL parallel interfaced 16 bit low glitch multiplying current output DAC operating in unipolar mode generating 0 – 10 V ramp using a LT1112 op amp and with secondary amplification provided by an OP97FPZ to produce a low impedance drive signal 0 – 18 V for the Siverts IMA VCO.

5.4 Target Screening and Localisation of Concealed Objects

Scanning a detector is a common way of increasing the detection volume of a system. This is implied for imaging systems where the detection element(s) can be scanned across the desired detection volume. Scanning can be achieved either mechanically or electronically and depends on the technology used.

If a detector is small and lightweight, a crude scanning regime can be undertaken by the operator by moving or aiming a detector over the target. This may be slower than mechanically or electrically scanned systems, but provides more control and is far simpler to implement.

The signals reflected from the body vary from different parts of the torso. Signals from the arms appear behind the chest and lead to interference effects very similar to the signature of explosive material. To mitigate this problem, microwave optics are used to focus illumination onto a small area of the subject, so only signals for one part of the body are being measured at a time. The decision to increase the operating frequency allowed the use of smaller optics and achieved the design goal of a compact and lightweight system.

5.4.1 Illumination Spot Size

For the technique to work optimally the object needs to be illuminated with a beam commensurate with the size of the object. Illuminating an area larger than the object under inspection reduces system performance, because that signal measured at the receivers contains information about not just the object but the surrounding area. Therefore it is crucial for optimum performance that the beam pattern is comparable in size to the object being scanned, and this depends on the gain of the transmitter and receiver antennas. The directionality of a pyramidal optimum horn antenna is a function of gain (Wikipedia contributors, 2012):

$$G = e_A \frac{4\pi A}{\lambda^2} \quad (5.25)$$

where e_A is the aperture efficiency (0.511 for a horn antenna) and A is the product of:

$$a_E = \sqrt{3\lambda L_E} \quad (5.26)$$

where L_E is slant length of the side in the E-field

$$a_H = \sqrt{2\lambda L_H} \quad (5.27)$$

where L_H is the slant length of the side in the H-field and combining to create:

$$G_{optimum} = e_A \frac{4\pi \sqrt{3\lambda L_E} \sqrt{2\lambda L_H}}{\lambda^2} \quad (5.28)$$

The beam width ω at range r for antenna gain G is defined as:

$$\omega \approx r \left(\frac{4\pi}{G} \right)^{\frac{1}{2}} \quad (5.29)$$

This is plotted in Figure 5.16 as a function of range r , for a 20 dB rectangular horn antenna.

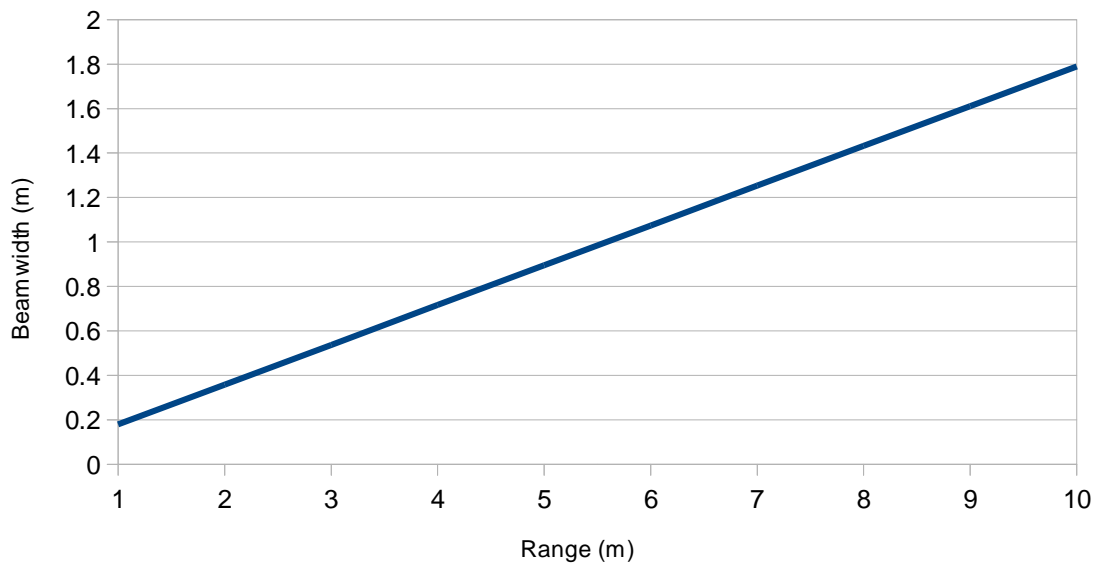


Figure 5.16: Spot size (half power) as a function of distance

Since the beam pattern is a function of range, the performance of the system varies on object size and the range of operation. This dynamic is partly mitigated by providing real-time feedback to the user by showing the beam pattern as an overlay on the live camera feed part of the GUI. This performance variation applies to guns, whereas for explosives a representative patch is needed due to its uniform nature.

Standard gain horns are available in 10, 15, 20 and 25 dB versions. Larger horns produce more gain. A 25db horn is approximately 3 times longer than the equivalent 20dB horn. The use of just an antenna to generate a small radiation spot on the target is impractical and therefore a horn antenna in combination with a lens was used. This increases the effective gain.

5.5 Prototype Two: Direct Detector Tripod Prototype

The first compact prototype is shown in Figure 5.17. The top level systems diagram for the prototype is shown in Figure 5.18.

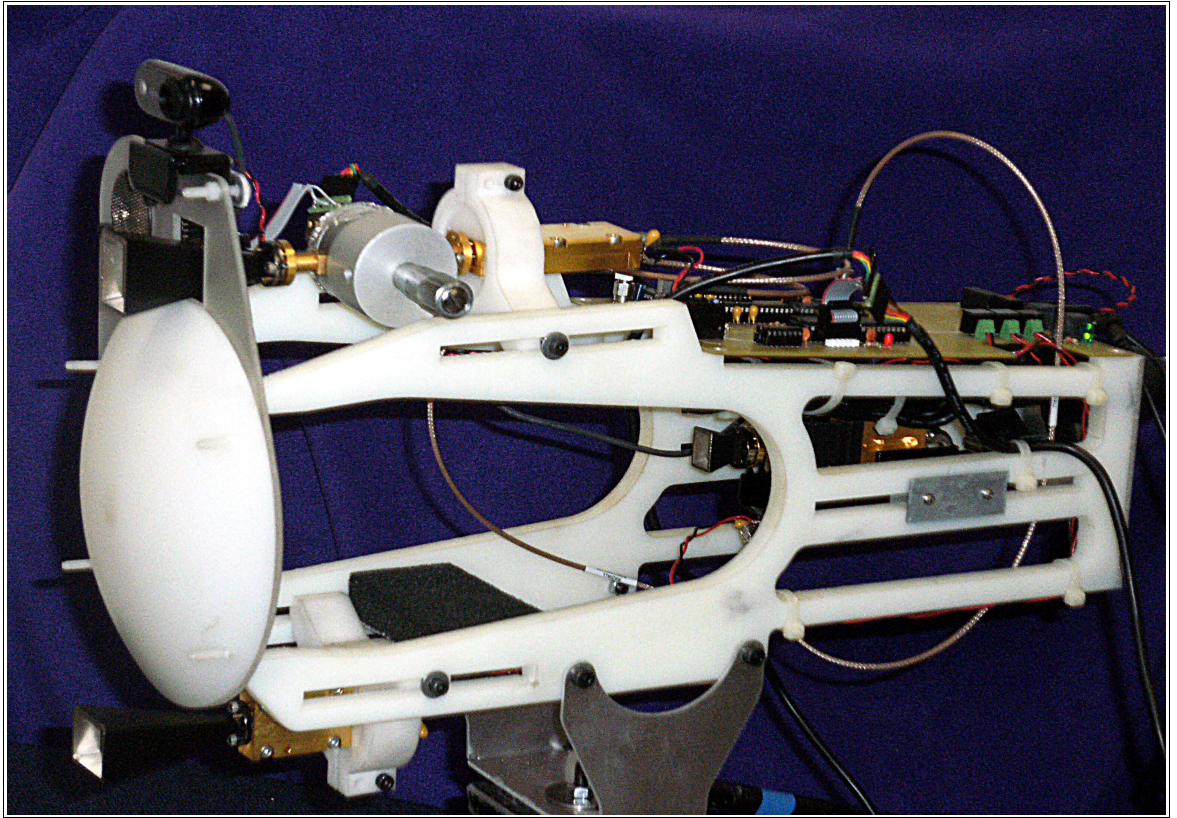


Figure 5.17: First portable direct detector prototype

This prototype is a self contained unit requiring no external bench equipment, except a laptop providing the user interface and running the MATLAB detection script.

Table 5.1 is a parts list of the top level systems. The following sections describe the design and operation of each individual subsystem.

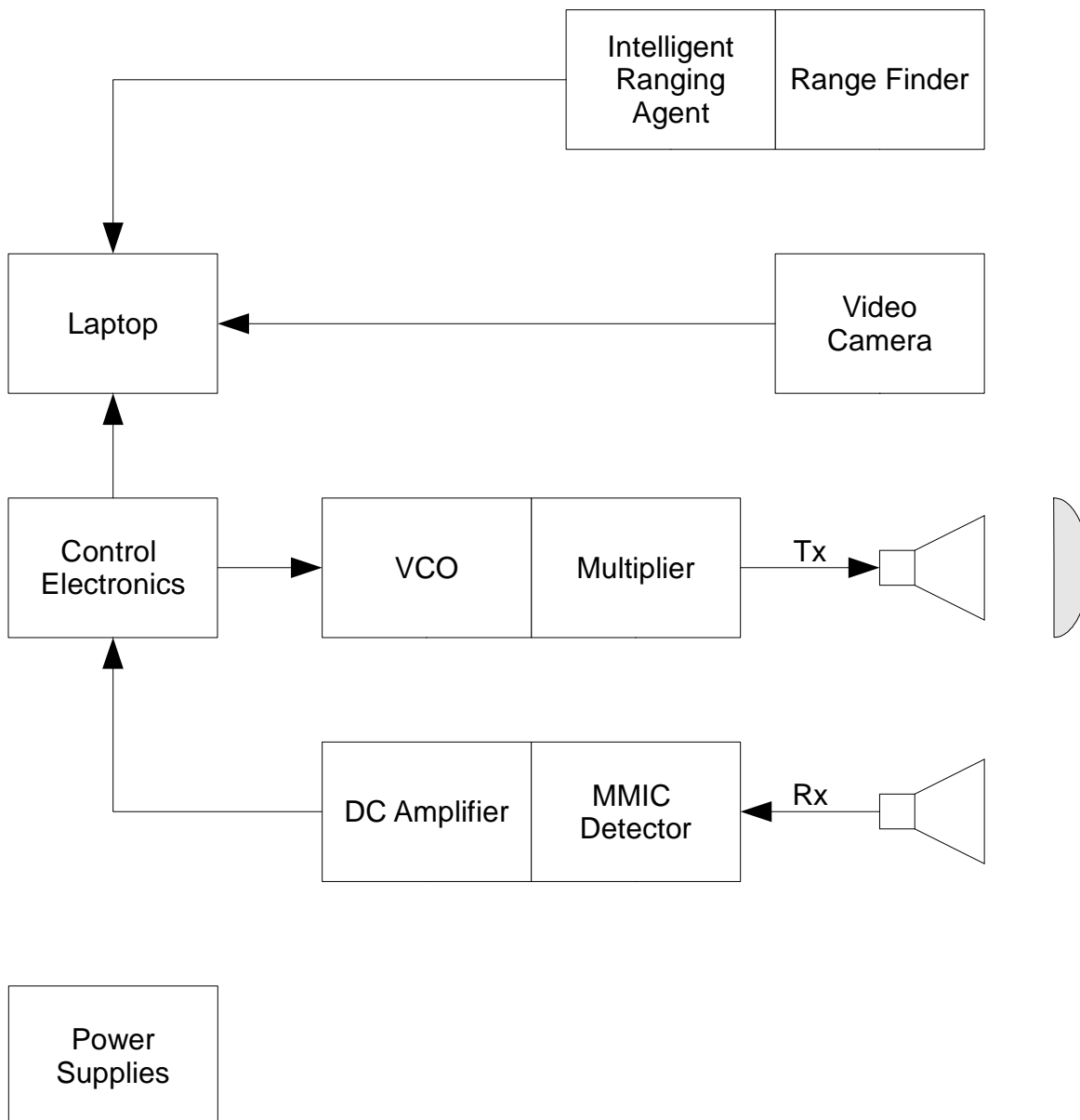


Figure 5.18: Top level systems of the first portable direct detector prototype, only one receive channel is shown

Video Camera	Trust HiRes USB camera
Multiplier	Millitech AMC-10-RFH00 active chain multiplier
VCO	Sivers IMA VO3260P/02 wide band voltage controlled oscillator
MMIC x2	MMIC 94GHz detector supplied by MMIC Solutions
Control Electronics	B253A
Range Finder	SensComp 615088 50kHz Instrument Grade Smart Sensor with smart slave interface
Lens	Polyethylene lens designed by Sarah Smith
Power Supplies	B272 Direct Detector RF PSU board
Laptop	Intel i5 with 4 GB RAM

Table 5.1: Prototype two top level parts list

To obtain a single inspection, the control electronics monitors the physical user interface. When a trigger event has occurred the control electronics loads the first value from the lookup table into the DAC and initialises the range finder. The voltage from the DAC causes the voltage controlled oscillator to generate a RF signal. This signal is multiplied to the desired frequency within the harmonic generator and transmitted via the transmitter horn. The lens focuses this energy onto the target with a beam size approximately commensurate with the size of a medium to large handgun. Energy returns from the target are captured by the receiver horns in co and cross polarisation, amplified and measured by the MMIC receivers, producing a voltage proportional to the detected RF energy. The ADCs digitise the respective voltages for processing by the control electronics. This sequence is repeated for each value in the lookup table. The receiver data is processed and compressed before transmission with accompanying data from the range finder to the PC

via the communications subsystem. The PC unpacks and analyses the data; updates the user interface and provides feedback if a threat is detected. The video feed is manipulated to show the scan area and calculated beam pattern.

The role of B253A board is to manage, configure, synchronise and power the hardware portion of the prototype. The VCO lookup table was created by the method described in Section 5.3.1 and refined by iteratively measuring and modifying the voltage curve to achieve the desired linear frequency ramp.

The host computer processes data sent by the control electronics and provides the graphical user interface. The laptop processor and memory specifications are an Intel multi-core i5 with 4 GB of RAM.

The transport of data and translation of protocol and physical signal translation is handled by multiple FTDI USB TTL converters. Data is packetised prior to transmission by micro-controllers to ensure synchronisation and data integrity.

This user interface consists of physical switches and buttons used to control the system software. The main push to scan trigger is part of this interface.

The video feed is provided by a Trust HiRes USB 2.0 web cam shown in Figure 5.19 connected to the host PC via a hub. This camera was chosen because of its diminutive size and video resolution of 640×480 at 25 fps.



Figure 5.19: Video feed provided by a Trust HiRes USB 2.0 Webcam

The target range is determined using a SensComp 50 kHz ultrasonic SmartSensor interfaced and controlled by board B246A running software P246B. This board makes for a self contained unit providing a simple serial interface for the host PC. The measurement and host update rate was set to 20Hz. The highest measurement rate is a function of target range and the speed of sound in dry air (Hyperphysics, 2008):

$$v_{sound} \approx 331.4 + 0.6T_c \quad (5.30)$$

where T_c is temperature in degrees Celsius. At 25 °C the speed of sound is 346 ms⁻¹, therefore the maximum measurement rate is:

$$Measurement\ Rate \approx \frac{v_{sound}}{2d} \quad (5.31)$$

where d is the maximum range of 8 m, the peak measurement rate is 21.6 Hz.

During trials a slower rate of 3 Hz was found to provide a responsive system while minimising unnecessary measurements.

Unlike airport scanners, this portable machine does not produce revealing images of the subject by using a standard camera to assist aiming. Professor Bowring told BBC News "It is designed to work out on the streets and is not (restricted) to a closed, controlled environment," (BBC, 2009a).

Active mm-wave illumination will be used by the prototype. It has already been decided to investigate detection methods utilising active illumination of the target to improve performance within uncontrolled environments. The decision on the frequency band used was based on the availability of parts for a 75 to 110 GHz radar. The increase in absolute bandwidth improved the radar resolution to 4.3 mm, compared to lower frequencies and requires physically smaller optics to focus.

The rapid sweeper used for this prototype is a compact version of the circuitry used to drive the VCO for a proposed super heterodyne radar. For more information about this sub-system refer to Section 5.3.1.

A full description of the VCO used was provided earlier in section 5.3.

Manufactured by Millitech the part number AMC-10 is a times six multiplier producing signals in the 75 - 110 GHz band. Requiring a nominal RF input power of 10dBm (max 13dBm) (Millitech, 2011), the target is illuminated using the radiation generated by this device.

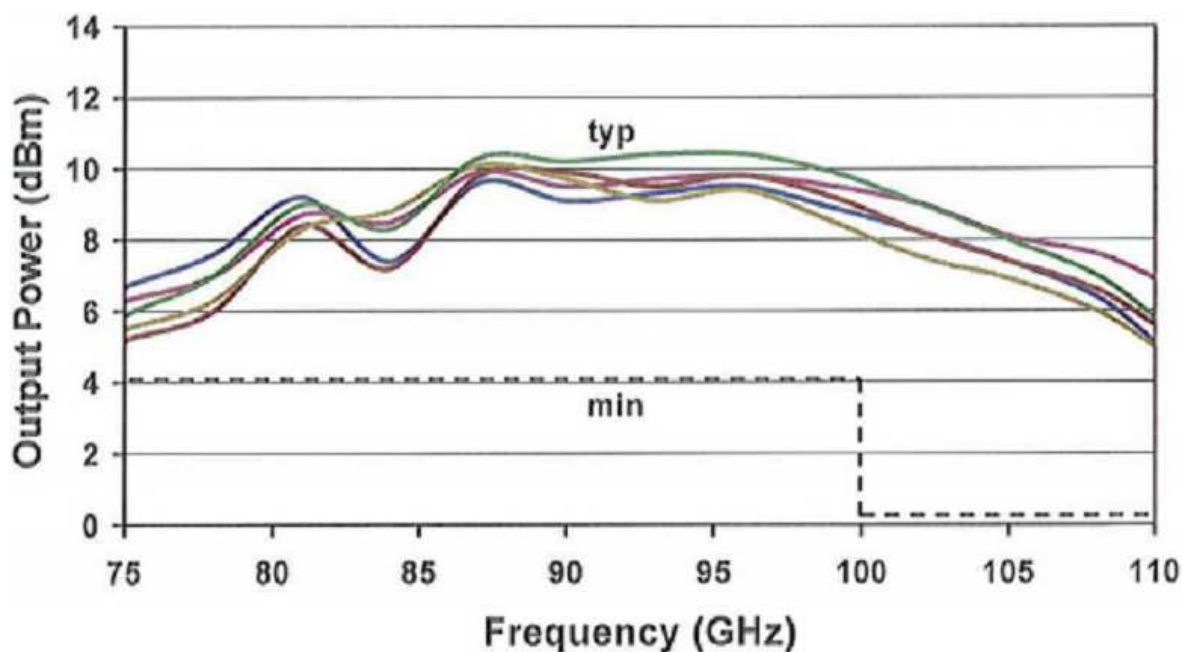


Figure 5.20: AMC-10 frequency against output power (Millitech, 2011)

Microwave horns are used to direct radiation. Antenna gain is calculable from the flare dimensions of the horn using Equation (3.3).

A single 20 dB horn is used to illuminate the the microwave lens.

The role of the microwave lens is to focus the diverging microwave beam as it exits the horn into as small a spot as possible at a distance of 8m.

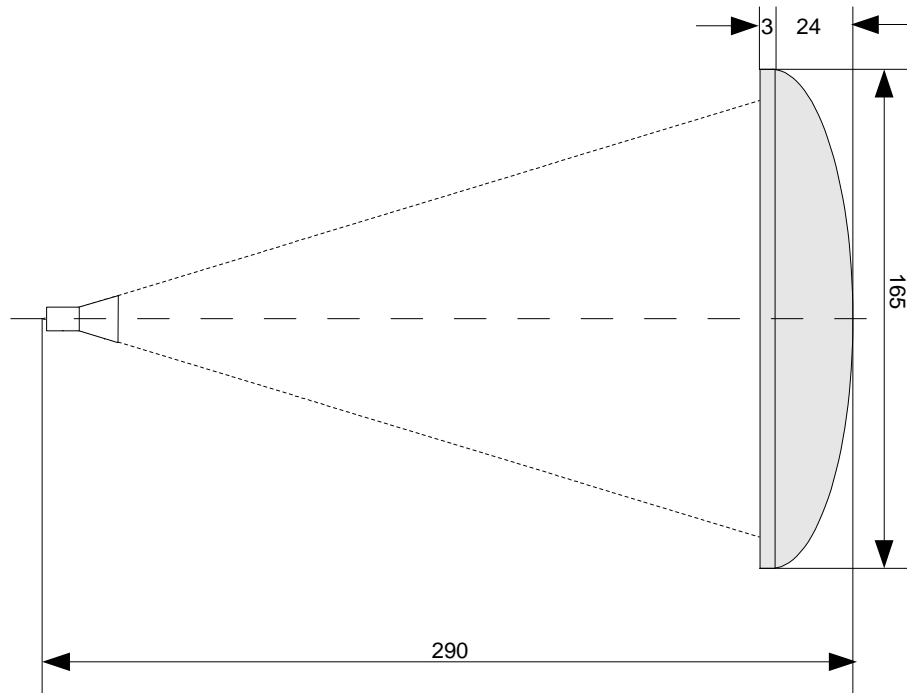


Figure 5.21: Diagram of lens

The lens used is planoconvex. The thin lens approximation for the focal length f is:

$$\frac{1}{f} = (n-1) \cdot \left(\frac{1}{R_1} + \frac{1}{R_2} \right) \quad (5.32)$$

where the radii of curvature of the lens surfaces are $R_1 = \infty$, $R_2 = 150$ mm and $n = 1.52$ for polyethylene, giving a focal length of approximately 290 mm. The beam size angle is defined as:

$$\theta_{FWHM} \approx 1.22 \frac{\lambda}{D} = 0.026 \text{ rad} \quad (5.33)$$

Where $\lambda = 3.3$ mm @ 90 GHz.

The gain of an ideal horn and lens combination is:

$$G \approx 6 \left(\frac{D}{\lambda} \right)^2 = 15000 = 42 \text{ dB} \quad (5.34)$$

Where the horn is at the point of focus:

$$\frac{D}{f} \approx \frac{165}{290} = 0.56 \text{ rad} \quad (5.35)$$

Typically, the optimal fill of a lens is:

$$\frac{D}{2f} \approx 0.28 \text{ rad} \quad (5.36)$$

which approximates to the beam angle of a 20dB horn antenna. The lens was designed by Sarah Smith and built in house. Smith (2012) provides a full description of the design.

Polyethylene was used instead of PTFE because of the difficulty of manufacture.

Figure 5.22 compares the theoretical beam size with 3 dB measurements taken in the lab at various distances.

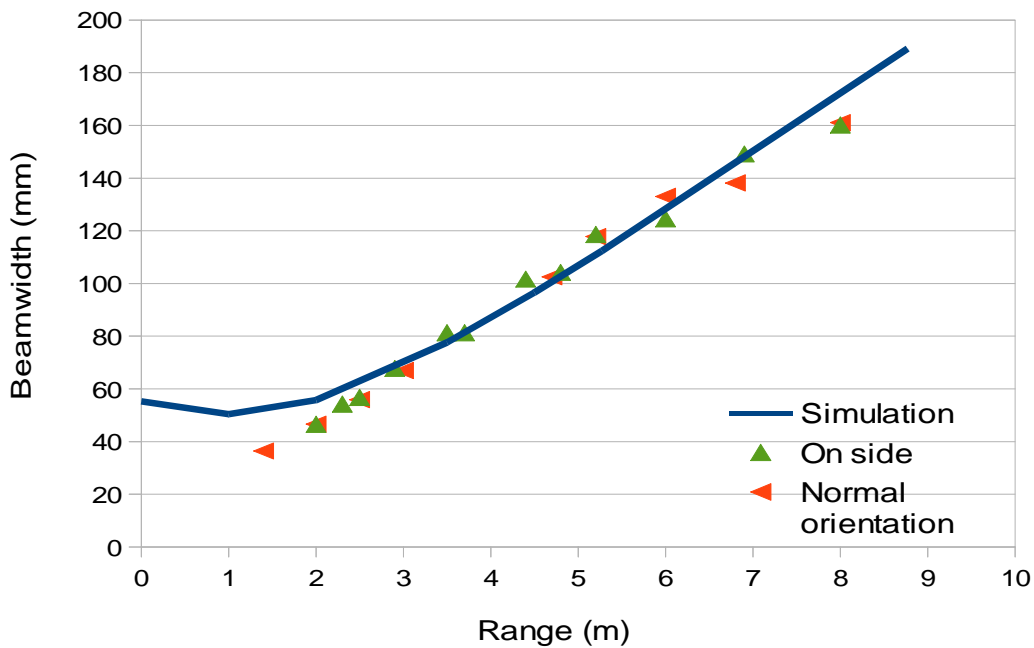


Figure 5.22: Spot size measurements with lens, range against beam-width

The receiver horns are used to provide signal gain and maximise the signal detectable by the MMICs. The horns are commercial off the shelf 75 – 110GHz 25dB gain antennas.

Their purpose is to enhance the directionality of the system and passively improve the system's signal to noise ratio by creating a beam profile that overlaps with the transmitted beam at all distances. By minimising the collection of radiation from extraneous clutter, a high signal to noise ratio is maintained.

The MMIC receivers are monolithic devices incorporating a microwave frequency integrated circuit low noise amplifier and RF detector. They produce a bandwidth limited signal with greater sensitivity than a comparable zero biased detector alone (they incorporate a zero biased detector after two LNA stages). The prototype employs two devices, one in co-polar orientation and another in cross polar orientation. The device is manufactured by MMIC Solutions. These parts are traditionally used in passive imaging applications operating around 94 GHz. These devices measure RF power and generate a DC voltage.

Property	Value
LNA response bandwidth	4 kHz
Sensitivity	3×10^9 mV/mW
Detector Bandwidth	72 – 110 GHz
Detector Noise	≈ 0.1 mV

Table 5.2: MMIC LNA and detector properties

The device output noise of 0.1 mV equates to an input noise power of 0.03 pW. Figure 5.23 shows the performance and voltage output of the two MMIC LNA receivers used in the prototype.

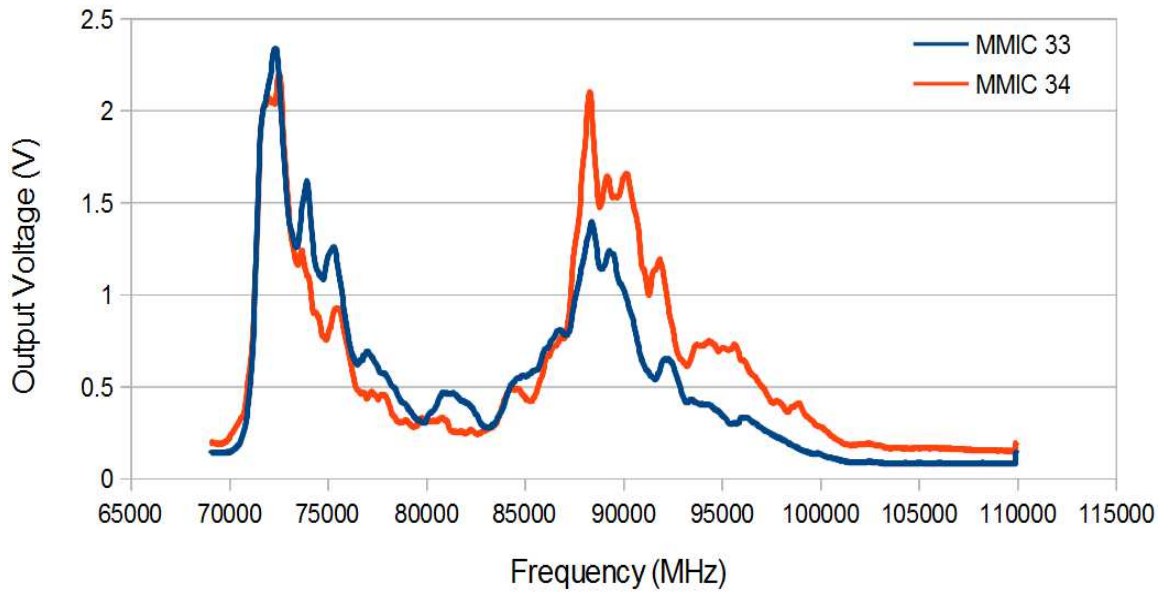


Figure 5.23: MMIC output voltage against frequency at room temperature

MMIC 33 and MMIC 34 are the serial numbers of the MMIC detectors under measurement. The measurement apparatus consisted of a VCO, AMC-10 harmonic generator and a series of attenuators connected to the MMIC detector input.

The Analog Devices' AD976A ADC was chosen to digitise the receiver signals for easy processing. The AD976A is a 200 kps, low power, 16 bit converter operating from a single 5 V supply. The converter resides with its controller on board B253A.

The power supply unit provides the numerous supply rails used by the different circuits and peripherals of the prototype from a single 12 V supply. The power supply circuitry consists of several buck, boost and linear regulators individually switched and current monitored using B240, running firmware P240.

A later version of board B241 incorporates a 4 x 20 character LCD displaying the status of the separate power circuits driven by another microcontroller running firmware P241.

Detection performance varied during experimentation and development of the rapid sweeper boards B226A and B226B. The cause of this variation was identified as temperature drift of the harmonic generator.

5.6 Prototype Three: Portable Direct Detector Prototype

The top level systems diagram for the prototype is shown in Figure 5.24.

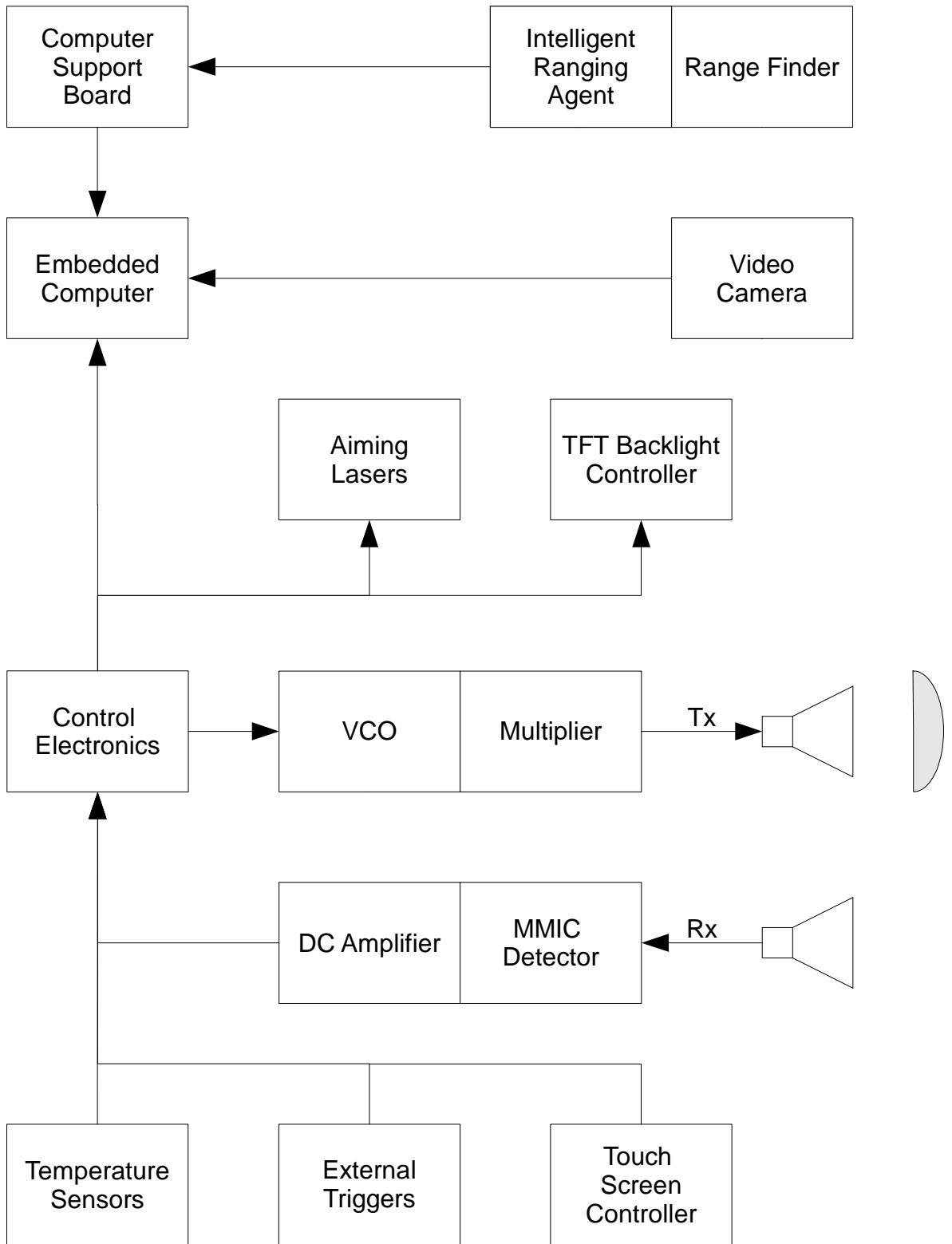


Figure 5.24: Top level systems of the first portable direct detector prototype, only one receive channel is shown

Video Camera	uEye UI-1226LE-C-HQ digital USB camera
Multiplier	Millitech AMC-10-RFH00 active chain multiplier
VCO	Sivers IMA VO3260P/02 wide band voltage controlled oscillator
MMIC x2	MMIC 94GHz detector supplied by MMIC Solutions
Control Electronics	B253B, B264, B270, B271, and B273
Range Finder	SensComp 615088 50kHz Instrument Grade Smart Sensor with smart slave interface board B246
Lens	Polyethylene lens designed by Sarah Smith
Power Supplies	B265, B266, B269
Laser Aiming	Four solid state laser diodes aligned as aiming guides without use of the video stream.
Computer Support Board	B273 provides power conditioning, data connection aggregation, battery backup for the RTC and an external buzzer interface.
Temperature Sensors	Incorporated onto B253B is a four channel temperature monitoring system with host reporting functionality.
Embedded PC	A Eurotech ISIS PC-104 embedded PC

Table 5.3: Prototype three top level parts list

System operation varies from the previous prototype in three major ways. A low power Intel Atom based embedded PC running software running Windows XP Embedded using a LCD and touch screen, handles user input and processing, removing the need for an external computer. The detector software is coded in C# rather than MATLAB, enabling the neural the network classification algorithm to run at full speed, in addition to enhancing the communication links. Temperature sensors have been included to monitor the environmental and RF subsystem temperatures to provide some stability in operation over a wider range of operating temperatures. Board B253B interfaces to and monitors the temperature sensors relaying digitised measurements to the embedded PC.

The power supply has been changed with all circuits running off a single 24 VDC supply provided by an external DC supply or battery pack including the LED LCD back-light which requires a boost converter producing 28 V. The revised PSU board B265 is significantly smaller than the previous revision, but lacks the capability of monitoring and switching individual supplies.

The criteria for selecting the video camera was, size, optics and connectivity. The uEye UI-1226LE is small and has the ubiquitous USB interface and supporting API. The optics contain an autofocus functionality so images are clear regardless of range.

The software consists of two versions for the direct detector, LabVIEW and a later C# versions. The C# version was developed in conjunction with some custom data acquisition electronics to vastly reduce data acquisition times and improve capture rates. The desired scan rate was 15 fps. The custom board was designed to be easily swapped between different computers to facilitate testing and be small enough to fit into a portable prototype. The custom board interfaced over a USB link, providing a single digitisation channel with a resolution of better than 19 mV. In one respect the custom board was inferior to the National Instruments' PCI-6132, which has a voltage resolution of better than 1.3 mV. In all other respects it was better (twenty four times faster), compact and lightweight. Later versions of this board are capable of resolutions of better than 0.1 mV and even faster acquisition rates were used when reliable true real-time data acquisition was needed.

Issues with the prototype were that the range finding ability was limited to 7 m and associated noise and alignment issues using acoustics. The embedded processor was regularly fully loaded and the MMIC receivers from MMIC Solutions Ltd are no longer manufactured.

5.6.1 Proposed Improvements

Several potential improvements were considered. For example, the incorporation of a homodyne radar replacing the ultrasonic range finder to improve the alignment and size of the range finder was considered. In order to reduce the processing load of the embedded computer, some of pre-processing of the data from the receiver may be offloaded onto a 32 bit PIC, freeing up the embedded PC to focus on the video stream and user interface. The receivers used in this and earlier prototypes are no longer available due to the closure of MMIC Solutions Ltd and identification of alternative parts will be necessary.

5.7 Prototype Four: Mirlin



Figure 5.25: Image of prototype four

Mirlin is the latest portable prototype, and with homodyne RF ranging capabilities. FFT processing has been offloaded to a 32 bit micro controller, freeing up the embedded PC to process video and GUI. Signal acquisition rates have increased to minimise spatial blurring of the ranger finder data and the MMIC receivers have been replaced with alternatives manufactured by Farran. The system top level diagram is shown in Figure 5.26.

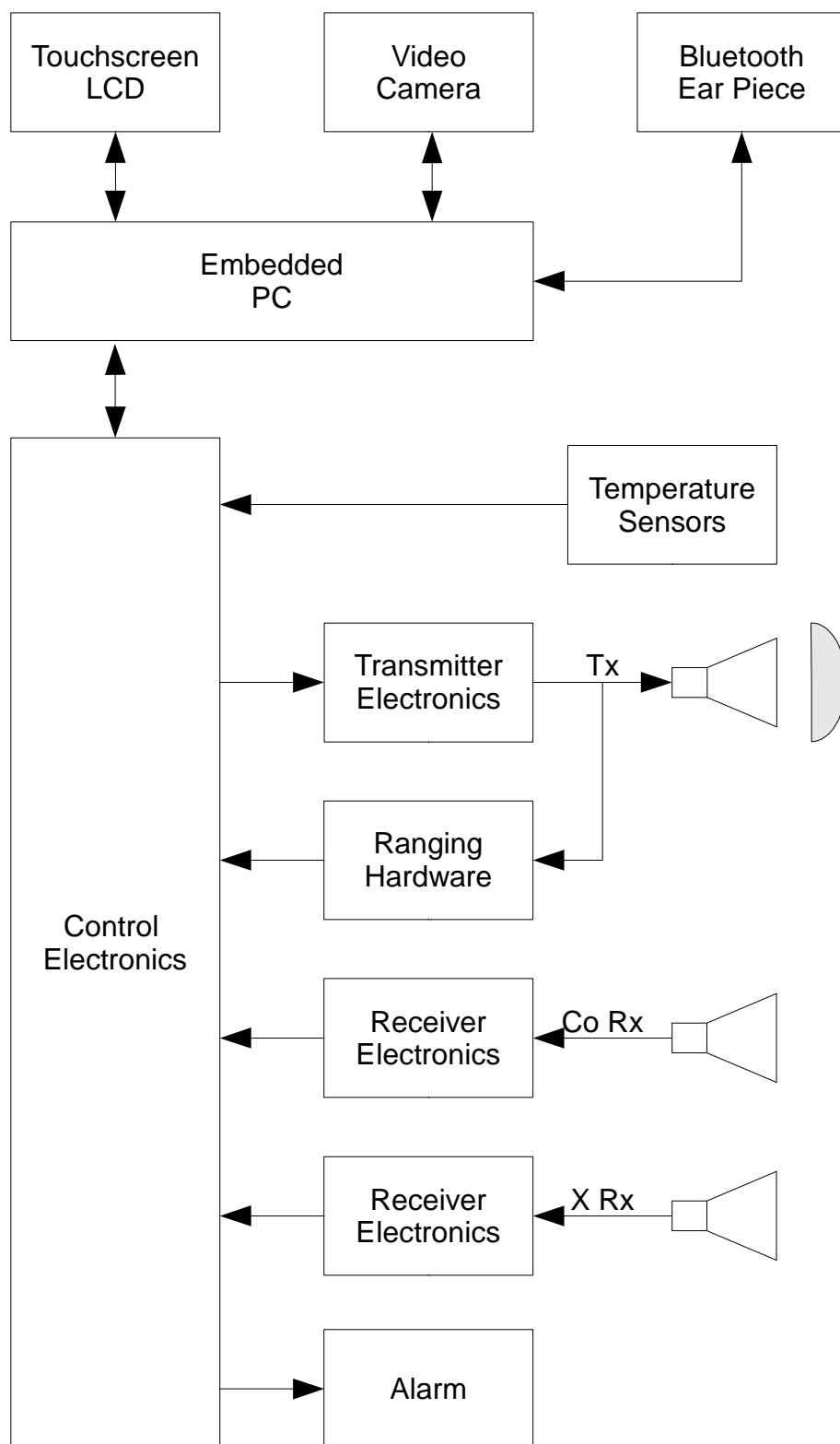


Figure 5.26: Top level system diagram for Mirlin

Video Camera	uEye UI-1226LE-C-HQ digital USB camera
Multiplier	Millitech AMC-10-RFH00 active chain multiplier
VCO	Sivers IMA VO3260P/02 wide band voltage controlled oscillator
Detectors	Farran FLNA40 and Farran WDP-10
Control Electronics	B269, B271, B273, B276, B277, B278, B279 and PIC32 DM320001 board.
Range Finder	Homodyne
Lens	Polyethylene lens designed by Sarah Smith
Power Supplies	B272 Direct Detector RF PSU board
Computer Support Board	B273 provides power conditioning, data connection aggregation, battery backup for the RTC and an external buzzer interface.
Temperature Sensors	Four channel temperature monitoring system.
Embedded PC	A Eurotech ISIS PC-104 embedded PC

Table 5.4: Prototype four top level parts list

Mirlin differs from the previous prototype by reducing the load on the host PC by performing the Fourier transform required for ranging and converting frequency domain data into the time domain for classification by the ANN. The additional processing capability is provided by a 32 bit PIC32. Replacing the MMIC receivers, with a part consisting of an ultra wide band low noise amplifier (LNA) with matched zero biased detector manufactured by Farran. Replacement of the ultrasonic range finder with a homodyne radar providing an unambiguous target detection range of 8.78 m. Co and cross receiver signals remain at 256 samples per channel, but the rate of sampling has increased to 170 kHz to improve inspection speed and system responsiveness.

The control electronics consists of a Microchip PIC32 DM320001 development board with various custom made daughter boards to handle signal conversion.

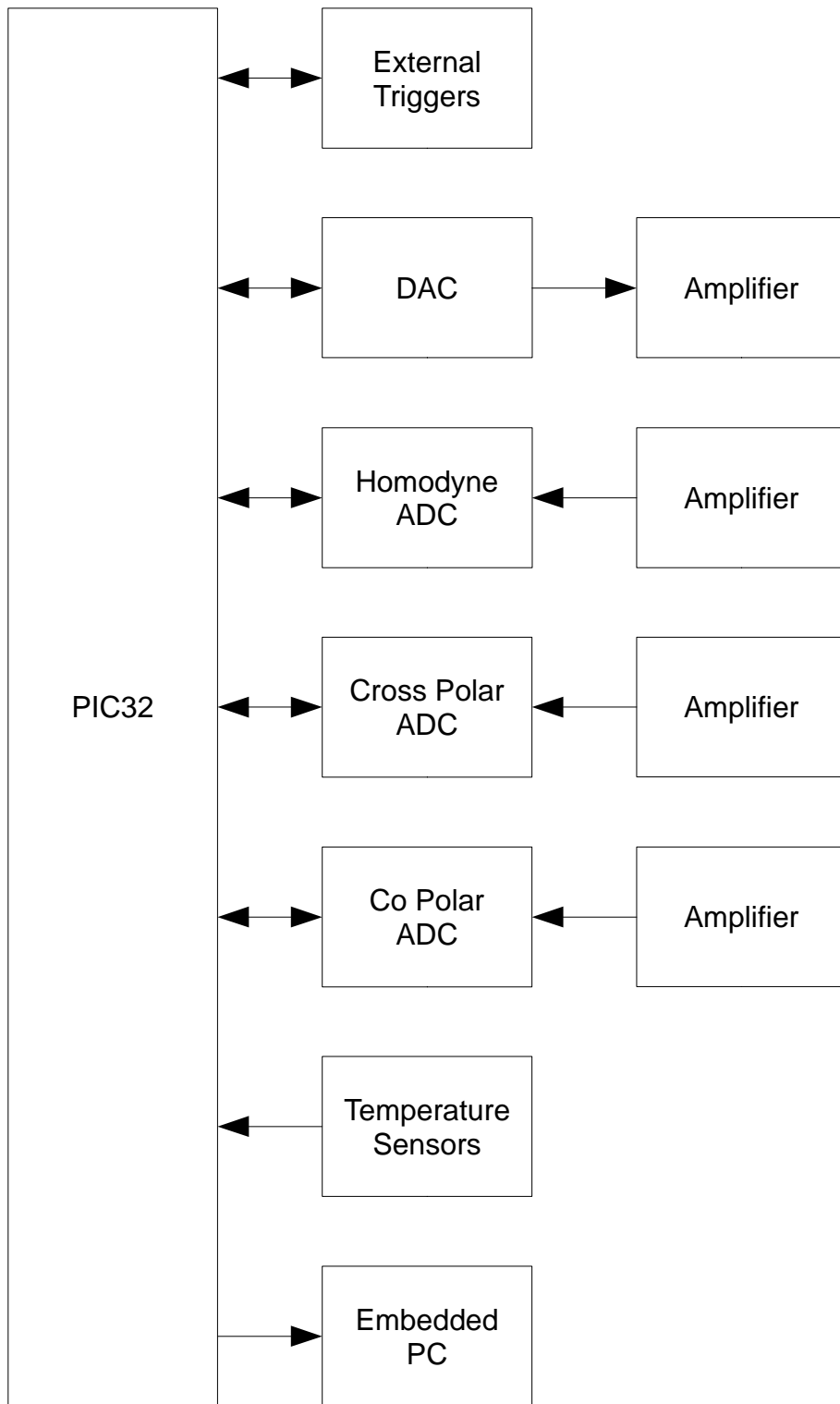


Figure 5.27: Top level system diagram of Mirlin control electronics

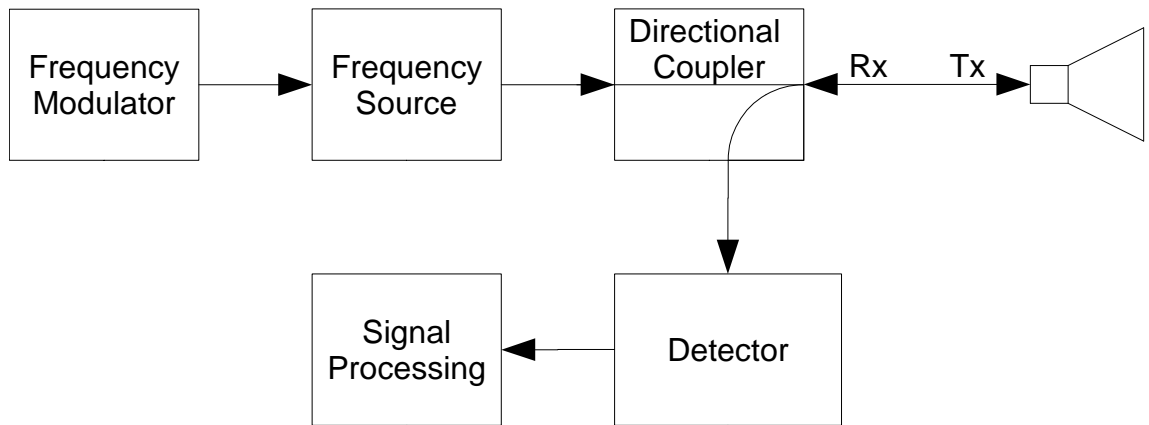


Figure 5.28: Mirlin homodyne range finder top level system diagram

The homodyne range finder works by mixing a fraction of the transmitted signal with the received signal directly at the detector to generate a phase sensitive baseband signal. The non-ideal behaviour of the directional coupler permits a fraction of the transmitted signal onto the detector due to leakage. The detector acts as the first interface of Equation (4.25) in Section 4.6, with $L_1 = 0$ and the front surface of the target acts as the second interface at distance L_2 . By applying a Fourier Transform to the swept frequency phase sensitive baseband response, the time domain response may be obtained and the distance to the target determined (Currie et al., 1992).

5.7.1 Future Work

Testing and experimentation with the prototype identified scope for improvement. For example, normalisation of the received signal may be enhanced by amplifying it electrically with a programmable front-end amplifier prior to conversion using a DAC, instead of numerically by multiplying the digitised value. Optical depth resolution could be improved by either increasing the bandwidth of the system or by interpolation. This would allow signal analysis to work at a finer granularity, maybe improving detection performance. Off loading processing of the neural network into hardware will improve inspection rates and is another step closer to making the embedded PC redundant and its removal.

5.8 Interpolation of FFT Binned Data for Improved Dielectric Detection

Using a FFT to process the FMCW signal results in a range of measurement bins of finite size and the binning error can be up to one half a bin (± 0.5). Interpolation can be used to improve the resolution by accounting for the influence of adjacent bins.

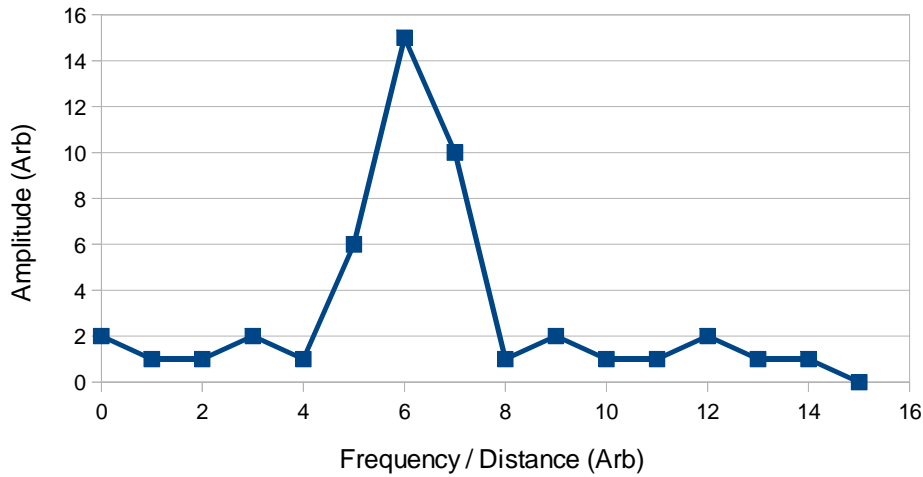


Figure 5.29: Interpolation of FFT example

The nominal optical depth of a dielectric block is the bin with the greatest amplitude and without interpolation the optical depth of the dielectric would be determined to be 6 in the example shown in Figure 5.27. With interpolation, if the adjacent bins are equal, then it can be concluded the measurement is correct. However when as in Figure 5.29 the adjacent bins are not equal the true measurement lies somewhere between the two bins of greatest amplitude.

Quadratic interpolation may be used to improve the measurement using the output of the FFT. For a quadratic defined by:

$$y = ax^2 + bx + c \quad (5.37)$$

where the peak lies at an offset from the central bin given that the centre bin is y_0 , the bins either side are y_{-1} and y_1 respectively the interpolated peak will be found at (Smith et al., 2011):

$$\hat{x} = \frac{y_{-1} - y_1}{2(y_{-1} + y_1 - 2y_0)} \quad (5.38)$$

Therefore using values from Figure 5.29, $y_{-1} = 6$, $y_0 = 15$ and $y_1 = 10$:

$$\hat{x} = \frac{6 - 10}{2(6 + 10 - 30)} = \frac{-4}{2(-14)} = \frac{1}{7} \quad (5.39)$$

therefore the interpolated peak may be found at $6 + 1/7$. For example, with a radar resolution of 4.3 mm and a target refractive index of 1.5 the physical optical thickness of the dielectric can be determined:

Blank page

6 Data Classification and Results

*Results! Why, man, I have gotten a lot of results. I know
several thousand things that won't work.*

THOMAS A. EDISON

This Chapter describes the classification techniques implemented by the prototypes for object detection and discrimination. The results of classified data are presented with a discussion of the effects of post processing of neural network outputs on threat detection performance.

6.1 Artificial Neural Networks

A good data analysis engine is needed to discriminate the characteristic signature of a concealed threat from that of a body only and body with mundane item target. The Artificial Neural Network (ANN) is an established pattern recognition tool (Tsai et al., 1996) and is able to generate the probability that a concealed threat is present from a dataset. It has been shown that ANN are effective for the classification of RADAR returns (Tatuzov, 2002) to identify remote targets, for example aircraft (Guo & Li, 2010), weather (Li et al., 2003; Yong et al., 2010) and even concealed threats (Hausner, 2009; Andrews, 2008).

Other techniques for the classification of radar returns include signature and model based approaches; feature vectors; and data fusion methods. Each approach has advantages and limitations (Zyweck & Bogner, 1996; Li & Yang, 1993; Subotic et al., 1998; Jain et al.,

2000). ANN are favoured because knowledge of underlying patterns within a data set are not required to apply them, unlike rule based approaches and the availability of efficient training methods (Guo & Li, 2010). ANNs are biologically inspired software models, simulating the parallel processing of information by the brain. An ANN is formed from hundreds of single units, artificial neurons or processing elements (PE), connected by coefficients (weights). All ANNs consists of an input layer, an output layer and zero or more hidden layers. Generally modern ANNs contain one or more hidden layers, the addition of which permits the modelling of more complex systems.

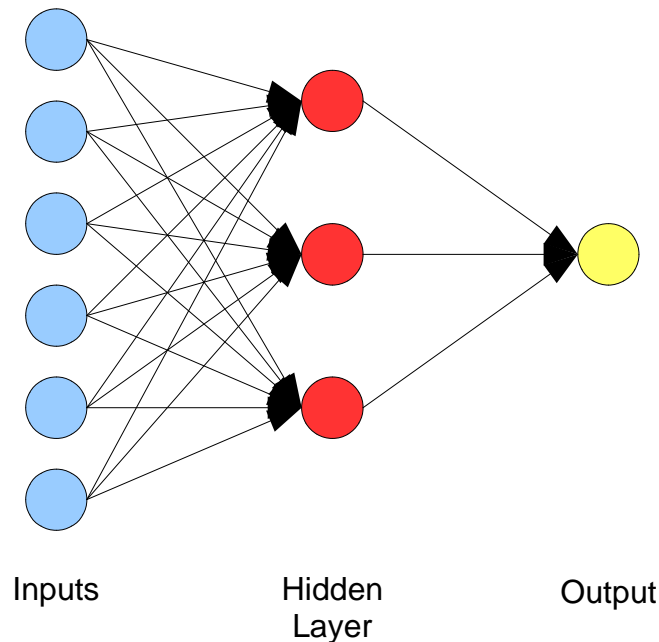


Figure 6.1: ANN with six inputs, a hidden layer of three neurons and a single output

Figure 6.1 shows the basic structure of an ANN with an input layer of six neurons connected to a single hidden layer of three neurons; and an output layer consisting of a single neuron. The behaviour of the neural network is determined by the transfer function of the neurons, the training method and the structure of the network. Each neuron has one or more weighted inputs, a transfer function and a single output. The sum of weighted inputs is the activation level of the neuron and the transfer function introduces non-linearity to the network. The connection weights are adaptable and during training are

modified until the network achieves a specified level of accuracy (Negnevitsky, 2005). Construction and training of an optimally generalised ANN can be fraught with difficulty. Identifying the correct number of layers and neurons and their type to sufficiently generalise without over training can be challenging (Lawrence et al., 1998) although the problem of local minima is generally ignored (Whittle et al., 1994)

There are three major ways of training an ANN. These are supervised learning, unsupervised learning and reinforcement learning. Training occurs until predefined training criteria (tolerances) are met or there is no remaining training data left.

Supervised Learning is the approach adopted for the project and the most widely used algorithm for supervised learning of ANN with feed-forward structures (Guo & Li, 2010). The ANN is provided with input data X and the desired output Y .

$$(x, y), x \in X, y \in Y \quad (6.1)$$

Knowledge of the correct output is required for supervised training. The aim of this approach is to adjust the set weights or connection strengths between the inputs and the output(s) such that the network produces the correct outputs when exposed to previously unseen inputs.

$$f : X \rightarrow Y \quad (6.2)$$

Unsupervised learning consists of providing the ANN with inputs x and a cost function f to be minimised. The cost function is designed to produce a correct classification for the minimum cost and the network is left to make sense of its inputs.

6.1.1 Prototype Artificial Neural Network Structure

The final neural network used by the prototypes is a feed forward three layer back propagation network with a single hidden layer consisting of ten sigmoid neurons. A hidden layer with ten neurons was selected after varying the number of neurons in the layer between three and twenty and grading the performance. The input layer was configured to accept preprocessed and distance normalised target data.

The artificial neural network produces a linear output between 0 and 100% representing the confidence that a threat item is present. By thresholding the linear output at 50% a binary classifier was created.

It was found that the best results were achieved by normalising the data before processing by the ANN; this was achieved by scaling the data based on range. Data was simplified and normalised prior to classification by the ANN as either a threat or benign item.

Fragmentation-based explosives can be detected in the same way as guns, using the polarisation altering property. Non-fragmentation-based explosives generate a return signal containing a depth spectrum of related to the optical distance between the front and back surfaces of the object. To train the ANN, static and dynamic sets of data for body only; threat and body; and body and mundane object were compiled for the scenarios described in section 4.2. The ANN was then optimised to produce the correct output through supervised learning.

The fragmentation-based explosives and gun detection algorithm is trained on the amplitude of the signal scattered from the target. The detection algorithm for non-fragmentation-based explosives is trained on the optical depth of the target. Therefore two different detection algorithms can be employed, each suited to a different target type.

6.2 Alternative Classifiers

6.2.1 Principal Component Analysis

Principal Component Analysis (PCA) is a mathematical technique for feature extraction. Useful for dimensionality reduction, PCA can be applied to a system consisting of many independent variables, to extract the eigenvectors describing the most significant variables. Applications are varied and include classification of RADAR signatures of aircraft (Jia et al., 2008), weather classification (Bajwa & Hyder, 2005) and face detection (Gottumukkal & Asari, 2003; Lang & Gu, 2009; Paul & Gavrilova, 2011). It was thought that PCA could be applied to the raw radar returns to reduce the dimensionality and thereby reduce the complexity of the ANN. However trials of applying PCA to the raw data to find patterns and features it was concluded that it was unsuitable due to a lack of repeatability.

6.2.2 Thresholding

Thresholding is programmatic and possibly the simplest approach to classification of a input. The linear input is compared with a threshold value and the classification generated. Thresholding is computationally efficient, but does requires an understanding and knowledge of the input to be processed and also the threshold level to generate a correct classification.

The frequency components of the radar returns were checked individually and also their collective intensity were checked. It was found that complex metal objects could be detected by thresholding the sum of the intensities of the cross-polar return, see section 4.10, but guns could not be distinguished from other benign objects with polarisation altering properties.

6.2.3 Self Organising Maps

A neural network that undergoes unsupervised training is a Self Organising Map (SOM). The technique leaves the neural network to form its own classifications of the training data and assumes the network will be able to classification those features across the range of

input patterns. Training consists is based on competitive learning, where output neurons compete to be activated with an end result is that only one is active at any one time.

SOM object detection performance was found to be similar to that of simple thresholding and provided inferior discrimination between objects compared to a neural network generated with supervised training.

6.3 Performance Metrics

Performance metrics provide a means of comparing the performance of different systems and configurations in a standardised manner. The results presented later in this chapter use these metrics to assist comparison.

The combination of user and prototype make for an overall system that is less than 100% accurate for detecting concealed objects. The system provides an indication of the presence of a concealed threat, as a probability. To assess and compare the performance of a detection system, the combination of the classification, probability of detection (PD), the probability of false alarm (PFA) and the confidence in these figures must be considered.

The following section describes this process. A basic approach to classifying the performance is shown in the confusion matrix, see Table 6.1.

		Predicted Classification	
		Negative	Positive
True Classification	Negative	True Negative (TN)	False Positive (FP)
	Positive	False Negatives(FN)	True Positives (TP)

Table 6.1: Performance metric confusion matrix

TN = number of correct predictions that an instance is negative

FP = number of incorrect predictions that an instance is positive

FN = number of incorrect predictions that an instance is negative

TP = number of correct predictions that an instance is positive

Several standard terms have been defined for the matrix:

The accuracy (AC) is the proportion of the total predictions that were correct and is determined by:

$$AC = \frac{TN + TP}{TN + TP + FN + FP} \quad (6.3)$$

The true positive rate (TPR) is the proportion of positive cases that were correctly identified, given by:

$$TPR = \frac{TP}{FN + TP} \quad (6.4)$$

The false positive rate (FPR) is the proportion of negative cases that were incorrectly classified as positive, given by:

$$FPR = \frac{FP}{TN + FP} \quad (6.5)$$

The true negative rate (TNR) is the proportion of negative cases that were correctly classified, determined by:

$$TNR = \frac{TN}{TN + FP} \quad (6.6)$$

The false negative rate (FNR) is the proportion of positive cases that were incorrectly classified as negative, determined by:

$$FNR = \frac{FN}{FN + TP} \quad (6.7)$$

The accuracy stated by Equation 6.3, relies on a comparable count of positive and negative cases.

6.4 Detection of Non-Fragmentation Based Explosives

In this section practical results taken in a manner similar to the laboratory test results described in section 4.6.5, using a VNA system, are presented and analysed using ANN techniques. The target movement with body rotation of approximately $\pm 10^\circ$ combined

with Doppler blur, produces a complex response from the body as seen in Figure 6.2. Therefore it would be necessary to scan faster than the VNA in a practical system. The VNA takes approximately 200 ms to complete the aforementioned scan. To overcome the complication of responses varying with different body position, multiple scans were aligned on the front edge of the body peak as shown in Figure 6.2.

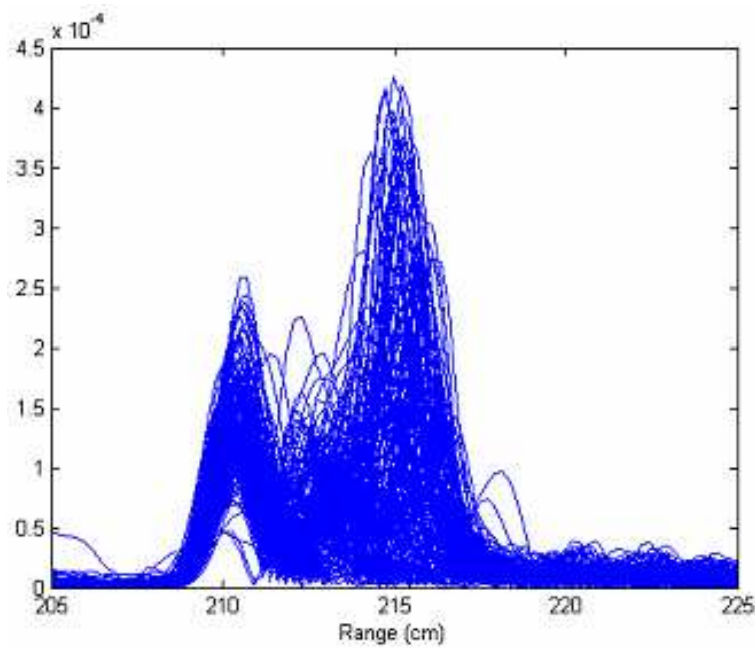


Figure 6.2: Superimposed time domain scans for body only aligned on the body peak

The presence of an extra peak in front of the main body peaks, shown by the arrow in Figure 6.3, indicates the presence of the wax block. This peak is absent in Figure 6.2, when the wax block was not present.

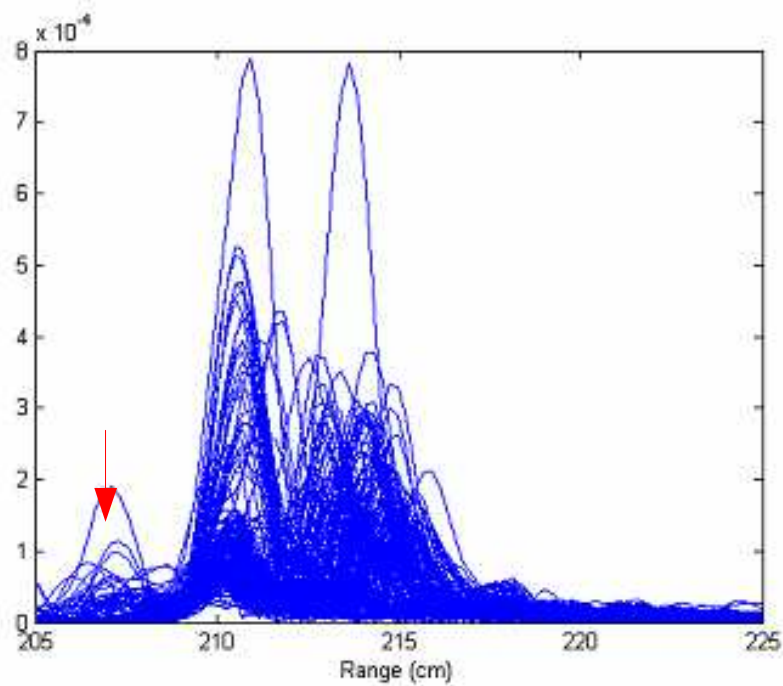


Figure 6.3: Superimposed time domain scans for body and wax block aligned on the body peak

The method of aligning multiple scans from (Andrews et al., 2008b) was to translate in time the signal so that it reaches a fixed fraction (25%) of its maximum height at a fixed time. This process was used to align the heterodyne generated data for processing. For direct detector generated data, this process is unnecessary.

6.4.1 ANN Classification of Direct Detector Generated Data

Using a direct detection based system operating between 75 and 110 GHz with a back end ANN configured with a confidence threshold of 50%, normalised datasets consisting of 40 scans for body only and body with wax block and using the depth spectrum data, produced the results below, in Table 6.2 and continued in Table 6.3. Training datasets are shaded.

Dataset	Range (m)	Optical Depth Spectrum		Frequency Spectrum	
		Threat	No Threat	Threat	No Threat
Body only 1	2	0	40	0	40
Body only 2		13	27	13	27
Body only 3		14	26	9	31
Body with wax 1		40	0	40	0
Body with wax 2		27	13	33	7
Body with wax 3		27	13	25	15
Body only 1	3	0	40	0	40
Body only 2		14	26	11	29
Body only 3		9	31	9	31
Body with wax 1		40	0	40	0
Body with wax 2		18	22	33	7
Body with wax 3		40	0	36	4
Body only 1*	4	0	40	0	40
Body only 2		11	29	10	30
Body only 3		13	27	9	31
Body with wax 1		40	0	39	1
Body with wax 2		18	22	24	16
Body with wax 3		18	22	23	17

Table 6.2: ANN classification of body only and body with wax for normalised datasets generated using a direct detector system

Range	Optical Depth Spectrum		Frequency Spectrum	
	Correct	Incorrect	Correct	Incorrect
2	107	53	116	44
3	115	45	129	31
4	92	68	108	52

Table 6.3: Sum of test data results for correctly and incorrectly classified by ANN supplied with dataset from a direct detection system operating between 75 – 105 GHz

This data can be expressed for comparison purposes in the performance metrics of TP, TN, FP and FN, shown in Figures 6.4 and 6.5.

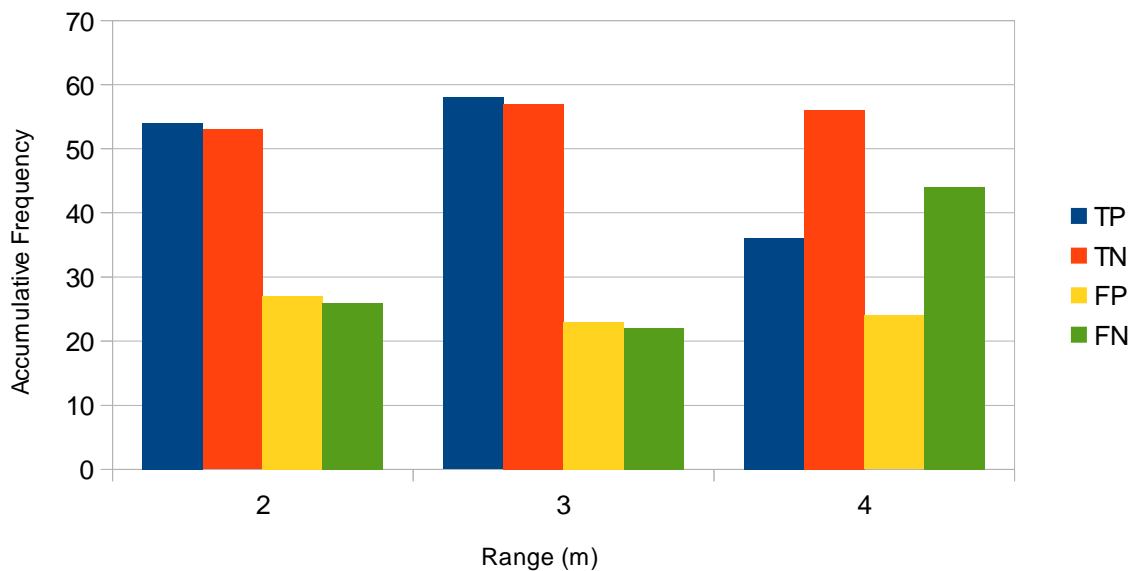


Figure 6.4: Performance metrics for ANN classification of direct detector generated optical depth spectrum in the 75 – 105 GHz band at ranges 2 – 4 m

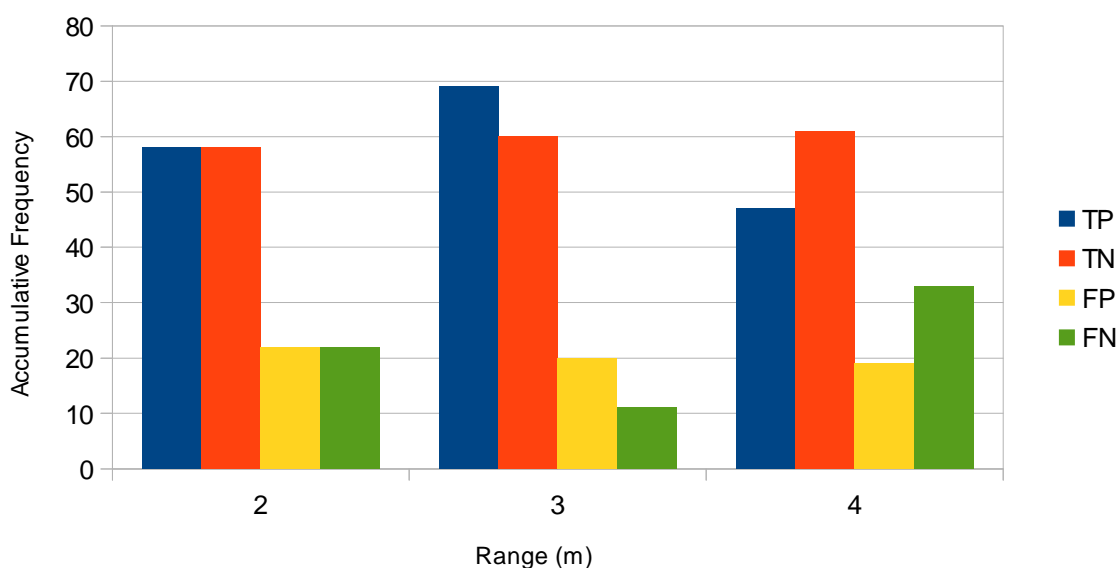


Figure 6.5: Performance metrics for ANN classification of direct detector generated frequency spectrum in the 75 – 105 GHz band at ranges 2 – 4 m

Tables 6.4 and 6.5 contain the performance rates against range for ANN classification of optical depth and frequency spectrum respectively.

Range (m)	AC	TPR	FPR	TNR	FNR
2	66.88%	67.50%	33.75%	66.25%	32.50%
3	71.88%	72.50%	28.75%	71.25%	27.50%
4	57.50%	45.00%	30.00%	70.00%	55.00%

Table 6.4: Optical depth spectrum performance metrics for direct detector operating between 75 – 105 GHz using a concealed paraffin wax block

Range (m)	AC	TPR	FPR	TNR	FNR
2	72.50%	72.50%	27.50%	72.50%	27.50%
3	80.63%	86.25%	25.00%	75.00%	13.75%
4	67.50%	58.75%	23.75%	76.25%	41.25%

Table 6.5: Frequency spectrum performance metrics for direct detector operating between 75 – 105 GHz using a concealed paraffin wax block

These results show the direct detector system is capable of target discrimination at ranges of at least 3 m. Ideally for this type of the system the TPR should be as high as possible, while the FNR should be as small as possible. For the case of the direct detector, the frequency spectrum data provides the better results.

The accuracy of the system could be improved by combining successive measurements thereby averaging out the variability of the body response and also including different orientations of the explosive target, hence potentially reducing the FNR.

6.4.2 ANN Classification of Super-heterodyne Generated Data

With a thresholded confidence of 50% the ANN classification for the super-heterodyne data is given in Table 6.6 for datasets containing 200 scans. The range gated limits are varied and shown for each data set. Training datasets are shaded.

Dataset	205 – 270 cm		205 – 225 cm only		205 – 215 cm only	
	Threat	No threat	Threat	No threat	Threat	No threat
Body only 1	40	160	23	177	11	189
Body only 2	49	151	38	162	10	190
Body only 3	0	200	0	200	7	193
Body with wax 1	154	46	140	60	113	87
Body with wax 2	162	38	156	44	193	7
Body with wax 3	200	0	200	0	200	0

Table 6.6: ANN classification of body only and body with wax for normalised, body aligned datasets generated using a super-heterodyne detector

The effect of segmenting the signal in time and using a reduced range of signals for training and testing the ANN, focuses on the response of the dielectric and generally improves accuracy of detection, by removing unrelated data from the classification process.

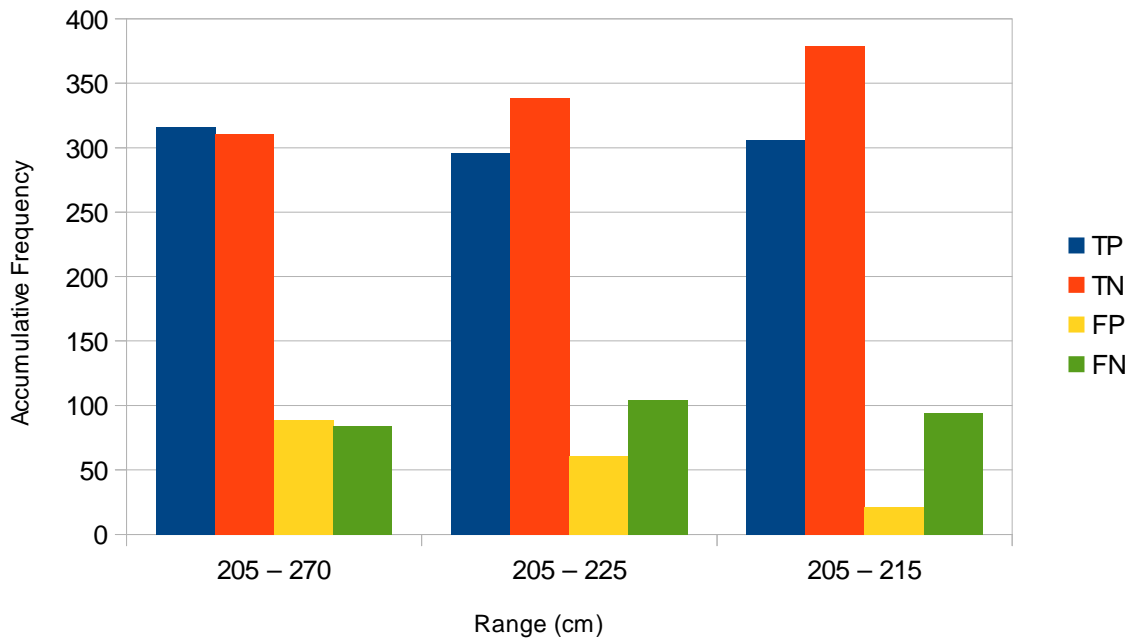


Figure 6.6: Performance metrics for ANN classification of super-heterodyne generated data in the 14 – 40 GHz for concealed wax block with segmented range

These results produce the performance metrics shown in table 6.7.

Range (cm)	AC	TPR	FPR	TNR	FNR
205 – 270	78.38%	79.00%	22.25%	77.75%	21.00%
205 – 225	79.38%	74.00%	15.25%	84.75%	26.00%
205 – 215	85.63%	76.50%	5.25%	94.75%	23.50%

Table 6.7: Performance metrics for super-heterodyne data, segmented by range for body only and body with wax

These results indicate that accuracy rates can be improved by selectively range gating the data to remove clutter, unrelated to the range of interest and classifying only data relating to the region immediately in front of the target.

The results show the possibility of remotely detecting the presence of a pure dielectric explosive stimulant concealed upon the human body by everyday clothing. The mechanism of detection is based on the interference of reflected radiation from the front and back surfaces of the dielectric. Using the phase of the return signal allows the removal of background clutter and on the whole improves the rate of accuracy, compared to direct detector generated data.

6.5 Detection of Fragmentation Based Explosives

Fragmentation based explosives give a clear radar signal, due to the embedded particles. The embedded particles give the explosive a complex structure with many scattering corners and the property similar to that of guns, see section Error: Reference source not found, of altering the polarisation of scattered radiation and this property is used as the detection mechanism. The behaviour of networks for classification of fragmentation based explosives is found to be similar or somewhat easier to that found for gun detection, which is discussed in the next section.

6.6 Detection of Concealed Handguns

Hand guns, like fragmentation based explosives, exhibit a clear radar signal. However an important difference is that unlike fragmentation based explosives, with the random distribution of embedded particles, the signal return produced by a handgun has more structure. For example the aspect independent return from a gun barrel is a distinctive feature and that does not exist with fragmentation based explosives.

Typically a handgun is carried against the body in the waistband either in front of or behind the torso. Aligning the scans at 25% of the largest signal Figure 6.8 shows the range gated results for a handgun in front of a moving torso. Note in this case only the co-polar receiver is used and classification is based on changes to the co-polar signal alone.

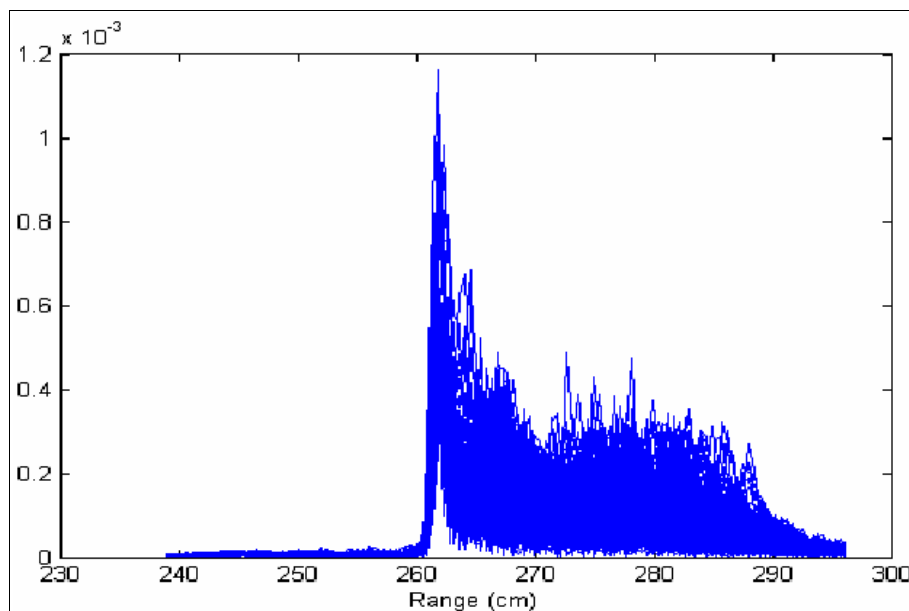


Figure 6.7: Aligned time domain responses of a stationary body 14 – 40 GHz

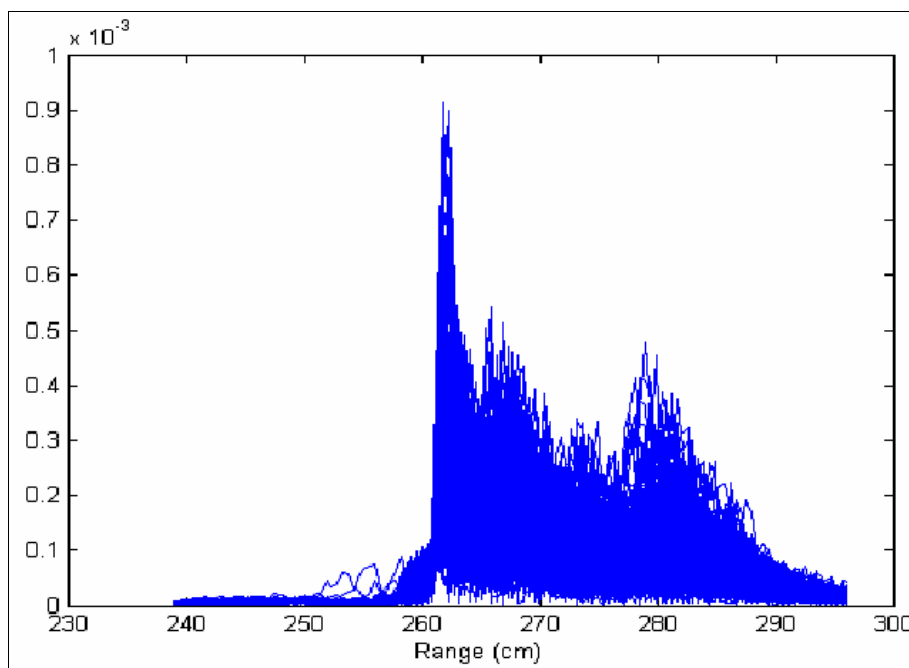


Figure 6.8: Aligned time domain responses of body with gun in front 14 – 40 GHz

The effect on the time domain response by the handgun can be clearly seen in Figure 6.8, with an early time response in front of the main peak produced by the surface of the body.

The results of classifying the data using the ANN are presented in Table 6.8 and shows clearly that the ANN can already clearly identify the presence of a gun.

Dataset	Threat	No threat
Body 1	0	200
Body 2	19	181
Body 1 and starter pistol	200	0
Body 2 and starter pistol	167	33
Body 1 and Glock	197	3
Body 2 and Glock	199	1

Table 6.8: ANN classification of body only and body with gun for normalised, distance gated, body aligned datasets generated using a co-polar heterodyne detector

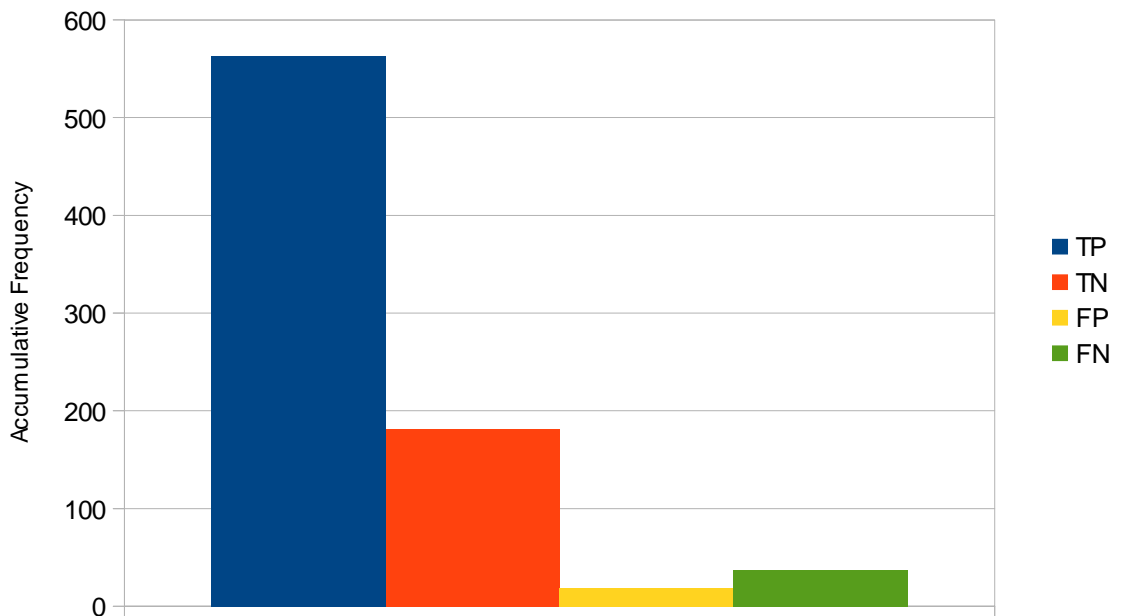


Figure 6.9: Performance for ANN classification of heterodyne range gated data between 14 – 40 GHz for concealed guns

AC	TPR	FPR	TNR	FNR
93.00%	93.83%	9.50%	90.50%	6.17%

Table 6.9: Performance metrics for the ANN classification of range gated co-polar heterodyne generated data between 14 – 40 GHz for concealed guns

Since an ANN can be configured with multiple outputs, a modified network was configured and trained to identify not only the presence but also the type of gun. Table 6.10 show the results with training datasets indicated with shading.

Dataset	No threat	Threat – starter pistol	Threat – Glock
Body 1	200	0	0
Body 2	156	36	0
Body 1 and starter pistol	0	200	0
Body 2 and starter pistol	23	132	43
Body 1 and Glock	0	0	200
Body 2 and Glock	0	25	175

Table 6.10: ANN classification of body only, body with two different guns for normalised, distance gated, body aligned datasets generated using a co-polar heterodyne detector

Figure 6.10 shows the performance for each training set and cross tested for the presence a gun.

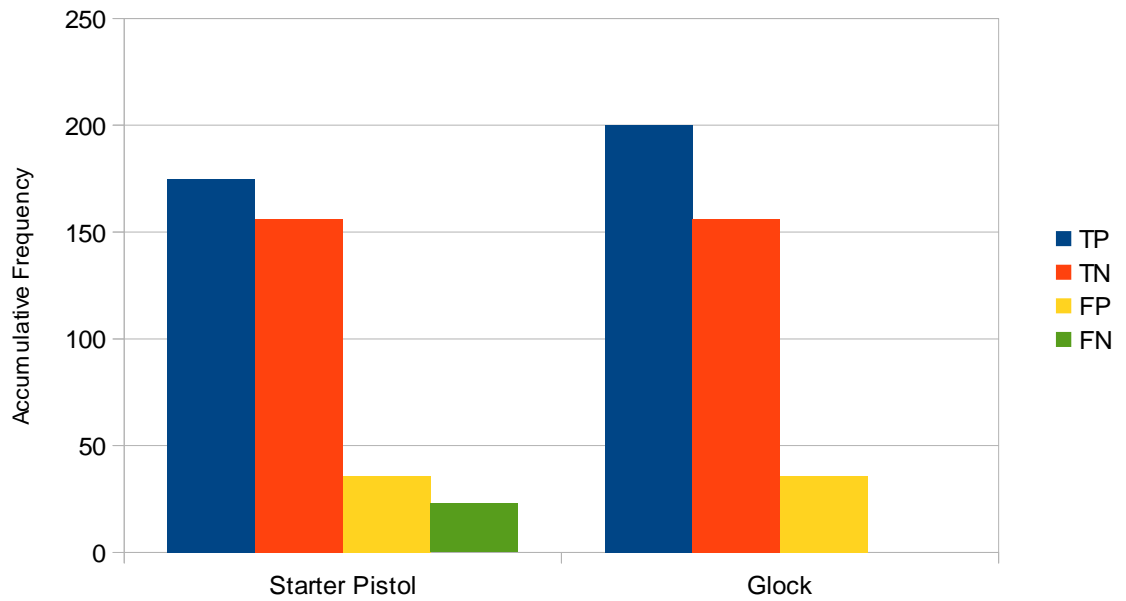


Figure 5.9: Performance of two ANN trained on a starter pistol or Glock and cross tested using range gated data from a heterodyne system operating between 14 – 40 GHz

The performance metrics are:

Type of gun	AC	TPR	FPR	TNR	FNR
Starter Pistol	84.87%	88.38%	18.75%	81.25%	11.62%
Glock	90.82%	100.00%	18.75%	81.25%	0.00%

Table 6.11: Performance metrics for cross testing of two ANNs trained on a starter pistol and Glock using range gated data from a heterodyne system between 14 – 40 GHz

Though the classification is less definite for the simpler decision 'gun' or 'no gun', these results show the feasibility of detecting gun type, as well as gun presence.

The network trained on the Glock dataset is more accurate by almost 6% and a lower false negative rate compared to the starter pistol dataset. This information can be used to produce better training datasets, resulting in a superior classification accuracy.

Analysis of the cross-polar return of a target can be included be analysed to provide further confirmation of the target type present. Objects with smooth conducting surfaces like a metal plate or the human torso are polarisation conserving – in that they do not significantly change the polarisation of reflected radiation. Conversely, our investigations confirm that complex objects or objects with lots of edges or points, generate multiple reflections, resulting in multiple reflections and a change of polarisation of the reflected radiation. The gun in this case is a Brocock, a small handgun.

Dataset	Threat	No threat	Threat 90%	No threat 90%
Body 1	0	40	0	40
Body 2	5	35	2	31
Body 3	3	37	0	32
Body 1 and gun	40	0	40	0
Body 2 and gun	38	2	38	0
Body 3 and gun	36	4	25	1

Table 6.12: ANN classification with 50% threshold of body only and body and gun using a heterodyne system operating between 14 – 40 GHz

The results given in Table 6.12, show that the classification is very good with low false positive rates (FPR).

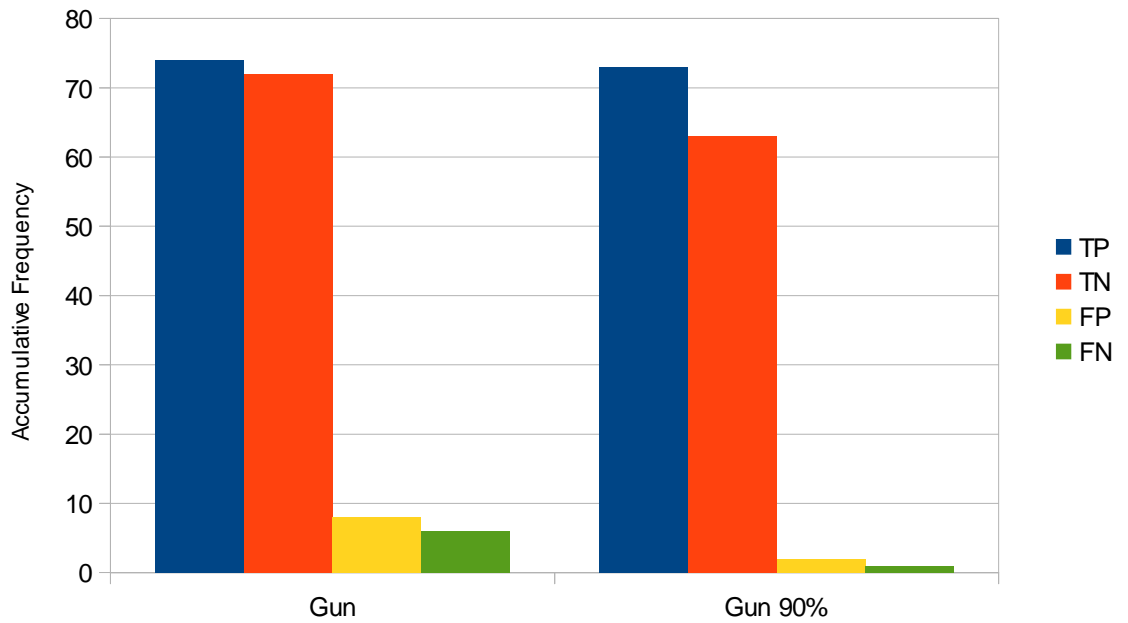


Figure 6.10: Performance of an ANN with variable output thresholding using range gated data from a heterodyne system operating between 14 – 40 GHz

Confidence	AC	TPR	FPR	TNR	FNR
Gun 50%	91.25%	92.50%	10.00%	90.00%	7.50%
Gun 90%	97.84%	98.65%	3.08%	96.92%	1.35%

Table 6.13: Performance metrics for an ANN network with variable output thresholding using range gated data from a heterodyne system operating between 14 – 40 GHz

Also shown in Table 6.12, is the effect of including only results where the ANN output was above a 90% threshold. This process rejects inspections, which the ANN is uncertain in its classification and leaves these as unclassified. The effect of output thresholding in this case generates 13.125% fewer outputs, requiring a longer inspection time. However, remaining classifications yield a better than four-fold reduction in false responses and the subsequent improvement of accuracy, increasing from 91.25% to 97.84%. The effect upon dataset utility and accurate classification is explored later in this chapter.

6.7 Identifying The Effect Of Thresholding On Accuracy and Data Utility

The measured TPR, PNR, FPR and FNR are functions of the threshold levels applied to the output of the ANN. The effects of various thresholds are shown in tabular format with desirable regions highlighted in progressively lighter shades of green. The ideal result for TPR and TNR is 1 and for FNR and FPR it is 0. Tables 6.14 to 6.17 show the effect of various confidence thresholds on TPR, FPR, TNR and FNR, for a dataset consisting of body only; camera in the waistband; keys; gun held in the waistband and in the hand, at ranges of 2, 4 and 6 metres. The upper confidence threshold is across the top of the table and the lower confidence threshold is down the left hand side of the table. Table elements containing hashes denote an invalid result, likely this is due a divide by zero.

		TPR = TP/(TP+FN)																						
		TP	0	0	0	286	421	522	603	667	724	786	852	901	949	990	1037	1087	1125	1149	1177	1198	1200	
		FP	0	0	0	1	11	28	42	67	97	135	169	221	287	381	485	611	764	922	1155	1553	1799	
TN	FN	resho	1.00	0.95	0.90	0.85	0.80	0.75	0.70	0.65	0.60	0.55	0.50	0.45	0.40	0.35	0.30	0.25	0.20	0.15	0.10	0.05	0.00	
0	0	0.00	###	###	###	1.00	1.00	1.00	1.00	1.00	1.00	1.00	1.00	1.00	1.00	1.00	1.00	1.00	1.00	1.00	1.00	1.00	1.00	
246	2	0.05	0.00	0.00	0.00	0.99	1.00	1.00	1.00	1.00	1.00	1.00	1.00	1.00	1.00	1.00	1.00	1.00	1.00	1.00	1.00	1.00	1.00	
644	23	0.10	0.00	0.00	0.00	0.93	0.95	0.96	0.96	0.97	0.97	0.97	0.97	0.98	0.98	0.98	0.98	0.98	0.98	0.98	0.98	0.98	0.98	0.98
877	51	0.15	0.00	0.00	0.00	0.85	0.89	0.91	0.92	0.93	0.93	0.94	0.94	0.95	0.95	0.95	0.95	0.96	0.96	0.96	0.96	0.96	0.96	0.96
1035	75	0.20	0.00	0.00	0.00	0.79	0.85	0.87	0.89	0.90	0.91	0.91	0.92	0.92	0.93	0.93	0.93	0.94	0.94	0.94	0.94	0.94	0.94	0.94
1188	113	0.25	0.00	0.00	0.00	0.72	0.79	0.82	0.84	0.86	0.86	0.87	0.88	0.89	0.89	0.90	0.90	0.91	0.91	0.91	0.91	0.91	0.91	0.91
1314	163	0.30	0.00	0.00	0.00	0.64	0.72	0.76	0.79	0.80	0.82	0.83	0.84	0.85	0.85	0.86	0.86	0.87	0.87	0.88	0.88	0.88	0.88	0.88
1418	210	0.35	0.00	0.00	0.00	0.58	0.67	0.71	0.74	0.76	0.78	0.79	0.80	0.81	0.82	0.83	0.83	0.84	0.84	0.85	0.85	0.85	0.85	0.85
1512	251	0.40	0.00	0.00	0.00	0.53	0.63	0.68	0.71	0.73	0.74	0.76	0.77	0.78	0.79	0.80	0.81	0.81	0.82	0.82	0.82	0.83	0.83	0.83
1578	299	0.45	0.00	0.00	0.00	0.49	0.58	0.64	0.67	0.69	0.71	0.72	0.74	0.75	0.76	0.77	0.78	0.78	0.79	0.79	0.80	0.80	0.80	0.80
1630	348	0.50	0.00	0.00	0.00	0.45	0.55	0.60	0.63	0.66	0.68	0.69	0.71	0.72	0.73	0.74	0.75	0.76	0.76	0.77	0.77	0.77	0.77	0.78
1664	414	0.55	0.00	0.00	0.00	0.41	0.50	0.56	0.59	0.62	0.64	0.66	0.67	0.69	0.70	0.71	0.71	0.72	0.73	0.74	0.74	0.74	0.74	0.74
1702	476	0.60	0.00	0.00	0.00	0.38	0.47	0.52	0.56	0.58	0.60	0.62	0.64	0.65	0.67	0.68	0.69	0.70	0.70	0.71	0.71	0.72	0.72	0.72
1732	533	0.65	0.00	0.00	0.00	0.35	0.44	0.49	0.53	0.56	0.58	0.60	0.62	0.63	0.64	0.65	0.66	0.67	0.68	0.68	0.69	0.69	0.69	0.69
1757	597	0.70	0.00	0.00	0.00	0.32	0.41	0.47	0.50	0.53	0.55	0.57	0.59	0.60	0.61	0.62	0.63	0.65	0.65	0.66	0.66	0.67	0.67	0.67
1771	678	0.75	0.00	0.00	0.00	0.30	0.38	0.44	0.47	0.50	0.52	0.54	0.56	0.57	0.58	0.59	0.60	0.62	0.62	0.63	0.63	0.64	0.64	0.64
1788	779	0.80	0.00	0.00	0.00	0.27	0.35	0.40	0.44	0.46	0.48	0.50	0.52	0.54	0.55	0.56	0.57	0.58	0.59	0.60	0.60	0.61	0.61	0.61
1798	914	0.85	0.00	0.00	0.00	0.24	0.32	0.36	0.40	0.42	0.44	0.46	0.48	0.50	0.51	0.52	0.53	0.54	0.55	0.56	0.56	0.57	0.57	0.57
1799	1200	0.90	0.00	0.00	0.00	0.19	0.26	0.30	0.33	0.36	0.38	0.40	0.42	0.43	0.44	0.45	0.46	0.48	0.48	0.49	0.50	0.50	0.50	0.50
1799	1200	0.95	0.00	0.00	0.00	0.19	0.26	0.30	0.33	0.36	0.38	0.40	0.42	0.43	0.44	0.45	0.46	0.48	0.48	0.49	0.50	0.50	0.50	0.50
1799	1200	1.00	0.00	0.00	0.00	0.19	0.26	0.30	0.33	0.36	0.38	0.40	0.42	0.43	0.44	0.45	0.46	0.48	0.48	0.49	0.50	0.50	0.50	0.50

Table 6.14: TPR for various confidence thresholds on gun and mundane item classification using a direct detection system operating between 75 – 110 GHz

		FPR = FP/(FP+TN)																					
		TP	0	0	0	286	421	522	603	667	724	786	852	901	949	990	1037	1087	1125	1149	1177	1198	1200
		FP	0	0	0	1	11	28	42	67	97	135	169	221	287	381	485	611	764	922	1155	1553	1799
TN	FN	resho	1.00	0.95	0.90	0.85	0.80	0.75	0.70	0.65	0.60	0.55	0.50	0.45	0.40	0.35	0.30	0.25	0.20	0.15	0.10	0.05	0.00
0	0	0.00	###	###	###	1.00	1.00	1.00	1.00	1.00	1.00	1.00	1.00	1.00	1.00	1.00	1.00	1.00	1.00	1.00	1.00	1.00	1.00
246	2	0.05	0.00	0.00	0.00	0.00	0.04	0.10	0.15	0.21	0.28	0.35	0.41	0.47	0.54	0.61	0.66	0.71	0.76	0.79	0.82	0.86	0.88
644	23	0.10	0.00	0.00	0.00	0.00	0.02	0.04	0.06	0.09	0.13	0.17	0.21	0.26	0.31	0.37	0.43	0.49	0.54	0.59	0.64	0.71	0.74
877	51	0.15	0.00	0.00	0.00	0.00	0.01	0.03	0.05	0.07	0.10	0.13	0.16	0.20	0.25	0.30	0.36	0.41	0.47	0.51	0.57	0.64	0.67
1035	75	0.20	0.00	0.00	0.00	0.00	0.01	0.03	0.04	0.06	0.09	0.12	0.14	0.18	0.22	0.27	0.32	0.37	0.42	0.47	0.53	0.60	0.63
1188	113	0.25	0.00	0.00	0.00	0.00	0.01	0.02	0.03	0.05	0.08	0.10	0.12	0.16	0.19	0.24	0.29	0.34	0.39	0.44	0.49	0.57	0.60
1314	163	0.30	0.00	0.00	0.00	0.00	0.01	0.02	0.03	0.05	0.07	0.09	0.11	0.14	0.18	0.22	0.27	0.32	0.37	0.41	0.47	0.54	0.58
1418	210	0.35	0.00	0.00	0.00	0.00	0.01	0.02	0.03	0.05	0.06	0.09	0.11	0.13	0.17	0.21	0.25	0.30	0.35	0.39	0.45	0.52	0.56
1512	251	0.40	0.00	0.00	0.00	0.00	0.01	0.02	0.03	0.04	0.06	0.08	0.10	0.13	0.16	0.20	0.24	0.29	0.34	0.38	0.43	0.51	0.54
1578	299	0.45	0.00	0.00	0.00	0.00	0.01	0.02	0.03	0.04	0.06	0.08	0.10	0.12	0.15	0.19	0.24	0.28	0.33	0.37	0.42	0.50	0.53
1630	348	0.50	0.00	0.00	0.00	0.00	0.01	0.02	0.03	0.04	0.06	0.08	0.09	0.12	0.15	0.19	0.23	0.27	0.32	0.36	0.41	0.49	0.52
1664	414	0.55	0.00	0.00	0.00	0.00	0.01	0.02	0.02	0.04	0.06	0.08	0.09	0.12	0.15	0.19	0.23	0.27	0.31	0.36	0.41	0.48	0.52
1702	476	0.60	0.00	0.00	0.00	0.00	0.01	0.02	0.02	0.04	0.05	0.07	0.09	0.11	0.14	0.18	0.22	0.26	0.31	0.35	0.40	0.48	0.51
1732	533	0.65	0.00	0.00	0.00	0.00	0.01	0.02	0.02	0.04	0.05	0.07	0.09	0.11	0.14	0.18	0.22	0.26	0.31	0.35	0.40	0.47	0.51
1757	597	0.70	0.00	0.00	0.00	0.00	0.01	0.02	0.02	0.04	0.05	0.07	0.09	0.11	0.14	0.18	0.22	0.26	0.30	0.34	0.40	0.47	0.51
1771	678	0.75	0.00	0.00	0.00	0.00	0.01	0.02	0.02	0.04	0.05	0.07	0.09	0.11	0.14	0.18	0.21	0.26	0.30	0.34	0.39	0.47	0.50
1788	779	0.80	0.00	0.00	0.00	0.00	0.01	0.02	0.02	0.04	0.05	0.07	0.09	0.11	0.14	0.18	0.21	0.25	0.30	0.34	0.39	0.46	0.50
1798	914	0.85	0.00	0.00	0.00	0.00	0.01	0.02	0.02	0.04	0.05	0.07	0.09	0.11	0.14	0.17	0.21	0.25	0.30	0.34	0.39	0.46	0.50
1799	1200	0.90	0.00	0.00	0.00	0.00	0.01	0.02	0.02	0.04	0.05	0.07	0.09	0.11	0.14	0.17	0.21	0.25	0.30	0.34	0.39	0.46	0.50
1799	1200	0.95	0.00	0.00	0.00	0.00	0.01	0.02	0.02	0.04	0.05	0.07	0.09	0.11	0.14	0.17	0.21	0.25	0.30	0.34	0.39	0.46	0.50
1799	1200	1.00	0.00	0.00	0.00	0.00	0.01	0.02	0.02	0.04	0.05	0.07	0.09	0.11	0.14	0.17	0.21	0.25	0.30	0.34	0.39	0.46	0.50

Table 6.15: FPR for various confidence thresholds on gun and mundane item classification using a direct detection system operating between 75 – 110 GHz

		TNR = TN/(TN+FP)																					
		TP	0	0	0	286	421	522	603	667	724	786	852	901	949	990	1037	1087	1125	1149	1177	1198	1200
		FP	0	0	0	1	11	28	42	67	97	135	169	221	287	381	485	611	764	922	1155	1553	1799
TN	FN	resho	1.00	0.95	0.90	0.85	0.80	0.75	0.70	0.65	0.60	0.55	0.50	0.45	0.40	0.35	0.30	0.25	0.20	0.15	0.10	0.05	0.00
0	0	0.00	###	###	###	0.00	0.00	0.00	0.00	0.00	0.00	0.00	0.00	0.00	0.00	0.00	0.00	0.00	0.00	0.00	0.00	0.00	0.00
246	2	0.05	1.00	1.00	1.00	1.00	0.96	0.90	0.85	0.79	0.72	0.65	0.59	0.53	0.46	0.39	0.34	0.29	0.24	0.21	0.18	0.14	0.12
644	23	0.10	1.00	1.00	1.00	1.00	0.98	0.96	0.94	0.91	0.87	0.83	0.79	0.74	0.69	0.63	0.57	0.51	0.46	0.41	0.36	0.29	0.26
877	51	0.15	1.00	1.00	1.00	1.00	0.99	0.97	0.95	0.93	0.90	0.87	0.84	0.80	0.75	0.70	0.64	0.59	0.53	0.49	0.43	0.36	0.33
1035	75	0.20	1.00	1.00	1.00	1.00	0.99	0.97	0.96	0.94	0.91	0.88	0.86	0.82	0.78	0.73	0.68	0.63	0.58	0.53	0.47	0.40	0.37
1188	113	0.25	1.00	1.00	1.00	1.00	0.99	0.98	0.97	0.95	0.92	0.90	0.88	0.84	0.81	0.76	0.71	0.66	0.61	0.56	0.51	0.43	0.40
1314	163	0.30	1.00	1.00	1.00	1.00	0.99	0.98	0.97	0.95	0.93	0.91	0.89	0.86	0.82	0.78	0.73	0.68	0.63	0.59	0.53	0.46	0.42
1418	210	0.35	1.00	1.00	1.00	1.00	0.99	0.98	0.97	0.95	0.94	0.91	0.89	0.87	0.83	0.79	0.75	0.70	0.65	0.61	0.55	0.48	0.44
1512	251	0.40	1.00	1.00	1.00	1.00	0.99	0.98	0.97	0.96	0.94	0.92	0.90	0.87	0.84	0.80	0.76	0.71	0.66	0.62	0.57	0.49	0.46
1578	299	0.45	1.00	1.00	1.00	1.00	0.99	0.98	0.97	0.96	0.94	0.92	0.90	0.88	0.85	0.81	0.76	0.72	0.67	0.63	0.58	0.50	0.47
1630	348	0.50	1.00	1.00	1.00	1.00	0.99	0.98	0.97	0.96	0.94	0.92	0.91	0.88	0.85	0.81	0.77	0.73	0.68	0.64	0.59	0.51	0.48
1664	414	0.55	1.00	1.00	1.00	1.00	0.99	0.98	0.98	0.96	0.94	0.92	0.91	0.88	0.85	0.81	0.77	0.73	0.69	0.64	0.59	0.52	0.48
1702	476	0.60	1.00	1.00	1.00	1.00	0.99	0.98	0.98	0.96	0.95	0.93	0.91	0.89	0.86	0.82	0.78	0.74	0.69	0.65	0.60	0.52	0.49
1732	533	0.65	1.00	1.00	1.00	1.00	0.99	0.98	0.98	0.96	0.95	0.93	0.91	0.89	0.86	0.82	0.78	0.74	0.69	0.65	0.60	0.53	0.49
1757	597	0.70	1.00	1.00	1.00	1.00	0.99	0.98	0.98	0.96	0.95	0.93	0.91	0.89	0.86	0.82	0.78	0.74	0.70	0.66	0.60	0.53	0.49
1771	678	0.75	1.00	1.00	1.00	1.00	0.99	0.98	0.98	0.96	0.95	0.93	0.91	0.89	0.86	0.82	0.79	0.74	0.70	0.66	0.61	0.53	0.50
1788	779	0.80	1.00	1.00	1.00	1.00	0.99	0.98	0.98	0.96	0.95	0.93	0.91	0.89	0.86	0.82	0.79	0.75	0.70	0.66	0.61	0.54	0.50
1798	914	0.85	1.00	1.00	1.00	1.00	0.99	0.98	0.98	0.96	0.95	0.93	0.91	0.89	0.86	0.83	0.79	0.75	0.70	0.66	0.61	0.54	0.50
1799	1200	0.90	1.00	1.00	1.00	1.00	0.99	0.98	0.98	0.96	0.95	0.93	0.91	0.89	0.86	0.83	0.79	0.75	0.70	0.66	0.61	0.54	0.50
1799	1200	0.95	1.00	1.00	1.00	1.00	0.99	0.98	0.98	0.96	0.95	0.93	0.91	0.89	0.86	0.83	0.79	0.75	0.70	0.66	0.61	0.54	0.50
1799	1200	1.00	1.00	1.00	1.00	1.00	0.99	0.98	0.98	0.96	0.95	0.93	0.91	0.89	0.86	0.83	0.79	0.75	0.70	0.66	0.61	0.54	0.50

Table 6.16: TNR for various confidence thresholds on gun and mundane item classification using a direct detection system operating between 75 – 110 GHz

		FNR = FN/(FN+TP)																					
		TP	0	0	0	286	421	522	603	667	724	786	852	901	949	990	1037	1087	1125	1149	1177	1198	1200
		FP	0	0	0	1	11	28	42	67	97	135	169	221	287	381	485	611	764	922	1155	1553	1799
TN	FN	resho	1.00	0.95	0.90	0.85	0.80	0.75	0.70	0.65	0.60	0.55	0.50	0.45	0.40	0.35	0.30	0.25	0.20	0.15	0.10	0.05	0.00
0	0	0.00	###	###	###	0.00	0.00	0.00	0.00	0.00	0.00	0.00	0.00	0.00	0.00	0.00	0.00	0.00	0.00	0.00	0.00	0.00	0.00
246	2	0.05	1.00	1.00	1.00	0.01	0.00	0.00	0.00	0.00	0.00	0.00	0.00	0.00	0.00	0.00	0.00	0.00	0.00	0.00	0.00	0.00	0.00
644	23	0.10	1.00	1.00	1.00	0.07	0.05	0.04	0.04	0.03	0.03	0.03	0.03	0.02	0.02	0.02	0.02	0.02	0.02	0.02	0.02	0.02	0.02
877	51	0.15	1.00	1.00	1.00	0.15	0.11	0.09	0.08	0.07	0.07	0.06	0.06	0.05	0.05	0.05	0.05	0.04	0.04	0.04	0.04	0.04	0.04
1035	75	0.20	1.00	1.00	1.00	0.21	0.15	0.13	0.11	0.10	0.09	0.09	0.08	0.08	0.07	0.07	0.07	0.06	0.06	0.06	0.06	0.06	0.06
1188	113	0.25	1.00	1.00	1.00	0.28	0.21	0.18	0.16	0.14	0.14	0.13	0.12	0.11	0.11	0.10	0.10	0.09	0.09	0.09	0.09	0.09	0.09
1314	163	0.30	1.00	1.00	1.00	0.36	0.28	0.24	0.21	0.20	0.18	0.17	0.16	0.15	0.15	0.14	0.14	0.13	0.13	0.12	0.12	0.12	0.12
1418	210	0.35	1.00	1.00	1.00	0.42	0.33	0.29	0.26	0.24	0.22	0.21	0.20	0.19	0.18	0.18	0.17	0.16	0.16	0.15	0.15	0.15	0.15
1512	251	0.40	1.00	1.00	1.00	0.47	0.37	0.32	0.29	0.27	0.26	0.24	0.23	0.22	0.21	0.20	0.19	0.19	0.18	0.18	0.18	0.17	0.17
1578	299	0.45	1.00	1.00	1.00	0.51	0.42	0.36	0.33	0.31	0.29	0.28	0.26	0.25	0.24	0.23	0.22	0.22	0.21	0.21	0.20	0.20	0.20
1630	348	0.50	1.00	1.00	1.00	0.55	0.45	0.40	0.37	0.34	0.32	0.31	0.29	0.28	0.27	0.26	0.25	0.24	0.24	0.23	0.23	0.23	0.22
1664	414	0.55	1.00	1.00	1.00	0.59	0.50	0.44	0.41	0.38	0.36	0.35	0.33	0.31	0.30	0.29	0.29	0.28	0.27	0.26	0.26	0.26	0.26
1702	476	0.60	1.00	1.00	1.00	0.62	0.53	0.48	0.44	0.42	0.40	0.38	0.36	0.35	0.33	0.32	0.31	0.30	0.30	0.29	0.29	0.28	0.28
1732	533	0.65	1.00	1.00	1.00	0.65	0.56	0.51	0.47	0.44	0.42	0.40	0.38	0.37	0.36	0.35	0.34	0.33	0.32	0.32	0.31	0.31	0.31
1757	597	0.70	1.00	1.00	1.00	0.68	0.59	0.53	0.50	0.47	0.45	0.43	0.41	0.40	0.39	0.38	0.37	0.35	0.35	0.34	0.34	0.33	0.33
1771	678	0.75	1.00	1.00	1.00	0.70	0.62	0.57	0.53	0.50	0.48	0.46	0.44	0.43	0.42	0.41	0.40	0.38	0.38	0.37	0.37	0.36	0.36
1788	779	0.80	1.00	1.00	1.00	0.73	0.65	0.60	0.56	0.54	0.52	0.50	0.48	0.46	0.45	0.44	0.43	0.42	0.41	0.40	0.40	0.39	0.39
1798	914	0.85	1.00	1.00	1.00	0.76	0.68	0.64	0.60	0.58	0.56	0.54	0.52	0.50	0.49	0.48	0.47	0.46	0.45	0.44	0.44	0.43	0.43
1799	1200	0.90	1.00	1.00	1.00	0.81	0.74	0.70	0.67	0.64	0.62	0.60	0.58	0.57	0.56	0.55	0.54	0.52	0.52	0.51	0.50	0.50	0.50
1799	1200	0.95	1.00	1.00	1.00	0.81	0.74	0.70	0.67	0.64	0.62	0.60	0.58	0.57	0.56	0.55	0.54	0.52	0.52	0.51	0.50	0.50	0.50
1799	1200	1.00	1.00	1.00	1.00	0.81	0.74	0.70	0.67	0.64	0.62	0.60	0.58	0.57	0.56	0.55	0.54	0.52	0.52	0.51	0.50	0.50	0.50

Table 6.17: FNR for various confidence thresholds on gun and mundane item classification using a direct detection system operating between 75 – 110 GHz

By inspection, the areas containing preferred results overlap in a very small area. Table

6.18 combines the previous four tables using the accuracy metric, see Equation (6.3).

		Accuracy = (TP+TN)/(TP+TN+FP+FN)																					
		TP	0	0	0	286	421	522	603	667	724	786	852	901	949	990	1037	1087	1125	1149	1177	1198	1200
		FP	0	0	0	1	11	28	42	67	97	135	169	221	287	381	485	611	764	922	1155	1553	1799
TN	FN	resho	1.00	0.95	0.90	0.85	0.80	0.75	0.70	0.65	0.60	0.55	0.50	0.45	0.40	0.35	0.30	0.25	0.20	0.15	0.10	0.05	0.00
0	0	0.00	###	###	###	1.00	0.97	0.95	0.93	0.91	0.88	0.85	0.83	0.80	0.77	0.72	0.68	0.64	0.60	0.55	0.50	0.44	0.40
246	2	0.05	0.99	0.99	0.99	0.99	0.98	0.96	0.95	0.93	0.91	0.88	0.87	0.84	0.81	0.76	0.72	0.68	0.64	0.60	0.55	0.48	0.45
644	23	0.10	0.97	0.97	0.97	0.97	0.97	0.96	0.95	0.94	0.92	0.90	0.89	0.86	0.84	0.80	0.77	0.73	0.69	0.65	0.61	0.54	0.50
877	51	0.15	0.95	0.95	0.95	0.96	0.95	0.95	0.94	0.93	0.92	0.90	0.89	0.87	0.84	0.81	0.78	0.75	0.71	0.68	0.63	0.56	0.53
1035	75	0.20	0.93	0.93	0.93	0.95	0.94	0.94	0.93	0.92	0.91	0.90	0.89	0.87	0.85	0.82	0.79	0.76	0.72	0.69	0.64	0.58	0.54
1188	113	0.25	0.91	0.91	0.91	0.93	0.93	0.92	0.92	0.91	0.90	0.89	0.88	0.86	0.84	0.82	0.79	0.76	0.73	0.69	0.65	0.59	0.56
1314	163	0.30	0.89	0.89	0.89	0.91	0.91	0.91	0.90	0.90	0.89	0.88	0.87	0.85	0.83	0.81	0.78	0.76	0.72	0.69	0.65	0.59	0.56
1418	210	0.35	0.87	0.87	0.87	0.89	0.89	0.89	0.89	0.88	0.87	0.86	0.86	0.84	0.83	0.80	0.78	0.75	0.72	0.69	0.66	0.60	0.57
1512	251	0.40	0.86	0.86	0.86	0.88	0.88	0.88	0.88	0.87	0.87	0.86	0.85	0.84	0.82	0.80	0.78	0.75	0.72	0.69	0.66	0.60	0.57
1578	299	0.45	0.84	0.84	0.84	0.86	0.87	0.87	0.86	0.86	0.85	0.84	0.84	0.83	0.81	0.79	0.77	0.75	0.72	0.69	0.65	0.60	0.57
1630	348	0.50	0.82	0.82	0.82	0.85	0.85	0.85	0.85	0.85	0.84	0.83	0.83	0.82	0.80	0.78	0.76	0.74	0.71	0.69	0.65	0.60	0.57
1664	414	0.55	0.80	0.80	0.80	0.82	0.83	0.83	0.83	0.83	0.82	0.82	0.81	0.80	0.79	0.77	0.75	0.73	0.70	0.68	0.64	0.59	0.56
1702	476	0.60	0.78	0.78	0.78	0.81	0.81	0.82	0.82	0.81	0.81	0.80	0.80	0.79	0.78	0.76	0.74	0.72	0.70	0.67	0.64	0.59	0.56
1732	533	0.65	0.76	0.76	0.76	0.79	0.80	0.80	0.80	0.80	0.79	0.79	0.78	0.77	0.75	0.73	0.71	0.69	0.66	0.63	0.58	0.56	0.56
1757	597	0.70	0.75	0.75	0.75	0.77	0.78	0.78	0.79	0.78	0.78	0.78	0.77	0.76	0.75	0.74	0.72	0.70	0.68	0.66	0.63	0.58	0.55
1771	678	0.75	0.72	0.72	0.72	0.75	0.76	0.76	0.77	0.77	0.76	0.76	0.76	0.75	0.74	0.72	0.71	0.69	0.67	0.65	0.62	0.57	0.55
1788	779	0.80	0.70	0.70	0.70	0.73	0.74	0.74	0.74	0.74	0.74	0.74	0.73	0.72	0.71	0.69	0.67	0.65	0.63	0.61	0.56	0.54	0.54
1798	914	0.85	0.66	0.66	0.66	0.69	0.71	0.71	0.72	0.72	0.71	0.71	0.71	0.70	0.70	0.68	0.67	0.65	0.64	0.62	0.59	0.55	0.52
1799	1200	0.90	0.60	0.60	0.60	0.63	0.65	0.65	0.66	0.66	0.66	0.66	0.66	0.66	0.65	0.64	0.63	0.61	0.60	0.58	0.56	0.52	0.50
1799	1200	0.95	0.60	0.60	0.60	0.63	0.65	0.65	0.66	0.66	0.66	0.66	0.66	0.66	0.65	0.64	0.63	0.61	0.60	0.58	0.56	0.52	0.50
1799	1200	1.00	0.60	0.60	0.60	0.63	0.65	0.65	0.66	0.66	0.66	0.66	0.66	0.66	0.65	0.64	0.63	0.61	0.60	0.58	0.56	0.52	0.50

Table 6.18: Accuracy for various confidence thresholds on gun and mundane item classification using a direct detection system operating between 75 – 110 GHz

By inspection an accuracy of almost 1 could be achieved by selecting a lower threshold

near 0% and upper threshold near 100%, however this also discards the most data. To

account for this a metric for data utility was created and defined as:

$$Utility = \frac{\text{Number of valid classifications}}{\text{Total number of classifications}} \quad (6.8)$$

Table 6.19 shows the utility of the original dataset for different confidence thresholds.

Lower utility is highlighted in darker shades of red.

		Dataset Utility % of original dataset used																					
TP	0	0	0	286	421	522	603	667	724	786	852	901	949	990	1037	1087	1125	1149	1177	1198	1200		
FN	0	0	0	1	11	28	42	67	97	135	169	221	287	381	485	611	764	922	1155	1553	1799		
resho	1.00	0.95	0.90	0.85	0.80	0.75	0.70	0.65	0.60	0.55	0.50	0.45	0.40	0.35	0.30	0.25	0.20	0.15	0.10	0.05	0.00		
0	0	0.00	0.00	0.00	0.10	0.14	0.18	0.22	0.24	0.27	0.31	0.34	0.37	0.41	0.46	0.51	0.57	0.63	0.69	0.78	0.92	1.00	
246	2	0.05	0.08	0.08	0.08	0.18	0.23	0.27	0.30	0.33	0.36	0.39	0.42	0.46	0.49	0.54	0.59	0.65	0.71	0.77	0.86	1.00	1.08
644	23	0.10	0.22	0.22	0.22	0.32	0.37	0.41	0.44	0.47	0.50	0.53	0.56	0.60	0.63	0.68	0.73	0.79	0.85	0.91	1.00	1.14	1.22
877	51	0.15	0.31	0.31	0.31	0.41	0.45	0.49	0.52	0.55	0.58	0.62	0.65	0.68	0.72	0.77	0.82	0.88	0.94	1.00	1.09	1.23	1.31
1035	75	0.20	0.37	0.37	0.37	0.47	0.51	0.55	0.59	0.61	0.64	0.68	0.71	0.74	0.78	0.83	0.88	0.94	1.00	1.06	1.15	1.29	1.37
1188	113	0.25	0.43	0.43	0.43	0.53	0.58	0.62	0.65	0.68	0.71	0.74	0.77	0.81	0.85	0.89	0.94	1.00	1.06	1.12	1.21	1.35	1.43
1314	163	0.30	0.49	0.49	0.49	0.59	0.64	0.68	0.71	0.74	0.77	0.80	0.83	0.87	0.90	0.95	1.00	1.06	1.12	1.18	1.27	1.41	1.49
1418	210	0.35	0.54	0.54	0.54	0.64	0.69	0.73	0.76	0.79	0.82	0.85	0.88	0.92	0.95	1.00	1.05	1.11	1.17	1.23	1.32	1.46	1.54
1512	251	0.40	0.59	0.59	0.59	0.68	0.73	0.77	0.80	0.83	0.86	0.89	0.93	0.96	1.00	1.05	1.10	1.15	1.22	1.28	1.37	1.51	1.59
1578	299	0.45	0.63	0.63	0.63	0.72	0.77	0.81	0.84	0.87	0.90	0.93	0.97	1.00	1.04	1.08	1.13	1.19	1.26	1.32	1.40	1.54	1.63
1630	348	0.50	0.66	0.66	0.66	0.76	0.80	0.84	0.87	0.90	0.93	0.97	1.00	1.03	1.07	1.12	1.17	1.23	1.29	1.35	1.44	1.58	1.66
1664	414	0.55	0.69	0.69	0.69	0.79	0.84	0.88	0.91	0.94	0.97	1.00	1.03	1.07	1.11	1.15	1.20	1.26	1.32	1.38	1.47	1.61	1.69
1702	476	0.60	0.73	0.73	0.73	0.82	0.87	0.91	0.94	0.97	1.00	1.03	1.07	1.10	1.14	1.18	1.23	1.29	1.36	1.42	1.50	1.64	1.73
1732	533	0.65	0.76	0.76	0.76	0.85	0.90	0.94	0.97	1.00	1.03	1.06	1.10	1.13	1.17	1.21	1.26	1.32	1.39	1.45	1.53	1.67	1.76
1757	597	0.70	0.78	0.78	0.78	0.88	0.93	0.97	1.00	1.03	1.06	1.09	1.13	1.16	1.20	1.24	1.29	1.35	1.41	1.48	1.56	1.70	1.78
1771	678	0.75	0.82	0.82	0.82	0.91	0.96	1.00	1.03	1.06	1.09	1.12	1.16	1.19	1.23	1.27	1.32	1.38	1.45	1.51	1.59	1.73	1.82
1788	779	0.80	0.86	0.86	0.86	0.95	1.00	1.04	1.07	1.10	1.13	1.16	1.20	1.23	1.27	1.31	1.36	1.42	1.49	1.55	1.63	1.77	1.86
1798	914	0.85	0.90	0.90	0.90	1.00	1.05	1.09	1.12	1.15	1.18	1.21	1.24	1.28	1.32	1.36	1.41	1.47	1.53	1.59	1.68	1.82	1.90
1799	1200	0.90	1.00	1.00	1.00	1.10	1.14	1.18	1.22	1.24	1.27	1.31	1.34	1.37	1.41	1.46	1.51	1.57	1.63	1.69	1.78	1.92	2.00
1799	1200	0.95	1.00	1.00	1.00	1.10	1.14	1.18	1.22	1.24	1.27	1.31	1.34	1.37	1.41	1.46	1.51	1.57	1.63	1.69	1.78	1.92	2.00
1799	1200	1.00	1.00	1.00	1.00	1.10	1.14	1.18	1.22	1.24	1.27	1.31	1.34	1.37	1.41	1.46	1.51	1.57	1.63	1.69	1.78	1.92	2.00

Table 6.19: Data Utility (%) for various confidence thresholds on gun and mundane item classification using a direct detection system operating between 75 – 110 GHz

It is clear by comparison of Tables 6.18 and 6.19 that more data is discarded as accuracy improves. To aid selection of an optimum threshold pair, an efficiency metric was created to allow simultaneous optimisation of both accuracy and data utility and is defined as:

$$Efficiency = \frac{Utility}{(1 - Accuracy)} \quad (6.9)$$

The aim of the Efficiency metric was to balance the conflicting requirements of a detection system with finite processing and data acquisition to produce an accurate and timely classification. Table 6.20 shows the calculated Efficiency for the dataset in tabular form.

		Efficiency = Utility / (1 - Accuracy)																					
		TP	1200	1198	1177	1149	1125	1087	1037	990	949	901	852	786	724	667	603	522	421	286	0	0	0
		FP	1799	1553	1155	922	764	611	485	381	287	221	169	135	97	67	42	28	11	1	0	0	0
TN	FN	resho	1.00	0.95	0.90	0.85	0.80	0.75	0.70	0.65	0.60	0.55	0.50	0.45	0.40	0.35	0.30	0.25	0.20	0.15	0.10	0.05	0.00
0	0	0.00	#DIV/0!	#DIV/0!	#DIV/0!	27	6	4	3	3	2	2	2	2	2	2	2	2	2	2	2	2	2
246	2	0.05	10	10	10	32	12	7	6	5	4	3	3	3	3	2	2	2	2	2	2	2	2
644	23	0.10	6	6	6	13	12	10	9	7	6	5	5	4	4	3	3	3	3	3	3	2	2
877	51	0.15	6	6	6	9	10	9	9	8	7	6	6	5	5	4	4	3	3	3	3	3	3
1035	75	0.20	5	5	5	9	9	9	9	8	7	7	6	6	5	5	4	4	4	3	3	3	3
1188	113	0.25	5	5	5	7	8	8	8	8	7	7	6	6	5	5	4	4	4	4	3	3	3
1314	163	0.30	4	4	4	6	7	7	7	7	7	6	6	6	5	5	5	4	4	4	4	3	3
1418	210	0.35	4	4	4	6	6	7	7	7	7	6	6	6	6	5	5	4	4	4	4	4	4
1512	251	0.40	4	4	4	6	6	6	7	7	6	6	6	6	6	5	5	5	4	4	4	4	4
1578	299	0.45	4	4	4	5	6	6	6	6	6	6	6	6	6	5	5	5	4	4	4	4	4
1630	348	0.50	4	4	4	5	5	6	6	6	6	6	6	6	5	5	5	4	4	4	4	4	4
1664	414	0.55	3	3	3	4	5	5	5	5	5	5	5	5	5	5	5	4	4	4	4	4	4
1702	476	0.60	3	3	3	4	5	5	5	5	5	5	5	5	5	5	5	4	4	4	4	4	4
1732	533	0.65	3	3	3	4	4	5	5	5	5	5	5	5	5	5	5	4	4	4	4	4	4
1757	597	0.70	3	3	3	4	4	4	5	5	5	5	5	5	5	5	5	4	4	4	4	4	4
1771	678	0.75	3	3	3	4	4	4	4	5	5	5	5	5	5	5	5	4	4	4	4	4	4
1788	779	0.80	3	3	3	3	4	4	4	4	4	4	5	5	5	4	4	4	4	4	4	4	4
1798	914	0.85	3	3	3	3	4	4	4	4	4	4	4	4	4	4	4	4	4	4	4	4	4
1799	1200	0.90	2	2	2	3	3	3	4	4	4	4	4	4	4	4	4	4	4	4	4	4	4
1799	1200	0.95	2	2	2	3	3	3	4	4	4	4	4	4	4	4	4	4	4	4	4	4	4
1799	1200	1.00	2	2	2	3	3	3	4	4	4	4	4	4	4	4	4	4	4	4	4	4	4

Table 6.20: Efficiency metric for various confidence thresholds on gun and mundane item classification using a direct detection system operating between 75 – 110 GHz

Figure 6.11 shows the plot of Efficiency with respect to upper and lower thresholds, illustrating graphically the effect of confidence thresholds upon Utility and Accuracy.

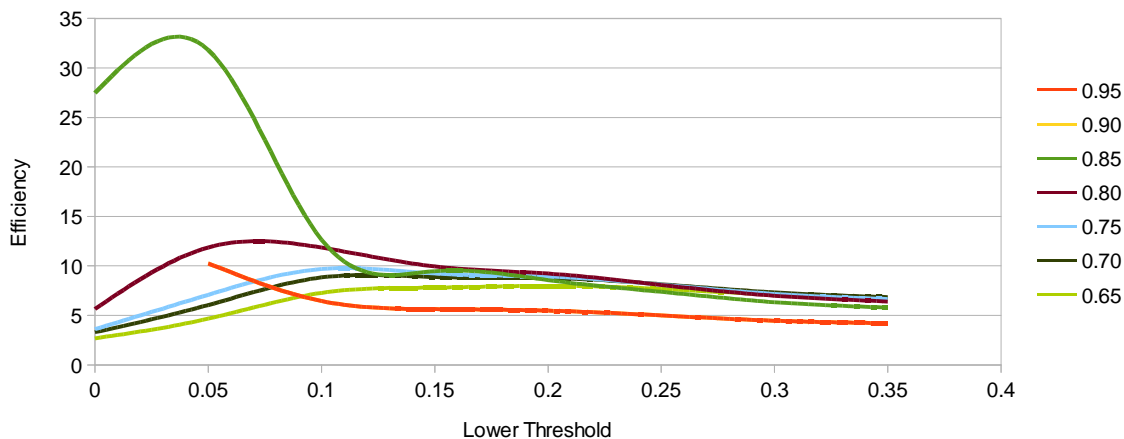


Figure 6.11: Plot of Efficiency metric for various confidence upper thresholds on gun and mundane item classification using a direct detection system operating between 75 – 110 GHz

For this particular network and training set, the greatest value of Efficiency is obtained with upper and lower confidence thresholds of 0.85 and 0.05 respectively. Note the asymmetry of the thresholds and the sum of the pair is not equal to 1. For classification

without emphasis on a particular metric primitive (TPR, TNR, FPR and FNR), the Efficiency metric may be used to select an optimal threshold pair for a real time system, by concurrently maximising both Accuracy and Utility.

6.7.1 Receiver Operating Characteristic (ROC) Space

ROC curves are graphical plots within the ROC space to show the performance of a binary classifier by comparing TPR and FPR. Conventionally a single ROC curve is plotted from a number of points generated by varying a threshold within the ROC space. Figure 6.12 shows the ROC space with marked points to assist with an explanation.

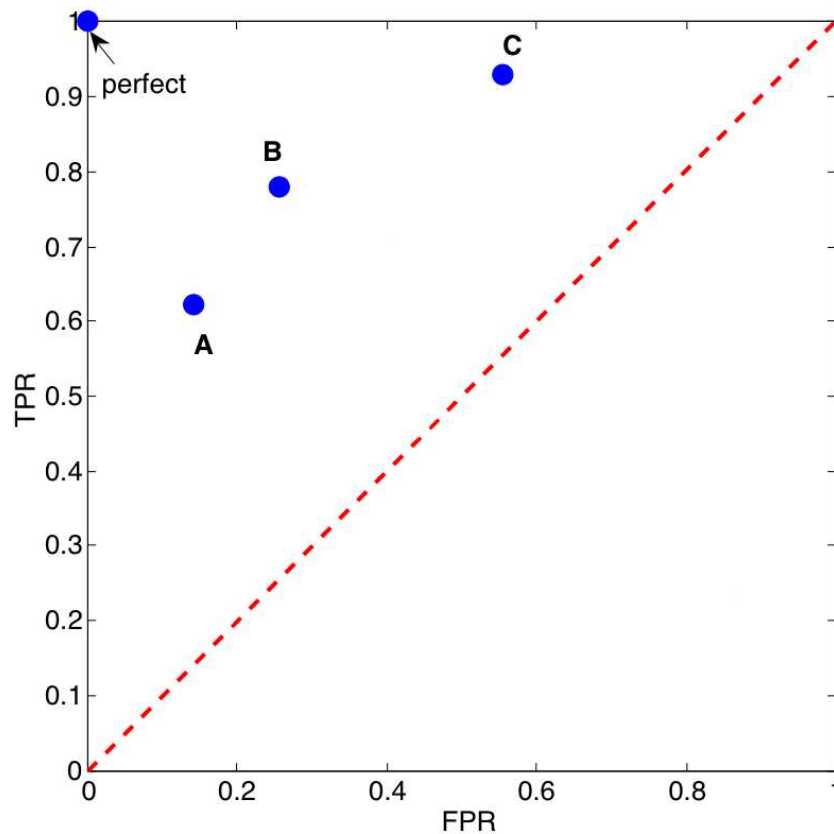


Figure 6.12: ROC space

The dashed line shows the performance of a classifier with a randomised output with an Accuracy of 0.5. The perfect classifier has a TPR of 1 and FPR of 0, a point representing its performance is indicated on the plot at (0,1). When comparing thresholds a point closer to perfect is generally considered superior, however the selection of an optimal point is a trade-off. Each point in has different characteristics and maybe or may not be more suited

to a specific application. Point A for example, has the lowest TPR, but also the lowest FPR; point B has a better TPR, but suffers from an increased FPR and similarly point C has the best TPR, but a suffers from the greatest FPR. For an application that requires the lowest FPR point A would be selected despite having the lowest TPR. It is the ability to easily interpret independently of all other operating parameters that makes ROC space so useful. As mentioned earlier conventionally the points making up a ROC curve represent a single varying threshold; fortunately with dual thresholding of the output the plot is only a little more complex with the ROC space containing multiple curves. Each ROC curve shown in Figure 6.13 represents a single upper threshold value with points obtained by varying the lower threshold.

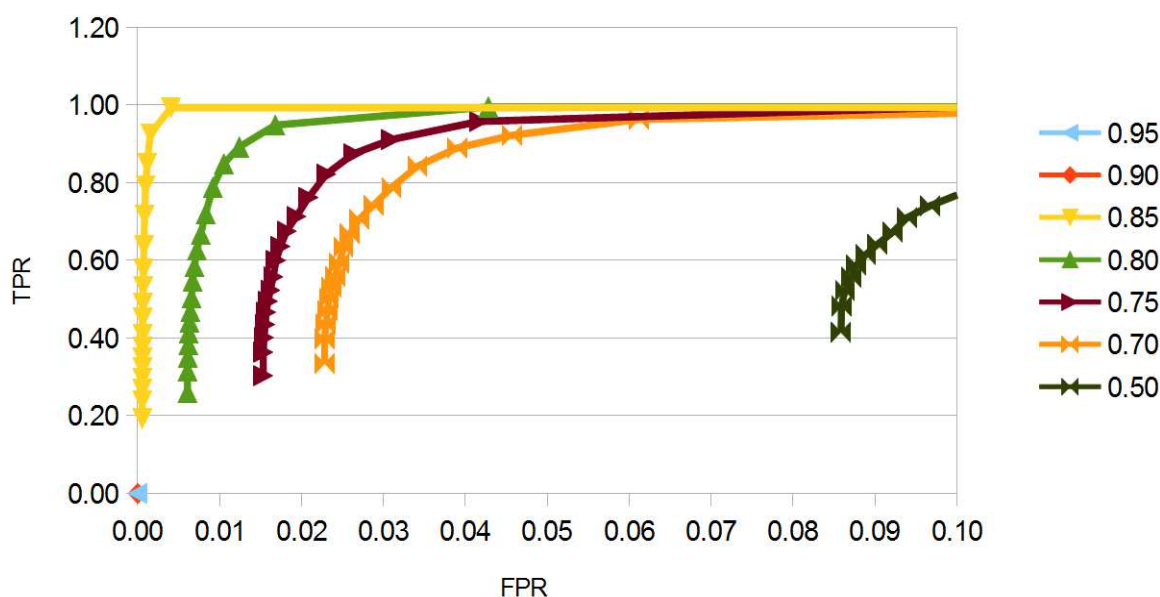


Figure 6.13: ROC curves for various upper thresholds of an unseen dataset consisting of body only; camera in the waistband; keys; gun held in the waistband and in the hand, at ranges of 2, 4 and 6 metres

ROC curves for upper thresholds of 0.95 and 0.90 are not shown due to a lack of classifications meeting the threshold. By inspection, the 0.85 upper threshold represents the best performance with a higher TPR and lower FPR than the other curves. However,

ROC curves do not indicate Utility, TNR and FNR. These metrics are also important when designing a real-time detection system. The Efficiency metric does not suffer this limitation, as it incorporates these essential metrics.

A comparison of optimally thresholded (85/05) and unthresholded (50/50) ANN classifications of an unseen dataset consisting of body only; camera in the waistband; keys; gun held in the waistband and in the hand, at ranges of 2, 4 and 6 metres, is given in Table 6.21.

Metric	Efficiency selected thresholds	Unthresholded classification
	(85/05)	(50/50)
TPR	0.99	0.71
TNR	1.00	0.91
FPR	0.00	0.09
FNR	0.01	0.29
Accuracy	0.99	0.83
Dataset utility	0.18	1.00
Efficiency	32.00	6.00

Table 6.21: Comparison of Efficiency selected threshold pair (85/05) with the standard classification threshold (50/50) for an unseen dataset of body only; camera in the waistband; keys; gun held in the waistband and in the hand, at ranges of 2, 4 and 6 metres

The Efficiency selected threshold pair provide an performance improvement compared to unthresholded classification at the expense of discarding 72% of the data.

6.8 Identification of Features Used In Classification: Signal Intensity or Structure

Another feature which was investigated was whether the network is classifying the shape of signals or analysing just the amplitude. In this particular example, horn antennas were used as simple polarisers and tests were conducted with a variety of objects concealed on

different areas of the body. The following results, shown in Table 6.22 were generated by a direct power detector based system with a single cross-polar receiver to establish whether the ANN was classifying the structure or just the magnitude of the returns. In the 'scaled' column the data has been rescaled so all the signals were of the same magnitude. The results show that even after rescaling, the ANN is able to correctly classify in most cases. This indicates that the shape as well as the magnitude of the cross polar signal is important and has implications in the selection of measured signals to be presented to the ANN.

Dataset	Range	Threat	No Threat	Threat (scaled)	No Threat (scaled)
Body 1	2	0	40	0	40
Body 2	2	0	40	1	39
Body 3	2	0	40	3	37
Body 1 and gun	2	40	0	40	0
Body 2 and gun	2	40	0	37	3
Body 3 and gun	2	40	0	38	2
Body 4	5	0	40	0	40
Body 5	5	0	40	4	36
Body 6	5	0	40	2	38
Body 4 and gun	5	40	0	40	0
Body 5 and gun	5	40	0	32	8
Body 6 and gun	5	40	0	27	13

Table 6.22: ANN classification results for original and normalised data from a direct power detector based system with a single cross-polar receiver between 80 – 100 GHz

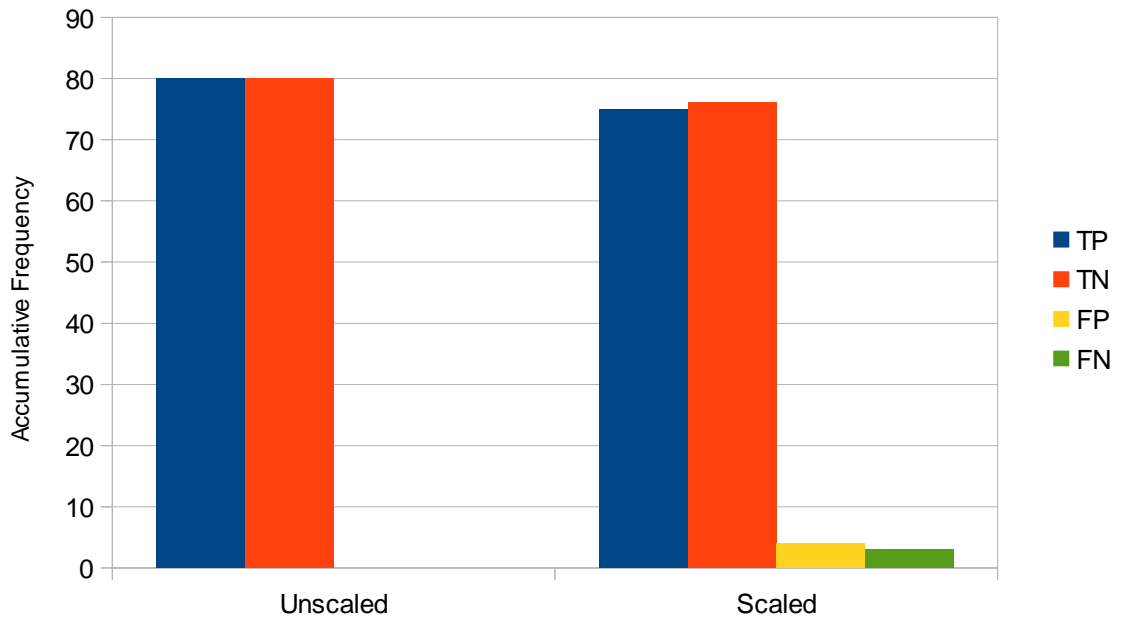


Figure 6.14: Performance of an ANN classifying unscaled and scaled data for body only and body with gun at 2 m using a direct power detect based system with a single cross-polar receiver operating between 80 – 100 GHz

Dataset	AC	TPR	FPR	TNR	FNR
Unscaled	100.00%	100.00%	0.00%	100.00%	0.00%
Scaled	95.57%	96.15%	5.00%	95.00%	3.85%

Table 6.23: Performance metrics for ANN classifying unscaled and scaled data for body only and body with gun at 2 m using a direct power detect based system with a single cross-polar receiver operating between 80 – 100 GHz

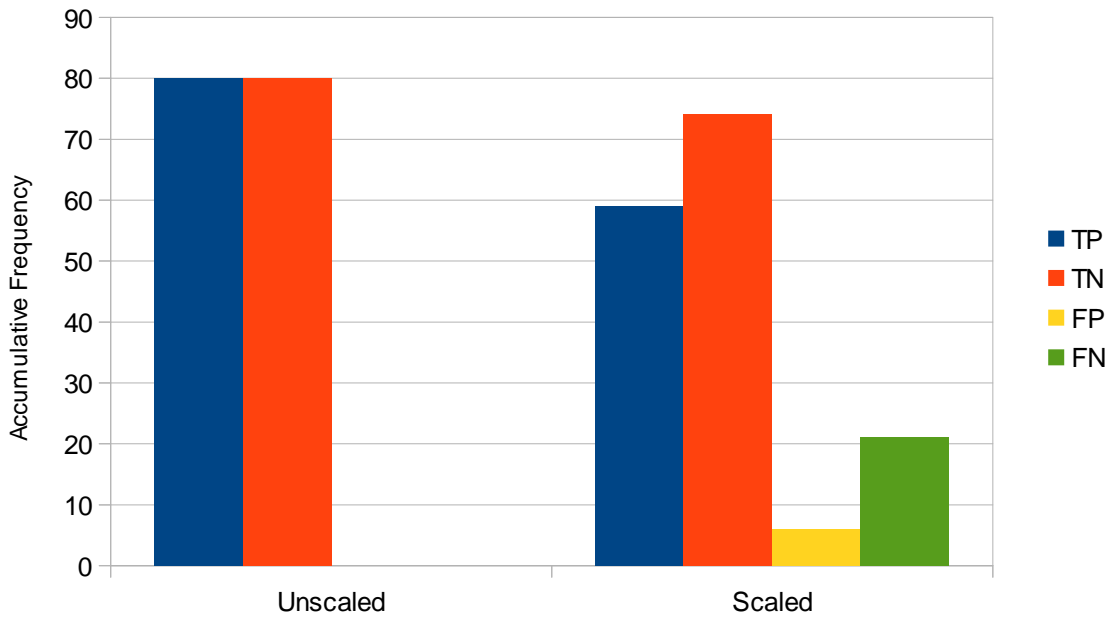


Figure 6.15: Performance of an ANN classifying unscaled and scaled data for body only and body with gun at 5 m using a direct power detect based system with a single cross-polar receiver operating between 80 – 100 GHz

Dataset	AC	TPR	FPR	TNR	FNR
Unscaled	100.00%	100.00%	0.00%	100.00%	0.00%
Scaled	83.13%	73.75%	7.50%	92.50%	26.25%

Table 6.24: Performance metrics for ANN classifying unscaled and scaled data for body only and body with gun at 5 m using a direct power detect based system with a single cross-polar receiver operating between 80 – 100 GHz

6.9 Evaluation

To be effective a stand-off screening system must satisfy several very substantial performance requirements. The energy used by the system must be able to penetrate commonly worn materials and reveal information about concealed objects with sufficient detail that they can be identified or detected as suspicious. The system must be able to

operate at sufficiently high rate of frames per second to provide prompt identification. Information presented to the user must be easy to interpret or be automatically analysed and interpreted.

The original remit of this work was the investigation, design and evaluation of signal processing and classification techniques for metallic items concealed upon a human body. During the project it was evident that the capability to detect explosives was also possible, although not necessarily as reliably for fragmentation free explosives and this ability increases the usefulness of the prototype.

The results earlier in this Chapter show the constructed device has strengths in different areas. The device is strong at detecting metallic items and fragmentation based explosives. Analysis of the return signal also indicates the likelihood that a metallic object is a threat or benign item. The main advantages of the prototype are:

- ◆ High throughput - detects concealed objects in as little as 0.5 second.
- ◆ Privacy - no anatomical details; personal privacy issues eliminated.
- ◆ Safe – use of non-ionising radiation is at levels well below agreed safe levels, see Appendix A.
- ◆ Seamless integration – the prototype can use in conjunction with existing systems.
- ◆ Real-time - monitoring and detection status is displayed for the operator in real-time.
- ◆ Stand-off detection – the prototype can be deployed remotely further reducing the level of danger the operator may be exposed to.
- ◆ Minimal training required to use the prototype with its automated threat detection algorithms.

The final prototype compares favourably with the similar Kapilevich hand held and bench-top systems described in Section 2.3.3.2. The specifications of these systems are compared in Table 6.25.

Property	(Kapilevich & Einat, 2007)	(Kapilevich et al., 2011)	Mirlin
Operating frequency	94 GHz	90 – 96 GHz	75 – 110 GHz
Operating mode	AM	FM	FM
Spatial resolution	N/A	25 mm	4.3 mm
Unambiguous Range	N/A	Estimated at 20 m	8.78 m
Maximum operating range	< 3 m	< 10 m	7 m
Receiver polarisations	1	1	Co and cross-polar
3 dB spot size at 3 m	0.38 m	0.11 m	0.07 m
Size	Hand-held unit approx. 30 x 25 x 40 cm	Approx. 1500 x 1000 x 600 cm	26 x 18 x 40 cm
Weight	Unknown	Static deployment	Approx. 3 kg
Indicates object nature	No	No	Yes
Self contained	No, a computer running LabVIEW and MATLAB is required	No, a computer and bench equipment are required	Yes

Table 6.25: Comparison of Kapilevich detection systems and Mirlin

7 Conclusion and Future Work

If you want something done well, do it yourself.

NAPOLEON BONAPARTE

7.1 Conclusion

The aim of the project was to develop and realise a system for the remote detection of guns and explosives concealed upon the human body. A bench top feasibility system was initially built and successfully tested. This system was succeeded by a series of three incremental portable active non-imaging prototypes operating in the 75 to 110 GHz frequency band as FMCW radars. The final system has a range of 7 m using a highly directional antenna and lens arrangement to focus the EM radiation on to the target during inspection and can be used effectively inside or outdoors. Inspection of targets is achieved by manually scanning the beam over the target to indicate the presence, location, size, shape and nature of concealed object upon the body of an individual.

The significant contribution to knowledge represented by this project, is a system capable of remotely indicating the nature of concealed objects in addition to identifying their presence, location, size and shape and operating at multiple times per second. Results indicate it is possible to detect the presence of a concealed threat by numerical analysis of the target's signal response.

Discoveries identified during the project include:

- There exist different mechanisms of detection for hand guns and explosives.
- A small area of fragmentation and non-fragmentation based explosives is representative of the whole device.
- The area of illumination required for detection varies with target - hand guns should be completely illuminated, whereas only a representative patch is needed for explosives.
- The optimum beam size for effective illumination of concealed threats is approximately 20 – 30 cm.
- The non-polarisation conserving property of complex metal objects is a good indicator that a handgun is present.
- A ultra-wideband system is required to detect thin sections of non-fragmentation based explosives.
- The mechanism of detection for fragmentation-based explosives and guns is similar and uses of the polarisation altering properties of the object.
- Classification of radar returns using ANNs enables threat objects to be detected and distinguished from mundane objects.
- The creation of an Efficiency metric to aid the selection of ANN confidence thresholds optimising both Accuracy and Utility metrics for use by real-time systems.

Seven publications have been made (Bowring et al., 2007b; Andrews et al., 2008b; Rezgui et al., 2008; Andrews et al., 2008a, 2009; Harmer et al., 2011, 2012) describing aspects of the work undertaken.

The Academic Aims defined in Section 1 have been fulfilled, see Table 7.1 below.

Academic Aim	Section
Identification of optimum frequency bands and power levels	2.3.1 - 2.3.4, 4.4, 4.5, 4.6 and Appendix A
The effects of commonly worn materials on EM transmissions	4.5
The use of continuous and pulsed illumination for the use of concealed object detection	3.2.2, 3.3.1 and 4.3.2
Signal processing and classification	4.2.2, 4.3.1, 4.3.2, 4.6, 4.7, 5.2, 5.8, 6.1.1 and 6.7
Construction of radar	4.9, 5.5, 5.6 and 5.7
Development of analysis routines	3.2.4 - 3.2.8, 4.7.2, 5.4, 6.1.1 6.4, 6.6, 6.7 and 6.8

Table 7.1: Sections relating to fulfilment of Academic Aims

Independent trials carried out in conjunction with our sponsors using Prototypes 3 and 4 have shown that the system provides a real time remote threat detection capability in an easily deployable, robust and lightweight unit for use inside or outdoors, which could satisfy an operational need not currently being addressed. These trials have provided essential feedback about system effectiveness during simulated deployment scenarios for comparison with our lab results.

7.2 Future Work

User feedback has helped identify areas for potential future development. These include:

- ◆ Increasing the operating frequency and hence reducing the size of the radar optics.
- ◆ Construction of a super heterodyne system for improved sensitivity.
- ◆ Incorporation of target contextual awareness, by automatically matching the part of the target being inspected with appropriate detection algorithms.
- ◆ Incorporation of gyroscopic sensors to aid image stabilisation during a manual inspection.
- ◆ Ruggedisation for use in operational environments.
- ◆ Improved power management systems for improved battery life.
- ◆ Enhance the hardware to to acquire and process inspections at higher rates.
- ◆ Investigate the use of genetic algorithms to improve ANN training by automatic selection of datasets for peak detection performance.

The technology and expertise gained during the development of the prototypes describe in this thesis, have been successfully employed within the Sensing and Imaging Group to develop a longer range device for detecting PBIEDs at distances up to 25m (Harmer et al., 2011). This has bigger radar optics and is also pedestal mounted, but otherwise uses similar technology and data processing, that has been developed for the hand held devices described here.

Bibliography

- Abramowitz & Stegun (1965). *Handbook of Mathematical Functions: with Formulas, Graphs, and Mathematical Tables*. Dover Publications.
- Achanta, A., McKenna, M. & Heyman, J. (2005). Nonlinear acoustic concealed weapons detection. In: *Applied Imagery and Pattern Recognition Workshop, 2005. Proceedings. 34th*. 2005, p. 7 pp.–27.
- Agilent (2012). *E8363B PNA Series [Discontinued] | Agilent*. [Online]. 2012. Available from: <http://www.home.agilent.com/agilent/product.jsp?cc=GB&lc=eng&ckey=72321&nid=-536902667.536882572.00&id=72321&pselect=SR.GENERAL>. [Accessed: 2 April 2012].
- Agurto, A., Li, Y., Tian, G.Y., Bowring, N. & Lockwood, S. (2007). A Review of Concealed Weapon Detection and Research in Perspective. In: *Proc. IEEE International Conference on Networking, Sensing and Control*. 2007, pp. 443–448.
- Alba (2006). *Microwave Optics: Refraction and Polarization*. [Online]. Available from: <http://www.physics.rutgers.edu/ugrad/205/manuals/micro.pdf>. [Accessed: 10 July 2012].
- Allen, G.I. (1999). Initial evaluation and follow-on investigation of the Quantum Magnetics laboratory prototype, room-temperature gradiometer for ordnance location. In: *Proceedings of SPIE*. [Online]. 1999, Orlando, FL, USA, pp. 103–112. Available from: http://spie.org/x648.html?product_id=354646. [Accessed: 14 March 2011].
- Andrews, D.A. (2008). *Detection of Concealed Explosives at Stand-off Distances using Wide Band Swept Millimetre Waves*.
- Andrews, D.A., Bowring, N., Rezgui, N.D., Southgate, M., Guest, E., Harmer, S. & Atiah, A. (2008a). A multifaceted active swept millimetre-wave approach to the detection

of concealed weapons. In: K. A. Krapels & N. A. Salmon (eds.). *Millimetre Wave and Terahertz Sensors and Technology*. [Online]. 2008, SPIE, p. 711707+. Available from: <http://dx.doi.org/10.1117/12.800360>.

Andrews, D.A., Rezgui, N.D., Smith, S.E., Bowring, N., Southgate, M. & Baker, J.G. (2008b). Detection of concealed explosives at stand-off distances using wide band swept millimetre waves. *Proceedings of SPIE*. 7117 (1). p.p. 71170J–71170J–9. Available from: [Accessed: 2 April 2012].

Andrews, D.A., Smith, S., Rezgui, N., Bowring, N., Southgate, M. & Harmer, S. (2009). A swept millimeter-wave technique for the detection of concealed weapons and thin layers of dielectric material with or without fragmentation. In: R. Appleby & D. A. Wikner (eds.). *Passive Millimeter-Wave Imaging Technology XII*. [Online]. 2009, SPIE, p. 73090H+. Available from: <http://dx.doi.org/10.1117/12.818875>.

Annaratone, D. (2009). *Engineering Heat Transfer*. Springer.

Anscombe, N. (2005). No place to hide [millimeter wave imaging]. *IEE Review*. 51 (12). p.pp. p26 – 30.

Appleby, R. (2004a). Passive millimetre-wave imaging and how it differs from terahertz imaging. *Philosophical Transactions of the Royal Society A: Mathematical, Physical and Engineering Sciences*. 362 (1815). p.pp. 379–393. Available from: [Accessed: 22 February 2012].

Appleby, R. (2004b). Passive millimetre-wave imaging and how it differs from terahertz imaging. *Philosophical Transactions of the Royal Society A: Mathematical, Physical and Engineering Sciences*. 362 (1815). p.pp. 379–393. Available from: [Accessed: 28 May 2012].

Appleby, R. (2008). *Security and Inspection Sector*.

Appleby, R. & Wallace, H.B. (2007). Standoff Detection of Weapons and Contraband in the 100 GHz to 1 THz Region. *Antennas and Propagation, IEEE Transactions on*. 55 (11). p.pp. 2944–2956.

Bajwa, I.S. & Hyder, S.I. (2005). PCA based image classification of single-layered cloud types. In: *Proceedings of the IEEE Symposium on Emerging Technologies, 2005*. 2005, pp. 365–369.

Baker, J. (n.d.). *Plastic Explosive Simulants*.

- BBC (2010a). Body scanners raise privacy fears. *BBC*. [Online]. 17 January. Available from: <http://news.bbc.co.uk/1/hi/8464266.stm>. [Accessed: 25 November 2010].
- BBC (2010b). MI5 head in terror attack warning. *BBC*. [Online]. 17 September. Available from: <http://www.bbc.co.uk/news/uk-11335412>. [Accessed: 2 March 2011].
- BBC (2009a). Mobile scanner could detect guns. *BBC*. [Online]. 8 June. Available from: <http://news.bbc.co.uk/1/hi/8089959.stm>. [Accessed: 11 February 2011].
- BBC (2009b). 'Naked' scanner in airport trial. *BBC*. [Online]. 13 October. Available from: <http://news.bbc.co.uk/1/hi/8303983.stm>. [Accessed: 24 November 2010].
- Bertl, S. & Detlefsen, J. (2010). Security-related active imaging of dielectric objects attached to human bodies. In: *Electromagnetic Theory (EMTS), 2010 URSI International Symposium on*. 2010, pp. 950–953.
- Bevelacqua, P. (2008). *Waveguides*. [Online]. August 2008. Antenna Theory. Available from: <http://www.antenna-theory.com/tutorial/waveguides/waveguide.php>. [Accessed: 6 June 2012].
- Bjarnason, J.E., Chan, T.L.J., Lee, A.W.M., Celis, M.A. & Brown, E.R. (2004). Millimeter-wave, terahertz, and mid-infrared transmission through common clothing. *Applied Physics Letters*. 85 (4). p.p. 519–521.
- Bowring, N. (2006). *Stand off distances*.
- Bowring, N.J., Baker, J.G. & Alder, J.F. (2007a). Detection and Measurement of Thin Dielectric Layers Using Reflection of Frequency Scanned Millimetric Waves. In: *Proc. IEEE International Conference on Networking, Sensing and Control*. 2007, pp. 437–442.
- Bowring, N.J., Baker, J.G., Rezgui, N.D. & Alder, J.F. (2008). A sensor for the detection and measurement of thin dielectric layers using reflection of frequency scanned millimetric waves. *MEASUREMENT SCIENCE AND TECHNOLOGY*. 19 (2). p.p. 24004.
- Bowring, N.J., Baker, J.G., Rezgui, N.D., Southgate, M. & Alder, J.F. (2007b). Active millimeter wave detection of concealed layers of dielectric material. In: T. T. Saito, D. Lehrfeld, & M. J. DeWeert (eds.). *Optics and Photonics in Global Homeland Security III*. [Online]. 2007, SPIE, p. 65401M+. Available from: <http://dx.doi.org/10.1117/12.719268>.

- Brandwood, D. (2003). *Fourier Transforms in Radar and Signal Processing*. Artech House.
- Brooker, Bishop & Hennessey (2008). Evolution of a suite of millimetre wave radar systems for situational awareness and automation on mines. In: *Proceedings of the 2008 Australian Mining Technology Conference*. [Online]. 2008, Queensland, Australia, pp. 3–33. Available from: <http://www.cas.edu.au/content.php/237.html?publicationid=542>. [Accessed: 21 June 2012].
- Brooker, G.M., Scheduling, S., Bishop, M.V. & Hennessy, R.C. (2005). Development and application of millimeter wave radar sensors for underground mining. *IEEE Sensors Journal*. 5 (6). p.pp. 1270–1280. Available from: [Accessed: 21 June 2012].
- Cafe, R.F. (2008). *Atmospheric Absorption [Online]*. [Online]. Available from: http://www.rfcafe.com/references/electrical/atm_absorption.htm.
- CCS (2007). *CCS, Inc. - Home*. [Online]. 2007. Available from: <http://www.ccsinfo.com/>. [Accessed: 11 June 2012].
- Chalmers, A. (2005). *Three applications of backscatter x-ray imaging technology to homeland defense*. In: [Online]. 2005, SPIE, pp. 989–993. Available from: <http://link.aip.org/link/?PSI/5778/989/1&Agg=doi>. [Accessed: 22 February 2012].
- Connolly, C. (2006). Machine vision developments. *Sensor Review*. 26 (4). p.pp. 277–282.
- Cooley, J.W. & Tukey, J.W. (1965). An Algorithm for the Machine Calculation of Complex Fourier Series. *Mathematics of Computation*. 19 (90). p.pp. 297–301. Available from: [Accessed: 28 May 2012].
- Costianes, P.J. (2005). An Overview of Concealed Weapons Detection for Homeland Security. In: *Applied Image Pattern Recognition Workshop*,. 2005, Los Alamitos, CA, USA: IEEE Computer Society, pp. 2–6.
- Coward, P.R. & Appleby, R. (2003). Development of an illumination chamber for indoor millimeter-wave imaging. *Proceedings of SPIE*. 5077. p.p. 54.
- Crane, R. (1980). Prediction of Attenuation by Rain. *Communications, IEEE Transactions on [legacy, pre-1988]*. 28 (9). p.pp. 1717–1733.

- Currie, N. & Stiefvater, K. (2003). *Counter-Terrorism Technology Assessment and Methodology Study*. DTIC Document.
- Currie, N.C. & Brown, C.E. (1987). *Principles and Applications of Millimeter-Wave Radar*. Artech House.
- Currie, N.C., Hayes, R.D. & Trebits, R.N. (1992). *Millimeter-Wave Radar Clutter*. Artech House Publishers.
- Detection, S. (2006). TADAR Millimetre-Wave People Screening System [Online]. Available at: <http://www.tadarvision.com/downloads/Tadar%20Brochure%20May05.pdf> [accessed 17 July 2008].
- Dickinson, J.C., Goyette, T.M., Gatesman, A.J., Joseph, C.S., Root, Z.G., Giles, R.H., Waldman, J. & Nixon, W.E. (2006). Terahertz imaging of subjects with concealed weapons D. L. Woolard, R. J. Hwu, M. J. Rosker, & J. O. Jensen (eds.). *Terahertz for Military and Security Applications IV*. 6212 (1). p.p. 62120Q.
- Dunayevskiy, I., Bortnik, B., Geary, K., Lombardo, R., Jack, M. & Fetterman, H. (2007). Millimeter-and submillimeter-wave characterization of various fabrics. *Applied Optics*. 46 (24). p.pp. 6161–6165.
- Eleftheriades, G.V. & Balmain, K.G. (2005). *Negative-refraction metamaterials : fundamental principles and applications*. Hoboken, N.J.: Wiley-Interscience.
- Elias, B. (2011). *Changes in Airport Passenger Screening Technologies and Procedures: Frequently Asked Questions*. [Online]. Available from: <http://www.fas.org/sgp/crs/homsec/R41502.pdf>. [Accessed: 9 November 2011].
- European Commission (2011). *EUROPA - Press Releases - Aviation security: Commission adopts new rules on the use of security scanners at European airports*. [Online]. 14 November 2011. Available from: <http://europa.eu/rapid/pressReleasesAction.do?reference=IP/11/1343&format=HTML&aged=0&language=EN&guiLanguage=en>. [Accessed: 22 February 2012].
- Farinelli, P. & Roth, F. (2003). Frequency domain analysis of the polarimetric ground penetrating radar response of landmines and minelike targets. In: *Proceedings of SPIE - The International Society for Optical Engineering*. 2003, pp. 437–447.
- Felber, F.S. (1998). Handheld ultrasound concealed weapons detector. In: *Proceedings of SPIE*. [Online]. 1998, Boston, MA, USA, pp. 89–98. Available from:

<http://link.aip.org/link/?PSI/3575/89/1&Agg=doi>. [Accessed: 6 April 2011].

- Fernandez-Cull, C., Wikner, D.A., Mattheiss, M., Mait, J.N. & Brady, D. (2010). Sparse sampling and enhanced axial resolution in millimeter-wave holographic imaging. In: *Proceedings of SPIE - The International Society for Optical Engineering*. [Online]. 2010. Available from: <http://www.scopus.com/inward/record.url?eid=2-s2.0-77953551907&partnerID=40&md5=6084b9efea0de0b334952d77a7cccb00>. [Accessed: 8 April 2011].
- Foster, F. (2011). *BBC News - Fast Track - When does airport security become physical assault?* [Online]. 14 August 2011. When does airport security become physical assault? Available from: http://news.bbc.co.uk/1/hi/programmes/fast_track/9561167.stm. [Accessed: 9 November 2011].
- FTDI (2010). *FT232R USB UART IC Datasheet Version 2.10*. [Online]. Available from: http://www.bryankappa.com/Resume/Kappa_MSME_Paper.pdf. [Accessed: 21 June 2012].
- Gandhi, O.P. & Riaz, A. (1986). Absorption of millimeter waves by human beings and its biological implications. *Microwave Theory and Techniques, IEEE Transactions on*. 34 (2). p.pp. 228–235.
- Gashinova, M., Cherniakov, M. & Vasalos, A. (2006). UWB signature analysis for detection of body-worn weapons. *Radar, 2006. CIE'06. International Conference on*. p.pp. 1–4.
- Gatesman, A.J., Danylov, A., Goyette, T.M., Dickinson, J.C., Giles, R.H., Goodhue, W., Waldman, J., Nixon, W.E. & Hoen, W. (2006). Terahertz behavior of optical components and common materials. *Proceedings of SPIE*. 6212. p.pp. 101–112.
- Gottumukkal, R. & Asari, V.K. (2003). Real time face detection from color video stream based on PCA method. In: *Applied Imagery Pattern Recognition Workshop, 2003. Proceedings*. 32nd. 2003, pp. 146–150.
- Goya, A. & Sibley, M.J.. (2007). *New proposal for the detection of concealed weapons*.
- Guo, Z. & Li, S. (2010). One-Dimensional Frequency-Domain Features for Aircraft Recognition from Radar Range Profiles. *IEEE Transactions on Aerospace and Electronic Systems*. 46 (4). p.pp. 1880–1892.

- Harmer, S., Bowring, N., Andrews, D., Rezgui, N., Southgate, M. & Smith, S. (2012). A Review of Nonimaging Stand-Off Concealed Threat Detection with Millimeter-Wave Radar [Application Notes]. *Microwave Magazine, IEEE*. 13 (1). p.pp. 160–167.
- Harmer, S.W., Bowring, N., Andrews, D., Rezgui, N. & Southgate, M. (2011). *Millimetre radar threat level evaluation (MiRTLE) at standoff ranges*. In: [Online]. 2011, p. 81880L–81880L–11. Available from: <http://link.aip.org/link/PSISDG/v8188/i1/p81880L/s1&Agg=doi>. [Accessed: 22 February 2012].
- Harmer, S.W., Rezgui, N., Bowring, N., Luklinska, Z. & Ren, G. (2008). Determination of the complex permittivity of textiles and leather in the 14–40 GHz millimetre-wave band using a free-wave transmittance only method. *IET Microwaves, Antennas & Propagation*. 2 (6). p.p. 606. Available from: [Accessed: 22 February 2012].
- Hausner, J. (2009). Radar based concealed threat detector. In: *Proceedings of SPIE - The International Society for Optical Engineering*. [Online]. 2009. Available from: <http://www.scopus.com/inward/record.url?eid=2-s2.0-69749112198&partnerID=40&md5=479c999b8b98db2cd26c9e3785ecf1af>. [Accessed: 17 December 2010].
- Hecht, E. (2001). *Optics*. 4th Ed. Addison Wesley.
- Herald (2010). *Plymouth police get handheld metal detectors*. [Online]. 11 February 2010. Available from: <http://www.thisisplymouth.co.uk/news/Plymouth-police-handheld-metal-detectors/article-1822580-detail/article.html>. [Accessed: 7 April 2011].
- Heyman (2008). *Acoustic concealed item detector*. [Online]. Available from: <http://www.google.co.uk/patents?hl=en&lr=&vid=USPAT7319639&id=4D-nAAAAEBAJ&oi=fnd&dq=hand-held+remote+concealed+weapons+detector+final+technical+report&printsec=abstract>. [Accessed: 5 April 2011].
- Hill, E.J., Intelligence, U.S.C.S.S.C. on & Intelligence, U.S.C.H.P.S.C. on (2002). *Joint Inquiry Staff Statement*. United States Senate Select Committee on Intelligence.
- Hu, Y., Huang, P., Guo, L., Wang, X. & Zhang, C. (2006). Terahertz spectroscopic investigations of explosives. *Physics Letters A*. 359 (6). p.pp. 728–732. Available from: [Accessed: 18 June 2012].
- Huguenin, G.R. (1997). *Millimeter-wave video rate imagers*. In: [Online]. 1997, SPIE, pp.

34–45. Available from: <http://link.aip.org/link/?PSI/3064/34/1&Agg=doi>.
[Accessed: 21 February 2012].

Humphreys, R.G. & Keene, M.N. (2009). *United States Patent: 7545140 - Metal object detecting apparatus*. [Online]. Available from: <http://patft.uspto.gov/netacgi/nph-Parser?Sect1=PTO2&Sect2=HITOFF&p=1&u=%2Fnethtml%2FPTO%2Fsearch-bool.html&r=1&f=G&l=50&co1=AND&d=PTXT&s1=20080054893&OS=20080054893&RS=20080054893>. [Accessed: 7 April 2011].

Hunt, A.R. (2001). Demonstration of a Concealed Weapons Detection System Using Electromagnetic Resonances, Final Report. *National Institute of Justice US Department of Justice, NCJ Number. 190134*.

Hyperphysics (2008). *Speed of Sound*. [Online]. 2008. Available from: <http://hyperphysics.phy-astr.gsu.edu/hbase/sound/souspe.html>. [Accessed: 21 June 2012].

ICNIRP, I. (1998). Guidelines for limiting exposure to time-varying electric, magnetic, and electromagnetic fields (up to 300 GHz). *Health Phys.* 74 (4). p.pp. 494–522.

IEEE (1984). *IEEE Standard Dictionary of Electrical and Electronics Terms*. 3rd edition. John Wiley & Sons Inc.

Iizuka, K., Freundorfer, A.P., Wu, K.H., Mori, H., Ogura, H. & Nguyen, V. (1984). Step-frequency radar. *Journal of Applied Physics*. 56 (9). p.pp. 2572–2583.

Immoriev, I. (2003). *Ten questions on UWB [ultra wide band radar]*. 11.

Immoriev, I.Y. & Taylor, J.D. (2005). Ultrawideband radar special features & terminology. *Aerospace and Electronic Systems Magazine, IEEE*. 20 (5). p.pp. 13–15.

Infineon (2010). *LNA (Low noise amplifier) and MMIC - Infineon Technologies*. [Online]. 2010. Available from: <http://www.infineon.com/cms/en/product/rf/rf-mmic/general-purpose-mmics-and-fm-radio-lnas/channel.html?channel=db3a30431b3e89eb011bd4ee7aa07e61>. [Accessed: 28 May 2012].

Interconnective (2010). *Adams Metal Detectors | Interconnective Security Products*. [Online]. 2010. Available from: <http://www.interconnective.co.uk/products/metal-detection>. [Accessed: 7 April 2011].

- Jain, A.K., Duin, R.P.W. & Mao, J. (2000). Statistical pattern recognition: a review. *IEEE Transactions on Pattern Analysis and Machine Intelligence*. 22 (1). p.pp. 4–37.
- Jaycor (2002). *Acoustic Sensors*. [Online]. 2002. Available from: http://jaycor.com/eme_sens_acoustic_apps.htm. [Accessed: 6 April 2011].
- Jia, H., Zhang, W., Zhang, K., Zhang, C. & Dai, C. (2008). A whole scheme for aircraft target identification in HRRP. In: *International Conference on Communications, Circuits and Systems, 2008. ICCAS 2008*. 2008, pp. 871–875.
- Johnson, W.C. (1950). *Transmission lines and networks*. McGraw-Hill.
- Kapilevich, B. & Einat, M. (2010). Detecting Hidden Objects on Human Body Using Active Millimeter Wave Sensor. *IEEE Sensors Journal*. 10 (11). p.pp. 1746–1752. Available from: [Accessed: 3 May 2012].
- Kapilevich, B. & Einat, M. (2007). *Hand-held Device and Method for Detecting Concealed Weapons and Hidden Objects*. [Online]. 28 December 2007. Available from: <http://patentscope.wipo.int/search/en/detail.jsf?docId=WO2007148327&recNum=64&docAn=IL2007000736&queryString=pa/university%2520AND%2520DP/27/12/2007&maxRec=101>. [Accessed: 23 May 2012].
- Kapilevich, B., Pinhasi, Y., Anisimov, M., Litvak, B. & Hardon, D. (2011). FMCW MM-wave non-imaging sensor for detecting hidden objects. In: *Microwave Workshop Series on Millimeter Wave Integration Technologies (IMWS), 2011 IEEE MTT-S International*. 2011, pp. 101–104.
- Keene, M.N. (2003). *United States Patent: 6541966 - Precision metal locating apparatus*. [Online]. Available from: <http://patft.uspto.gov/netacgi/nph-Parser?Sect2=PTO1&Sect2=HITOFF&p=1&u=%2Fnetacgi%2FPTO%2Fsearch-bool.html&r=1&f=G&l=50&d=PALL&RefSrch=yes&Query=PN%2F6541966>. [Accessed: 8 April 2011].
- Keene, M.N., Humphrey, K.P. & Horton, T.J. (2005). Actively shielded, adaptively balanced SQUID gradiometer system for operation aboard moving platforms. *IEEE Transactions on Applied Superconductivity*. 15 (2 PART I). p.pp. 761–764. Available from: [Accessed: 6 April 2011].
- Keller, G.V. (1996). *United States Patent: 5552705 - Non-obtrusive weapon detection system and method for discriminating between a concealed weapon and other metal objects*. [Online]. Available from: <http://patft.uspto.gov/netacgi/nph-Parser?>

Sect1=PTO1&Sect2=HITOFF&d=PALL&p=1&u=%2Fnetahtml%2FPTO%2Fsrchnum.htm&r=1&f=G&l=50&s1=5552705.PN.&OS=PN/5552705&RS=PN/5552705. [Accessed: 8 April 2011].

Keller, H. (1999). *United States Patent: 5859532 - Method of and measuring arrangement for metal detection with a coil device having several separately controllable regions*. [Online]. Available from: <http://patft.uspto.gov/netacgi/nph-Parser?Sect1=PTO1&Sect2=HITOFF&d=PALL&p=1&u=%2Fnetahtml%2FPTO%2Fsrchnum.htm&r=1&f=G&l=50&s1=5859532.PN.&OS=PN/5859532&RS=PN/5859532>. [Accessed: 8 April 2011].

Kemp, M.C. (2006). *Millimetre wave and terahertz technology for the detection of concealed threats: a review*. In: [Online]. 2006, SPIE, p. 64020D–64020D–19. Available from: <http://link.aip.org/link/PSISDG/v6402/i1/p64020D/s1&Agg=doi>. [Accessed: 22 February 2012].

Kemp, M.C., Glauser, A. & Baker, C. (2006). Recent developments in people screening using terahertz technology: seeing the world through terahertz eyes. *Proceedings of SPIE*. 6212. p.p. 62120T.

Kennedy, L. (2010). *ThruVision Status 2010*. [Online]. January 2010. Available from: http://www.etn-uk.com/DesktopModules/Bring2mind/DMX/Download.aspx?Command=Core_Download&EntryId=800&PortalId=0&TabId=2200. [Accessed: 1 June 2012].

Kennedy, L. (2009). *ThruVision THz Platform*. [Online]. Available from: <http://www.etn-uk.com/Portals/0/Content/Terahertz/MtG%20at%20RS/S43%20-%20Kennedy.pdf>. [Accessed: 1 June 2012].

King, T.L., Horine, F.M., Daly, K.C. & Smith, B.H. (2004). Explosives detection with hard-wired moths. *Instrumentation and Measurement, IEEE Transactions on*. 53 (4). p.pp. 1113–1118.

Knox, R. (2010). *Scientists Question Safety Of New Airport Scanners : NPR*. [Online]. 17 May 2010. Scientists Question Safety Of New Airport Scanners. Available from: <http://www.npr.org/templates/story/story.php?storyId=126833083>. [Accessed: 30 November 2010].

Komarov, I.V. & Smolskiy, S.M. (2003). *Fundamentals of Short-Range Fm Radar*. Artech House.

Lamb, J.W. (1996). Miscellaneous data on materials for millimetre and submillimetre

optics. *International Journal of Infrared and Millimeter Waves*. 17 (12). p.pp. 1997–2034.

- Lang, L. & Gu, W. (2009). The Face Detection Algorithm Combined Skin Color Segmentation and PCA. In: *International Conference on Information Engineering and Computer Science, 2009. ICIECS 2009*. 2009, pp. 1–3.
- Langman, A., Dimaio, S.P., Burns, B.E. & Inggis, M.R. (1996). Development of a low cost SFCW ground penetrating radar. *Geoscience and Remote Sensing Symposium, 1996. IGARSS'96. 'Remote Sensing for a Sustainable Future.'*, International. 4.
- Lawrence, S., Giles, C.L. & Tsoi, A.C. (1998). *What size neural network gives optimal generalization? Convergence properties of backpropagation*. [Online]. Available from: <http://drum.lib.umd.edu/handle/1903/809>. [Accessed: 27 March 2013].
- Li, H.-J. & Yang, S.-H. (1993). Using range profiles as feature vectors to identify aerospace objects. *IEEE Transactions on Antennas and Propagation*. 41 (3). p.pp. 261–268.
- Li, W., Chandrasekar, V. & Xu, G. (2003). Investigations in radar rainfall estimation using neural networks. In: *Geoscience and Remote Sensing Symposium, 2003. IGARSS '03. Proceedings. 2003 IEEE International*. 2003, pp. 2347–2349 vol.4.
- Lide, D.R. (1996). *CRC Handbook of Chemistry and Physics: Special Student Edition, 77th Edition*. 77th Ed. CRC Press.
- Liebe, H.J. (1989). MPM An atmospheric millimeter-wave propagation model. *International Journal of Infrared and Millimeter Waves*. 10 (6). p.pp. 631–650.
- Lo, D.C.W., Dow, G.S., Allen, B.R., Yujiri, L., Mussetto, M., Huang, T.W., Wang, H. & Biedenbender, M. (1995). A monolithic W-band high-gain LNA/detector for millimeter wave radiometric imaging applications. In: *Microwave Symposium Digest, 1995., IEEE MTT-S International*. 1995, pp. 1117–1120.
- Markov, G. (1965). *Antennas*. Progress Publishers.
- McCullagh, D. (2010). *Feds admit storing checkpoint body scan images / Privacy Inc.* - *CNET News*. [Online]. 4 August 2010. Feds admit storing checkpoint body scan images. Available from: http://news.cnet.com/8301-31921_3-20012583-281.html?tag=contentMain;contentBody. [Accessed: 30 November 2010].

- McMillan, R., Currie, N., Ferris Jr, D. & Wicks, M. (1998). Concealed weapon detection using microwave and millimeter wave sensors. In: *Microwave and Millimeter Wave Technology Proceedings, 1998. ICMMT'98. 1998 International Conference on.* 1998, pp. 1–4.
- Met (2008). *Common Locations for Concealed Items.*
- Microchip (2010). *PIC18F2331/2431/4331/4431 Data Sheet.*
- Microchip (2008). *PIC18F2420 Datasheet.* [Online]. Available from: <http://ww1.microchip.com/downloads/en/DeviceDoc/39631E.pdf>. [Accessed: 4 June 2012].
- Microchip (2009). *PIC18F2455/2550/4455/4550 Data Sheet.* [Online]. Available from: <http://ww1.microchip.com/downloads/en/DeviceDoc/39632e.pdf>. [Accessed: 8 June 2012].
- Microchip (2007). *USB Framework for PIC18, PIC24 & PIC32.* [Online]. 2007. Available from: http://www.microchip.com/stellent/idcplg?IdcService=SS_GET_PAGE&nodeId=2680&dDocName=en537044. [Accessed: 11 June 2012].
- Mikhnev, V.A. (2008). Published: Available online: <http://www.ndt.net/article/wcndt00/papers/idn354/idn354.htm> [Accessed on 20/7/2008]. *Microwave Reconstruction Approach for Stepped-Frequency Radar.* [Online]. Available from: <http://www.ndt.net/article/wcndt00/papers/idn354/idn354.htm>.
- Millitech (2011). *Millitech Series Active Multiplier Chain.* [Online]. Available from: <http://www.millitech.com/pdfs/specsheets/IS000037-AMC.pdf>. [Accessed: 25 June 2012].
- Morris, E.J.L. (2005). *A backscattered x-ray imager for medical applications.* In: [Online]. 2005, SPIE, pp. 113–120. Available from: <http://link.aip.org/link/?PSI/5745/113/1&Agg=doi>. [Accessed: 22 February 2012].
- Motzer, J. (2000). A pulse radar gauge for level measurement and process control. In: *Microwave Symposium Digest., 2000 IEEE MTT-S International.* [Online]. 2000, pp. 1563–1566. Available from: http://ieeexplore.ieee.org/xpls/abs_all.jsp?arnumber=862274. [Accessed: 21 June 2012].

- Nacci, P.L. & Mockensturm, L. (2001). *Detecting Concealed Weapons: Technology Research at the National Institute of Justice*.
- Narayan, C.P. (2007). *Antennas And Propagation*. Technical Publications.
- NASA (2011). *MY NASA DATA ELECTROMAGNETIC SPECTRUM PAGE*. [Online]. 2011. Available from: <http://mynasadata.larc.nasa.gov/ElectroMag.html>. [Accessed: 19 January 2011].
- Negnevitsky, M. (2005). *Artificial Intelligence: A Guide To Intelligent Systems*. Pearson Education.
- Nelson, C.V. (2004). Metal detection and classification technologies. *Johns Hopkins APL technical digest*. 25 (1). p.pp. 62–67.
- Nelson, C.V. (2006a). *Three-Dimensional Steerable Magnetic Field (3DSMF) Sensor System for Classification of Buried Metal Targets*. JOHNS HOPKINS UNIV LAUREL MD APPLIED PHYSICS LAB.
- Nelson, C.V. (2003a). Three-dimensional steerable magnetic field antenna for metal target classification. In: *Proceedings of SPIE*. [Online]. 2003, Orlando, FL, USA, pp. 707–717. Available from: <http://link.aip.org/link/?PSI/5089/707/1&Agg=doi>. [Accessed: 7 April 2011].
- Nelson, C.V. (2006b). *United States Patent: 7030759 - Steerable three-dimensional magnetic field sensor system for detection and classification of metal targets*. [Online]. Available from: <http://patft.uspto.gov/netacgi/nph-Parser?Sect2=PTO1&Sect2=HITOFF&p=1&u=%2Fmetahtml%2FPTO%2Fsearchbool.html&r=1&f=G&l=50&d=PALL&RefSrch=yes&Query=PN%2F7030759>. [Accessed: 6 April 2011].
- Nelson, C.V. (2007). *United States Patent: 7227466 - Expendable metal detector*. [Online]. Available from: <http://patft.uspto.gov/netacgi/nph-Parser?Sect2=PTO1&Sect2=HITOFF&p=1&u=%2Fmetahtml%2FPTO%2Fsearchbool.html&r=1&f=G&l=50&d=PALL&RefSrch=yes&Query=PN%2F7227466>. [Accessed: 7 April 2011].
- Nelson, C.V. (2003b). Wide-area metal detection system for crowd screening. In: *Proceedings of SPIE - The International Society for Optical Engineering*. [Online]. 2003, pp. 380–387. Available from: <http://www.scopus.com/inward/record.url?eid=2-s2.0-1642556865&partnerID=40&md5=59f68b700f40fc492ecd4d518d8b8934>.

[Accessed: 7 April 2011].

Novak, D., Waterhouse, R. & Farnham, A. (2005). Millimeter-wave weapons detection system. In: *Applied Imagery and Pattern Recognition Workshop, 2005. Proceedings. 34th.* 2005, p. 6–pp.

Paul, P.P. & Gavrilova, M. (2011). PCA Based Geometric Modeling for Automatic Face Detection. In: *2011 International Conference on Computational Science and Its Applications (ICCSA).* 2011, pp. 33–38.

Paulter, N.G. (2001). *Guide to the Technologies of Concealed Weapon and Contraband Imaging and Detection.* National Institute of Standards and Technology: US Department of Justice, Office of Justice Program, National Institute of Justice.

Pickwell, E., Cole, B.E., Fitzgerald, A.J., Pepper, M. & Wallace, V.P. (2004). In vivo study of human skin using pulsed terahertz radiation. *Physics in Medicine and Biology.* 49 (9). p.pp. 1595–1607. Available from: [Accessed: 22 February 2012].

Polyanskiy, M. (2008). RefractiveIndex.INFO - A comprehensive refractive index database [Online]. Available at: <http://refractiveindex.info/index.php?group=PLASTICS&material=BK7&wavelength=0.6328> [accessed 21 September 2008]. [Online]. Available from: <http://refractiveindex.info/index.php?group=PLASTICS&material=BK7&wavelength=0.6328>.

QinitiQ (2012). *QinetiQ Technology Showcase - New Technology Products from QinetiQ.* [Online]. 2012. SPO-20 Technology Showcase. Available from: <http://technologyshowcase.qinetiq.com/>. [Accessed: 25 May 2012].

Rapiscan (2009). *Rapiscan Systems - People Screening - Rapiscan Secure 1000 - Backscatter Screening.* [Online]. 2009. Available from: <http://www.rapiscansystems.com/sec1000.html>. [Accessed: 4 April 2011].

Raza, M. (2012). PressCoverage-SecuringAsia2012-ContingencyToday-31.05.2012.pdf. *Contingency Today.* [Online]. 31 May. Available from: <http://securingasia2012.com/Press/PressCoverage-SecuringAsia2012-ContingencyToday-31.05.2012.pdf>. [Accessed: 12 June 2012].

Renato (2002). *RADAR BASICS.* [Online]. 2002. Available from: http://www.alphaalpha.org/radar/intro_e.html. [Accessed: 18 June 2012].

Rezgui, N., Andrews, D., Bowring, N., Harmer, S. & Southgate, M. (2008). Standoff

detection of concealed handguns. In: R. Appleby & D. A. Wikner (eds.). *Passive Millimeter-Wave Imaging Technology XI*. [Online]. 2008, SPIE, p. 69480L+. Available from: <http://dx.doi.org/10.1117/12.777719>.

Rønne, C. & Keiding, S.R. (2002). Low frequency spectroscopy of liquid water using THz-time domain spectroscopy. *Journal of Molecular Liquids*. 101 (1-3). p.pp. 199–218. Available from: [Accessed: 22 February 2012].

Roybal, L.G. (1997). *New approach for detecting and classifying concealed weapons*. In: [Online]. 1997, SPIE, pp. 96–107. Available from: <http://link.aip.org/link/?PSI/2935/96/1&Agg=doi>. [Accessed: 22 February 2012].

Schauer, D.A. (2011). Does Security Screening with Backscatter X-Rays Do More Good than Harm? *Radiology*. 259 (1). p.pp. 12–16. Available from: [Accessed: 22 February 2012].

SDN (2008). *Courting security*. [Online]. 30 2008. Security Director News. Available from: <http://www.securitydirectornews.com/general-news/courting-security>. [Accessed: 1 June 2012].

SensComp (2009). *SensComp Series 600 Smart Sensor*. [Online]. Available from: <http://www.senscomp.com/pdfs/smart-sensor.pdf>. [Accessed: 4 June 2012].

Seymour, C., Mann, C. & Kennedy, L. (2010). *Investigation into the Phenomenology and Physics of Sub-THz Imaging for Buried Object Detection*. In: [Online]. 2010, Edinburgh. Available from: <http://www.emrsdte.com/conferences/2010/downloads/papers/A3.pdf>. [Accessed: 1 June 2012].

Sheen, D.M., Hall, T.E., Severtsen, R.H., McMakin, D.L., Hatchell, B.K. & Valdez, P.L.J. (2010). *Standoff concealed weapon detection using a 350-GHz radar imaging system*. In: [Online]. 2010, Orlando, Florida, USA, pp. 767008–767008–12. Available from: <http://link.aip.org/link/PSISDG/v7670/i1/p767008/s1&Agg=doi>. [Accessed: 8 April 2011].

Sheen, D.M., McMakin, D.L. & Hall, T.E. (2001). Three-dimensional millimeter-wave imaging for concealed weapon detection. *Microwave Theory and Techniques, IEEE Transactions on*. 49 (9). p.pp. 1581–1592.

SiversIMA (2011). *Advantages and disadvantages of FMCW radar*. [Online]. Available from: <http://www.siversima.com/wp-content/uploads/2011/07/FMCW-Radar-App-Notes-Advantages-and-Disadvantages.pdf>. [Accessed: 7 June 2012].

- Skolnik, M. (2002). *Introduction to Radar Systems*. 3rd Ed. McGraw-Hill Science/Engineering/Math.
- Smith, J.O., Stanford University. Center for Computer Research in Music and Acoustics & Stanford University. Dept. of Music (2011). *Spectral audio signal processing*. [Stanford, Calif.?]: W3K.
- Smith, S. (2012). *Concealed Explosives Detection Using Swept Millimetre Waves*. Manchester Metropolitan University.
- Smith, S. (1991). *Patent US5181234 - X-ray backscatter detection system - Google Patents*. [Online]. May 1991. Available from: <http://www.google.co.uk/patents?hl=en&lr=&vid=USPAT5181234&id=9tMAAAAAEBAJ&oi=fnd&dq=soft+x-ray+concealed&printsec=abstract#v=onepage&q=soft%20x-ray%20concealed&f=false>. [Accessed: 22 February 2012].
- Smith, S.W. (1997). *The scientist and engineer's guide to digital signal processing*. San Diego, Calif.: California Technical Pub.
- Southgate, M. (2009). *Detection of Concealed Guns and Explosives at Standoff Distances*.
- Southgate, M., Harmer, S.W., Rezgui, N. & Bowring, N. (2008). *Determination of the complex permittivity of textiles and leather in the 75-110 GHz millimetre-wave band using a free-wave transmittance only method*.
- Stove, A.G. (1992). Linear FMCW radar techniques. In: *Radar and Signal Processing, IEE Proceedings F*. 1992, pp. 343–350.
- Subotic, N.S., Gorman, J.D. & Welby, S. (1998). *Hybrid Template- and Model-Based ATR Formulation*.
- Sutton, V. & Bromley, D.A. (2005). Understanding technologies of terror. *Technology in Society*. 27 (3). p.pp. 263–285. Available from: [Accessed: 14 March 2011].
- Tatuzov, A.L. (2002). Neural network methods for radar processing. In: *Proceedings of the 9th International Conference on Neural Information Processing, 2002. ICONIP '02*. 2002, pp. 1718–1722 vol.4.
- Taylor, J.D. (1995). *Introduction to ultra-wideband radar systems*. Boca Raton: CRC Press.

- Taylor, J.D. (2001). *Ultra-Wideband Radar Technology*. CRC Press.
- Telegraph (2009). Airport scanner ‘shows passengers naked’. *Telegraph.co.uk*. [Online]. October. Available from:
<http://www.telegraph.co.uk/travel/travelnews/6309898/Airport-scanner-shows-passengers-naked.html>. [Accessed: 25 November 2010].
- Teshirogi, T. & Yoneyama, T. (2001). *Modern Millimeter-Wave Technologies*. IOS Press.
- Transportation, N.R.C. (US). C. on A. of S.T. for (2007). *Assessment of millimeter-wave and terahertz technology for detection and identification of concealed explosive and weapons*. Natl Academy Pr.
- Tsai, C.Y., Rothwell, E.J. & Chen, K.M. (1996). Target discrimination using neural networks with time domain or spectrum magnitude response. *Journal of Electromagnetic Waves and Applications*. 10 (3). p.pp. 341–382. Available from:
 [Accessed: 4 April 2012].
- UK Government (2000). *Terrorism Act 2000*. [Online]. 2000. Available from:
<http://www.legislation.gov.uk/ukpga/2000/11/contents>. [Accessed: 2 March 2011].
- UKHO (2009). *Explosives and Weapons Detection: 2010 Call for Innovative R&D Proposals Bidder Information*.
- UKHO (2011). *Review of Counter-Terrorism and Security Powers - Review Findings and Recommendations*. [Online]. Available from:
<http://www.homeoffice.gov.uk/publications/counter-terrorism/review-of-ct-security-powers/review-findings-and-rec?view=Binary>. [Accessed: 2 March 2011].
- UKHO (2010). *The UK counter-terrorism strategy (CONTEST)*. [Online]. 2010. The UK counter-terrorism strategy (CONTEST). Available from:
<http://www.homeoffice.gov.uk/counter-terrorism/uk-counter-terrorism-strat/>. [Accessed: 2 March 2011].
- USB (2007). *USB.org*. [Online]. 2007. USB Implementors Forum. Available from:
<http://www.usb.org/developers/docs/>. [Accessed: 11 June 2012].
- Weib, M. & Knochel, R. (1997). A highly accurate multi-target microwave ranging system for measuring liquid levels in tanks. In: *Microwave Conference, 1997. 27th European*. [Online]. 1997, pp. 1103–1112. Available from:
http://ieeexplore.ieee.org/xpls/abs_all.jsp?arnumber=4138997. [Accessed: 21 June

2012].

Whittle, P., Kay, J., Hand, D.J., Tarassenko, L., Brown, P.J., Titterton, D.M., Taylor, C., Gilks, W.R., Critchley, F., Mayne, A.J., Wahba, G., Luttrell, S.P., Baczkowski, A.J., Mardia, K.V., Breiman, L., Buntine, W., Chatfield, C., Deveaux, R.D., Darken, C.J., Ungar, L.H., Glendinning, R.H., Hastie, T., Tibshirani, R., McLachlan, G.J., Michie, D., Owen, A.B., Wolpert, D.H. & Ripley, B.D. (1994). Neural Networks and Related Methods for Classification - Discussion. *Journal of the Royal Statistical Society Series B-Methodological*. 56 (3). p.pp. 437–456. Available from: [Accessed: 28 March 2013].

WHO (2012). *WHO / What are electromagnetic fields?* [Online]. 2012. WHO. Available from: <http://www.who.int/peh-emf/about/WhatisEMF/en/index3.html>. [Accessed: 12 June 2012].

Wikipedia contributors (2012). Horn antenna. *Wikipedia, the free encyclopedia*. [Online]. Available from: http://en.wikipedia.org/w/index.php?title=Horn_antenna&oldid=498673513. [Accessed: 22 June 2012].

Wild, N. (2003). *Handheld Concealed Weapons Detector Development*. JAYCOR SAN DIEGO CA.

Wild, N., Niederhaus, S., Lam, H. & Lum, C. (2001). *Handheld ultrasonic concealed weapon detector*. [Online]. 2001. Available from: <http://adsabs.harvard.edu/abs/2002SPIE.4708..122W>. [Accessed: 14 March 2011].

Wild, N.C. (2001). Handheld ultrasonic concealed weapon detector. In: *Proceedings of SPIE*. [Online]. 2001, Boston, MA, USA, pp. 152–158. Available from: http://spie.org/x648.html?product_id=417527. [Accessed: 6 April 2011].

Wolff (2009). *Radar Basics - Range Resolution*. [Online]. 2009. Available from: <http://www.radartutorial.eu/01.basics/rb18.en.html>. [Accessed: 20 June 2012].

Yamamoto, K., Yamaguchi, M., Miyamaru, F., Tani, M., Hangyo, M., Ikeda, T., Matsushita, A., Koide, K., Tatsuno, M. & Minami, Y. (2004). Noninvasive Inspection of C-4 Explosive in Mails by Terahertz Time-Domain Spectroscopy. *Japanese Journal of Applied Physics*. 43 (No. 3B). p.pp. L414–L417.

Yong, S., Lei, Y. & Yi, W. (2010). Application research on intelligent pattern recognition methods in hail identification of weather radar. In: *2010 International Conference on Computer Application and System Modeling (ICCA SM)*. 2010, pp. V11–554–V11–558.

- Yuehua, L., Xingguo, L. & Min, W. (1998). An analysis of signal of MMW step frequency high resolution radar with MUSIC algorithms. In: *Microwave and Millimeter Wave Technology Proceedings, 1998. ICMMT'98. 1998 International Conference on*. [Online]. 1998, pp. 443–447. Available from: http://ieeexplore.ieee.org/xpls/abs_all.jsp?arnumber=768321. [Accessed: 21 June 2012].
- Zanotti-Fregonara, P., Hindie, E. & Brenner, D.J. (2011). Radiation Risk from Airport X-ray Backscatter Scanners: Should We Fear the Microsievert? *Radiology*. 261 (1). p.pp. 330–331. Available from: [Accessed: 22 February 2012].
- Zollars, B.G. (1997). *Concealed weapons detection using low-frequency magnetic imaging*. In: [Online]. 1997, SPIE, pp. 108–119. Available from: <http://link.aip.org/link/?PSI/2935/108/1&Agg=doi>. [Accessed: 1 February 2012].
- Zyweck, A. & Bogner, R.E. (1996). Radar target classification of commercial aircraft. *IEEE Transactions on Aerospace and Electronic Systems*. 32 (2). p.pp. 598–606.

Blank page

Appendices

Blank page

A Radiation Safety

There are two types of radiation ionising and non-ionising. The difference is basically due to energy levels, non-ionising radiation does not carry enough energy to knock an electron from atoms or molecules that it passes through and ionising radiation has sufficient energy to do so. Ionising radiation consists of five major kinds: alpha particles, beta particles, gamma rays, x-rays and neutrons. Non-ionising radiation consists of extremely low frequencies waves, radio waves, microwaves and visible light.

Radiation intensity must be considered alongside its ability to ionise. In an ideal world the level of microwave radiation used for illuminating targets would be minuscule as no radiation is completely safe. The purpose of providing target illumination is to supplement and control the illumination already detected by the system, otherwise the system would be passive and have performance limitations.

‘Safe’ threshold levels have been devised by international regulators below which it is believed that people are not adversely affected by radiation. These levels have yet to be settled scientifically and there is a degree of controversy about them, so the recommended approach is to minimise unnecessary radiation exposure.

The current International Commission on Non-Ionising Radiation Protection (ICNIRP) guidelines specify maximum levels for general public and occupational exposure. The guidelines covering the frequencies of use give a power density limit for the general public of $10\text{W}/\text{m}^2$ and occupational exposure levels of $50\text{W}/\text{m}^2$. The calculations below use the public limit of $10\text{W}/\text{m}^2$ and our maximum output power of 10dBmW sufficient to drive multipliers are used. All values are to three significant figures.

$$\begin{aligned} Power(dBm) &= 10 \log_{10} Power(W) \\ \therefore 10dBm W &= 10mW = 0.01W \end{aligned} \quad (1)$$

Assuming range to target is one metre the power density with an isotropic antenna would be:

$$P_{density_isotropic} = \frac{P_t}{4\pi r^2} = \frac{0.01}{4\pi(1)^2} = 796 \times 10^{-6} Wm^{-2} \quad (2)$$

Using a 20dB gain horn antenna to focus the transmitted power the theoretical power density would be:

$$P_{density_20dB_horn} = (796 \times 10^{-6} Wm^{-2})^{20/10} = 79.6 \times 10^{-3} Wm^{-2} \quad (3)$$

Supporting this calculation a metal sheet reflector was used to empirically quantify the radiation pattern of the 20dB horns at one metre. The radiation pattern was approximately sixty centimetres wide by thirty centimetres tall. The power density assuming no losses for this area at one metre would be:

$$P_{density} = \frac{P_t}{P_{area}} = \frac{0.01}{0.60 \times 0.30} = \frac{0.01}{0.18} = 55.6 \times 10^{-3} Wm^{-2} \quad (4)$$

Hence the gain of the delivery system is approximately:

$$\begin{aligned} Gain &= \frac{P_{density_horn}}{P_{density_isotropic}} = \frac{55.6 \times 10^{-3} Wm^{-2}}{796 \times 10^{-6} Wm^{-2}} = 69.8 \\ P_{gain(dB)} &= 10 \log_{10} Gain \\ \therefore P_{gain(dB)} &= 10 \log_{10} 69.8 = 18.4dB \end{aligned} \quad (5)$$

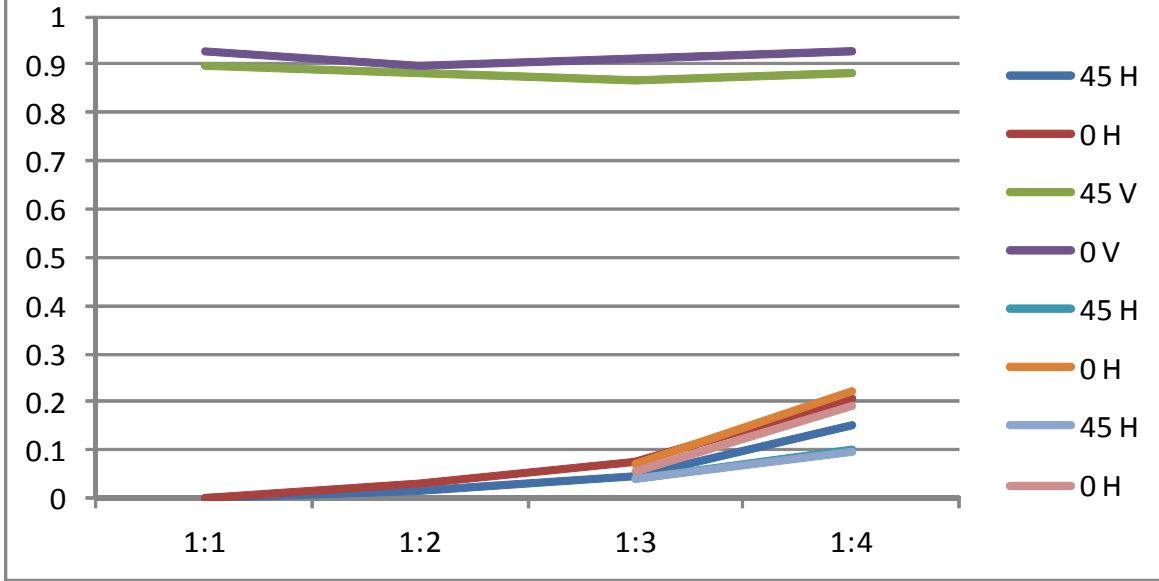
This value is similar and supports the theoretical value calculated above.

In summary, the power density generated at the target at a distance of one metre by our system is $79.6mWm^{-2}$, is approximately one hundred and thirty times smaller than the maximum level set by the ICNIRP of $10Wm^{-2}$.

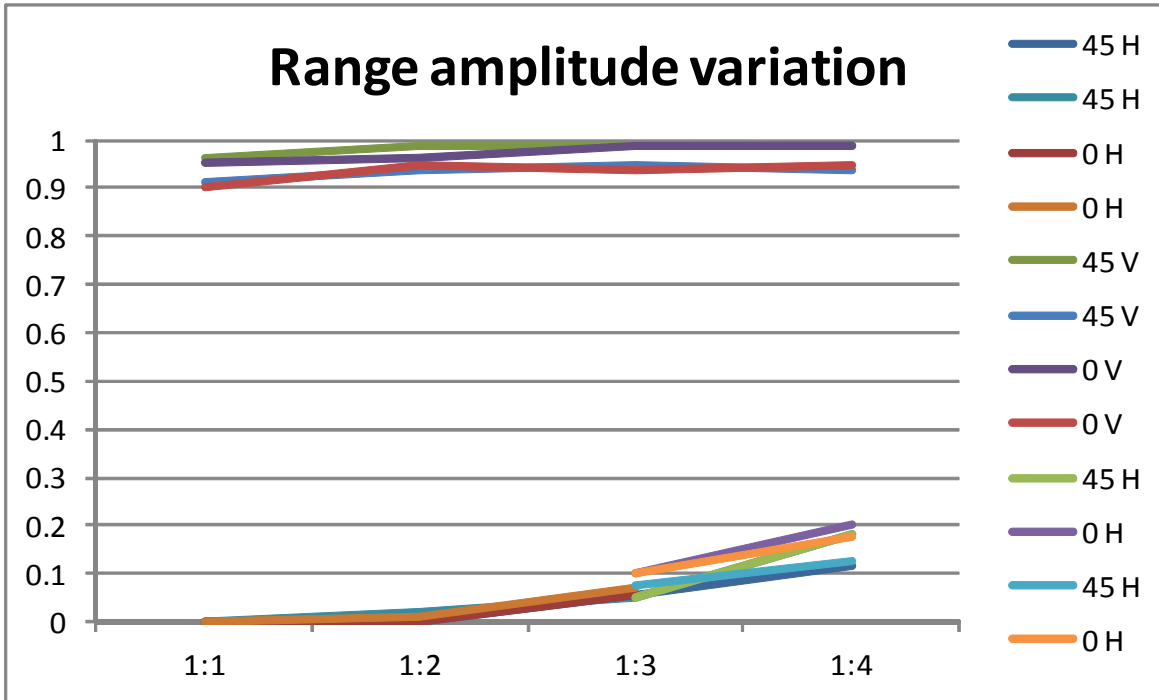
B PCB Polariser

Transmitter polarisation H		Fill ratio:						Normalised			
		1:1	1:2	1:3	1:4	None	1:1	1:2	1:3	1:4	
Mirror tilt angle	Mirror orientation	0.5	0.333333	0.25	0.2						
Co signal strength											
	45 H	0	0.01	0.03	0.1	0.67	0	0.014925	0.044776	0.149254	
	0 H	0	0.02	0.05	0.14	0.67	0	0.029851	0.074627	0.208955	
	45 V	0.6	0.59	0.58	0.59	0.67	0.895522	0.880597	0.865672	0.880597	
	0 V	0.62	0.6	0.61	0.62	0.67	0.925373	0.895522	0.910448	0.925373	
Range signal strength (3.4m)											
	45 H	0	0	0.05	0.1	0.86	0	0	0.05814	0.116279	
	0 H	0	0	0.05	0.5	0.86	0	0	0.05814		
	45 V	0.83	0.85	0.85	0.85	0.86	0.965116	0.988372	0.988372	0.988372	
	0 V	0.82	0.83	0.85	0.85	0.86	0.953488	0.965116	0.988372	0.988372	
Range signal strength (1m)											
	45 H	0	0.2	0.5	1.8	10	0	0.02	0.05	0.18	
	0 H	0	0.1	0.7	5	10	0	0.01	0.07		
	45 V	9.1	9.4	9.5	9.4	10	0.91	0.94	0.95	0.94	
	0 V	9	9.5	9.4	9.5	10	0.9	0.95	0.94	0.95	
Co signal strength again											
	45 H			0.04	0.1	0.99			0.040404	0.10101	
	0 H			0.07	0.22	0.99			0.070707	0.222222	
	45 H			0.02	0.05	0.52			0.038462	0.096154	
	0 H			0.03	0.1	0.52			0.057692	0.192308	
Range signal again											
	45 H			0.5	1.8	10			0.05	0.18	
	0 H			1	2	10			0.1	0.2	
	45 H			0.15	0.25	2			0.075	0.125	
	0 H			0.2	0.35	2			0.1	0.175	

Co Signal variation



Range amplitude variation



C Comparison of PIC Compiler USB Throughput

To aid USB development a C# application was written as a replacement for Windows Hyper Terminal to provide a means of benchmarking and verifying the integrity of hardware to host PC data transmissions. The lightweight code was written to interface at standard and arbitrary serial rates and support isochronous transmissions not supported by Hyper Terminal. The code was used extensively for C# applications that interfaced with hardware including the final analysis program. Figure 1 shows the original application GUI.

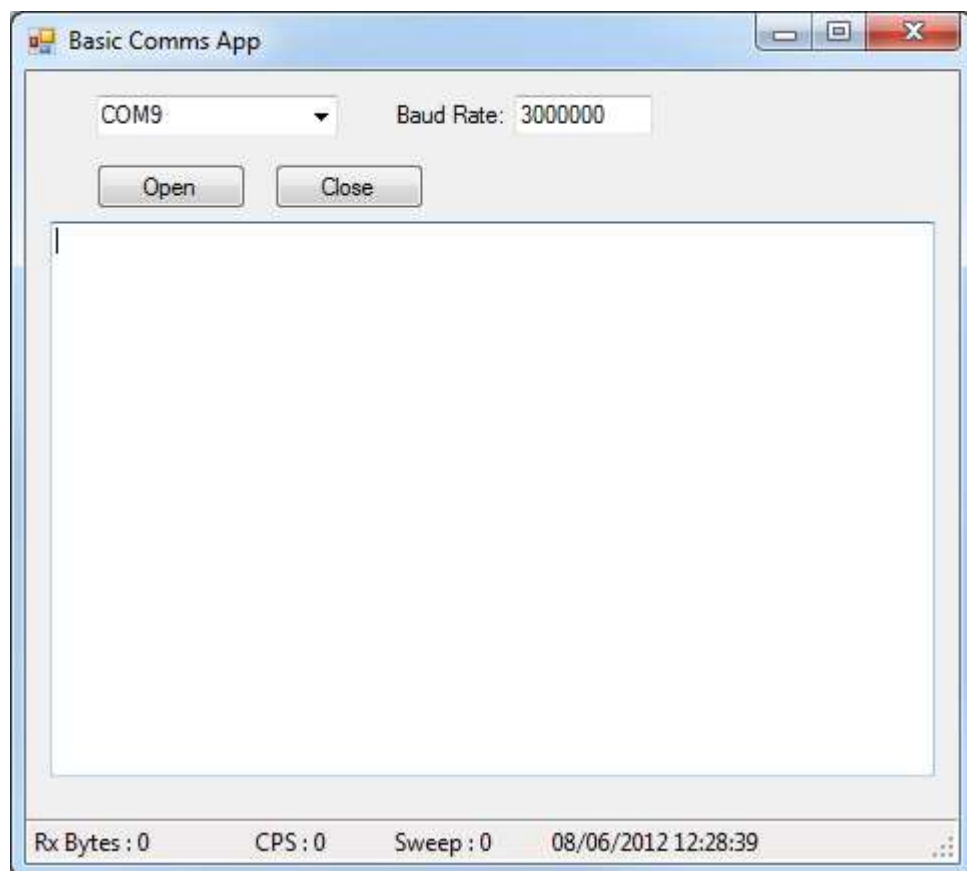


Figure 1: GUI of test and verify data terminal application

CCS (2007) and Microchip (2007) compilers, drivers and USB frameworks for the PIC18F2550 were tested. Data was sent using the USB functional calls in different size packets to establish small packet efficiency. Tests were conducted five times and the three median results averaged to produce a throughput. The best result from the two compilers is given.

ASCII Pattern (Length)	USB Throughput
01234 (5)	560 kbaud
0123456789 (10)	712 kbaud
01234567890123456789 (20)	710 kbaud
0123456789... (40)	714 kbaud
0123456789... (80)	712 kbaud
0123456789... (160)	712 kbaud

Table 1: PIC18F2550 USB data throughput using `usb_cdc_putc("payload")`

The Microchip drivers provided a slightly higher throughput for packetised data than the CCS drivers, but suffered poor throughput with small byte count packets. By using the alternate `usb_cdc_putc('')` within a loop the compilers were tested. The superior results of the CCS compiler are shown in in Table 2.

Loop size	USB Throughput
10	689 kbaud
20	687 kbaud
40	688 kbaud
80	692 kbaud
160	688 kbaud
250	680 kbaud

Table 2: PIC18F2550 USB data throughput using looped `usb_cdc_putc('')`

By using ten `usb_cdc_putc('1')` function calls within a loop an throughput was found to improve, see Table 3.

Loop size	USB Throughput
80	756 kbaud
500	750 kbaud
1000	750 kbaud
2000	750 kbaud

Table 3: PIC18F2550 USB data throughput using looped `usb_cdc_putc('1')`

A 750 kbaud data rate represents a significant 650% increase in throughput compared to a standard serial port at 115.2 kbaud. However this rate was insufficient for our needs and fell well short of the supported 12 Mbaud of Full Speed USB 1.0.

The library files were checked and it was found that Endpoint 2 in Bulk transfer mode was being used. For further details about USB coding refer to the official USB specifications (USB, 2007). Changing the default mode to isochronous transfers, not supported by Hyper Terminal and the reason for the custom application and manually flushing the Endpoint, produced the following results:

Message Length	USB Throughput
50	1020 kbaud
40	816 kbaud
30	609 kbaud
20	406 kbaud

Table 4: PIC18F2550 USB data throughput using isochronous transfers and manual buffer flushing of the Endpoint and sending data using `putsrsUSBUART` (“payload”)

From these results it appears the USB framework sends packets every 0.5 ms approximately. Checking for a maximum throughput using function call `putsUSBUART` a maximum packet size of 59 bytes was found to exist, anything larger was split into two packets before transmission, effective halving throughput.